FROM FOLDING TO FUNCTION THROUGH COMPARTMENTALISATION - INFLUENCE OF AMINOACID CHANGES AND PYRIDOXAL-5'-PHOSPHATE ON THE CELL BIOLOGY OF ALANINE:GLYOXYLATE AMINOTRANSFERASE.

A thesis presented by Sonia FARGUE
for the Degree of Doctor of Philosophy

University College London

2012

Declaration

I, Sonia Fargue, confirm that the work presented in this thesis is my own. Where information has been derived from other sources, I confirm that this has been indicated in the thesis

I.1 Abstract

From folding to function through compartmentalisation - influence of aminoacid changes and roles of pyridoxal-5'-phosphate on alanine:glyoxylate aminotransferase.

Primary hyperoxaluria type 1 (PH1), is a rare inherited disease caused by a deficiency in the liver-specific, pyridoxal-5'-phosphate (PLP)-dependent enzyme alanine:glyoxylate aminotransferase (AGT). AGT is normally localized to the peroxisomes where it catalyses the conversion of the intermediary metabolite glyoxylate to glycine. In a subset of patients with PH1, linked with the Gly170Arg mutation, AGT is mistargeted to mitochondria and patients may respond to pharmacological doses of pyridoxine, a precursor of PLP.

Using a model system of stably transformed CHO cells expressing different AGT variants, we have studied four mutations – Gly170Arg, Phe152Ile, Ile244Thr, Gly41Arg - on the background of a common polymorphism, Pro11Leu, characteristic of a minor *AGXT* allele. All four mutations unexpectedly result in the peroxisome-to-mitochondrion mistargeting of AGT. However, significant differences were found on AGT quaternary status and catalytic activity. These results emphasize the synergistic effect of the Pro11Leu polymorphism and disease-causing mutations and its potential to act as a mitochondrial targeting signal.

Varying the concentration of pyridoxine in cells had a biphasic effect on AGT expression, activity and compartmentalization that differed between constructs.

Where some mutants had improved function with additional pyridoxine, normal AGT was inhibited at higher levels. The results provide an explanation for the therapeutic effect of pyridoxine in some patients. Overall, PLP was shown to have both chaperone and prosthetic group effects on mutant AGTs.

Using a specially developed cell-based assay of indirect glycolate toxicity, we have shown the lower ability of mutant AGTs to detoxify glyoxylate. This is the basis for a functional assay of AGT in mammalian cells which could be used to screen drugs targeted at AGT.

I.2 Acknowledgments

I owe foremost thanks to my project supervisor Pr C Danpure. I am grateful for the knowledge he shared, his passion for teaching and enthusiasm for science, as well as his kindness. I have learned much about scientific reasoning during these years.

I would also like to thank my second supervisor Dr G Rumsby, who provided scientific and moral support during these four years.

Thanks also to Dr E Williams from UCLH, for teaching me about enzyme assays, to Dr B Cellini in Verona, for the collaboration on AGT-Δ, AGT-anc and many interesting discussions on AGT, to J Lewin at the Royal Free Hospital, who carried out the immunoelectron microscopy of CHO cells, to Dr P Cochat, who introduced me to the world of Primary Hyperoxaluria and sent the clinician I was, and am, on the path of research.

I owe thanks to The Oxalosis and Hyperoxaluria Foundation, the French Société de Néphrologie and the Association pour l'Information et la Recherche sur les maladies Rénales Génétiques (AIRG-France), Hospal, Amgen and Novartis who funded me during these four years.

I also wish to thanks my Tai Chi teacher Barry McGinlay, who has helped me stay rooted during that time.

Above all, I owe thanks to my family, who have provided unfailing support as well as technical advice throughout the years.

I.3 Table of Contents

I.4 List of Figures

I.5 List of Tables

I.6 List of Annexes

I.7 List of Figures on CD

I.8 List of abbreviations

AGT-152: AGT-F152I construct

AGT-170: AGT-G170R construct

AGT-244: AGT-I244T construct

AGT-41: AGT-G41R construct

AGT-anc: ancestral mammalian AGT

AGT-F152I: AGT with the phenylalanine to isoleucine substitution in position 152 on the background of the minor allele

AGT-G170R: AGT with the glycine to arginine substitution in position 170 on the background of the minor allele

AGT-G41R: AGT with the glycine to arginine substitution in position 41 on the background of the minor allele

AGT-I244T: AGT with the isoleucine to threonine substitution in position 244 on the background of the minor allele

AGT-MA: major allele of AGT, with a proline in position 11 and isoleucine in position 340.

AGT-mi: AGT-P11L, minor allele of AGT, with a leucine in position 11 and methionine in position 340.

AGT-P10L,P11L: AGT with a proline to leucine substitution in positions 10 and 11.

AGT: alanine:glyoxylate aminotransferase

AGXT: gene coding for AGT

AOA: amino-oxyacetic acid

B6: any of the vitamin B6 vitamers

BMOE: Bis(maleimido)ethane

$BS(PEG)_5$: bis-N-succinimidyl-(pentaethylene glycol)ester,

BS_3: bis(sulfosuccinimidyl)suberate

CaOx: calcium oxalate

CAT: carnitine acetyl transferase

CHO GO AGT: CHO cells transformed with both the *GOX1* and any of the *AGXT* variants plasmids

CHO GO: CHO cells transformed with the *GOX1* plasmid

CHO WT: wild-type non-transformed CHO cells

CHO: Chinese hamster ovary

COS: COS-1 cell line, African green monkey derived cell line (*C*V-1 *o*rigin, *S*V40)

DAO: D-amino acid oxidase

DMSO: dimethyl sulphoxide

EM: electron microscopy

FBS: foetal bovine serum

G418: Geneticin

GO: glycolate oxidase

GOX1: gene coding for GO (also called *HAOX1*)

GR: glyoxylate reductase

GR/HPR: gene coding for the GR and HPR enzymes

HOGA: 4-hydroxy-2-oxoglutarate aldolase

HPR: hydroxypyruvate reductase

IEM: immunoelectron microscopy

IMF: immunofluorescence

LDH: lactate dehydrogenase

MTS: mitochondrial targeting signal

OKT: ornithine ketoacid transaminase

PA: pyridoxic acid

PAM: presequence translocase associated motor

PBA: 4-phenyl butyric acid

PDXK: pyridoxal kinase

PDXP: pyridoxal phosphatase

PH: primary hyperoxaluria

PH1: primary hyperoxaluria type 1

PH2: primary hyperoxaluria type 2

PH3: primary hyperoxaluria type 3

PL: pyridoxal

PLP: pyridoxal-5'-phosphate

PM: pyridoxamine

PMP: pyridoxamine-5'-phosphate

PN: pyridoxine

PNP: pyridoxine-5'-phosphate

PNPO: pyridoxine 5'-phosphate oxidase

PTS: peroxisomal targeting signal

SDS-PAGE: sodium dodecyl sulfate polyacrylamide gel electrophoresis

SDS: sodium dodecyl sulfate

$SM(PEG)_2$: Succinimidyl-[(N-maleimidopropionamido)-diethyleneglycol] ester

TAT: tyrosine aminotransferase

TEM: transmission electron microscopy

TIM: translocase of the inner membrane

TMAO: trimethylamine-N-oxide

TOM: translocase of the outer membrane

VNTR: variable number of tandem repeats

WB: western blotting

II INTRODUCTION

II.1 The primary hyperoxalurias

Inborn errors in the metabolism of glyoxylate and oxalate in humans are the causes of primary hyperoxaluria (PH). An excessive production of oxalate, a metabolic end-product, characterizes these diseases. Three distinct hereditary enzyme deficiencies have been identified that cause PH: 1) a deficiency of the liver-specific, peroxisomal, pyridoxal-phosphate-dependent enzyme alanine:glyoxylate aminotransferase (AGT) in the case of PH type 1 (PH1, OMIM #259900) (Danpure and Jennings, 1986a), 2) a deficiency in glyoxylate reductase[1] (GR) in the case of PH type 2 (PH2, OMIM #260000) (Williams and Smith, 1968; Mistry J, 1988) and 3) a deficiency in 4-hydroxy-2-oxoglutarate aldolase 1 (HOGA, formerly called KHGA) [2] in the case of PH type 3 (PH3, OMIM #613616) (Belostotsky et al., 2010).

In some instances, hyperoxaluria also appears to be genetic but cannot be linked to any of these enzymes and remains, as yet, unexplained. The PHs are rare diseases with an estimated prevalence for PH1 of 1 to 3 per million population in Europe, occurring in 1/120,000 live births in central Europe (Cochat et al., 1995; Hoppe et al., 2005; Cochat et al., 2006; Hoppe et al., 2009). PH1 represents approximately 80% of patients with PH. PH2 is less frequent than type 1 and represents less than 10 % of PH patients (Lieske et al., 2005), the real frequency of PH3 is still unknown but might be higher than that of PH2.

The majority of urinary oxalate is derived from endogenous sources. Dietary sources of oxalate only contributes to about 10-20%, most of which is excreted in the faeces complexed to calcium or degraded by the gut flora, like *Oxalobacter formigenes* (Danpure, 2001). The main elimination of oxalate occurs through the kidney, where it is freely filtered in the glomerulus. There is conflicting evidence as to whether oxalate has a net tubular secretion or absorption (Watts et al., 1983; Danpure, 2001).

In patients with PH the urinary excretion of oxalate is very high, typically >1mmol/1.73m^2 per day (normal < 0.5). In patients with chronic renal failure, the plasma levels of oxalate are also increased (normal limits 1-6 μmol/l) and can reach 100-150 μmol/l.

The excessive endogenous production of oxalate that characterizes PH leads to the increase of its calcium salt, which is poorly soluble at physiological pH. Concentration of calcium oxalate (CaOx) above the saturation levels (>30 μmol/l) result in the formation of crystals or

---

[1] *Glyoxylate reductase was first known as D-glyceric dehydrogenase (DGDH). The enzyme known as GR also catalyses a different reaction for which it is called hydroxypyruvate reductase (HPR).*

[2] *HOGA is the gene product of dihydrodipicolinate synthase-like (DHDPSL) whose approved name is now HOGA1.*

deposits in tissues. When the overall renal function decreases below a critical level, CaOx accumulates and deposits manifest in the kidney. The level at which this starts to happen is debated but could still be relatively high, around or above a glomerular filtration rate (GFR) of 40 ml/mn/1.73m^2 (normal range 100-130 ml/mn/1.73m^2) (Morgan et al., 1987).

Using [C^{14}]oxalate infusion in normal subjects and patients with PH, it has been shown that oxalate can become part of a metabolic pool, in equilibrium, but added to the extra-cellular fluid (Watts et al., 1983, 1985b). It seems that a major storage compartment is represented by bones (Marangella et al., 1995). In PH patients with renal impairment there is a net accretion of oxalate and the oxalate pool can be a hundred times greater than in normal subjects (Watts et al., 1984). In rats with chronic renal failure and hyperoxalemia, oxalate has been shown to be excreted in the colon (Hatch et al., 1999; Hatch and Freel, 2003), but the relevance to patients with PH is unclear as if present, it would be only expected to be a minor contribution to oxalate metabolism (Watts et al., 1983).

In PH patients, the first organs to manifest symptoms are usually the kidney and urinary tract, where CaOx deposition occurs first as stones (urolithiasis) or as interstitial deposition in the renal parenchyma (nephrocalcinosis) {reviewed in (Cochat et al., 2006; Hoppe et al., 2009)}. As a consequence, renal function declines and CaOx deposits occur more widely in the body (systemic oxalosis). These deposits can involve the retina, heart and blood vessels, peripheral nerves, skin, joints and bones. As the excessive endogenous synthesis of oxalate is continuous and massive, the progression of oxalosis is ineluctable in the absence of curative treatment.

The quality of life of PH patients is very poor in the absence of treatment and the life expectancy decreased {reviewed in (Cochat et al., 2006; Hoppe et al., 2009)}. There is a great phenotypic heterogeneity and clinical presentation can even vary between siblings (Hoppe et al., 1997; Danpure, 2001). The first symptoms of PH usually manifest early, with a median age at first symptoms of 4 (range: 0.3-58.5) years (Harambat et al., 2010). Despite this, the greatest sign of the clinical heterogeneity is shown by the fact that end-stage renal failure can be reached anytime between the first months of life and the 6th decade of life.

The medical treatment of PH is supportive and essentially relies on decreasing the solubility product of CaOx in the urine with high fluid intake (> 3 l/m^2 per day) and urine alkalinisation with citrate (Leumann et al., 1993; Milliner et al., 1994; Broyer et al., 1996). In PH1, the oral administration of pharmacological doses of pyridoxine (vitamin B6) has been shown to be associated with a decrease in urinary and plasma oxalate, as well as the oxalate metabolic pool size, in a subset of PH1 patients (Gibbs and Watts, 1970; Watts et al., 1985b). The mechanisms by which pyridoxine reduces oxalate excretion are currently not understood.

Once end-stage renal failure is reached, renal replacement therapy, *i.e.* dialysis or kidney transplantation, has to be instituted but classically cannot match the high rate of endogenous

production and accumulation of CaOx (Watts et al., 1984). Peritoneal dialysis is much less efficient than hemodialysis, which following standard regimen is itself insufficient to clear the oxalate and decrease sufficiently long-enough the CaOx saturation (Watts et al., 1984; Marangella et al., 1993; Hoppe et al., 1996, 1999). In some patients with PH1 it has been estimated that the overall oxalate generated reached 4-7 mmol per day and that despite dialysis the tissue deposition was greater than 50 μmol/kg body weight per day (Marangella et al., 1992). The actual recommendations for dialysis are an intensive, daily, nocturnal hemodialysis and/or a combination of hemodialysis and peritoneal dialysis.

Isolated kidney transplantation has a poor prognosis, as it does not stop the liver production of oxalate, and can lead to recurrence of kidney failure in a very short time (Broyer et al., 1990; Cibrik et al., 2002; Harambat et al., 2010, 2012).

Aside from pyridoxine treatment in responsive patients, the only true disease-specific approach is liver transplantation, which has been performed in patients with PH1 for decades, either isolated or combined with kidney transplantation, with very good success (Watts et al., 1985a, 1987; Cibrik et al., 2002; Jamieson, 2005; Harambat et al., 2010, 2012). Since AGT is liver-specific, the excessive production of oxalate by PH1-liver will continue in patients as long as the native liver is left in place (Danpure, C.J., 1991). Therefore the removal of the native liver is required in liver transplantation for PH1 patients and auxiliary liver transplantation is useless.

Since, apart from the AGT deficiency, the patient's liver is functional, a few attempts at domino liver transplantation in liver cancer patients have been performed using PH1 patients' liver (Donckier et al., 2001; Casas-Melley et al., 2002; Farese et al., 2005; Franchello et al., 2005; Saner et al., 2010). The domino transplantations have been followed by the appearance of hyperoxaluria confirming the central role of the liver in the proximal disease process (Donckier et al., 2001; Farese et al., 2005).

After liver transplantation in PH1 patients, the urinary glycolate quickly returns to normal levels. Elevated plasma oxalate also returns to normal levels but urinary oxalate levels may take years to normalize due to the secondary release of systemic CaOx, probably mainly from the bone compartment (Watts et al., 1987; de Pauw et al., 1990; Inoue et al., 2003; Bergstralh et al., 2010). Clinically, oxalate osteopathy can improve as well as cutaneous deposits (Toussaint et al., 1993). Oxalate cardiomyopathy have been described as being amenable to normalization after transplantation (Detry et al., 2002).

However, liver transplantation can only be proposed for a subset of patients, exposes patients to life-long risks related to immunosuppression and there is still controversy on the timing of such a step during the course of the disease (Cochat and Mahmoud, 1995; Cochat et al., 2010).

Models for the study of PH1 are available, they range from recombinant protein, to yeast (Hopper et al., 2008), mammalian cells (Behnam et al., 2006) and animal models (KO and induced hyperoxaluria) (Chetyrkin et al., 2005; Salido et al., 2006).

II.2 Metabolism of glyoxylate and oxalate in the liver

AGT is involved in the oxalate and glyoxylate metabolic pathway (Fig.1) (Crawhall et al., 1959; Noguchi and Takada, 1979; Danpure and Jennings, 1986a).

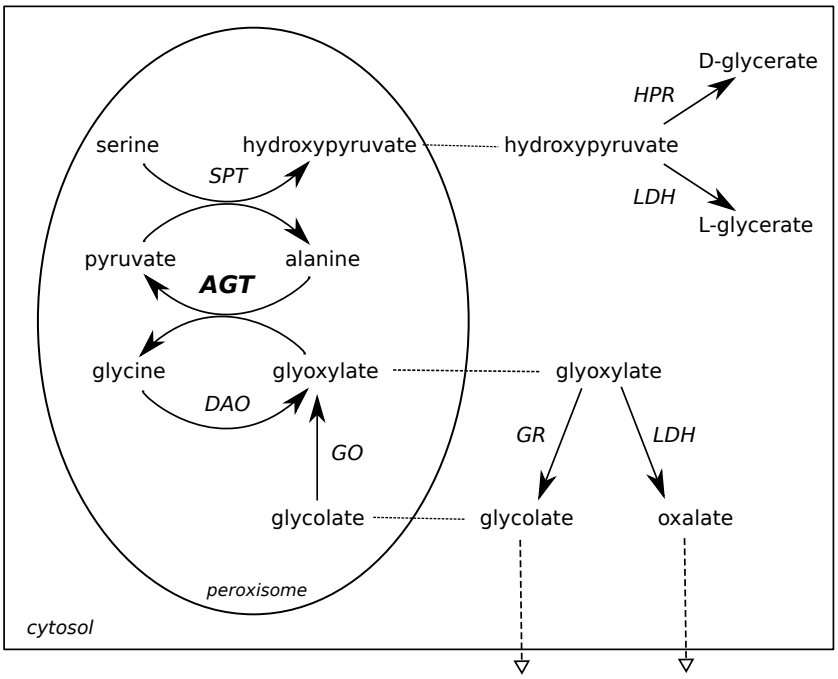

Figure II-1. **Glyoxylate and oxalate metabolism in human hepatocytes**. AGT: alanine:glyoxylate aminotransferase, SPT: serine:pyruvate aminotransferase, GO: glycolate oxidase, GR: glyoxylate reductase, HPR: hydroxypyruvate reductase, LDH: lactate dehydrogenase, DAO: D-amino acid oxidase. AGT and SPT are different appellations of the same enzyme, the same is true for GR and HPR. Dashed line: diffusion, dashed empty arrow: diffusion out of the cell and excretion in the urine.

AGT (EC 2.6.1.44) catalyses the transamination of glyoxylate to glycine while alanine is converted to pyruvate (fig II.1) (Danpure and Jennings, 1986a).The same enzyme is also responsible for the conversion of serine to hydroxypyruvate (serine:pyruvate aminotransferase (SPT) activity), but this reaction does not seem to play any role in (human) disease.

Other enzymes involved in the glyoxylate and oxalate pathway are known, but their relative importance is imperfectly understood.

Glycolate oxidase (GO), another peroxisomal enzyme, also found in the liver, catalyses the oxidation of glycolate to glyoxylate (fig II.1) (Fry and Richardson, 1979; Jones et al., 2000;

Williams et al., 2000; Williams, E. L., 2003). GO has been shown to be able to convert glyoxylate to oxalate *in vitro*, but it is unlikely to contribute to oxalate production in human liver (Fry and Richardson, 1979).

LDH, a cytosolic enzyme, catalyses the oxidation of glyoxylate to oxalate, which is presumably the reaction responsible for oxalate production in PH (Gibbs et al., 1977; Poore et al., 1997; Sharma and Schwille, 1997; Mdluli et al., 2005).

Glyoxylate reductase (GR) catalyses the reduction of glyoxylate to glycolate and also has another catalytic activity, reducing hydroxypyruvate to D-glycerate (hydroxypyruvate reductase (HPR) activity) (Williams and Smith, 1968; Mistry J, 1988; Giafi and Rumsby, 1998; Cramer et al., 1999; Rumsby and Cregeen, 1999; Cregeen et al., 2003; Mdluli et al., 2005, 205).

Another aminotransferase can catalyse the conversion of glyoxylate to glycine, as well as glutamate to 2-oxoglutarate, called glutamate:glyoxylate aminotransferase, GGT, (EC 2.6.1.4) (Thompson and Richardson, 1967, 1968). However, this enzyme has a lower activity than AGT in human liver and is cytosolic, so that it is not expected to compete for the same substrate as AGT - although correction for GGT activity when measuring AGT activity in human liver has been necessary for some diagnostic assays.

Finally, D-amino acid oxidase, DAO (EC 1.4.3.3) a peroxisomal enzyme, can catalyse the conversion of glycine to glyoxylate, but studies in pure protein and animals have suggested that its contribution to the glyoxylate pool is minor compared to the conversion of glycolate to glyoxylate catalysed by GO {reviewed in (Poore et al., 1997; Williams, E. L., 2003)}.

Humans also express another PLP-dependent alanine:glyoxylate aminotransferase, AGT2 (EC 2.6.1.44). In rats, mice and some other species, agt2 is localized in mitochondria (Takada and Noguchi, 1982). It has recently been shown that human AGT2 is also targeted to mitochondria (Rodionov et al., 2010). The sequence of AGT2, which forms a tetramer, is different from that of AGT1. In addition to its alanine:glyoxylate aminotransferase activity, AGT2 also can accept, as amino donor, asymmetric dimethylarginine (ADMA), which is an endogenous inhibitor of nitric-oxide (NO) synthase and may be involved in cardiovascular regulations (Lee et al., 1995).

In primary hyperoxaluria, the metabolism of glyoxylate is perturbed. In PH1, glyoxylate cannot be detoxified to glycine, reaction catalysed by AGT in the peroxisome, anymore. It can be oxidised, however, to oxalate by cytosolic LDH and reduced to glycolate by cytosolic GR. The classical biochemical hallmarks of PH1 are elevated urinary oxalate and glycolate. Glycolate is considered innocuous in itself. However glyoxylate, which is an intermediary metabolite, and oxalate, which is a metabolic end-product in humans, are harmful.

Although there is evidence for a cytotoxic effect of both oxalate and glyoxylate, at least in cell studies, the clinical consequence of the alteration of the glyoxylate metabolism at the level

of the whole organism, is dominated by the physico-chemical properties of oxalate (Poore et al., 1997; Holmes and Assimos, 1998; Poldelski et al., 2001; Knight and Holmes, 2005; Guo et al., 2007). That is, its propensity to crystallize as a calcium oxalate salt and form intra-renal deposits. The potential cytotoxic damage caused by glyoxylate or oxalate themselves is difficult to evaluate and still subject to debate.

II.3 Alanine:glyoxylate aminotransferase

II.3.1 *AGXT*

The gene encoding human AGT is *AGXT*. *AGXT* is situated on chromosome 2 (2q37.3), spans 11 exons and codes for one transcript, with a cDNA clone of 1176 nucleotides in the open reading frame (Takada et al., 1990; Purdue et al., 1991c). There are two main polymorphic variants of *AGXT* in the Caucasian population. The "major" *AGXT* allele is found in ~80% of the Caucasian population whereas the "minor" allele's frequency is ~15-20%. The minor allele is characterised by several changes that co-segregate: the replacement of a proline in position 11 by a leucine (c.32C>T), a 74 bp duplication in intron 1 (c.165+19_165+92dup74) , a type I (29 to 32 copy number) variable number tandem repeat (VNTR) in intron 4 and the replacement of isoleucine 340 by methionine (c.1020A>G) (Purdue et al., 1990, 1991b, 1992; Danpure et al., 1994a). The frequency of this minor allele in non-Caucasian populations is about 2% in the Japanese population (Danpure et al., 1994a) and in a population of black South African a so-called "African minor allele" with a frequency of 12% has been found to include only the intron 1 duplication and intron 4 VNTR without the P11L or I340M changes (Coulter-Mackie et al., 2003). However, in patients with PH1 the frequency of the (Caucasian) minor allele is greatly increased to 35-50% (Purdue et al., 1990, 1991b; Williams and Rumsby, 2007).

II.3.2 AGT protein

II.3.2.1 General properties of the AGT protein

AGT is a homodimer, of which each subunit contains 392 aminoacids with a molecular mass of 43 kDa (Noguchi and Takada, 1979). The cofactor of AGT is pyridoxal 5'-phosphate (PLP), one of the B6 vitamers. The functional (biophysical, structural, catalytic, cell biological) characteristics of AGT have been determined by several groups, both in animals and humans, and also on pure protein (Purdue et al., 1991a; Motley et al., 1995; Lumb et al., 1999; Lumb and Danpure, 2000; Coulter-Mackie et al., 2005; Coulter-Mackie and Lian, 2006; Williams and Rumsby, 2007; Hopper et al., 2008; Cellini et al., 2010a).

II.3.2.2 Catalytic properties of AGT

The most physiologically relevant reaction catalysed by AGT is the interconversion of L-alanine and glyoxylate to pyruvate and glycine (fig II.2). AGT follows a ping-pong mechanism and the kinetic parameters of AGT encoded by the major allele (AGT-MA) for the alanine/glyoxylate pair have been determined in human liver (Noguchi and Takada, 1979; Kamoda et al., 1980; Wanders et al., 1990; Rumsby et al., 1997) and on purified His-tagged protein (Lumb and Danpure, 2000; Cellini et al., 2007). The Km for alanine has been found between 7.5 and 13.5 mmol/l and the Km for glyoxylate between 0.21 and 2.5 mmol/l in human liver (Noguchi and Takada, 1979; Kamoda et al., 1980; Wanders et al., 1990; Rumsby et al., 1997). The optimal pH was between 7.5 and 8.5 for Lumb *et al.* and 8.0 for Wanders *et al.* and Rumsby *et al.,* whereas the maximum activity was found for PLP concentrations at or above 100 µmol/l (Wanders et al., 1990; Rumsby et al., 1997; Lumb and Danpure, 2000). AGT is inhibited by high concentrations of glyoxylate (>10 mmol/l) (Allsop et al., 1987; Danpure and Jennings, 1988; Wanders et al., 1990; Rumsby et al., 1997). The AGT activity varies according to the different publications and methods used. In human liver, using a diagnostic method, the normal AGT activity ranges between 17.9 and 38.5 µmol/h/mg of protein (Rumsby et al., 1997). The K_D for the binding of PLP to AGT has been determined on purified His-tagged AGT at 0.27 ± 0.03 nmol/l (Cellini et al., 2007). Pyridoxamine 5'-phosphate (PMP), another form of the B6 co-factor, has a higher affinity for AGT than PLP ($K_{D(PMP)}$ <0.1 µmol/l), which could explain how it remains bound to AGT during the catalytic cycle (Cellini et al., 2007, 2011).

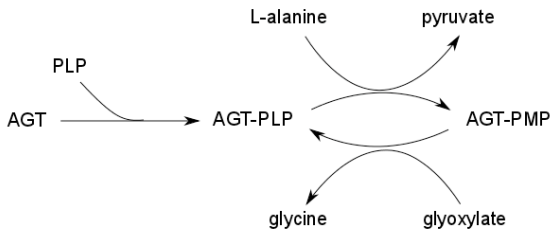

Figure II-2. **Mechanism of the alanine:glyoxylate transamination catalysed by AGT.** AGT: alanine:glyoxylate aminotransferase, PLP: pyridoxal 5'-phosphate, PMP: pyridoxamine 5'-phosphate. The two half-reactions are shown with the corresponding form of cofactor bound to the AGT.

The kinetic characteristics of AGT encoded by the minor allele (AGT-mi) have been determined on purified recombinant protein (Lumb and Danpure, 2000; Cellini et al., 2007; Hopper et al., 2008; Cellini et al., 2010a) and *E. coli* lysates (Coulter-Mackie et al., 2005; Coulter-Mackie and Lian, 2006; Williams and Rumsby, 2007). Depending on the study, the activity of AGT-mi ranges from 45% (Lumb and Danpure, 2000) to 100% of the activity of the

major isoform of AGT (Coulter-Mackie et al., 2005). In a yeast complementation assay, Hopper et al. have shown a decreased activity of AGT-mi compared with AGT-MA, along with a slight decrease in protein expression by western blotting in yeast expressing AGT (Hopper et al., 2008). It is to be noted that the decrease in activity of AGT-mi seems to be due to the P11L substitution, which has been demonstrated by Lumb *et al.* who compared the activity of AGT-P11L (30%) versus AGT-I340M (90%) and AGT-mi (*i.e.* P11l and I340M: 45%) (Lumb and Danpure, 2000).

II.3.2.3 Biophysical properties of AGT

The stability of AGT, encoded both by the major and minor alleles, has been studied by different groups and different techniques.

The stability of AGT-mi has been shown to be decreased compared to that of AGT-MA. This has been shown by studies on purified recombinant AGT. Hopper et al. showed that the thermal inactivation of AGT-mi occurred at lower temperatures than for AGT-MA (Hopper et al., 2008). In addition these authors used mass spectrometry-based analysis using SUPREX technique and showed lower $C^{1/2}_{SUPREX}$ for AGT-mi and lower melting temperatures (T_m) in differential scanning fluorimetry analysis.

Although the half-life of AGT-mi was not different from that of AGT-MA (>23h) on pulse-chase experiments performed on cell-free transcription/translation, Coulter-Mackie and Lian have shown that AGT-mi was susceptible to form aggregates to the detriment of the dimer/monomer forms over the duration of the pulse-chase in the cell-free experiments, whereas AGT-MA did not and increased its proportion of dimer/monomer (Coulter-Mackie and Lian, 2006). In another study the same authors have also noted a slight sensitivity to partial trypsin digestion on the part of AGT-mi but not AGT-MA (Coulter-Mackie and Lian, 2008).

In addition, studies have been performed to distinguish the stability of the holo- versus the apo-form of AGT, in minor and major allele-encoded AGTs. The holo-form of AGT has been found to be more stable than the apo-form, in terms of apparent melting temperature and transition midpoints of thermal inactivation (Cellini et al., 2007, 2009). Cellini et al. have further studied the stability of holo- and apo-AGT (both AGT-MA and AGT-mi) using urea-induced equilibrium unfolding techniques (Cellini et al., 2010a). They have shown that the sensitivity to chemical stress of holo- AGT-MA and AGT-mi are different, AGT-mi being less stable than AGT-MA, with the formation of aggregated intermediates. This lower stability was also found in the apo-forms and more precisely a lower stability was found for AGT carrying the P11L substitution only (instead of the characteristics of the minor allele: P11L and I340M). The relative instability of AGT-mi seems therefore to reflect changes due to the P11L substitution.

II.3.2.4 Structural properties of AGT

The x-ray crystal structure of AGT has been solved (pdb 1hoc) (fig II.3 & fig II.4) to a resolution of 2.5 Å, in complex with PLP and amino-oxyacetic acid (AOA), an inhibitor of AGT, taking the place of alanine (Zhang et al., 2003). Each subunit is composed of a large N-terminal domain (residues 1-282), containing the dimerization interface and most of the catalytic site, and a smaller C-terminal domain (residues 283-392). The first (1-22) residues of the N-terminal domain form an N-terminal arm of irregular coil, which wraps around the opposing subunit and is thought to play a role in the proper dimerization of AGT (Zhang et al., 2003). The peroxisomal targeting sequence (PTS) is located at the C-terminus. The PLP binds next to where the inhibitor, AOA substituting for alanine, was shown to bind. In the absence of substrate, the aldehyde group of PLP forms a Schiff-base linkage with the ε-amino group of Lys209 but residues (Tyr360 and Thr363) from the opposing subunit also form hydrogen bonds with the coenzyme.

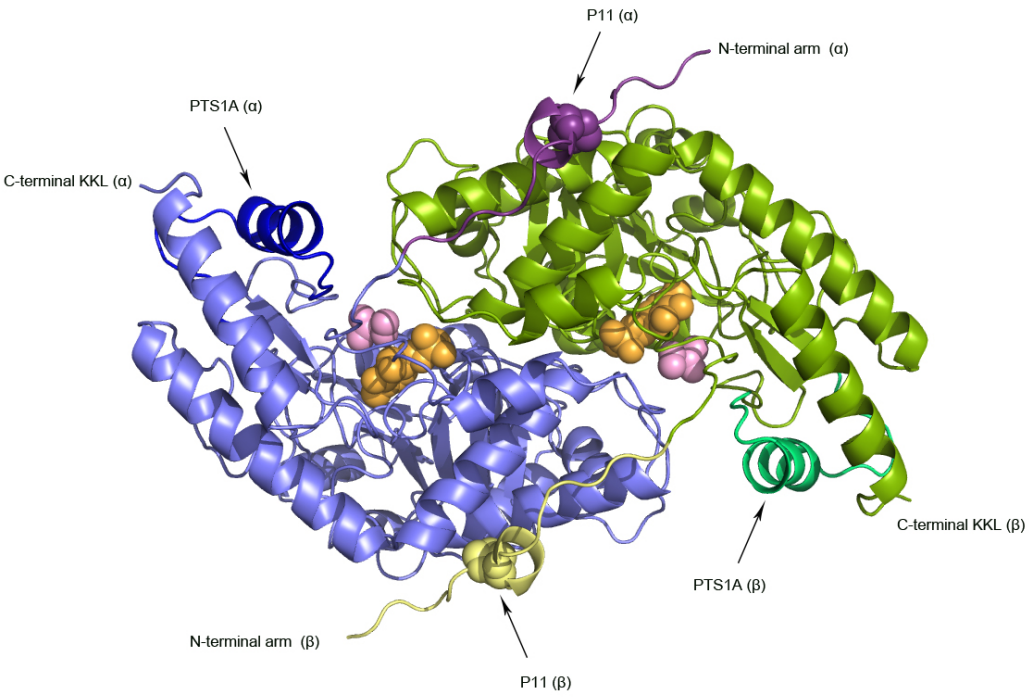

Figure II-3. **Structure of the AGT homodimer. Cartoon representation**. AGT alpha subunit in blue, beta subunit in green. PLP: pyridoxal phosphate in orange (space-filling representation), AOA: amino-oxyacetic acid in pink (substituting for alanine, space-filling representation).The proline residues in position 11 are shown on the N-terminal arms (space-filling representation), The PTS1A is shown in contrasting blue and green colours. Pdb file: pdb 1hoc.

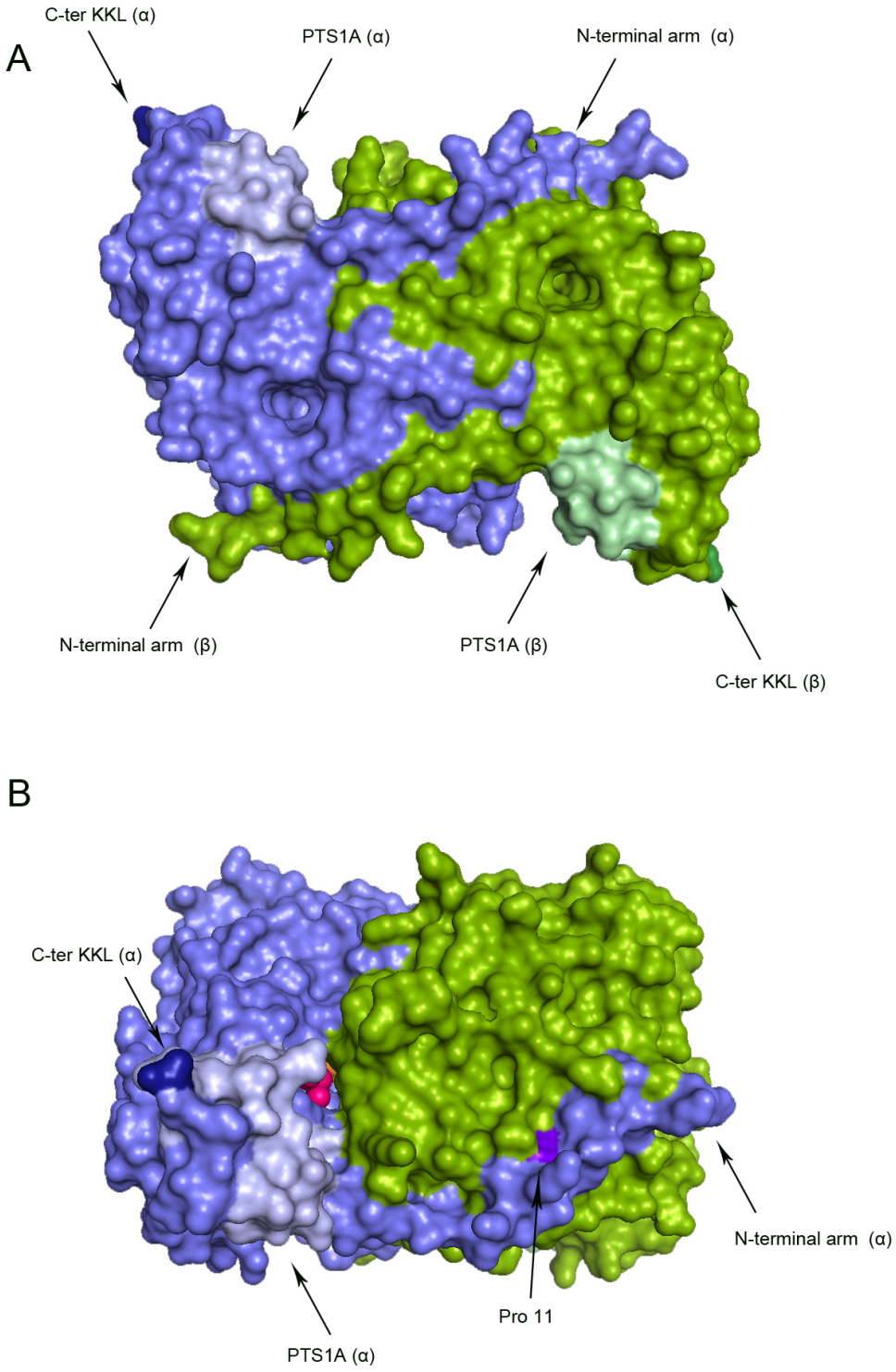

Figure II-4. **Surface views of the AGT homodimer.** Alpha subunit in blue, beta subunit in green. The C-terminal KKL is shown in dark blue (alpha) and dark green (beta), putative PTS1A in light blue (alpha) and light green (beta). The alpha-proline 11 is shown in violet in (B). The AOA: amino-oxyacetic acid can been seen as space-filling in pink (B). Pdb file: pdb 1hoc.

II.3.2.5 Cell biological properties of AGT

In humans, AGT is almost entirely expressed in the liver (Kamoda et al., 1980) and its subcellular localization is in the peroxisomal matrix (Noguchi and Takada, 1979; Cooper et al., 1988).

AGT has an atypical peroxisomal targeting signal (PTS1) at the C-terminus composed of a KKL sequence (Motley et al., 1995). The presence of this PTS1 allows it to bind to pex5 in the cytosol, which in turn probably interacts with the peroxisomal translocation apparatus, via pex13. The non-consensus nature of the AGT PTS1 has been shown to result in a less efficient binding of AGT to Pex5p compared to an AGT construct with the consensus -SKL PTS1 (Knott et al., 2000) and GFP-AGT constructs have shown the inefficiency of the AGT PTS1 on its own (Huber et al., 2005). The presence of an ancillary region (PTS1A) involved in the peroxisomal targeting of AGT was therefore suggested and the region between amino acids 324 to 345 shown to be a candidate (Huber et al., 2005). This has recently found confirmation and additional residues involved in facilitating the interaction between AGT and Pex5p have been identified and x-ray crystal structure of AGT bound to Pex5 solved (pdb 3R9A) (Fig II.5) (Fodor et al., 2012).

In AGT encoded by the minor allele, the replacement of proline by a leucine is responsible for the potential generation of an amphiphilic α helix, a typical structure of MTS, and the generation of a LXXLL motif which can interact with TOM20, a mitochondrial import receptor (Abe et al., 2000). The presence of this MTS was shown to direct 5% of the AGT to the mitochondria in a liver biopsy of one individual homozygous for the minor allele (Purdue et al., 1990). The remaining AGT is targeted to peroxisomes, due to the presence of the PTS1. The rate of dimerization of AGT, relative to the rate of import into peroxisomes, which can import partially or fully folded proteins, and rate of mitochondrial import, which requires un- or loosely folded proteins, is thought to be crucial to the final targeting of AGT-mi (Purdue et al., 1991a; Leiper et al., 1996). If the dimerization can occur quickly enough, as in the case for AGT-MA and if there is no or only a weak MTS, the peroxisomal import will be predominant.

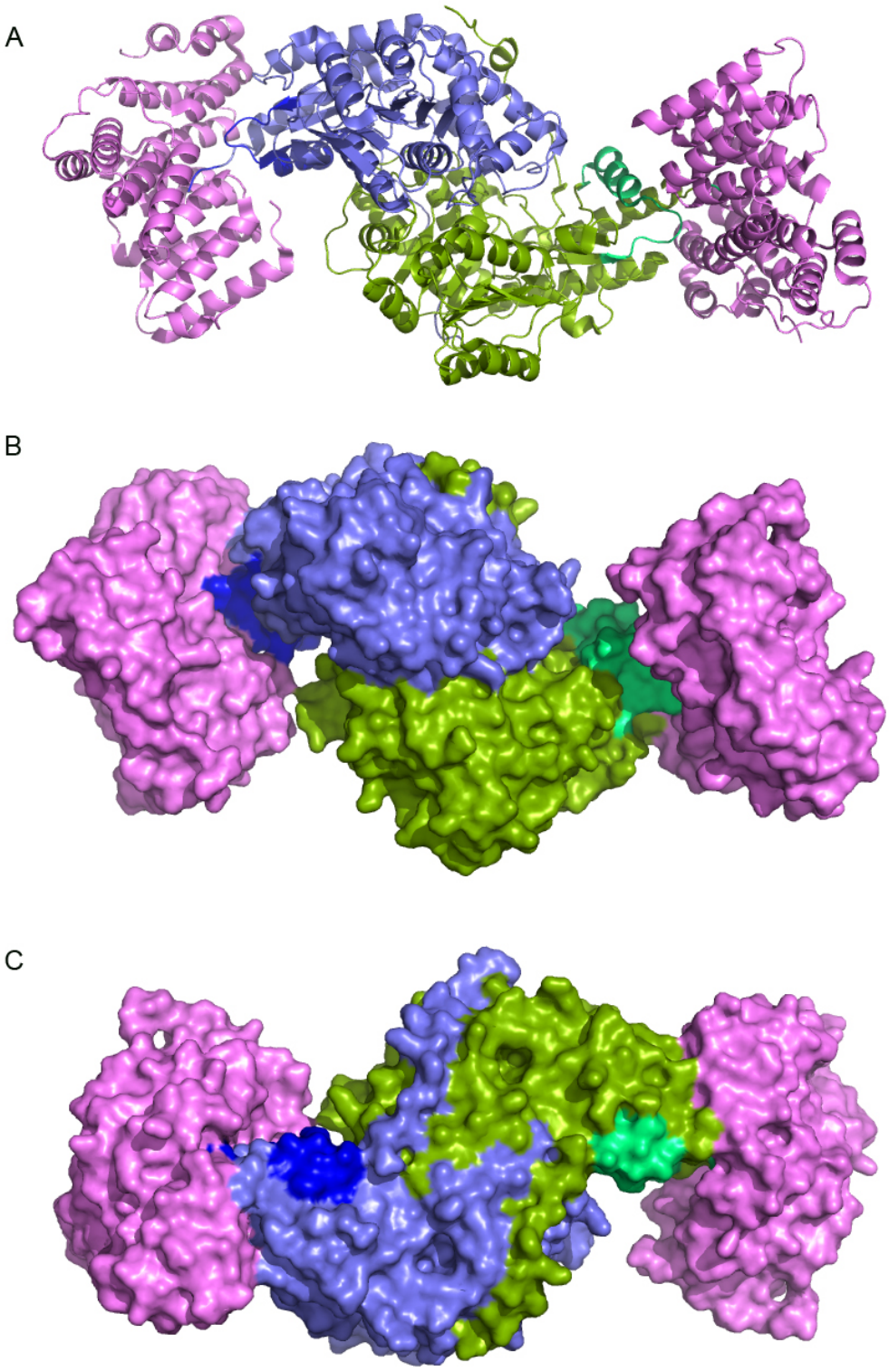

Figure II-5. **Structure of the TPR domains of PEX5P and the AGT dimer.** PEX5P in violet (2 separate PEX5P), alpha sub-unit of AGT in blue, beta in green. The C-terminal KKL and PTS1A from (Huber et al., 2005) are shown in contrasting blue and green. A: cartoon view, B: surface view, same orientation as A, C: surface view back orientation from B. Pdb file: 3R9A.

II.3.3 Evolution of the peroxisomal and mitochondrial import of AGT

The subcellular distribution of AGT is different between species and has changed several times during mammalian evolution (Danpure et al., 1990; Holbrook et al., 2000; Birdsey et al., 2005; Liu et al., 2012).

The archetypal ancestral mammalian AGT gene has two in-frame translation start sites, separated by a region which codes for a 22 amino acids mitochondrial targeting sequence (MTS). In addition to the MTS, a PTS1 is found at the C-terminus (Fig II.6). Two transcription start sites are found, one of which is upstream of the first translation start site and one between the first and second translation start sites. However, the Kozak initiation sequence of the first translation start site is poor compared to that of the second start site, leading to translational read-through by leaky ribosome scanning. The polypeptide with both MTS and PTS will be targeted to mitochondria in cells as the MTS takes precedence over the PTS (Oatey et al., 1996). Thus rat and marmoset, for instance, produce both mitochondrial and peroxisomal AGT. The human *AGXT* has lost the first translation start site so that the ancestral mitochondrial targeting sequence (MTS) of 22 amino acids at the N-terminus is lost, resulting in a protein with a PTS1, only targeted to the peroxisomes (Takada et al., 1990; Holbrook et al., 2000).

In other species, AGT can be wholly peroxisomal, as in rabbit and normal humans, mainly mitochondrial, as in cat, or distributed more equally in both as in the rat and marmoset. There is evidence that the AGT distribution is correlated with the natural diet, which might be explained by changes in dietary selection pressure (Birdsey et al., 2004, 2005). Natural herbivores tend to have peroxisomal AGT, carnivores mitochondrial AGT and omnivores both mitochondrial and peroxisomal AGT (Danpure et al., 1994b).

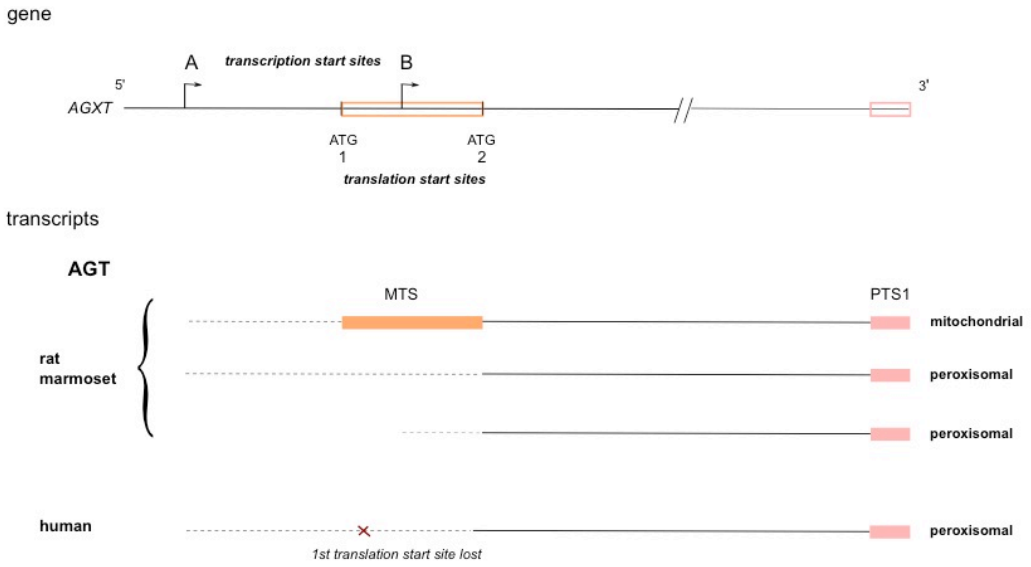

Figure II-6. **Ancestral mammalian *AGXT* gene and gene product in rat, marmoset and human species.** Adapted from (Danpure, 2001). The organization of *AGXT* is shown above and the possible AGT transcripts theoretically present in each species, as well as their subcellular localization, is shown beneath *AGXT*. The dotted line represents the 5'-UTR, the solid line represents the coding region. MTS: mitochondrial targeting sequence (orange box), PTS1: peroxisomal targeting sequence type 1 (pink box).

II.3.4 Subcellular targeting of AGT

In eucaryotes, proteins are sequestered in specific subcellular compartments and therefore need specific targeting information. The peroxisomal and mitochondrial targeting of proteins, although both relying on translation on membrane-free ribosomes in the cytosol, have different import mechanisms and characteristics.

All peroxisomal proteins are synthesised on free cytosolic polyribosomes and are imported post-translationally. Peroxisomal matrix proteins can be imported as fully-folded, cofactor-bound oligomers {reviewed in (Wolf et al., 2010; Rucktäschel et al., 2011; Ma et al., 2011)}. The most frequent PTS is a PTS1, a non-cleavable tripeptide motif at the C-terminus of the protein, -SKL or conserved variants (consensus sequence (S/A/C)-(K/R/H)-(L/M)) (Gould et al., 1989; Swinkels et al., 1992), whereas a minority of proteins carry an N-terminal PTS2 and follow a different import pathway (Swinkels et al., 1991; Ma et al., 2011). Proteins with a PTS1 signal are recognized in the cytosol by the receptor protein Pex5p {reviewed in (Wolf et al., 2010; Ma et al., 2011)}. The C-terminal TPR domains on Pex5p interact with the canonical PTS1. In the case of atypical PTS1, other residues both on the cargo and receptor are necessary

for a successful interaction (Fodor et al., 2012). Pex5p undergoes a conformational change after binding its cargo and interacts with the docking sub-complex part of the importomer. The receptor-cargo complex translocates across the peroxisomal membrane and releases the cargo in the peroxisomal matrix. The receptor Pex5p is recycled to the cytosol after ubiquitination and extracted from the membrane by a complex associating other proteins. The exact mechanisms by which the receptor and cargo cross the peroxisomal membrane and cargo is released are still not fully understood but recently the hypothesis of a transient protein-conducting channel has found some corroboration {reviewed in (Wolf et al., 2010; Rucktäschel et al., 2011; Ma et al., 2011)}.

The vast majority of mitochondrial proteins are encoded by nuclear genes, synthesized on membrane-free cytoplasmic ribosomes and most have to be imported post-translationally {reviewed in (Neupert and Herrmann, 2007; Schmidt et al., 2010)}. However, mitochondrial proteins can only be imported as unfolded or loosely folded monomers. Mitochondrial membrane or inter-membrane space proteins are imported differently from mitochondrial matrix proteins. Classical matrix proteins are synthesized as precursors with cleavable N-terminal extensions containing the mitochondrial targeting signals (MTS). Some hydrophobic proteins have internal non-cleavable targeting signals and follow a carrier import pathway, actively involving cytosolic chaperones in an ATP-dependent manner. For matrix proteins with an N-terminal MTS, the import route first takes place via the translocase of the outer membrane (TOM) complex followed by a transfer to the complex of the translocase of the inner membrane (TIM) and finally imported completely into the matrix by a presequence translocase associated motor (PAM). MTS presequences are typically up to 50 amino acids long and form positively charged amphiphilic α-helices, which are recognized by TOM and TIM complexes sequentially. The interaction with Tom20 involves hydrophobic interactions and uses a motif for recognition which follows a: - $\sigma\varphi\chi\beta\varphi\varphi$ - sequence (σ: hydrophilic, φ: hydrophobic, χ: any, β: basic residue) (Abe et al., 2000; Obita et al., 2003). The TOM complex is composed of a central barrel shaped Tom40 and preprotein receptors, Tom20, (recognizing the hydrophobic surface of the MTS helix) Tom22 (recognizing the positively charged surface), Tom70 as well as smaller proteins. The last steps of import into the matrix take place via the PAM which includes a mitochondrial chaperone, mtHsp70, and co-chaperones (5 identified so far) and a combination of trapping and pulling the protein is thought to happen. Once fully imported, most presequence are cleaved proteolytically by a mitochondrial processing peptidase (MPP), some proteins may be processed further by other enzymes.

Some proteins can be found in several subcellular compartments. For proteins encoded by the same gene the mechanisms that can be involved include the existence of multiple transcripts with multiple transcription initiation sites or alternative pre-mRNA processing. Single transcripts from a single gene can also lead to different proteins with different targeting

information due to an alternative translation start site. However, even single products from a single transcript can be targeted in different subcellular compartments.

The dual localization of a protein in eucaryotes can take place via several, non-exclusive mechanisms {reviewed in (Danpure, 1995; Karniely and Pines, 2005; Wolf et al., 2010)}.

In the case of AGT, in addition to the presence of two possible transcripts (in those species which have dual-localized AGT (Fig II.6) there can be a competition between the two different targeting signals. This is the mechanism for the small percentage of mitochondrial human AGT encoded by the minor allele (Purdue et al., 1990).

II.3.5 AGT mutants causing PH1

There are more than 150 mutations in PH1, most of them private mutations, but some very common, which are scattered over the gene (Williams et al., 2009). They include missense, nonsense and splice-site mutations. A minority (25%) of both small and large deletions and insertions has been found.

Many mutations segregate with either the major or the minor allele, while others can be found on both. For some mutations, such as the G170R mutation, the effect on AGT is dependent on its co-segregation with the minor allele, specifically the Pro11Leu replacement (Lumb and Danpure, 2000).

The mechanism of action of some of the most common mutations has been elucidated using a wide range of biochemical, biophysical, structural and cell biological techniques (Purdue et al., 1991a; Leiper et al., 1996; Lumb and Danpure, 2000; Santana et al., 2003; Zhang et al., 2003; Coulter-Mackie et al., 2005; Cellini et al., 2007; Williams and Rumsby, 2007; Coulter-Mackie and Lian, 2008; Hopper et al., 2008; Cellini et al., 2009, 2010a; b; Djordjevic et al., 2010). Missense mutations in AGT can affect the co-factor binding site, inhibit dimerization, decrease stability, cause aggregation or accelerate degradation or cause the AGT to be targeted to the wrong subcellular compartment (mitochondria instead of peroxisomes) (Fig II.7).

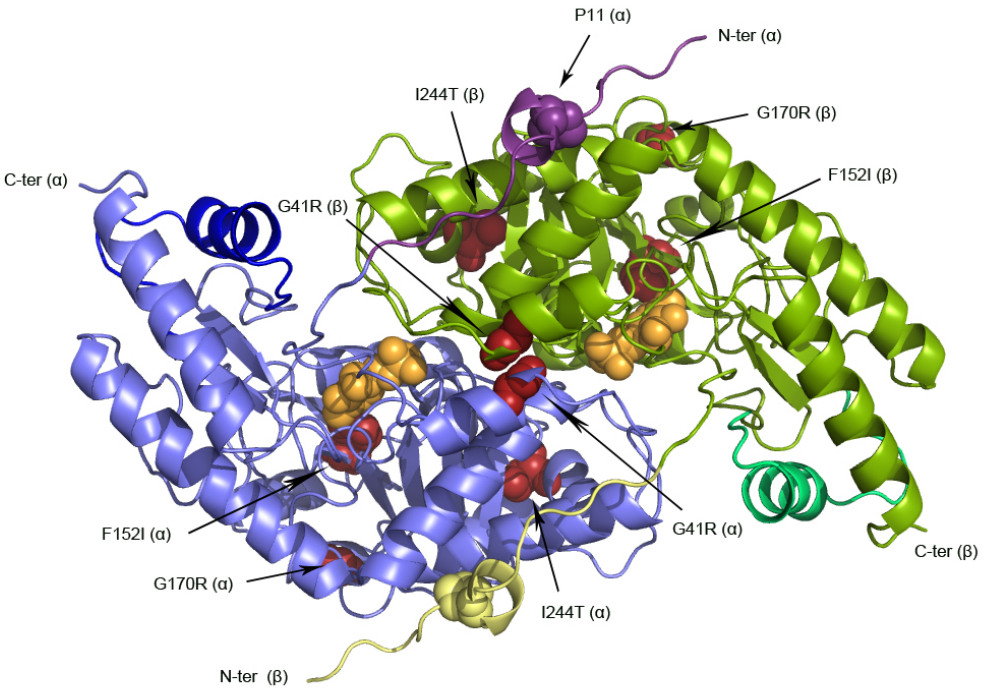

Figure II-7. **Position of common missense AGT mutations**. The AGT alpha subunit is shown in blue, beta subunit in green. PLP: pyridoxal phosphate in orange (as spheres). The proline residues in position 11 (as spheres) are shown on the N-terminal arms (in purple for subunit alpha, yellow for beta). Residues with known pathological mutations, which are studied in the present work, are shown in red on both chains (G41R, F152I, G170R, I244T) as spheres.

Some mutations have different frequencies in distinct populations. There is no international database recording their frequencies but several studies have reported the mutations found in different diagnostic centres (Fig II.8) (Santana et al., 2003; van Woerden et al., 2004; Williams and Rumsby, 2007; Coulter-Mackie et al., 2008; Harambat et al., 2010). When added together, 4 missense mutations (G170R, I244T, F152I, G41R) represent between 34 and 100% of the alleles in patients depending on the studies. The most frequent, G170R, accounts for 20 to 40% of alleles in Caucasian patients.

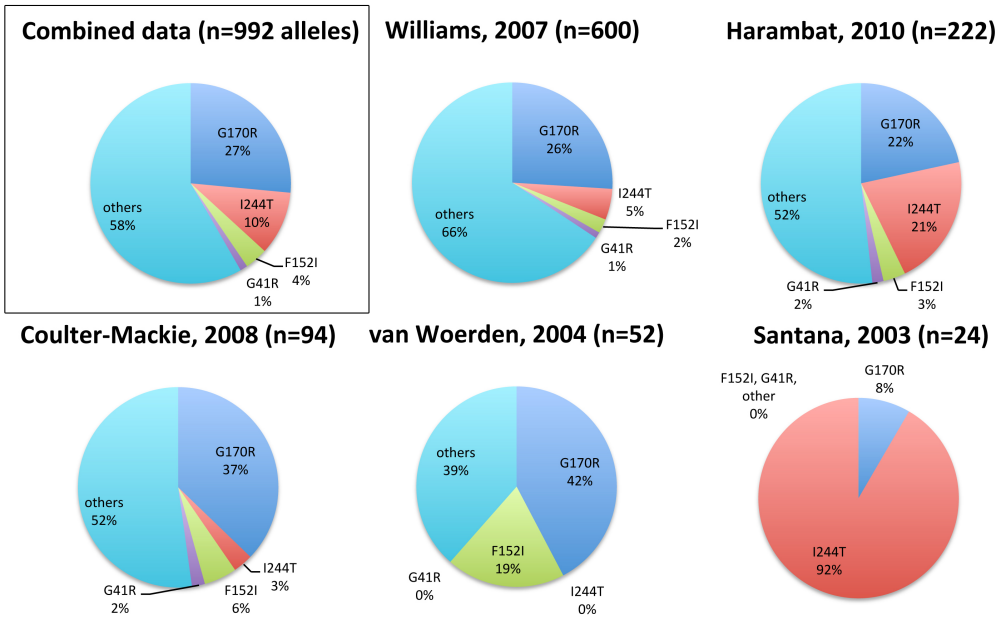

Figure II-8. **Allele frequencies of selected missense mutations in the published literature**. Combined data from published data of five diagnostic centres for PH1. Overlap between some patients has not been formally excluded. From (Santana et al., 2003; van Woerden et al., 2004; Williams and Rumsby, 2007; Coulter-Mackie et al., 2008; Harambat et al., 2010).

II.3.5.1 AGT-G170R

The most common mutation in PH1, the G170R missense mutation (c.508G>A), is also the most studied. This mutation always co-segregates with P11L on the minor allele and demonstrates a remarkable synergy with the polymorphism.

Homozygous patients bearing the G170R mutations have the highest catalytic activity compared to other mutant AGTs or heterozygotes, in the diagnostic enzyme assay, but can still greatly vary, between 0 to 70% of normal values (Purdue et al., 1990; van Woerden et al., 2004; Monico et al., 2005a; Williams and Rumsby, 2007; Harambat et al., 2010).

The crystal structure of AGT with the G170R mutation, on the background of the major allele however, is known and shows little difference with the structure of the AGT-MA apart from some structural changes next to the residue 170, so that the explanation for its effect in patients reflects more the functional interaction and synergy between mutation and polymorphism (Djordjevic et al., 2010).

Liver biopsies have been available from patients and have led to the discovery that 95% of the AGT-G170R is mistargeted to the mitochondria, whereas only 5% is targeted to peroxisomes (Danpure et al., 1989; Purdue et al., 1990) . Though the catalytic activity of such mistargeted AGT can be significant, it cannot be effective in cells, as its substrate is produced in a different compartment, the peroxisome. Studies in transiently transfected mammalian cells (COS cells) have shown that the G170R change is insufficient on its own to target AGT to the

mitochondria, while the P11L polymorphism on its own can direct 5% to the mitochondria. The presence of both these changes, however, leads to 95% of AGT being mistargeted to the mitochondria (Danpure et al., 1989; Purdue et al., 1990, 1991a; Leiper et al., 1996). It is thought that the slowed down dimerization, caused by the combined presence of the G170R mutation and the P11L polymorphism, allows the AGT to stay in a mitochondrial import-compatible conformation (*i.e.* unfolded or loosely folded monomer) long enough to be effectively mistargeted to mitochondria. This mitochondrial targeting is mediated by the availability of the polymorphic MTS caused by the P11L change. Once in the mitochondria, the mutant AGT can dimerize into an active form. Some dimer can be also formed and imported to peroxisome but the overall balance is shifted in favour of mitochondrial import (Purdue et al., 1991a).

Biochemical studies on purified AGT-G170R (on the minor allele background) have shown a decreased catalytic activity, which still remains high, between 60 and 76% (Coulter-Mackie and Lian, 2006; Hopper et al., 2008; Cellini et al., 2010a). The stability of the mutant is decreased compared with normal AGT, and the presence of the G170R mutation added to the P11L polymorphism resulted in aggregates for Lumb *et al.* (Lumb and Danpure, 2000). The synergy between mutation and polymorphism is again shown by the fact that the G170R mutation on its own resulted in non-aggregated AGT with a specific activity of approximately 40% of AGT-MA (Lumb and Danpure, 2000). Protein levels are lower both in *E. coli* and yeast systems and the sensitivity to trypsin digestion is increased (Coulter-Mackie and Lian, 2006, 2008; Hopper et al., 2008). More precisely it seems that the main instability occurs in the apoform, which is less stable than that of the minor allele of AGT (Cellini et al., 2010a).

The distribution of the mistargeted mutant form of AGT, AGT-G170R, has been studied in the presence of potentially stabilizing and destabilizing circumstances. Lumb *et al.* showed that decreasing the temperature to 30°C was able to redirect AGT-G170R from the mitochondrion to the peroxisomes in transiently transfected COS cells, while increasing the temperature to 42°C increased the mitochondrial targeting (Lumb et al., 2003). The non-specific stabilizer glycerol also had the ability to redirect AGT-G170R to peroxisomes in COS cells without affecting the efficiency of the mitochondrial import pathway. Thus stabilizing AGT shifted import to the correct intra-cellular target. Binding to cofactors and/or inhibitors is also known to improve the stability of proteins. However, neither pyridoxine, nor pyridoxal phosphate or AOA were shown to be able to change the distribution of AGT-G170R in COS cells (Lumb et al., 2003).

II.3.5.2 Other AGT mutants

Some AGT mutations interfere with PLP binding, such as the G82E mutation (with co-segregates with the major allele), resulting in the absence of catalytic activity, others have residual activity and a different pathophysiological mechanism (Purdue et al., 1992; Lumb and Danpure, 2000; Cellini et al., 2007).

AGT-I244T

The second most frequent missense mutation, the c.731T>C change, causing the I244T substitution, also has a very population specific distribution (fig II.8) (von Schnakenburg and Rumsby, 1997). It is the most common mutation in patients from the Canary Islands, with evidence for a founder effect, and also a common mutation among patients originating from North Africa (Santana et al., 2003; Harambat et al., 2010). This mutation almost always segregates with the minor allele but has also been found on the background of the major allele in one patient (Williams and Rumsby, 2007). The catalytic activity in patient's liver is usually very low but ranges between 0 and 36% (Williams and Rumsby, 2007). The catalytic activity of recombinant protein synthesized in *E. coli* ranges from 0 to 26% with evidence that it is less stable than AGT-MA and may form aggregates (Lumb and Danpure, 2000; Santana et al., 2003; Hopper et al., 2008). Lumb *et al.* showed aggregation in AGT-I244T on the minor allele background but measured significant AGT activity, around 50% in the absence of the P11L polymorphism (Lumb and Danpure, 2000). The synergistic effect on activity was confirmed by Santana et al. in *E. coli* lysates, who also found evidence that AGT-I244T formed aggregates when expressed in COS cells (Santana et al., 2003). These authors have also shown in transient transfection experiments, that the aggregation of AGT-I244T in COS-7 cells and subsequent low solubility in extracts was improved by the addition of betaine, and, to a lesser degree, pyridoxal phosphate. However, neither glycerol, DMSO, PBA, TMAO, nor amino-oxyacetic acid (AOA, a competitive inhibitor of AGT) showed any effect. Hopper et al. showed a decreased growth of yeast expressing AGT-I244T in a yeast complementation assay (12%) compared to yeast expressing AGT-MA and decreased expression of AGT-I244T in yeast compared to AGT-MA (Hopper et al., 2008).

The subcellular distribution of this mutant in patients is not published, but there is little detectable immunoreactivity in western blot performed on patient's liver (von Schnakenburg and Rumsby, 1997), suggesting that it has a low synthesis or high degradation rate. Immunoelectron microscopy in patient's liver has only been available in one homozygous patient and one heterozygous patient also carrying the G170R mutation. Whereas the detectable AGT was peroxisomal in the I244T homozygote, almost all the AGT was detected in the mitochondria in the compound heterozygote, probably due to the associated G170R mutation (personal communication from P Cochat, University of Lyon, France). It has been shown in transiently transfected COS cells that AGT-I244T can be targeted to peroxisomes (Santana et al., 2003).

AGT-F152I

The c.454T>A mutation leading to a F152I substitution is also found on the minor allele. It is highly represented in the Dutch population (19%) but has a lower frequency in other populations (2-6%) (Fig II.8). The catalytic activity in homozygotes has been described to be around 10% of the normal activity (van Woerden et al., 2004). There is no direct evidence as to whether it is localized in peroxisomes or mitochondria. However, the subcellular localization of 4 compound heterozygotes for AGT-F152I (2 F152I/G41R, 2 F152I/unknown) was shown to be partly mitochondrial on immunoelectron microscopy of liver biopsies, as was some of the AGT in the 2 parents carrying the F152I allele (Danpure et al., 1993).

The catalytic activity of AGT-F152I (on the minor allele background) in purified protein synthesized in *E. coli* has been described as having different activities depending on the study (14% to 80%) (Coulter-Mackie and Lian, 2006; Hopper et al., 2008; Cellini et al., 2009). Its stability is also decreased compared to AGT-MA. Lumb *et al.* showed for this mutation also a synergy with the P11L polymorphism. Whereas the F152I mutation alone resulted in decreased but significant activity around 50-60%, the presence of the P11L leads to aggregation of the purified recombinant AGT in *E. coli* (Lumb and Danpure, 2000). The main defect seems to be in the apoform, which is less stable that the holoform, and the tendency of the monomer to form aggregates. The affinity for PMP has also been shown to be greatly reduced (Cellini et al., 2009).

AGT-G41R

The c.121G>A, which leads to a G41R change on AGT, can be found both on minor and major alleles, but is not a frequent mutation (1-2%) (Danpure et al., 1993; Williams and Rumsby, 2007). A study of the liver from compound heterozygotes carrying the G41R mutation on the minor allele background (2 G41R/F152I, 1 G41R/G170R) has shown the presence of intra-peroxisomal cores staining with AGT, which were also present in the heterozygote parent carrying the G41R mutation (Danpure et al., 1993). The catalytic activity in patients is unknown in homozygotes. In purified protein, most of the protein aggregates (electrostatic driven aggregation process), and the activity on the soluble part has been found to be around 20% (Coulter-Mackie and Lian, 2006; Cellini et al., 2010b). Lumb *et al.* even showed that in the absence of P11L, the activity of AGT-G41R was very low, <10% (Lumb and Danpure, 2000). The purified recombinant G41R mutants are very unstable, with defects both in the apo and holo-forms. It has been suggested that the G41R change leads to a disruption of the active site loop 24-32 which, being transmitted to the active site, could explain the loss of activity and decreased PLP-binding (Cellini et al., 2010b).

In a study using *E. coli* and an *in vitro* translation system, Coulter-Mackie and Lian studied the effect of chemical chaperones on a model assessing proper folding of the mutant AGT based on partial trypsin digestion (Coulter-Mackie and Lian, 2008). Some degree of protection was found on AGT-G41R with the addition of PLP and AOA.

II.3.5.3 Genotype-phenotype correlations

Although there is a wide intra-and inter-familial phenotypic heterogeneity in PH1, a certain degree of correlation between genotype and enzyme phenotype can be described for AGT (Fig II.9) (Danpure et al., 1994c). The absence of catalytic activity can be accompanied by an absence or low levels of AGT immunoreactivity, as is the case for the rare Japanese S205P mutation (Nishiyama et al., 1991) or by a significant levels of immuoreactive protein, as with the G82E mutation (Purdue et al., 1992). A third type is characterized by the presence of immunoreactive protein and detectable, sometimes significant, enzyme activity. This is the case for the G170R mutation, which is further characterized by a mistargeting of the enzyme from peroxisomes to mitochondria, which explains its impaired metabolic effectiveness in PH1 patients (Purdue et al., 1990). However, even in patients with the same *AGXT* genotype, the enzyme activities may vary (Danpure, 2004; Williams and Rumsby, 2007).

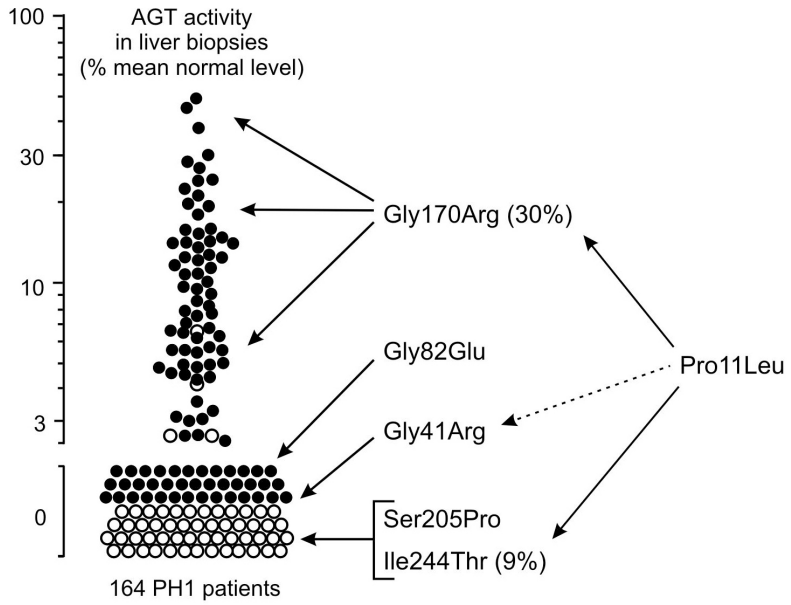

Figure II-9**. Genotype/enzyme phenotype relationships**. From (Danpure et al., 1994c). The catalytic activity of AGT in liver biopsies is represented on a logarithmic scale as a percentage of averaged normal value in human liver. Black circles: significant AGT immunoreactive protein detected, white circles: no significant immunoreactive AGT detected. Allelic frequencies in the population tested are indicated for the two common mutations. Segregation with the P11L polymorphism is indicated by an arrow linking the mutation and the polymorphism (dashed arrow: partial segregation). The G82E and S205P mutations segregate with the major allele.

The phenotypic heterogeneity within families can also be found at the clinical level, and this has been documented in siblings with PH1 who may present their first symptoms or even reach renal failure at very different ages, without taking into account the influence of medical treatment (Hoppe et al., 1997). Both an environmental effect and the role of modifier genes could explain this heterogeneity.

However, some degree of clinical phenotype-genotype correlation has been found for a few genotypes. The renal survival of patients carrying the G170R mutation is better than that of patients with other mutations (Fig II.10) (Harambat et al., 2010). Interestingly, patients carrying the G170R mutation have been shown to be able to respond to pharmacological doses of pyridoxine (van Woerden et al., 2004; Monico et al., 2005b). The response to pyridoxine is neither constant nor similar in all patients, but some patients can normalize the excretion of urinary oxalate with pyridoxine (Monico et al., 2005b). Another genotype has also been associated with response to pyridoxine, the F152I mutation (van Woerden et al., 2004). Other genotypes have not been described as responsive, although extensive pyridoxine testing has not been done on a sufficiently large cohort. Odd reports of B6-responsiveness, concerning other genotypes, have been mentioned by physicians. The two responsive mutations known have had the benefit of a large-enough pool of patients, either by virtue of their allele frequency in the Caucasian population for the G170R, or in the Dutch population, for F152I. Although pyridoxine is metabolized to PLP, the cofactor for AGT, the reason why these particular mutations should be responsive to pyridoxine is at present unclear.

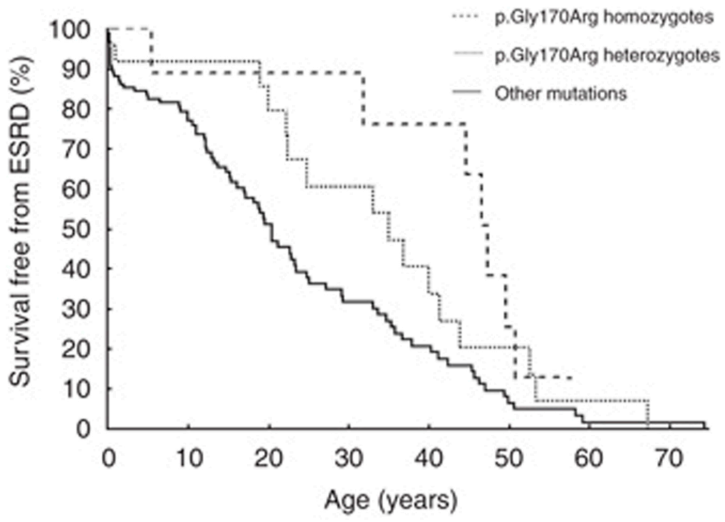

Figure II-10. **Renal survival in PH1 patients according to their genotype**, from (Harambat et al., 2010). Long-dashed line: renal survival (ESRD: end-stage renal disease) in patients homozygous for the G170R mutation, short-dashed line: renal survival in patients compound heterozygotes with one G170R mutation, full line: PH1 patients carrying non G170R mutations. ESRD: end-stage renal disease

II.3.6 AGT mutants and pyridoxine responsiveness

Vitamin B6, a water-soluble vitamin, is the cofactor of more than a 100 enzymes in humans. There are 6 vitamers present in the body and an inactive form (pyridoxic acid), which is the main urinary metabolite of B6. Pyridoxal 5'-phosphate is the active form of the cofactor. The fact that a deficiency in vitamin B6 could be associated with elevated urinary oxalate has been known for a long time (Gershoff et al., 1959; Takada et al., 1984).

The efficacy of pyridoxine in reducing the amount of oxalate excreted by certain patients with PH1 and improving clinical outcome has also been known for some time (Gibbs and Watts, 1970; Watts et al., 1979; Kopp and Leumann, 1995; Hoppe and Langman, 2003). Only 20 to 30% of patients with PH1 seem to be sensitive to B6-treatments, frequencies which match the prevalence of the common G170R mutation in the Caucasian population (Kopp and Leumann, 1995; Hoppe and Langman, 2003). The response to B6 has long been defined by experts as a minimum decrease of 30 % of urinary oxalate after a therapeutic test of administration of vitamin B6 (pyridoxine hydrochloride) for a maximum time of 3 month at a maximum dose of 20 mg/kg per day (Kopp and Leumann, 1995; Leumann and Hoppe, 2001), although evidence suggests that most responsive patients do so at lower doses (van Woerden et al., 2004; Monico et al., 2005b). The urinary oxalate levels have also been reported as near-completely normalized in some patients under medical treatment with pyridoxine. It has been suggested recently that those patients who are B6-responsive carry the P11L and G170R mutation (van Woerden et al., 2004; Monico et al., 2005a; b). The F152I mutation has also been shown to be associated with B6-sensitivity (van Woerden et al., 2004), but whether B6-response is limited to patients carrying these two mutations or can also be present, albeit at a lower degree, in other patients still remains to be proven (Hoppe et al., 2005). The G170R mutation is associated with significant residual enzymatic activity and the magnitude of the response to B6 treatment may vary between patients with homozygous or heterozygous [P11L, G170R] but no correlation between residual activity and degree of response has been shown so far (Purdue et al., 1990; Monico et al., 2005b; Williams and Rumsby, 2007). The effect of PLP on the stability and dimerization state of some purified recombinant AGT mutants has been studied by several groups, but most of all in studies on pure protein (Santana et al., 2003; Coulter-Mackie and Lian, 2006, 2008; Hopper et al., 2008; Cellini et al., 2009, 2010a; Oppici et al., 2012). Studies have shown by different methods that PLP is able to stabilize AGT encoded by the major allele as well as by the minor allele and may also stabilize some mutants such as AGT-G170R and AGT-G41R (Coulter-Mackie and Lian, 2006, 2008; Hopper et al., 2008). Other studies have shown that the main defect lies in the apoform of the enzyme, which is less stable and thus could be stabilized by the presence of the cofactor (Cellini et al., 2009, 2010a). The potential of pyridoxal phosphate to act as a chaperone for PLP-dependent enzyme has been shown on

tyrosine aminotransferase (TAT) in in vitro studies, although patients do not seem to be B6-responsive (Greengard and Gordon, 1963; Gross-Mesilaty et al., 1997).

How this translates to pyridoxine-responsiveness in PH1 patients remains unclear.

II.4 Rationale for current project

Several questions remain where AGT is concerned. This project is concerned with 3 main questions, which, based on certain hypotheses, lead to 3 main objectives.

1. What is the role of the P11L polymorphism, the N-terminal extensions and can these affect the function and targeting of AGT in cells, *i.e.* does it have a role in addition to generating a MTS and does it mediate proper dimerization?

The acquisition of a correct quaternary structure is linked to the subcellular targeting of AGT. The N-terminal extension and more precisely the residue at position 11, may play a determinant role on the folding of the protein and thus on its final targeting in the cell.

The first objective is therefore to study the relationship between dimerization of AGT, its acquisition of catalytic activity and intracellular targeting in a selection of PH1-specific AGT mutants as well as artificial constructs involving changes in the N-terminal arm in a mammalian cell system.

2. How can vitamin B6 lead to a decrease of oxalate in the urine? Is this accomplished by an increased metabolic effectiveness of remaining AGT? If so, how?

Pyridoxine therapy is effective in reducing oxalate excretion in some patients with PH1, most notably patients with G170R or F152I mutations, both mutations associated with the P11L polymorphism and for which mitochondrial mistargeting has been described or suspected. One or several mechanisms might be involved in the effectiveness of pyridoxine, the active form of which is pyridoxal-5-phosphate, and involve increasing the metabolic effectiveness of AGT. The mechanisms could include: affecting the rate of AGT dimerization, changing the subcellular targeting of AGT, increasing peroxisomal AGT, stabilizing AGT and reducing its degradation or inducing proper folding, thereby prolonging the half-life of AGT, increasing AGT enzyme activity, shifting the balance of apo/holo-enzyme.

The second objective is to investigate the effect of pyridoxine on mutant AGT. More specifically, study the effect of increasing concentration of pyridoxine in cells stably expressing AGT on catalytic activity, protein levels, subcellular targeting and metabolic efficiency.

3. Is there a way to test the metabolic activity of mutated AGT in a cell environment, which would take into account the catalytic activity and the subcellular targeting of AGT?

The previously published indirect glycolate toxicity assay, based on the cell toxicity of glyoxylate, can be used to identify agents that increase the metabolic effectiveness of mutated AGT.

The third objective is to study the metabolic effectiveness of different mutated AGTs in the presence or absence of vitamin B6 using the cell-based indirect toxicity assay

III METHODS

III.1 Plasmids and constructs

III.1.1 Expression constructs

The full-length cDNA of the genes encoding human AGT-MA, AGT-G170R and GO had been previously subcloned into the mammalian expression vector pcDNA3.1 (Invitrogen Ltd., Paisley, UK) (Behnam et al., 2006). For details of the AGT constructs (Fig III.1) see (Knott et al., 2000; Lumb et al., 2003), for the GO (Williams et al., 2000; Williams, E. L., 2003). For other mutant AGTs (AGT-G41R; AGT-F152I), AGT-mi and AGT-anc, constructs had already been made previously in the mammalian vector pHYK and were recloned in the pcDNA3.1 vector by directionally ligating the 1600 bp HindIII/BamHI digested from pHYK into pcDNA3.1 (+) neo (Motley et al., 1995; Oatey et al., 1996). The AGT-244T mutant was created by site directed mutagenesis using newly designed primers and AGT-mi as template (Appendix IX.1) The construct AGT-Δ[1-21] (AGT-Δ), was kindly provided by Dr. Cellini, University of Verona (Montioli et al., 2012). All plasmids were sequenced for verification before use with a combination of internal primers and the T7 forward primer (Appendix IX.2). The properties of constructs (Fig III.1) are shown in (Table III.1) and the correspondences between names and description in (Table III.2).

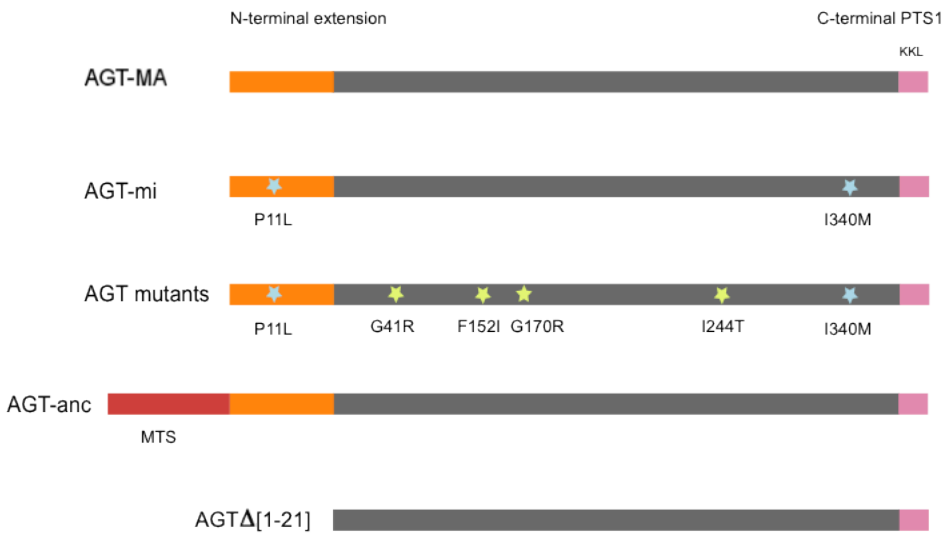

Figure III-1. **Schematic representation of the AGT constructs used in the present study**. The N-terminal arm (amino-acid 1 to 21) is represented in orange, the C-terminal peroxisomal targeting sequence type 1 (KKL) in pink, the ancestral mitochondrial targeting sequence (MTS) is in red. Amino acid changes are represented by stars: Pro11Leu and Ile340Met are in blue and define the minor allele (AGT-mi); the position of mutations is marked by yellow stars (Gly41Arg, Phe152Ile, Gly170Arg, Ile244Thr). For definition of the AGT constructs, see (Tables III.1 & III.2).

Table III-1. **Definition of the AGT constructs used.** (*): The MTS of AGT-anc is the same in sequence as that of New World primates like the marmoset with reconstruction of the more 5' ancestral translation start site lost during primate evolution (Oatey et al., 1996).

Name of the construct (synonym)	Description	Sequence change compared to NM_000030.2	Changes on the protein sequence compared to {Takada 1990}
AGT-MA	Normal human AGT encoded by the "major" *AGXT* allele		
AGT-mi	Normal human AGT encoded by the "minor" *AGXT* allele	c.32C>T; c.1020G>A	P11L, I340M
AGT-anc	Normal human AGT encoded by the "major" *AGXT* allele with additional N-terminal MTS *	c.-63A>G; c.-96-95CC>TT; c.-53T>C (Leu>Leu); CGCCCTGCTG> CAGCCCAAGG	MFQALAKASAAP GSRAAGWVRT- "AGT"
AGT-Δ	human AGT-MA, deletion of the N-terminal amino-acids 1-21		deletion of the N-terminal amino-acids 1-21
AGT-G170R (AGT-170)	human mutant AGT on the background of the minor allele	c.32C>T; c.264C>T; c.348G>A; c.508G>A; c.1020G>A	P11L, G170R, I340M
AGT-F152I (AGT-152)	human mutant AGT on the background of the minor allele	c.32C>T; c.454T>A; c.1020G>A	P11L, F152I, I340M
AGT-I244T (AGT-244)	human mutant AGT on the background of the minor allele	c.32C>T; c.731T>C; c.1020G>A	P11L, I244T, I340M
AGT-G41R (AGT-41)	human mutant AGT on the background of the minor allele	c.32C>T; c.121G>A; c.1020G>A	P11L, G41R, I340M

Table III-2. **Characteristics of the expression constructs used, corresponding vector and cloning sites.** (*): GO is the normal human GO.

Produced protein	Vector	Size of insert	Cloning sites	Antibiotic resistance
GO*	pcDNA3.1 (-) zeo	1180 bp	PstI/BamHI	zeocin
AGT-MA	pcDNA3.1 (+) neo	1600 bp	HindIII/Eco RV	neomycin, G418
AGT-mi	pcDNA3. (+) neo	1600 bp	HindIII/Bam HI	neomycin, G418
AGT-anc	pcDNA3.1 (+) neo	2120 bp	HindIII/Bam HI	neomycin, G418
AGTΔ	pcDNA3.1/V5-His TOPO	1122 bp	TA PCR product cloning	neomycin, G418
AGT-G170R	pcDNA3.1 (+) neo	1600 bp	HindIII/Bam HI	neomycin, G418
AGT-F152I	pcDNA3.1 (+) neo	1600 bp	HindIII/Bam HI	neomycin, G418
AGT-I244T	pcDNA3.1 (+) neo	1600 bp	HindIII/Bam HI	neomycin, G418
AGT-G41R	pcDNA3.1 (+) neo	1600 bp	HindIII/Bam HI	neomycin, G418

III.1.2 Sequencing of plasmids extracted from the stable CHO AGT transformants

Stably transformed cells were lysed (25 mM EDTA, 2% sodium dodecyl sulphate) and the protein precipitated in 10 M ammonium acetate. The DNA was subsequently precipitated with isopropanol, washed with 70% ethanol and resuspended in 10 mM TrisHCl, pH 8, 1 mM EDTA. A first step of amplification of the AGT constructs was performed with internal primers to *AGXT* (Mit1 and TAK1040) (Fig II.2; Appendix IX.2) before being sequenced with nested internal primers (*AGXT*-e2, *AGXT*-e4, *AGXT*-e6, (Fig III.2; Appendix IX.2)).

PCR conditions for sequencing plasmids extracted from stable CHO AGT transformants

step 1: 94° - 02'

step 2: 94° - 10"

step 3: 52° - 30 "

step 4: 68° - 2'

step 5: 10 times [steps 2-4]

step 6: 94° - 10"

step 7: 52° - 30"

step 8: 68° - 2' + 20"/cycle

step 9: 20 times [steps 6-8]

step 10: 68° - 7'

step 11: 4° end

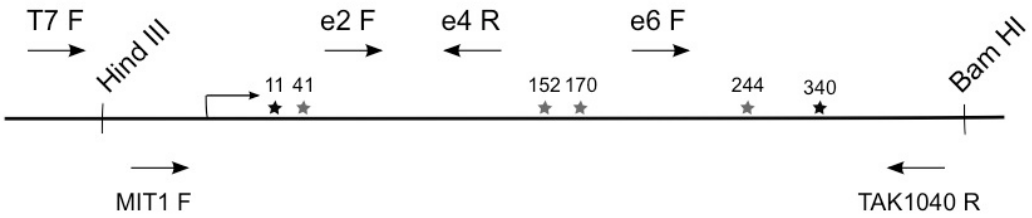

Figure III-2. **Localization of primers on pcDNA AGT.** The cDNA for AGT was cloned between Hind III and Bam HI. The primers used for PCR (MIT1 F and TAK1040R) in the sequencing of the plasmids from the cells are shown in (Appendix IX.2), primers used for sequencing are shown above the line (T7F, *AGXT* e2F, *AGXT* e4R, *AGXT* e6F). For characteristics of the primers, see (Appendix IX.2). Codon changes in the different AGT constructs are shown by stars: 11 = P11L; 41 = G41R; 152 = F152I; 170 = G170R; 244 = I244T; 340 = I340M.

III.2 Cell culture and transformation

III.2.1 Rationale

For stable transformation, Chinese hamster ovary (CHO) cell lines were chosen. This model system had already been published previously for AGT-MA (Behnam et al., 2006). The CHO cells have the characteristic of producing neither AGT, GO nor GR. The cell lines used in this project were re-cloned from the single GO transformed CHO cell line published previously. Therefore all GO and AGT double transformants are expected to express AGT and GO with a similar level of GO. This is required for the indirect glycolate toxicity assay, which requires GO expressing cells. In addition, since GO is a peroxisomal enzyme, antibodies raised against GO provide a useful peroxisomal marker in immunofluorescence experiments.

Tissue culture cell lines derived from hepatocytes were not used, as the endogenous AGT would have interfered with the interpretation of cells transformed with mutated AGT.

III.2.2 Method

Chinese hamster ovary (CHO) cells were cultured in Ham's F12 medium (Invitrogen Ltd.) supplemented with 10% foetal bovine serum (FBS), L-alanyl-L-glutamine (2 mM), penicillin (100 U/ml), streptomycin (100 μg/ml) and the appropriate antibiotic for selection pressure (Table III.2) at 37°C under 5% CO_2. For cells stably expressing GO, Zeocin was added at a concentration of 400 μg/ml for maintenance. For cells stably expressing AGT, G418 was added at a concentration of 800 μg/ml for maintenance (Table III.2). For experiments using COS-1a cells, these were grown in the same conditions as CHO cells, with DMEM (Invitrogen) replacing Ham's F12.

Cells were transfected with pcDNA3.1 plasmids containing the different AGT constructs. For transient transfections, cells were plated at a density of $2x10^4$ cells/well on 13 mm coverslips in 24-well plates. After 24h incubation at 37°C, the cells were transfected using Turbofect (Fermentas) following the manufacturer's instructions. Serum-free, antibiotic-free medium was mixed with 1 μg of DNA, 2 μl of Turbofect to a total volume of 100 μl and incubated at room temperature (22-24°C) for 15 min before adding 900 μl complete medium on cells previously washed with PBS. The transfection mixture was removed after 3-4h incubation and replaced by complete medium. Cells were analysed 24 to 48h later.

For stable transfection, cells were plated at a density of $3x10^6$ cell in 6 cm dishes 24h before transfection and the antibiotic selection for the new plasmid was added 24h after transfection. For the selection of new AGT stable transformants, Geneticin at 1000 μg/ml was used. For the re-cloning of stable GO transformants, Zeocin at 600 μg/ml was used. The cells were subcloned by the limiting dilution technique, 24 to 48h after transfection.

The normal and mutant AGT (AGT-MA, AGT-mi, AGT-G170R, AGT-F152I, AGT-G41R, AGT-I244T) plasmids were extracted from the established cell lines and the insert sequenced for verification (Methods III.1.2). The different cell types used and the appropriate medium and selection are shown in the table below (Table III.3).

All GO and AGT double transformed cell lines were created from one single CHO GO cell line retransformed with AGT in order to keep the levels of GO expression at comparable levels for the cell based toxicity assay.

Table III-3. **Characteristics of the cell lines used**: type of tissue culture cell, expression or GO or AGT, medium and selection antibiotics.

Cell line name	Enzyme expressed by the cell lines	Medium, antibiotics for selection maintenance
COS cells	none	DMEM
CHO wt	none	Ham's F12
CHO GO	GO	Ham's F12, zeocin: 400 µg/ml
CHO GO AGT(x)	GO, AGT (-MA, -mi, -anc, -G41R, -F152I, -G170R, -I244T, -Δ)	Ham's F12, zeocin: 400 µg /ml, G418: 800 µg /ml

III.2.3 Cell culture in varying levels of pyridoxine

In experiments where the effect of pyridoxine was studied on stable cells, the different cell lines were grown for a minimum of 4 weeks in the different conditions, to account for a wash-out period covering the intra-cellular decrease in B6 and the half-life of AGT. Five conditions were chosen (Table III.4).

The "normal" level of B6 was defined as culture in normal Ham's F12 and normal FBS.

For "high" and "very high" levels of B6, normal Ham's F12 and FBS were used and supplemented with pyridoxine hydrochloride solution to a final concentration of 50 µM and 250 µM, respectively.

A pyridoxine hydrochloride (Sigma, MW 205.64) 50 mM stock solution was prepared in PBS and the pH adjusted to 7.4 with NaOH. The solution was then filter sterilized and kept at 4ºC for up to 2 weeks.

For "low" and "no" B6 conditions, a specialty Ham's F12 medium without B6 vitamer was used (Invitrogen). For "low" B6, normal FBS was added and for "no" B6 condition, dialysed FBS was used (cut-off 10,000 MW) (Gibco).

The content in B6 vitamers of FBS is not guaranteed. Measuring the concentration of PLP in normal and dialysed FBS with a standard assay (Chromsystems, GmbH), showed levels of PLP below the level of sensitivity of the assay (<4 nM) with normal levels for human plasma between 15 and 75 nM. Other forms of vitamers are not routinely assayed and are not detected using this assay.

Table III-4. **Levels of pyridoxine in different culture conditions**. PN: pyridoxine, PN HCL: pyridoxine hydrochloride, PLP: pyridoxal-5'-phosphate, FBS: foetal bovine serum.

culture conditions for B6	final [PN]	Medium used	[PN HCl] in medium	FBS used	[PLP] in FBS	PN HCl added (final)
No B6	≈ 0 µmol/l	B6-free Ham's F12	0	dialysed FBS	< 4 nmol/l	0
low B6	< 0.3 µmol/l	B6-free Ham's F12	0	normal FBS	< 4 nmol/l	0
standard B6	≈ 0.3 µmol/l	normal Ham's F12	292 nmol/l	normal FBS	< 4 nmol/l	0
high B6	≈ 50 µmol/l	normal Ham's F12	292 nmol/l	normal FBS	< 4 nmol/l	50 µmol/l
very high B6	≈ 250 µmol/l	normal Ham's F12	292 nmol/l	normal FBS	< 4 nmol/l	250 µmol/l

III.3 Vitamin B6 vitamers measurements.

Cell pellets were harvested by trypsinisation, washed in PBS and freeze-thawed three times before being resuspended in water to 12-25 x10^3 cells/ µl of water. An aliquot of 0.8-1.5x 10^6 cell was mixed with TCA and deuterated B6 vitamin standards (TCA 0.15 N, d_2-PLP 50 nM, d_2-PN 50 nM, d_2-PA 50 nM, d_3-PL 50 nM) and incubated on ice for 1 hour. The supernatant was analysed first by HPLC and then by mass-spectrometry according to the method published by E Footitt (Midttun et al., 2005; Footitt et al., 2012) . Briefly, the B6 vitamers were separated on a reversed-phase column with acetonitrile gradient in a buffer containing acetic acid and heptafluorobutyric acid. The analytes were detected by tandem spectrometry in the positive-ion method. The measurements by HPLC-Tandem Mass Spectrometry was kindly performed by E Footitt at the Institute of Child Health (Clinical and Molecular Genetics Unit, UCL Institute of Child Health, London, UK).

The cell protein content was determined by a Bradford assay and the concentration of the intracellular B6 vitamers measured was expressed per g of cell protein. Only one full assay was performed, with intra-assay duplicates.

III.4 Cell-based indirect glycolate toxicity assay

Cells were plated at a density of 1-3 x10^5 cells in 6 cm round dishes. Glycolate was added after 24h to final concentrations of 0, 125, 250, 500, 750, 1000 to 1500 µM in culture medium and cells were grown under standard conditions, but without antibiotic selection pressure, for 48h before analysis. The toxicity was assessed by comparing the number of cells surviving to that of controls without glycolate. The cell number was counted using a Scepter (Millipore). The size of cells to be counted in experiments with 0 to 1500 µM glycolate or glyoxylate was fixed between 9.675 and 19.05 µm in order to include all cells in the controls while excluding

the peak of dead cells under toxic conditions (Appendix IX.3). The average diameter of CHO cells in normal growth conditions was 12 μm (volume 1 pl). The final cell number was normalised against the control without glycolate for each cell line to account for different growth rate between cell lines.

For experiments on the toxicity of glycolate metabolites (glyoxylate, glycine, oxalate) ranging between 0 and 10 mM (possible repercussions of osmolality on cell size), cells were counted manually with a Haemocytometer.The glycolate stock solution was prepared from glycolic acid (Sigma), buffered to pH 7.4 with sodium hydroxide, filter-sterilised and kept at -20ºC. Glyoxylate solution was prepared from glyoxylic acid (Sigma) in the same way, glycine and oxalate solution were also prepared following the same protocol.

III.5 Antibodies

The antibodies used in the present study are shown in (Table III.5).

The immunolabelling of GO, whether on immunofluorescence microscopy (IMF), immuno electron microscopy (IEM) or immunoblotting (IB), was carried out with polyclonal rabbit anti-human GO (Behnam et al., 2006; Williams, E. L., 2003).

The immunolabelling of peroxisomes in IMF was done with either anti-human GO antibodies or with guinea-pig anti-rat peroxisomes polyclonal antibodies. Briefly, peroxisomes were purified from rat liver and the peroxisome extract was used to raise antisera in guinea-pigs. The raising of the anti rat-peroxisomal proteins antibody was carried out previously, by J Allsop.

The immunolabelling of AGT in IMF, IEM or IB was carried out with either guinea-pig or rabbit anti-human AGT polyclonal antisera (Behnam et al., 2006).

In addition to anti-AGT antisera raised against total AGT, antisera raised against the N-terminus of AGT were used for IMF and IB. The sequence of the first 20 amino-acids characteristic of the major allele (Pro 11) was coupled to keyhole limpet hemocyanin and used to raise rabbit anti-AGT-MA antisera. Similarly, the sequence of the first 20 amino-acids characteristic of the minor allele (Leu 11) was coupled to keyhole limpet hemocyanin and used to raise rabbit anti-AGT-mi antisera. The raising of both anti-AGT-MA and anti AGT-mi antibodies was carried out previously, by J Allsop.

For IB, the anti-human GAPDH polyclonal antibody was purchased from Santa Cruz (#25778).

Table III-5. **Antibodies used in the present study**. Protein or organelle targeted, characteristics and techniques in which the antibodies have been used. GO: glycolate oxidase; AGT: alanine:glyoxylate aminotransferase; GAPDH: glyceraldehyde_3-phosphate_dehydrogenase; IMF: immunofluorescence microscopy; IEM: immuno electron microscopy; IB: immunoblotting. Anti-AGT and anti-peroxisome antibodies were provided by Pr CJ Danpure, UCL, London (c.danpure@ucl.ac.uk). Anti-GO antibodies were provided by Dr G Rumsby, UCLH, London (gill.rumsby@uclh.nhs.uk). Anti-GAPDH were from Santa-Cruz Biotechnology.

target	antibody		use
GO	anti-human GO	(rabbit, polyclonal, serum)	IMF, IEM, IB
peroxisomes	anti-human GO	(rabbit, polyclonal, serum)	IMF, IEM
	anti-rat peroxisome, non-specific	(guinea-pig, polyclonal, serum)	IMF
AGT	anti-human AGT	(rabbit, polyclonal, serum)	IMF, IEM, IB
	anti-human AGT	(guinea-pig, polyclonal serum)	IMF, IEM, IB
	anti-human AGT-MA: AGT-N-terminus Pro11	(rabbit, polyclonal, serum)	IMF, IB
	anti-human AGT-mi: AGT-N-terminus Leu11	(rabbit, polyclonal, serum)	IMF, IB
GAPDH	anti-human GAPDH (Santa Cruz #25778)	(rabbit IgG, polyclonal)	IB

III.6 Immunofluorescence

III.6.1 Immunofluorescence microscopy

Cells on 13 mm glass coverslips were lightly fixed in 4% w/v paraformaldehyde or formaldehyde for 15 minutes at room temperature before permeabilization with 0.3% Triton X-100 in phosphate buffered saline (PBS) and 3% bovine serum albumin (BSA) for 15 minutes followed by labelling. All incubations were performed at room temperature for 1-2 hour or overnight at 4ºC, and antibodies diluted in PBS plus 3% BSA. For primary antibodies, various combinations of guinea-pig polyclonal anti-peroxisomes, rabbit or guinea-pig polyclonal anti-human AGT, rabbit polyclonal anti-human GO were used (Behnam et al., 2006). For mitochondrial staining, a vital stain, Mitotracker (Red CMXRos version, Molecular Probes, Invitrogen Ltd) was used prior to fixation following the manufacturer's instructions. Nuclei were stained with Hoechst 33258 after fixing and the coverslips mounted over slides in Citifluor AF1 mounting medium (Citifluor). The fluorescence images were captured sequentially using a confocal laser-scanning fluorescence microscope (Leica TCS SPE) with a 40x or 63x oil immersion lens (apochromat, NA: 1.33). The focal z-step was kept between 200 and 300 nm.

For imaging, cells with abnormal nuclei (fragmented or multi-nucleated cells) and giant CHO cells were excluded, along with cells non expressing AGT or GO. For colocalization analysis, non-overlapping cells in monolayers were selected and a total of 10 to 20 cells between different experiments were imaged.

III.6.2 Image analysis

Images were processed using ImageJ software or Fiji (ImageJ, Fiji Is Just ImageJ) , and Adobe Photoshop. A shift between green and red channel was regularly observed and imputable to the system. When necessary, the correction of registration was based on beads (Appendices IX.4 & IX.5) and calculated using the TransformJ/Translate plugin in ImageJ developed by E Meijering using the following settings on the green channel: {x: -1.7; y: +1; z: 0; interpolation: quantic B spline} (Appendix IX.4) and {x: -1.5; y: 0; z: 0; interpolation: quantic B spline} for the far red channel (Appendix IX.5) (TransformJ). A registration correction was performed when a shift was observed and corrected with these settings, on the control AGT-MA. For colocalization analysis, the exposure settings and gain of laser were kept fixed during the experiment. Colocalization visualization was performed by dye-overlay method, merging the channels involved, and displayed in figures as either magenta/green/blue or red/green/blue/grey combinations (Fig III.3 & III.4).

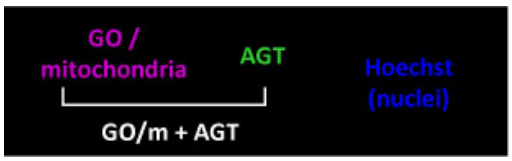

Figure III-3. **False-colour combination on three-channel immunofluorescence pictures.** The peroxisomal or mitochondrial marker is displayed in magenta, AGT in green and Hoechst-stained nuclei are displayed in blue. In this combination, the colocalization of AGT and the other marker is shown as white.

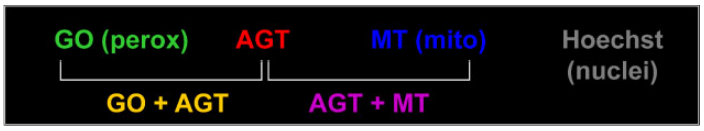

Figure III-4. **False-colour combination on four-channel immunofluorescence pictures**. The peroxisomal marker is displayed in green, AGT in red, Mitotracker is displayed in blue and the Hoechst-stained nuclei are displayed in grey. In this combination, colocalization of AGT and peroxisomal marker is shown as yellow, and colocalization of AGT and mitochondria as magenta.

The colocalization was analysed on stacks by cytofluorograms and Li's ICA graphs as well as Mander's and Pearson's colocalization coefficients (Manders et al., 1992) (Table III.6) through the ImageJ JACoP plugin developed by Bolte and Cordelieres (Bolte and Cordelières, 2006) (JACoP). Throughout this work, Manders' colocalization coefficient M(mitochondria) is the coefficient for mitochondria in the channel in which AGT is stained; M(GO) or M(Perox) is the coefficient for GO, or peroxisomes in the channel in which AGT is stained. M(AGT) designates the coefficient for AGT in the other channel staining either for GO, peroxisome or mitochondria.

Table III-6. **Formula for Pearson's and Manders' colocalization analyses**. A_i:channel A intensity of voxel i; a: mean voxel intensity in channel A; B_i: channel B intensity of voxel i; b: mean voxel intensity in channel B; A_{icoloc}: channel A intensity of colocalized voxel i; B_{icoloc}: channel A intensity of colocalized voxel i.

Colocalisation method	Formula		
Pearson's coefficient	$(r) = \Sigma_i (A_i - a)(B_i - b) / \sqrt{[\Sigma_i (A_i - a)^2 \times \Sigma_i (B_i - b)^2]}$		
Manders' coefficients	$M1 = \Sigma_i A_{i\,coloc} / \Sigma_i A_i$	where	$A_{i\,coloc} = A_i$ if $B_i > 0$
		or	$A_{i\,coloc} = 0$ if $B_i = 0$
	$M2 = \Sigma_i B_{i\,coloc} / \Sigma_i B_i$	where	$B_{i\,coloc} = B_i$ if $A_i > 0$
		or	$B_{i\,coloc} = 0$ if $A_i = 0$

III.7 Electron microscopy and immunoelectron microscopy

For transmission electron microscopy, cells were fixed by suspension in 1.5% glutaraldehyde, post-fixed in 1% osmium tetroxide, and dehydrated with increasing concentrations of ethanol. Finally the pellets were embedded in Lemix (TAAB) epoxy resin. Ultrathin sections (100 nm) were cut and collected on copper grids and stained with uranyl acetate and lead citrate.

For the colloidal gold immuno-electron microscopy, cells were fixed in a mixture of 1% paraformaldehyde and 1.5% glutaraldehyde, dehydrated in increasing concentrations of ethanol, and embedded in LRWhite resin. Ultrathin sections (70-90 nm) sections were incubated with rabbit anti-human AGT and anti-GO antisera and then colloidal gold (10 or 20 nm) conjugated to anti-rabbit IgG. Finally the sections were stained with uranyl acetate and lead citrate. All the electron- and immunoelectron- microscopy and photography was kindly performed by Jackie Lewin (EM Unit, Royal Free and University College Medical School, London NW3 2PF).

III.8 Catalytic activity

The catalytic activities of AGT and GO were measured spectrophotometrically as have been reported elsewhere (Rumsby et al., 1997; Williams et al., 2000; Williams, E. L., 2003). For catalytic activities, the cells were harvested and sonicated in buffer (sucrose 240 mM, potassium phosphate 0.1 M; pH 8.0).

III.8.1 AGT assay

The AGT activity was measured on cell sonicates, by the detection of the pyruvate formed with alanine (150 mM) and glyoxylate (10 mM) as substrate in the presence of 150 µM PLP, in potassium phosphate buffer (0.1 M), pH 8.0 (Fig III.5). The incubation time was 60 min at 37ºC. The reaction was stopped by the addition of trichloroacetic acid (7% final). The amount of pyruvate formed was indirectly estimated via the reduction in NADH absorbance at 340 nm occurring by a secondary reaction: pyruvate reduction to lactate catalysed by LDH (16 UI/ml) in the presence of NADH (0.25 mM), the other potential contaminating substrate of LDH, glyoxylate, being complexed with TrisHCl (0.5 M), pH 8.0. For assays done without B6 (Fig III.6), PLP was omitted from the reaction and replaced with buffer in the first reaction, and the assay performed in the same conditions (Fig III.6). The limit of detection of the assay is 2 µmol /h/mg of protein (3 µmol /h/mg of protein for the assay in the absence of PLP) (Table III.7).

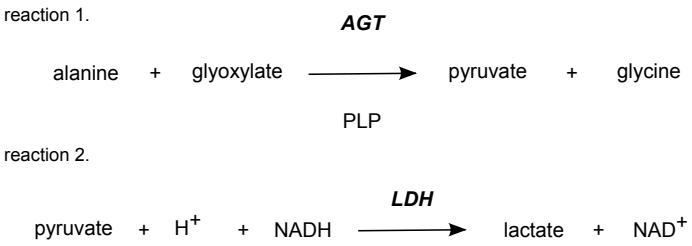

Figure III-5. **Catalytic reactions used in the AGT assay.** AGT: alanine:glyoxylate aminotransferase; PLP: pyridoxal-5'-phosphate; NADH/NAD: nicotinamide adenine dinucleotide.

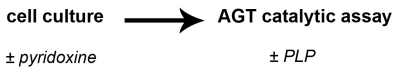

Figure III-6. **Vitamin B6 in culture and AGT catalytic assay**. Transformed CHO cells were grown in different pyridoxine concentrations (0 to 250 µmol/l), and prepared for the AGT catalytic assay. For AGT assay with vitamin B6, PLP was added to the reaction mix (150 µmol/l, final concentration in the reaction) or replaced with buffer.

Table III-7. **Limit of detection for the AGT assay in CHO cells**. Determined on CHO WT cells and CHO cells transformed with GO grown in 0.3 µmol/l of pyridoxine, with or without PLP during the assay. SD: standard deviation.

AGT assay (B6: 0.3 uM)		mean	SD	mean +3SD
µmol pyruvate/h/mg protein	+PLP (n=25)	0.54	0.46	1.93
	-PLP (n=12)	0.86	0.64	2.77

III.8.2 GO assay

For GO activity, cell sonicates were dialysed overnight against phosphate buffer (KH_2PO_4 0.05 M; pH7.0; EDTA 0.1 mM). GO activity was measured indirectly, by measuring the production of H_2O_2 which accompanies the oxidation of glycolate (5 mmol/l) into glyoxylate, in a secondary concomitant reaction (Fig III.7). In the presence of horseradish peroxidase the H_2O_2 formed couples oxidatively sulphonated 2,4-dichlorophenolindophenol (DCIP, 0.1 mM) and 4-aminophenazone and yields a soluble quinoneimine dye (Trinder reaction). The amount of dye produced is monitored by the change in absorbance at 515 nm. The limit of detection of the assay is 4 nmol substrate transformed/min/mg protein (Table III.8).

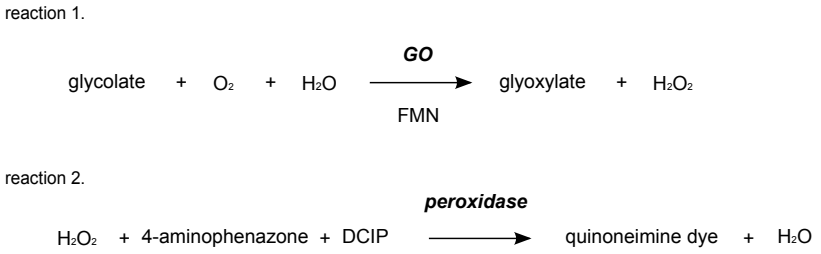

Figure III-7. **Catalytic reactions used in the GO assay**. GO: glycolate oxidase, FMN: flavin mononucleotide, DCIP: 2,6-dichlorophenolindophenol.

Table III-8. **Limit of detection for the GO assay in CHO cells**. Determined on CHO WT cells (n=18). SD: standard deviation.

GO assay (n=18)	mean	SD	mean +3SD
(nmol/min/mg protein)	0.61	0.86	3.19

III.9 Western blotting

Cells were resuspended in lysis buffer (1% v/v Triton X100, 3mM EDTA, protease inhibitor cocktail (Roche) in PBS) and frozen on dry ice before thawing out at 37°, followed by 4 cycles of sonication (Bioruptor, Diagenode) with a medium output. Protein concentration was determined on sonicates using the Bradford Reagent kit (Sigma-Aldrich). Aliquots of 2-5 µg of cell protein were loaded into each lane of precast Bis-Tris 10 % NuPAGE gels (Invitrogen Ltd). The samples were prepared with NuPAGE LDS loading Buffer (106 mM tris HCl, 141 mM Tris base, 2% LDS, 10% glycerol, 0.51 mM EDTA, 0.22 mM SERVA Blue G250, 0.175 mM phenol red, pH 8.5), NuPAGE reducing agent (dithiotreitiol 500 mM) and heated at 70 ºC for 10

min. The samples were run with NupAGE anti-oxidant (proprietary reagent) in NupAGE MOPS SDS buffer at 180-200 V for 1 to 1h30.

After wet transfer onto a Westran PVDF membrane (Whatman) in Tris-Glycine buffer (25 mM Tris HCl, 52 mM glycine), the membranes were blocked in 5 % non-fat dry milk in TBS-T (154 mM NaCl, 15 mM Tris HCl, pH 7.5, 0.5 % Tween 20) and incubated with polyclonal rabbit or guinea-pig primary anti human AGT or human GO antisera (dilution 1/5000) (Purdue et al., 1990; Behnam et al., 2006), secondary antibodies were the appropriate peroxidase conjugated goat anti IgG (dilution 1/10000). The signal was detected using an EZ-ECL chemiluminescence kit (Biological Industries) and either recorded by exposure to film (Hyperfilm ECL, Amersham) or to a camera (ImageQuant LAS 4000 mini, GE Healthcare).

III.10 Densitometry analysis

For densitometry analysis of western blots, films were exposed to the membranes without saturation and scanned at high resolution. Alternatively, the ECL signal was recorded from the membrane with a Camera (ImageQuant LAS 4000). The non-compressed digital file was analysed using the measure tool in ImageJ (ImageJ). Measurements were taken for bands in each lane in a fixed size area. A background measurement of the same area size was recorded above and below each band and subtracted from the measured band to give a corrected densitometry. Results were expressed relative to the densitometry of AGT-MA in each gel analysed. For autoradiography, films were treated as for western blots and scanned before analysis.

III.11 Chemical cross-linking

Cross-linking was performed with either bis(sulfosuccinimidyl)suberate (BS_3; Pierce), bis-N-succinimidyl-(pentaethylene glycol)ester, $BS(PEG)_5$, Succinimidyl-[(N-maleimidopropionamido)-diethyleneglycol] ester ($SM(PEG)_2$) or Bis(maleimido)ethane (BMOE) (all, Pierce) (Fig III.8, Table III.9). Cells were harvested as above, by trypsinization, rinsed twice in cold PBS buffer and resuspended in 0.5 ml cold cross-linking buffer (PBS pH 7.2, protease inhibitor cocktail (Roche)). The cells were lysed as described above. Protein concentration was determined with the Bradford reagent kit and the cell lysate (0.25 mg/ml total protein concentration) was incubated with cross-linkers at concentrations of 30 to 1250 μM of BS_3 or $BS(PEG)_5$, at room temperature for 30 minutes. Samples were then quenched in Tris-HCl, pH 7.5, 20 mM for 20 minutes at room temperature. Samples of 1.7 μg cell protein were then loaded per lane on a SDS-PAGE gel and western blotted as described above.

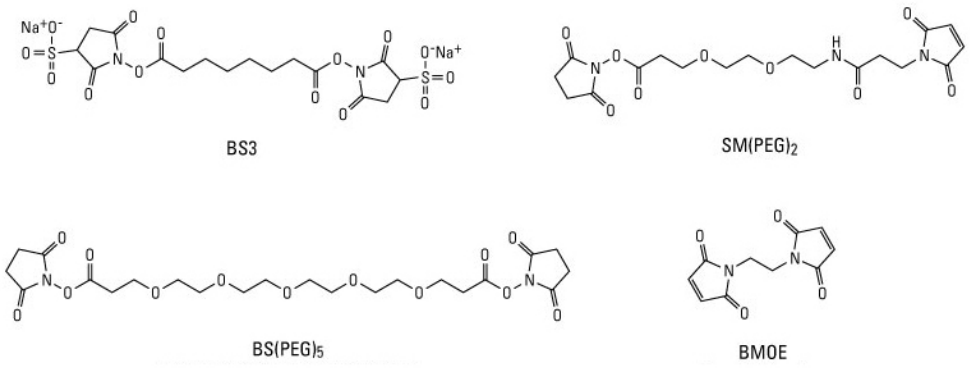

Figure III-8. **Cross-linkers used for AGT and GO cross-linking**.
BS3: bis(sulfosuccinimidyl)suberate; BS(PEG)5: bis-N-succinimidyl-(pentaethylene glycol)ester; SM(PEG)2: Succinimidyl-[(N-maleimidopropionamido)-diethyleneglycol] ester; BMOE: : Bis(maleimido)ethane.

Table III-9. **Characteristics of the cross-linkers used**.
BS3: bis(sulfosuccinimidyl)suberate; BS(PEG)5: bis-N-succinimidyl-(pentaethylene glycol)ester; SM(PEG)2: Succinimidyl-[(N-maleimidopropionamido)-diethyleneglycol] ester; BMOE: : Bis(maleimido)ethane.

	BS3	SM(PEG)2	BS(PEG)5	BMOE
chemical name	Bis(sulfosuccinimidyl)suberate	Succinimidyl-[(N-maleimidopropionamido)-diethyleneglycol] ester	Bis-N-succinimidyl-(pentaethylene glycol) ester	Bis(maleimido)ethane
alternative names	sulfo-DSS	NHS-PEG2-Maliemide	Bis(NHS)PEG5	
Molecular weight	572.43	425.39	532.5	220.18
spacer arm	11.4 Å	17.6 Å	21.7 Å	8.0 Å
	homobifunctional	heterobifunctional	homobifunctional	homobifunctional
reactive towards	-NH2	-NH2 -SH	-NH2	-SH

III.12 Immunoprecipitation

Immunoprecipitation was performed using columns prepared with agarose beads cross-linked with polyclonal rabbit anti human AGT IgG (Cross-link Immunoprecipitation Kit, Pierce), following the manufacturer's instructions.

Cells were lysed with lysis buffer (0.025 M TrisHCl, 0.15 M NaCl, 0.001 M EDTA, 1% NP-40, 5% glycerol, pH 7.4, Pierce) supplemented with protease inhibitor (Protease Inhibitor Cocktail, Roche). The cell lysate was centrifuged for 10 minutes at 13 000g, except for radiolabelled samples which were directly incubated on the columns, without preclearing. For non-radiolabelled samples, the supernatant incubated at 4ºC for 1h with control resin in order to preclear the lysate. The supernatant was then incubated overnight at 4ºC with rotation, on the

prepared columns. AGT was eluted with Pierce elution buffer (pH 2.8) and the samples analysed on SDS-PAGE gels followed by western blotting or autoradiography if pulse-chase was performed.

III.13 Pulse-chase

CHO cells were starved for 20 min in DMEM without cysteine/methionine (Sigma) supplemented with 10% FBS and L-glutamine (2 mM). Cells were pulse-labelled for 20 min with ^{35}S-methionine and cysteine (50 μCi/dish, Easytag ™ Express protein Labeling Mix, Perkin Elmer) and chased in normal Ham's F12 medium supplemented with 5 mM methionine and cysteine for different chasing times ranging from 0 to 72 hours for determination of the half-life of AGT. AGT was immunoprecipitated from the radiolabeled lysate as above, without preclearing or centrifugation, using polyclonal rabbit anti-AGT prepared columns. The samples were analysed on SDS-PAGE gels, stained for protein using Bluestain (Pierce), dried and exposed to film (Hyperfilm MP, Amersham) for autoradiography or treated for western blotting as above.

To determine protein half-lives, the intensities of the AGT band was measured by densitometry (Methods III.10) using Image J. The decay of radio-labelled protein was assumed to follow the equation:

$$P(t) = P_0 e^{-\alpha.t}$$

Where P_0 is the protein intensity at time t = 0. The degradation rate, α, was calculated after applying a linear regression in Excel (Microsoft) to the following equation:

$$\ln(P(t)) = \ln(P_0) - \alpha.t$$

IV RESULTS part 1: Role of the N-terminal extension and amino acid changes on AGT

IV.1 Introduction

The mutation the most studied in PH1 is the G170R change in AGT, which co-segregates with the minor allele of AGT (*i.e.* AGT containing P11L and I340M polymorphisms). This mutation has been shown to lead to a change in the subcellular distribution of AGT in human liver, from the peroxisomes to the mitochondria (Danpure et al., 1989). Since the ancestral MTS present in some species with mitochondrial AGT is lost in humans, this retargeting of an AGT variant with near normal catalytic activity in vitro has raised a number of questions on the role of the N-terminus of AGT and the P11L polymorphism, as well as the interaction between this polymorphism and the mutation (Danpure, 1993; Lumb and Danpure, 2000; Williams and Rumsby, 2007).

Published studies on purified recombinant AGT as well as transient transfection in COS cells have shown that the P11L replacement generates a functionally weak MTS in AGT. The P11L-generated MTS is not intrinsically weak as it has been shown to target monomeric GFP to mitochondria but is less efficient in AGT on its own as it cannot prevent AGT from acquiring rapidly a conformation incompatible with mitochondrial import (unfolded monomer) (Purdue et al., 1991a; Leiper et al., 1996; Lumb et al., 1999). It has been suggested that the enhancing of the functional efficiency of the polymorphic MTS by the G170R mutation was due to a change in the molecular environment of AGT. This new environment would allow the polymorphic MTS to fold more efficiently into an α-helix, retarding the folding and/or dimerization of AGT (normally rapid) and thereby increasing the efficiency of the polymorphic MTS (Leiper et al., 1996; Lumb et al., 1999). An artificial construct which replaces both the proline in position 11 by a leucine and the proline in position 10 by a leucine, was predicted to form an α-helix more easily than the P11L alone and was shown to be able to target AGT to mitochondria without additional mutation (Lumb et al., 1999). This same artificial AGT variant, AGT-P10L, P11L was also shown to be unable to dimerize in in vitro translation experiments, like the variant with both P11L and G170R change and unlike the P11L alone (Lumb et al., 1999). Conversely, stabilizing the mutant AGT-170 by lowering the temperature in transiently transfected COS cells was shown to result in peroxisomal targeting (Lumb et al., 2003). The synergistic effect of the P11L polymorphism and AGT mutation was shown not only for AGT-170 but also for other AGT variants on studies in purified recombinant AGT (Lumb and Danpure, 2000). Four AGT mutants, AGT-170, AGT-152, AGT-244 and AGT-41, were shown to have less deleterious consequences (in terms of catalytic activity and stability) in the absence of the P11L

polymorphism. Such consequences might be expected to result more generally into a mitochondrial mistargeting in mutants on the minor allele of AGT, which had only been suggested for the F152I mutation in addition to the G170R in patients (Danpure et al., 1993). However, immunoelectron microscopy of PH1 patients' liver is rare and so far suggested that both AGT-41 and AGT-244 would be peroxisomal (Table IV.1).

In order to understand the effects of these mutations on the properties of AGT and to try to understand the importance of the N-terminus and the P11L change, CHO cells have been stably transformed with AGT variants and the intra-cellular distribution, oligomeric state and catalytic activity of these variants have been studied.

Table IV-1. **Known characteristics of the AGT constructs used in the present work.** The intracellular distribution relies on IEM studies in human liver except for (*) which relies on IEM in marmoset liver and in IMF studies for transfected COS. (**):extrapolation from compound heterozygotes and heterozygotes (Danpure et al., 1993); (***), IEM on one patient (personal communication, P Cochat, University of Lyon, France); (-): not known. P: peroxisomal targeting, M: mitochondrial targeting. (m) or (p) denote a minor distribution. (Danpure, 1993; Danpure et al., 1993; Lumb et al., 1999; Lumb and Danpure, 2000; Santana et al., 2003; van Woerden et al., 2004; Coulter-Mackie et al., 2005; Monico et al., 2005a; Cellini et al., 2007; Williams and Rumsby, 2007; Cellini et al., 2009, 2010b; Harambat et al., 2010).

AGT construct		enzyme activity		targeting		treatment in PH1 patients
		recombinant protein	human liver	in cells (transient in COS)	in liver	
AGT-MA	normal	100%	100%	P	P	
AGT-mi		45-100%	90%	P	P (m)	
AGT-anc	artificial constructs	–	–	M (p)	M + P *	
AGT-Δ		–	–	–	–	
AGT-G170R	natural occuring mutants *(on AGT-mi background)*	<10-76%	10-72%	M (p)	M (p)	B6 responsive
AGT-F152I		<10-80%	0-16%	–	M **	
AGT-I244T		<10-26%	0-36%	P	P***	
AGT-G41R		<10-24%	0%	–	P **	

IV.2 Subcellular targeting of the AGT variants in mammalian cells

IV.2.1 Stable transfection in CHO cells

In order to study the subcellular distribution of AGT in mammalian cells, AGT was transformed in mammalian tissue culture cells as previously described (Behnam et al., 2006). Both transient transfection and stable transfection were used in CHO cells and only transient transfection in COS cells. Since expression levels and catalytic activities required high and reproduceable levels of expression, stable cell lines were created in CHO cells, following the methods of Behnam *et al.* (Behnam et al., 2006).

The cell line in which all AGT variants were transformed was the same CHO GO cell line published in (Behnam et al., 2006). The expression of GO was required for the metabolic assay (see VI Results part 3) and was used as a peroxisomal marker as its expression was both peroxisome-specific and high.

In more simple labelling (nuclei, AGT and peroxisomes), anti-AGT and anti-GO antibodies were used. For more complex labelling (mitochondria, nuclei, AGT, peroxisomes), a combination of MitoTracker, anti-AGT and anti-rat peroxisomal proteins was used for double transformants and CHO WT cells

IV.2.1.1 CHO GO and WT

IV.2.1.1.1 IMF of CHO WT and CHO GO

The staining for mitochondria and peroxisomes was checked on CHO WT and CHO GO cells. In CHO WT cells the co-localization analysis performed showed parameters characteristic of exclusion between peroxisomes and mitochondria as expected (Fig IV.1). The peroxisomal antibody (polyclonal anti rat-peroxisomal membrane or anti-peroxisomal proteins) showed some background cytosolic staining in addition to the peroxisomal staining.

In CHO GO cells, the GO was shown to be peroxisomal and there was no background due to the AGT antibody (Fig IV.2 & IV.3). Background cytosolic staining for GO was variable.

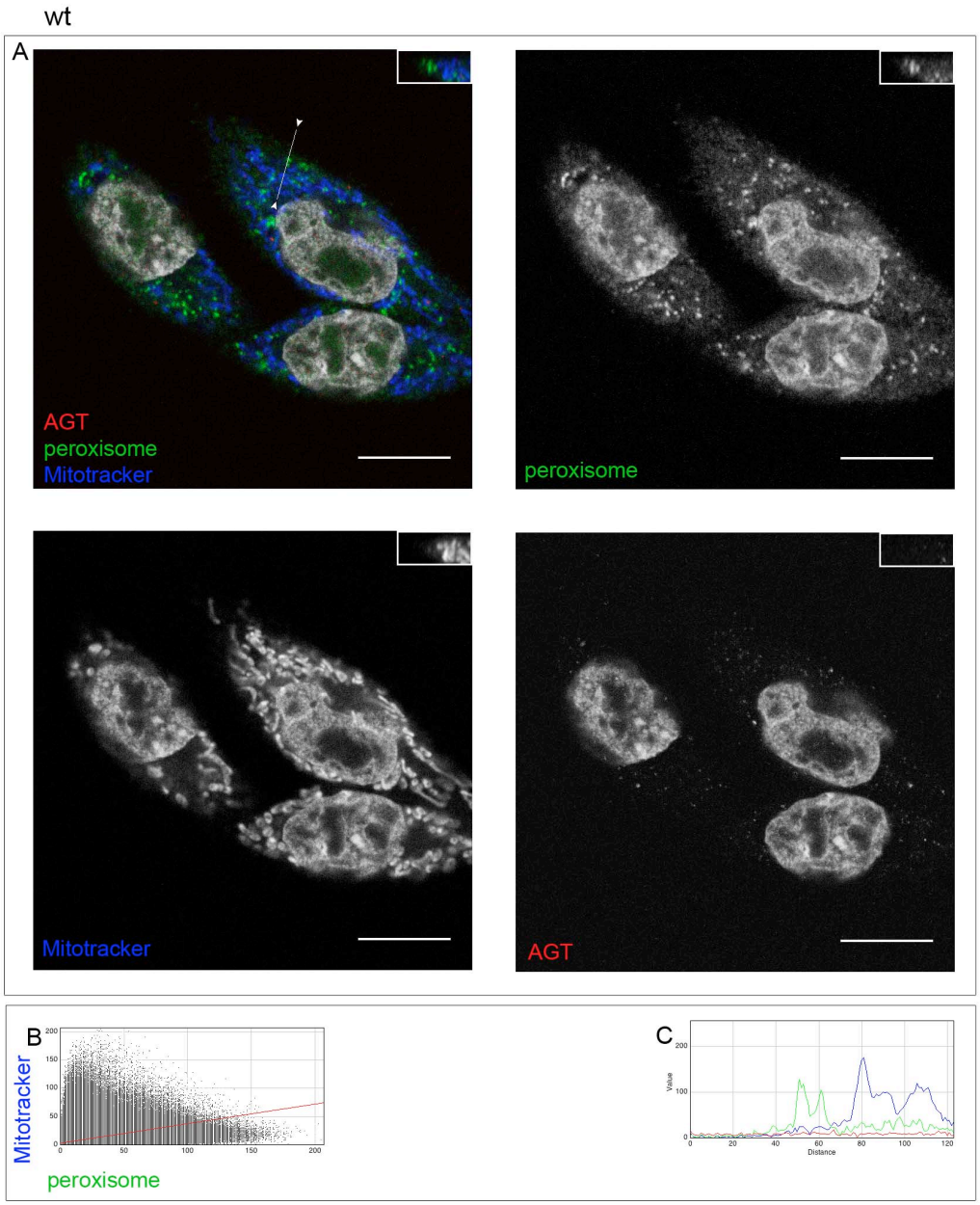

Figure IV-1. **Subcellular organelles staining in CHO WT as shown by immunofluorescence microscopy.** A: CHO WT were cultured in standard conditions (see Methods III.2), stained with anti AGT (red), anti peroxisomes (green), MitoTracker (blue). Nuclei stained with Hoechst (grey). Scale bar : 10 µm. Merged and single channel images from a single z-plane (A). Insert: reslice along the z-axis along the line drawn in the merged image in (A). B: scatter plot showing MitoTracker (y-axis) and peroxisomes (x-axis). C: RGB profile plotted along the line drawn in merged image. Colocalization coefficients for the couple mitochondria/ peroxisomes: Pearson's coefficient 0.488, Manders' coefficient (thresholded): M1 (mitochondria): 0.037, M2 (peroxisomes): 0.270.

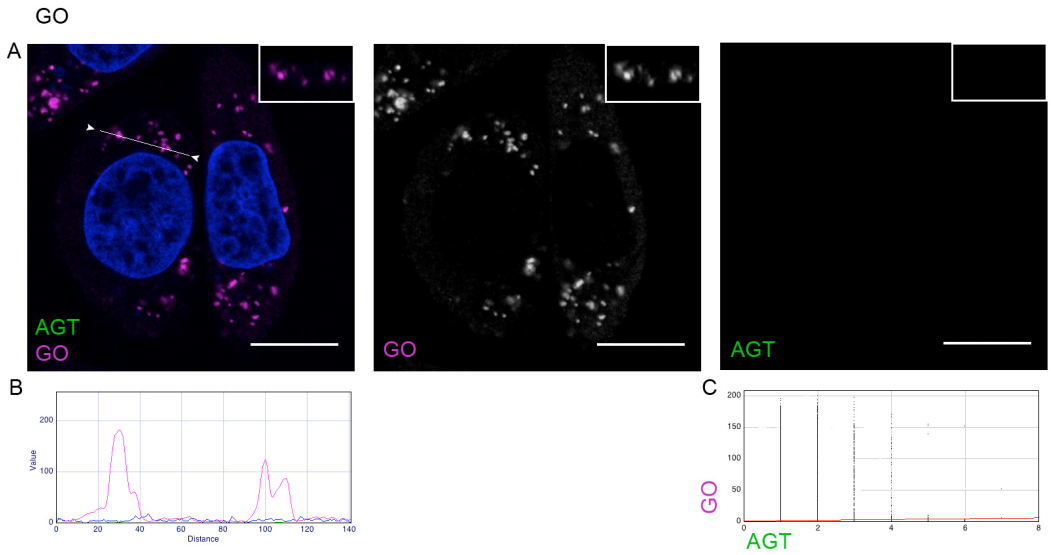

Figure IV-2. **Characteristics of CHO GO cells as shown by immunofluorescence microscopy.** CHO GO cells were cultured in standard conditions (see Methods III.2), stained with anti AGT (green), anti GO (magenta), Hoechst (blue). Merged and single channel images from a single z-plane are shown in (A). Insert: reslice along the z-axis along the line drawn in the merged image (A). The RGB profile (B) is plotted along the line drawn in the merged image, the scatter plot (C)shows AGT (x-axis) and GO (y-axis). Scale bar: 10 µm. Pearson's coefficient 0.057, Manders' coefficient (thresholded): M1 (AGT): 0.243, M2 (GO): 0.001.

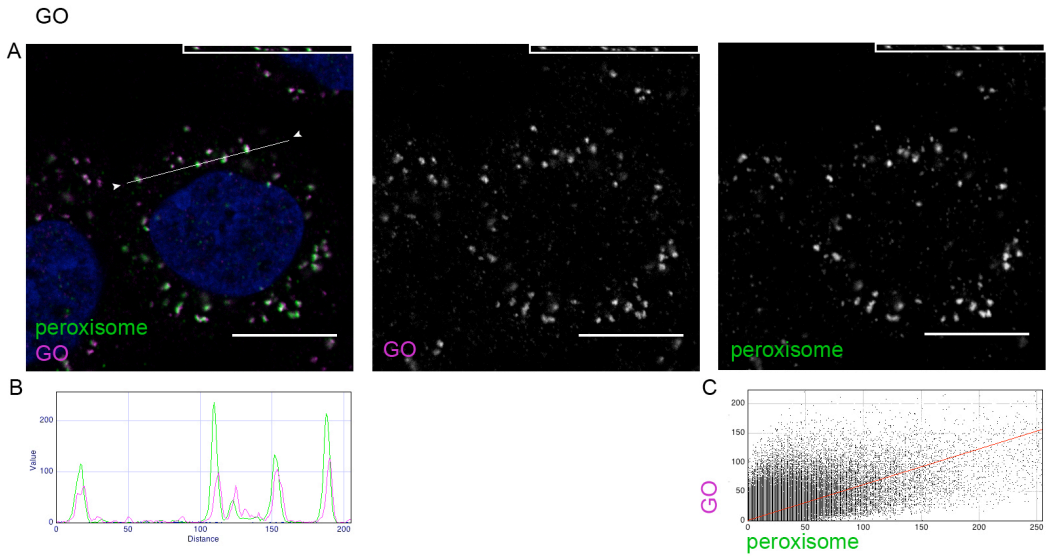

Figure IV-3. **Subcellular distribution of GO as shown by immunofluorescence microscopy.** CHO GO cells were cultured in standard conditions (see Methods III.2), stained with anti peroxisome (green), anti GO (magenta), Hoechst (blue). Merged and single channel images from a single z-plane are shown in (A). Insert: reslice along the z-axis along the line drawn in the merged image (A). The RGB profile (B) is plotted along the line drawn in the merged image, the scatter plot (C)shows peroxisomes (x-axis) and GO (y-axis). Scale bar: 10 µm. Pearson's coefficient 0.687, Manders' coefficient (thresholded): M1 (peroxisomes): 0.777, M2 (GO): 0.454.

IV.2.1.1.2 EM of CHO WT and CHO GO

The IEM study of CHO WT showed an absence of staining for either AGT or GO antibodies. The structure of peroxisomes or mitochondria was unremarkable (Fig IV.4).

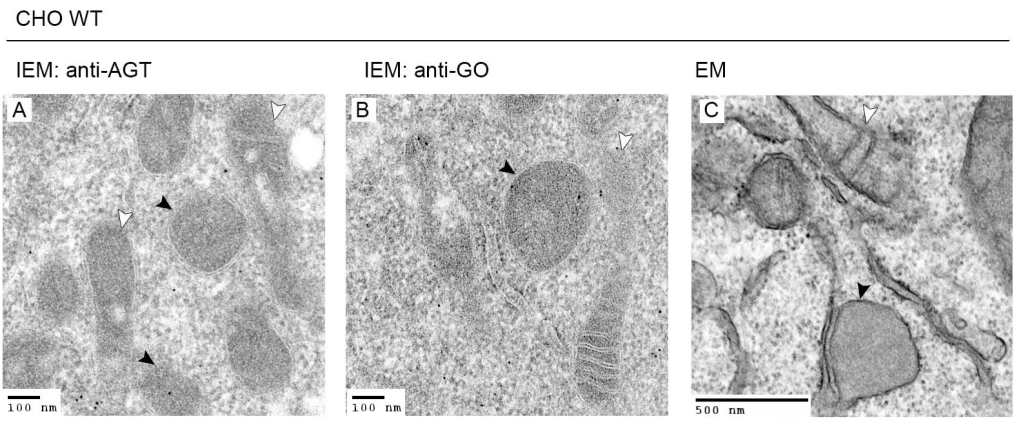

Figure IV-4. **Subcellular structures in CHO WT cells, as shown by electron microscopy**. A: immuno-electron microscopy, staining with anti-AGT (10 nm gold particles); B: immuno-electron microscopy, staining with anti-GO (10 nm gold particles); C: transmission electron microscopy. Black arrowheads: peroxisomes, white arrowheads: mitochondria (electron microscopy kindly carried out by J Lewin, see Methods III.7).

In CHO GO cells, GO staining localized to peroxisomes (single membrane organelles) and not mitochondria (double membrane organelles). A few peroxisomes contained a small dense structure staining with GO (Fig IV.5).

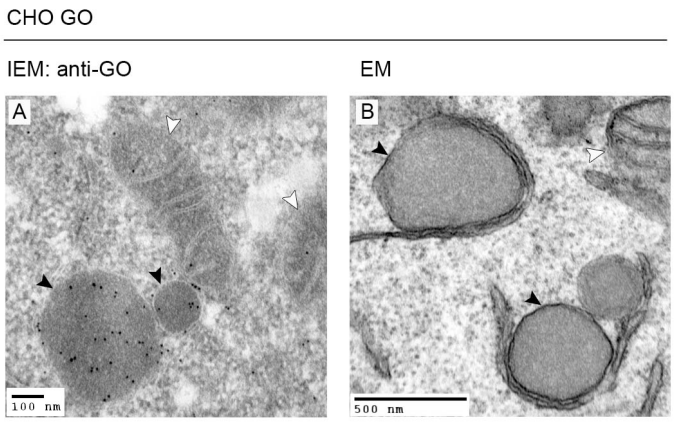

Figure IV-5. **Subcellular distribution of GO in CHO GO cells as shown by electron microscopy**. A: immuno-electron microscopy, staining with anti-GO (10 nm gold particles); B: transmission electron microscopy. Black arrowheads: peroxisomes, white arrowheads: mitochondria (electron microscopy kindly carried out by J Lewin, see Methods III.7).

IV.2.1.2 Homogeneity of expression in the stably transformed CHO cell lines

The CHO cell lines were re-cloned to obtain cell lines, which expressed GO and AGT almost completely homogenously (Fig IV.6). The fraction of cells expressing AGT or GO was kept above 90% for studies on stable CHO cells.

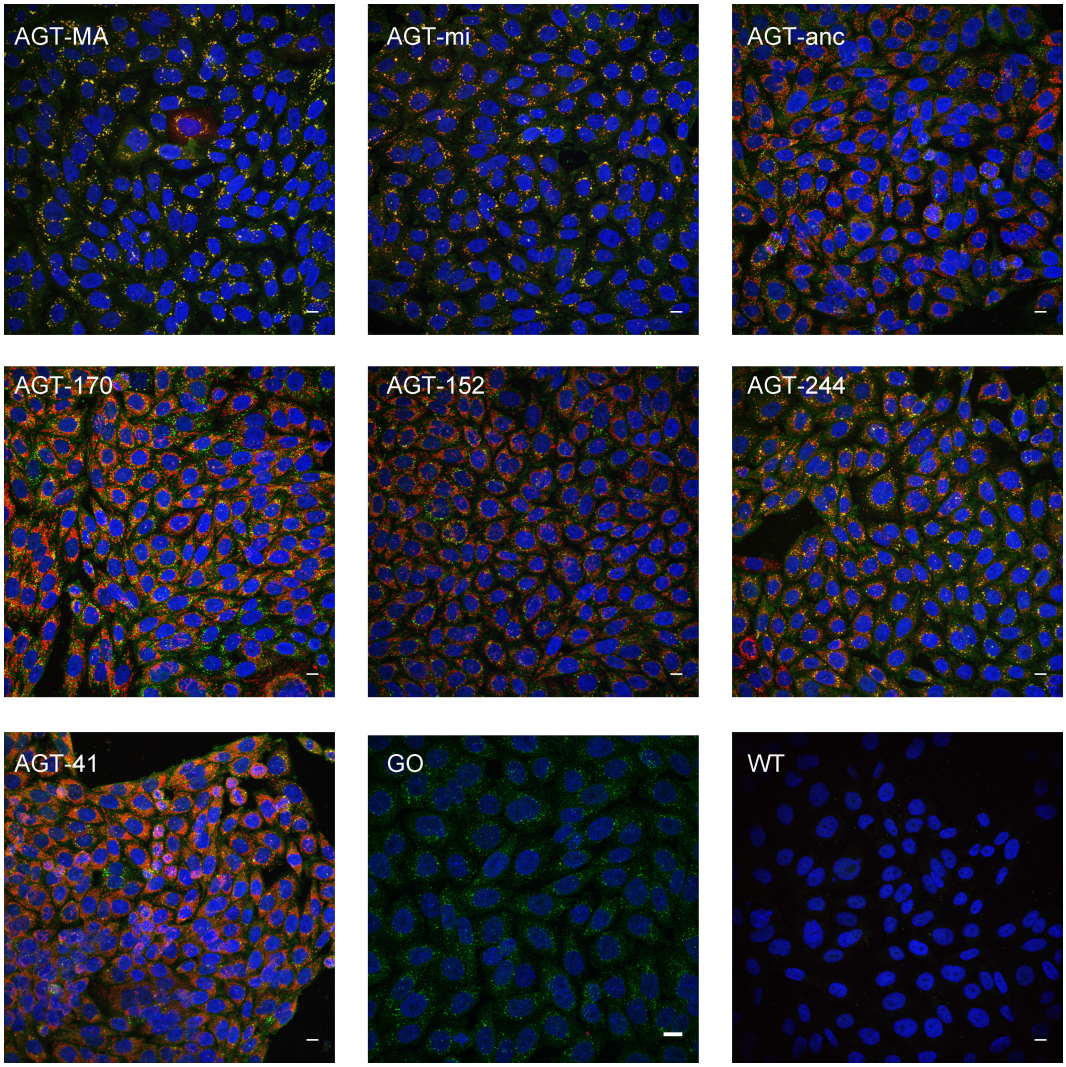

Figure IV-6. **Homogeneity of expression of AGT and GO in the stably transformed CHO cell lines as shown by immunofluorescence microscopy.** CHO GO AGT(x)- cells in standard culture conditions, stained with anti AGT (magenta), anti GO (green), Hoechst (blue). Magnification: objective 40X. Scale bar: 10 µm.

IV.2.1.3 AGT-MA

IV.2.1.3.1 IMF of CHO GO AGT-MA

As has been previously reported in human liver and transiently transfected COS cells, AGT-MA in stably transformed CHO cells is peroxisomal and co-localizes with the peroxisomal enzyme GO as is shown on the single z-plane in (Fig IV.7) and in the orthogonal view in the insert. The profile of red, green and blue intensities along a line passing through peroxisomes shows matched peaks of intensities in the AGT and GO channels. The scatter plot shows a correlation between intensities in the GO and AGT channels with a slant towards the AGT channel, explained by the higher intensities of the AGT staining versus GO staining. The Pearson coefficient and Manders' M1 and M2 coefficients all indicated correlation between the two channels, supporting colocalization. The exclusive peroxisomal localization of AGT-MA can also be seen by concomitant exclusion from mitochondria (Fig IV.8). The RGB profile of a section passing through peroxisome (staining with antiperoxisomal antibody) and mitochondria (staining with MitoTracker) shows peaks corresponding to the AGT that match the peaks of peroxisomes and not mitochondria. The scatter plot between AGT and mitochondria shows an exclusion pattern with Pearson and Manders' coefficient characteristic of non-colocalization, while the scatter plot between AGT and peroxisome shows a correlation, as do the co-localization coefficients.

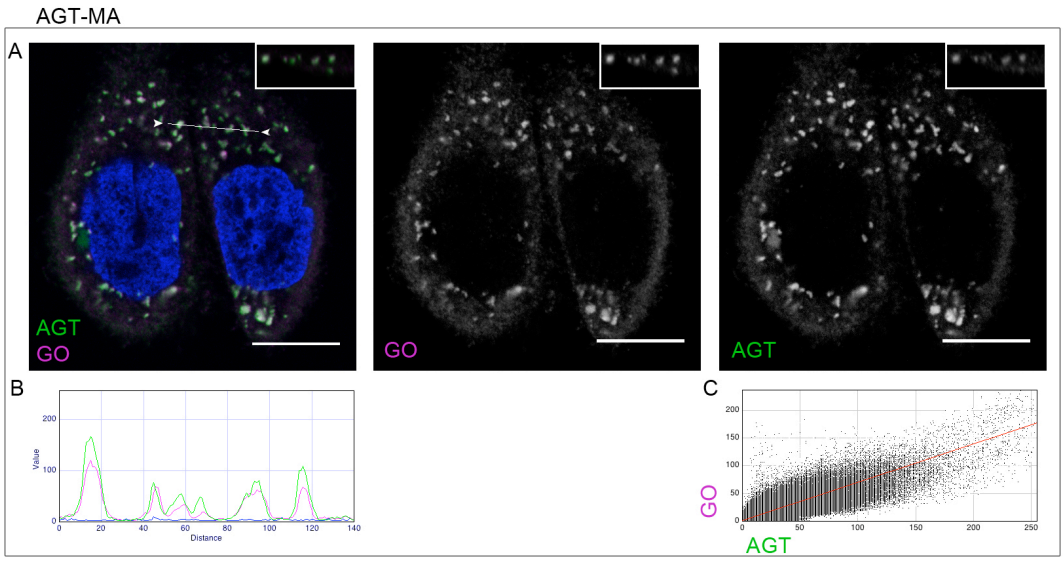

Figure IV-7. **Subcellular distribution of AGT-MA, as shown by immunofluorescence microscopy - 1.** CHO GO AGT-MA cells were cultured in standard conditions (see Methods III.2), stained with anti AGT (green), anti GO (magenta), Hoechst (blue). Scale bar: 10 µm. Merged and single channel images from a single z-plane are shown in (A). Insert: reslice along the z-axis along the line drawn in the merged image (A). The RGB profile (B) is plotted along the line drawn in the merged image, the scatter plot (C)shows AGT (x-axis) and GO (y-axis). Pearson's coefficient 0.853, Manders' coefficient (thresholded): M1 (AGT): 0.773, M2 (GO): 0.712.

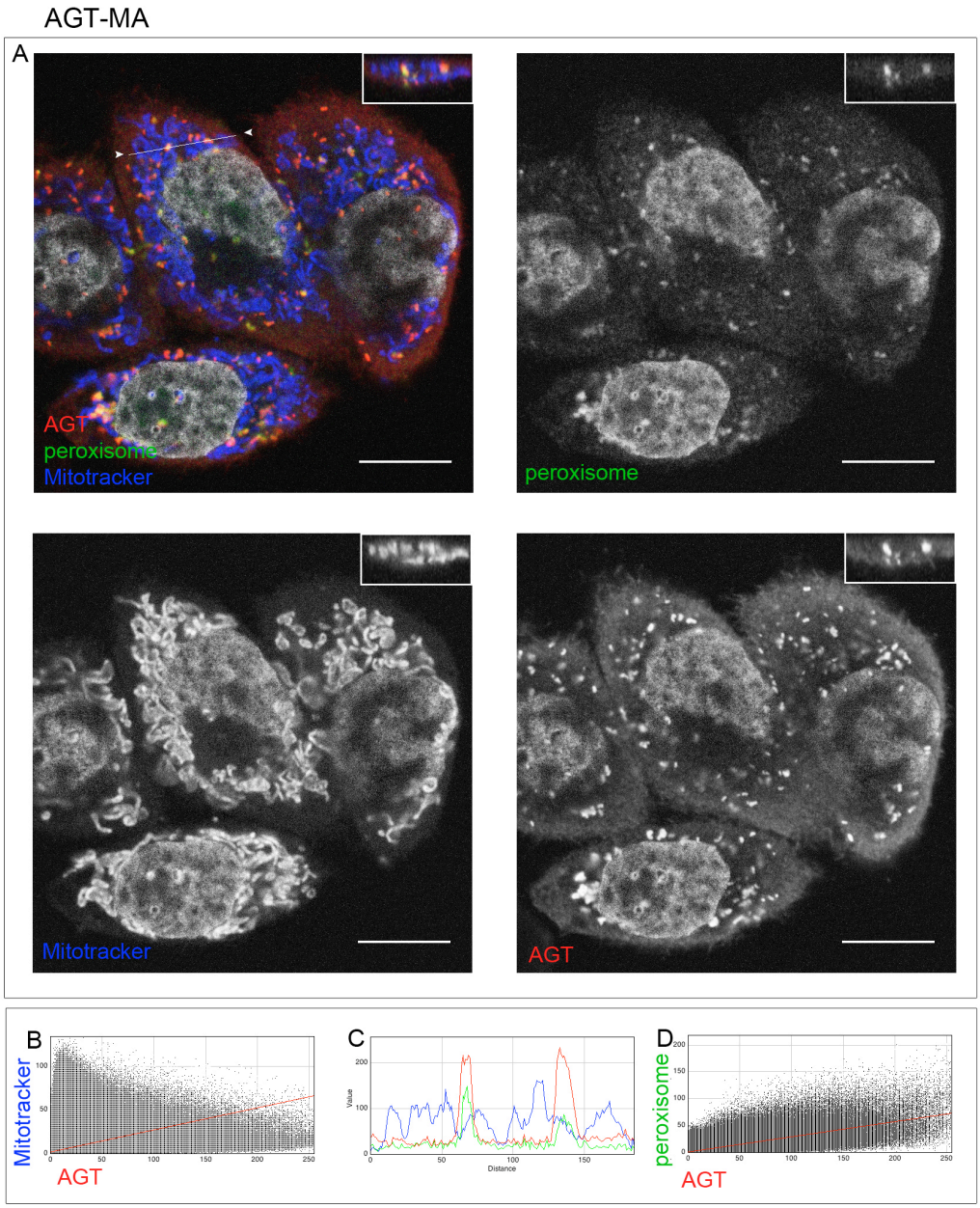

Figure IV-8. **Subcellular distribution of AGT-MA, as shown by immunofluorescence microscopy - 2.** A: CHO GO AGT-MA cells were cultured in standard conditions (Methods III.2), stained with anti AGT (red), anti peroxisomes (green), MitoTracker (blue). Nuclei stained with Hoechst (grey). Scale bar : 10 µm. Merged and single channel images from a single z-plane (A). Insert: reslice along the z-axis along the line drawn in the merged image in (A). B & D: scatter plots showing AGT (x-axis) and MitoTracker (y-axis) (B) and AGT (x-axis) and peroxisomes (y-axis) (D). C: RGB profile plotted along the line drawn. Colocalization coefficients for the couples AGT / peroxisomes and AGT / mitochondria are as follows. For the couple AGT-MA / peroxisomes: Pearson's coefficient: 0.675, Manders' coefficient (thresholded): M1 (AGT): 0.280, M2 (peroxisomes): 0.904. For the couple AGT-MA / mitochondria: Pearson's coefficient 0.383, Manders' coefficient (thresholded): M1 (AGT): 0.063, M2 (mitochondria): 0.079.

IV.2.1.3.2 EM of CHO GO AGT-MA

CHO GO AGT-MA cells were immuno-labelled for AGT or GO using post-embedding colloidal gold immune-electron microscopy. Both GO and AGT localized to single-membrane-limited structures, characteristic of peroxisomes (Fig IV.9). The distribution of colloidal-gold particles was spread throughout the peroxisomal matrix for both AGT and GO. The peroxisomal structure was normal when compared to CHO WT on transmission electron microscopy, with a frequent proximity of peroxisomes to endoplasmic reticulum structures.

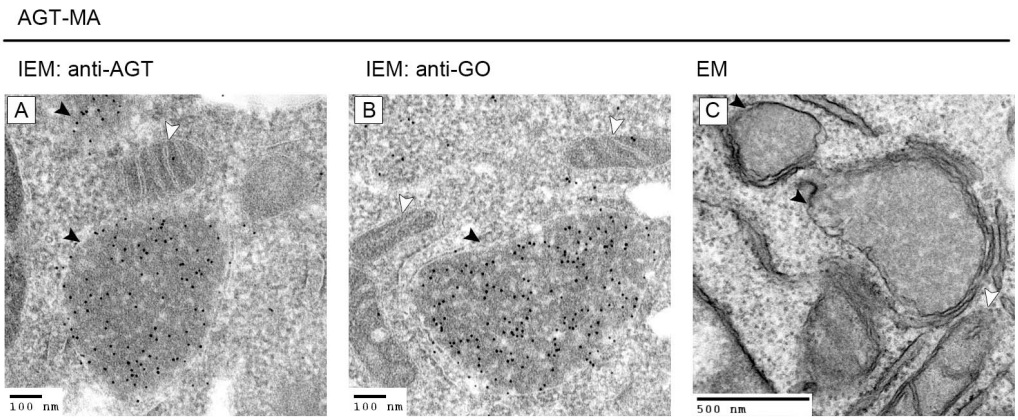

Figure IV-9. **Subcellular distribution of AGT-MA (A) and GO (B) in CHO GO AGT-MA cells as shown by electron microscopy**. A: immuno-electron microscopy, staining with anti-AGT (10 nm gold particles); B: immuno-electron microscopy, staining with anti-GO (10 nm gold particles); C: transmission electron microscopy. Black arrowheads: peroxisomes, white arrowheads: mitochondria (electron microscopy kindly carried out by J Lewin, see Methods III.7).

IV.2.1.4 AGT-mi

IV.2.1.4.1 IMF of CHO GO AGT-mi

As has been reported previously in transiently transfected COS cells the distribution of AGT-mi is peroxisomal (Motley et al., 1995; Lumb et al., 1999). The profile of AGT-mi in CHO GO AGT-mi cells shown by IMF microscopy matched that of GO (Fig IV.10) and peroxisomal marker (Fig IV.11) but not that of MitoTracker (Fig IV.11). The co-localization coefficients and scatter plots show a correlation with peroxisomes (Pearson 0.849 and 0.809, Mander's M1: 0.794 – 0.753, M2: 0.815 – 0.822) and not significantly mitochondria (Pearson: 0.529, M1: 0.107, M2: 0.050). The evidence based on IMF is that of a complete peroxisomal localization of AGT-mi.

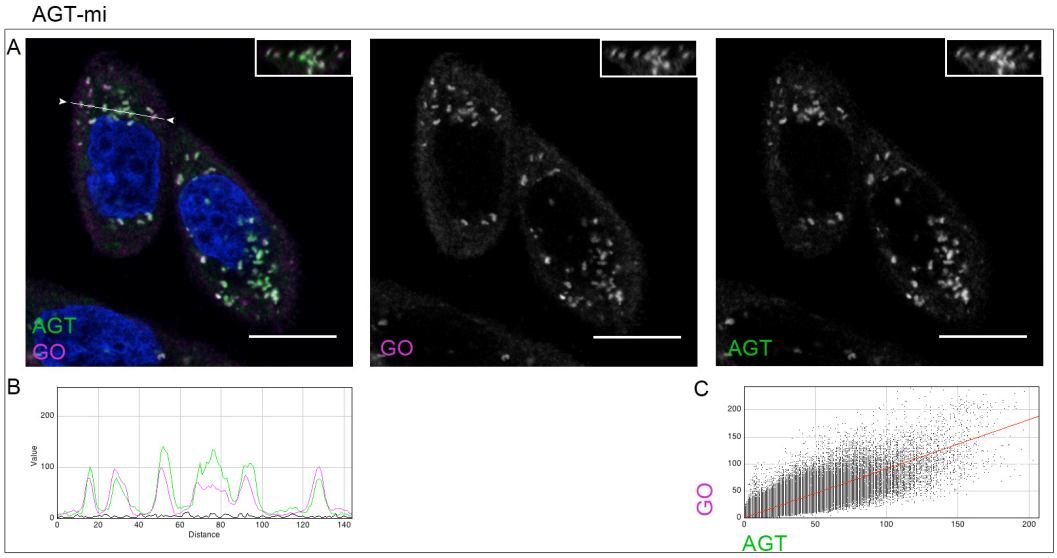

Figure IV-10. **Subcellular distribution of AGT-mi, as shown by immunofluorescence microscopy - 1.** CHO GO AGT-mi cells were cultured in standard conditions (see Methods III.2), stained with anti AGT (green), anti GO (magenta), Hoechst (blue). Scale bar: 10 µm. Merged and single channel images from a single z-plane are shown in (A). Insert: reslice along the z-axis along the line drawn in the merged image (A). The RGB profile (B) is plotted along the line drawn in the merged image, the scatter plot (C)shows AGT (x-axis) and GO (y-axis). Pearson's coefficient 0.849, Manders' coefficient (thresholded): M1 (AGT): 0.794, M2 (GO): 0.815.

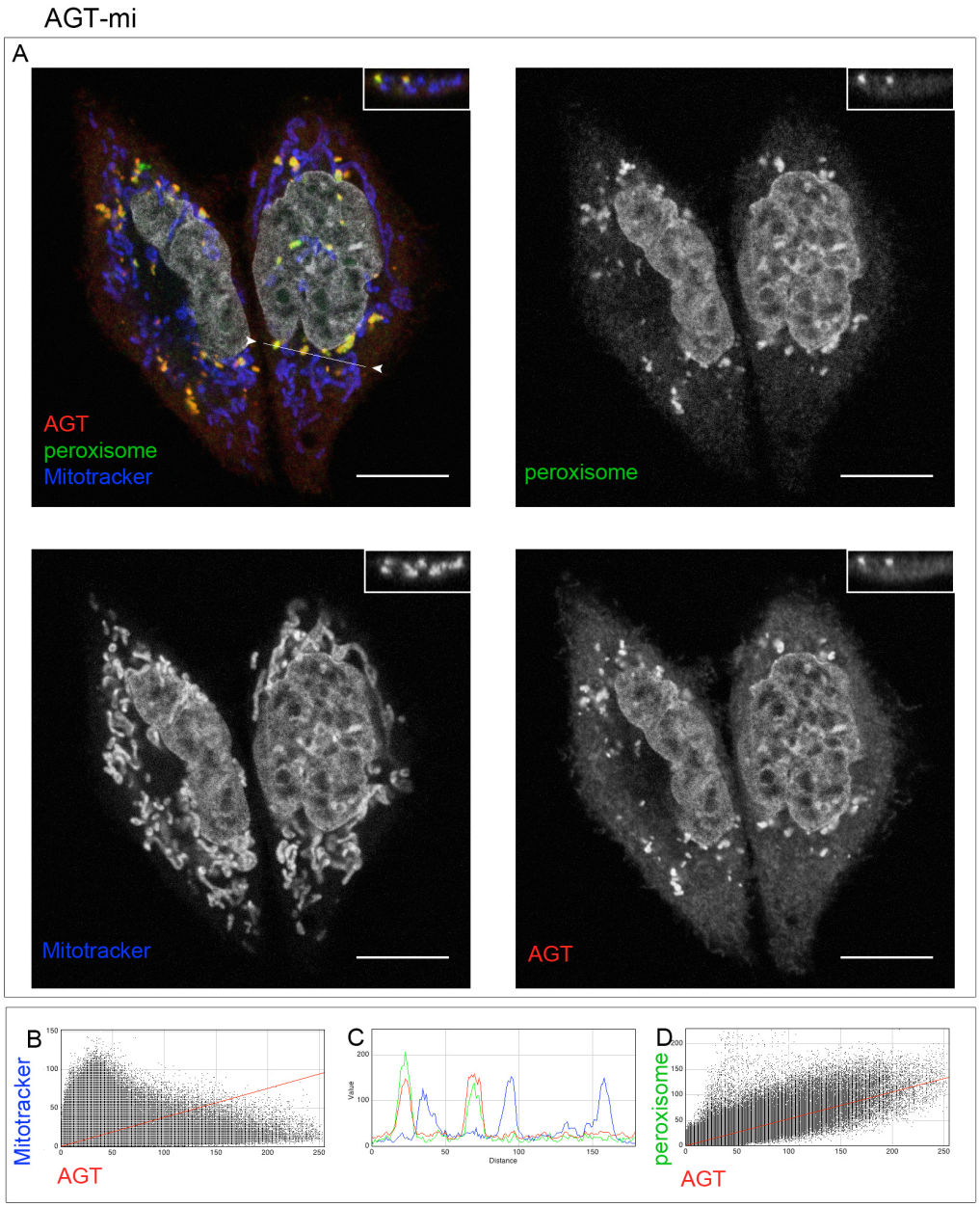

Figure IV-11. **Subcellular distribution of AGT-mi as shown by immunofluorescence microscopy - 2.** A: CHO GO AGT-mi cells were cultured in standard conditions (see Methods III.2), stained with anti AGT (red), anti peroxisomes (green), MitoTracker (blue). Nuclei stained with Hoechst (grey). Scale bar : 10 µm. Merged and single channel images from a single z-plane (A). Insert: reslice along the z-axis along the line drawn in the merged image in (A). B & D: scatter plots showing AGT (x-axis) and MitoTracker (y-axis) (B) and AGT (x-axis) and peroxisomes (y-axis) (D). C: RGB profile plotted along the line drawn in the merged image. Colocalization coefficients for the couples AGT / peroxisomes and AGT / mitochondria are as follows. For the couple AGT-mi / peroxisomes: Pearson's coefficient: 0.809, Manders' coefficient (thresholded): M1 (AGT): 0.753, M2 (peroxisomes): 0.822. For the couple AGT-mi / mitochondria: Pearson's coefficient 0.529, Manders' coefficient (thresholded): M1 (AGT): 0.107, M2 (mitochondria): 0.050.

IV.2.1.4.2 EM of CHO GO AGT-mi

Immunoelectron microscopy (IEM) study of AGT-mi showed that the vast majority of AGT-mi was peroxisomal. However there was also staining for AGT in mitochondria although the level was just above that of background staining (cytosolic) (Fig IV.12).

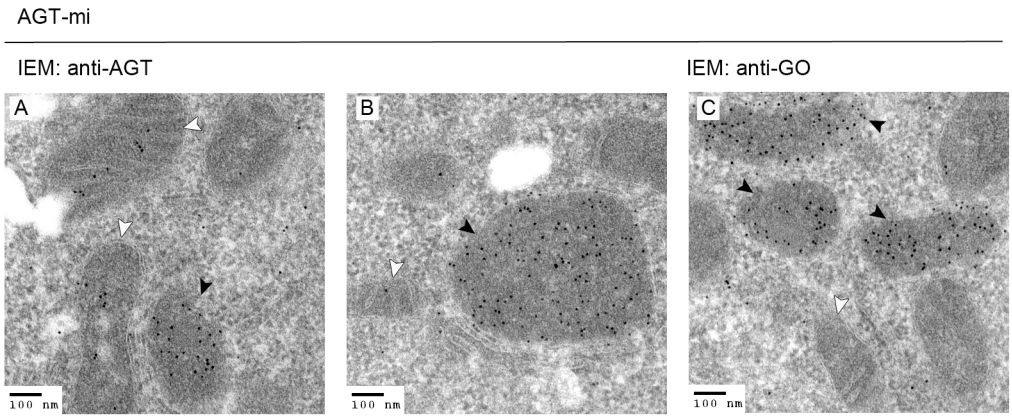

Figure IV-12. **Subcellular distribution of AGT-mi (A) and GO (B) in CHO GO AGT-mi cells as shown by immuno-electron microscopy**. A,B: immuno-electron microscopy, staining with anti-AGT (10 nm gold particles); C: immuno-electron microscopy, staining with anti-GO (10 nm gold particles). Black arrowheads: peroxisomes, white arrowheads: mitochondria (electron microscopy kindly carried out by J Lewin, see Methods).

IV.2.1.5 AGT-anc

IV.2.1.5.1 IMF of CHO GO AGT-anc

The subcellular localization of AGT-anc was both mitochondrial and peroxisomal in all transfected cells, stable and transient CHO cells, transient COS cells (data not shown). Immunofluorescence staining of stably transformed CHO cells with anti-GO (Fig IV.13) showed that a fraction of AGT-anc co-localized with GO (common subcellular structures, matching peaks on RGB profiles). Since the co-localization with peroxisomal markers was not exclusive, general markers of co-localization such as scatter plot, Pearson and Manders' coefficients do not give standard marks of co-localization. The combined anti-peroxisomal and mitochondrial staining (Fig IV.14) showed that the majority of AGT-anc was mitochondrial with local and general markers agreeing (common structures, matching peaks on RGB profile as well as Pearson's and Manders' coefficient > 0.5). However the proportion of peroxisomal AGT-anc is biologically significant for this study and a more careful analysis of co-localization markers allow us to identify a population of peroxisomal AGT-anc as well as a different population of mitochondrial AGT-anc on the scatter plots between peroxisomes and AGT-anc

that show two distinct clouds. One population of GO-pixels is spread over AGT-pixel of low to medium intensity (in accordance with the lower intensity seen on IMF pictures). A second population of AGT-pixels is spread over the complete range of intensities and only has no or low GO intensities (Fig IV.13 C & IV.14 C). The fact that almost all peroxisomes are populated with AGT-anc whereas a minority of AGT-anc is peroxisomal can be supported by the discrepancy between the two Manders' coefficients (higher for GO compared to AGT).

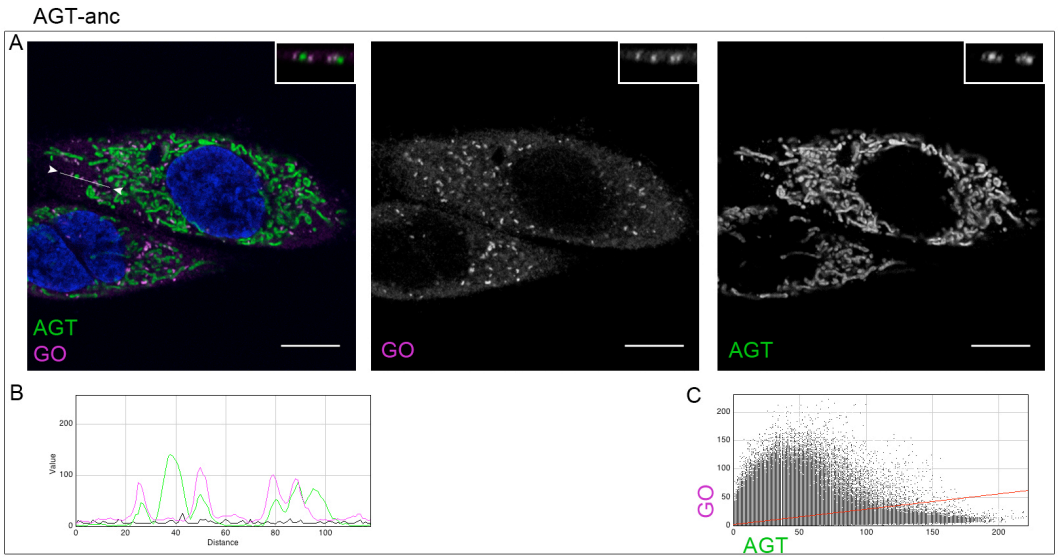

Figure IV-13. **Subcellular distribution of AGT-anc as shown by immunofluorescence microscopy - 1.** CHO GO AGT-anc cells were cultured in standard conditions (see Methods III.2), stained with anti AGT (green), anti GO (magenta), Hoechst (blue). Scale bar: 10 µm. Merged and single channel images from a single z-plane are shown in (A). Insert: reslice along the z-axis along the line drawn in the merged image (A). The RGB profile (B) is plotted along the line drawn in the merged image, the scatter plot (C)shows AGT (x-axis) and GO (y-axis). Pearson's coefficient 0.473, Manders' coefficient (thresholded): M1 (AGT): 0.081, M2 (GO): 0.291.

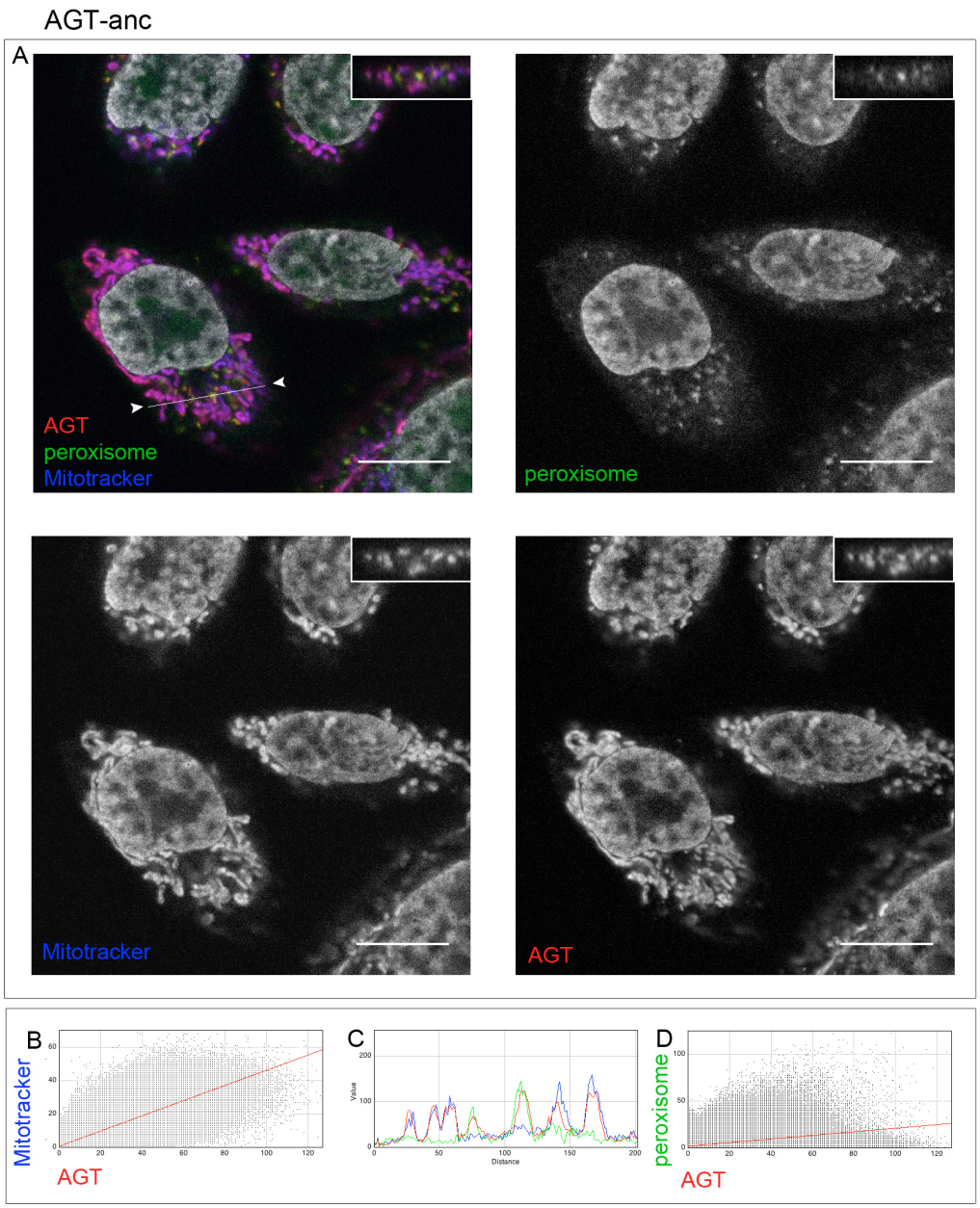

Figure IV-14. **Subcellular distribution of AGT-anc as shown by immunofluorescence microscopy - 2.** A: CHO GO AGT-anc cells were cultured in standard conditions (see Methods III.2), stained with anti AGT (red), anti peroxisomes (green), MitoTracker (blue). Nuclei stained with Hoechst (grey). Scale bar : 10 µm. Merged and single channel images from a single z-plane (A). Insert: reslice along the z-axis along the line drawn in the merged image in (A). B & D: scatter plots showing AGT (x-axis) and MitoTracker (y-axis) (B) and AGT (x-axis) and peroxisomes (y-axis) (D). C: RGB profile plotted along the line drawn in the merged image. Colocalization coefficients for the couples AGT / peroxisomes and AGT / mitochondria are as follows. For the couple AGT-anc / peroxisomes: Pearson's coefficient: 0.382, Manders' coefficient (thresholded): M1 (AGT): 0.035, M2 (peroxisomes): 0.376. For the couple AGT-anc / mitochondria: Pearson's coefficient 0.852, Manders' coefficient (thresholded): M1 (AGT): 0.561, M2 (mitochondria):0.526.

IV.2.1.5.2 EM of CHO GO AGT-anc

The dual localization of AGT-anc in peroxisomes and mitochondria was confirmed by IEM study. As with AGT-MA and AGT-mi, the global structure of organelles on transmission electron microscopy was normal (Fig IV.15).

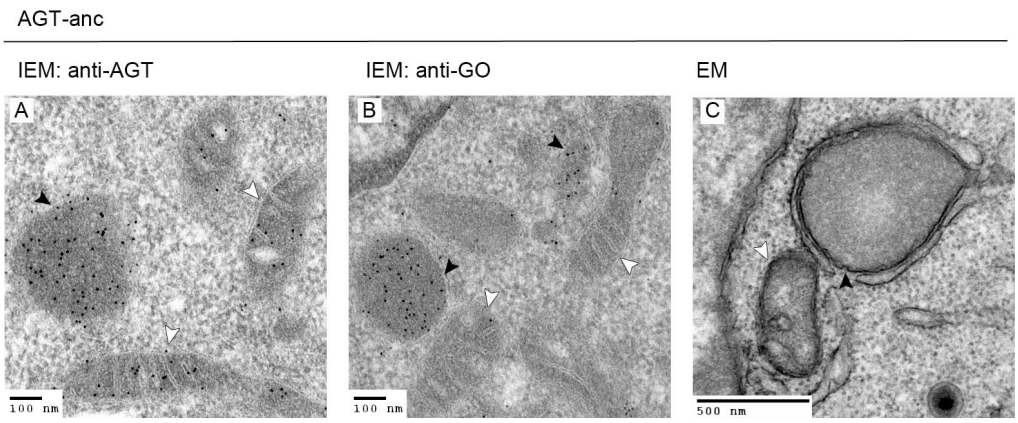

Figure IV-15. **Subcellular distribution of AGT-anc (A) and GO (B) in CHO GO AGT-anc cells as shown by electron microscopy**. A: immuno-electron microscopy, staining with anti-AGT (10 nm gold particles); B: immuno-electron microscopy, staining with anti-GO (10 nm gold particles); C: transmission electron microscopy. Black arrowheads: peroxisomes, white arrowheads: mitochondria (electron microscopy kindly carried out by J Lewin, see Methods III.7).

IV.2.1.6 AGT-Δ

IV.2.1.6.1 IMF of CHO GO AGT-Δ

The localization of the artificial variant AGT-Δ, devoid of the N-terminal arm, was entirely peroxisomal as was shown by complete colocalization with GO (Fig IV.16) and peroxisomal antibodies (Fig IV.17) and co-localization indexes >0.5 as well as exclusion with the mitochondrial marker (Fig IV.17) and low indexes (<0/5) for AGT/mitochondria analysis.

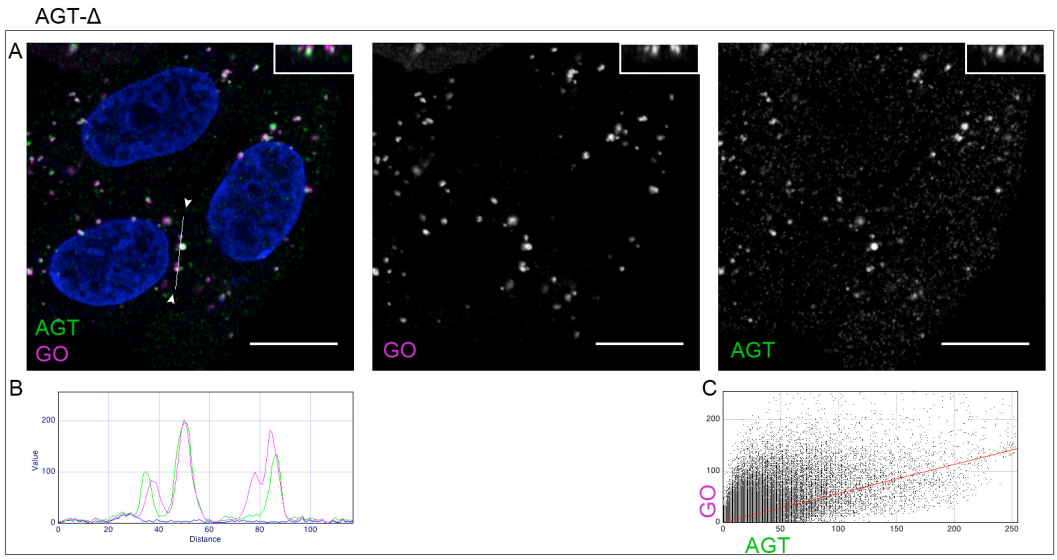

Figure IV-16. **Subcellular distribution of AGT-Δ as shown by immunofluorescence microscopy - 1.** CHO GO AGT-Δ cells were cultured in standard conditions (see Methods III.2), stained with anti AGT (green), anti GO (magenta), Hoechst (blue). Scale bar: 10 µm. Merged and single channel images from a single z-plane are shown in (A). Insert: reslice along the z-axis along the line drawn in the merged image (A). The RGB profile (B) is plotted along the line drawn in the merged image, the scatter plot (C)shows AGT (x-axis) and GO (y-axis). Pearson's coefficient 0.642, Manders' coefficient (thresholded): M1 (AGT): 0.634, M2 (GO): 0.584.

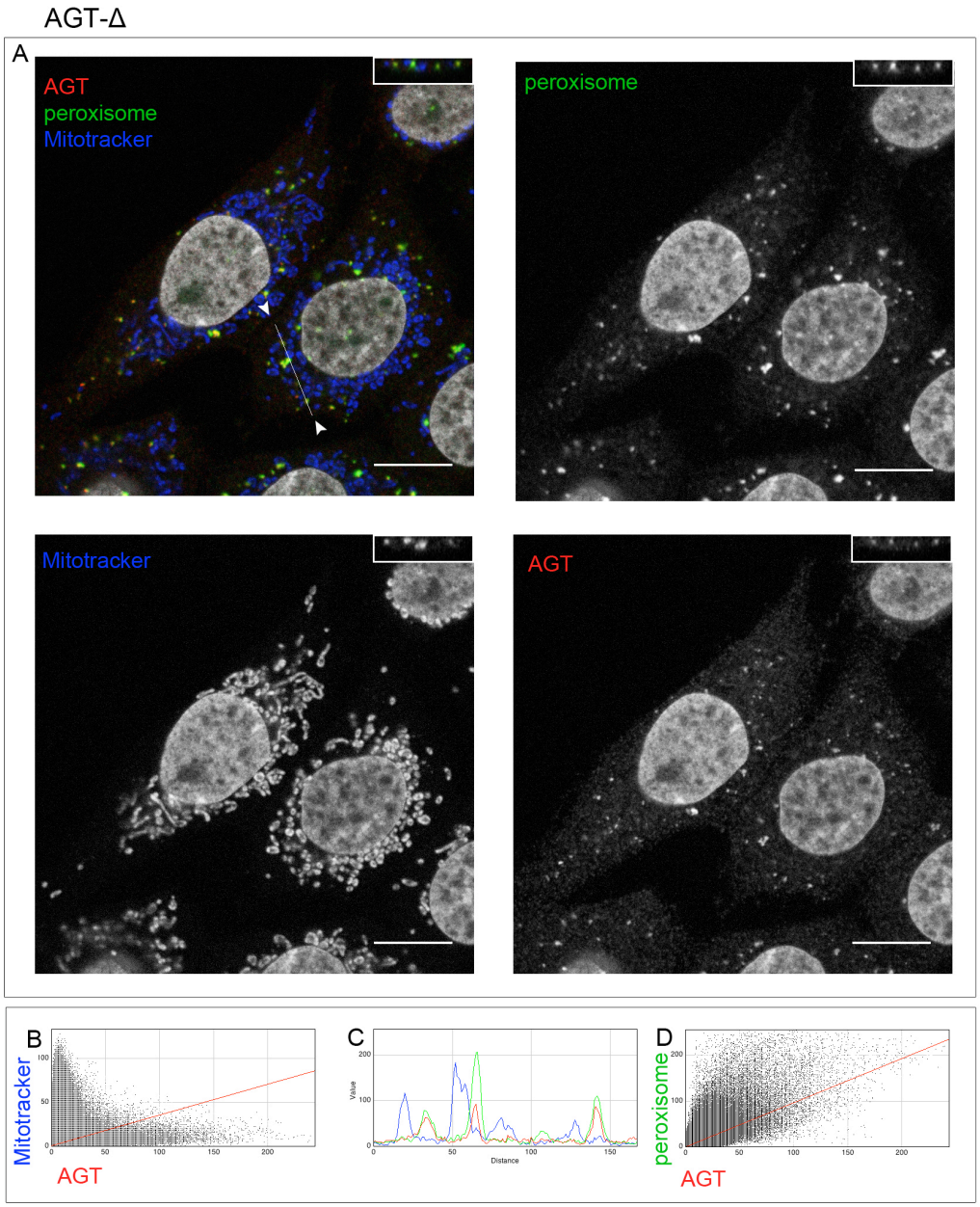

Figure IV-17. **Subcellular distribution of AGT-Δ as shown by immunofluorescence microscopy - 2.** A: CHO GO AGT-Δ cells were cultured in standard conditions (see Methods III.2), stained with anti AGT (red), anti peroxisomes (green), MitoTracker (blue). Nuclei stained with Hoechst (grey). Scale bar : 10 µm. Merged and single channel images from a single z-plane (A). Insert: reslice along the z-axis along the line drawn in the merged image in (A). B & D: scatter plots showing AGT (x-axis) and MitoTracker (y-axis) (B) and AGT (x-axis) and peroxisomes (y-axis) (D). C: RGB profile plotted along the line drawn in the merged image. Colocalization coefficients for the couples AGT / peroxisomes and AGT / mitochondria are as follows. For the couple AGT-Δ / peroxisomes: Pearson's coefficient 0.711, Manders' coefficient (thresholded): M1 (AGT): 0.702, M2 (peroxisomes): 0.639. For the couple AGT-Δ / mitochondria: Pearson's coefficient 0.267, Manders' coefficient (thresholded): M1 (AGT): 0.109, M2 (mitochondria): 0.010.

IV.2.1.6.2 EM of CHO GO AGT-Δ

The peroxisomal localization of AGT-Δ was confirmed by IEM. Most of the peroxisomes contained in addition to a normal matrix staining with AGT and GO, also contained a amorphous structure. This structure stained non-exclusively with AGT. Staining with GO, although less than the AGT staining, could be observed in the intra-peroxisomal structure (Fig IV.18). The size of the dense peroxisomal structure was much larger than the occasional similar structure seen in the transformed cells expressing normal AGT or GO.

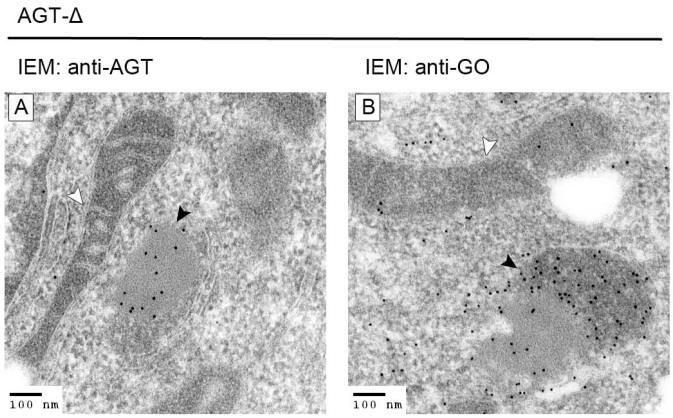

Figure IV-18. **Subcellular distribution of AGT-Δ (A) and GO (B) in CHO GO AGT-Δ cells as shown by immuno-electron microscopy**. A: immuno-electron microscopy, staining with anti-AGT (10 nm gold particles); B: immuno-electron microscopy, staining with anti-GO (10 nm gold particles). Black arrowheads: peroxisomes, white arrowheads: mitochondria (electron microscopy kindly carried out by J Lewin, see Methods III.7).

IV.2.1.7 AGT-G170R

IV.2.1.7.1 IMF of CHO GO AGT-170

The subcellular localization of AGT-170 was both mitochondrial and peroxisomal in stable (Fig IV.19 & IV.20) or transiently transfected cells (data not shown). Peroxisomes staining with AGT could be identified (Fig IV.19, IV.20, insert & B). However the intensity of AGT in peroxisomes was very low in contrast with the mitochondrial fraction (Fig IV.20). In addition there was inter-cell and inter-experimental variability in the amount of peroxisomal localization, ranging from non detectable on IMF to moderate and significant staining in IMF. As with AGT-anc the two populations of AGT, peroxisomal and mitochondrial, can be identified on scatter plots (Fig IV.20 B&D).

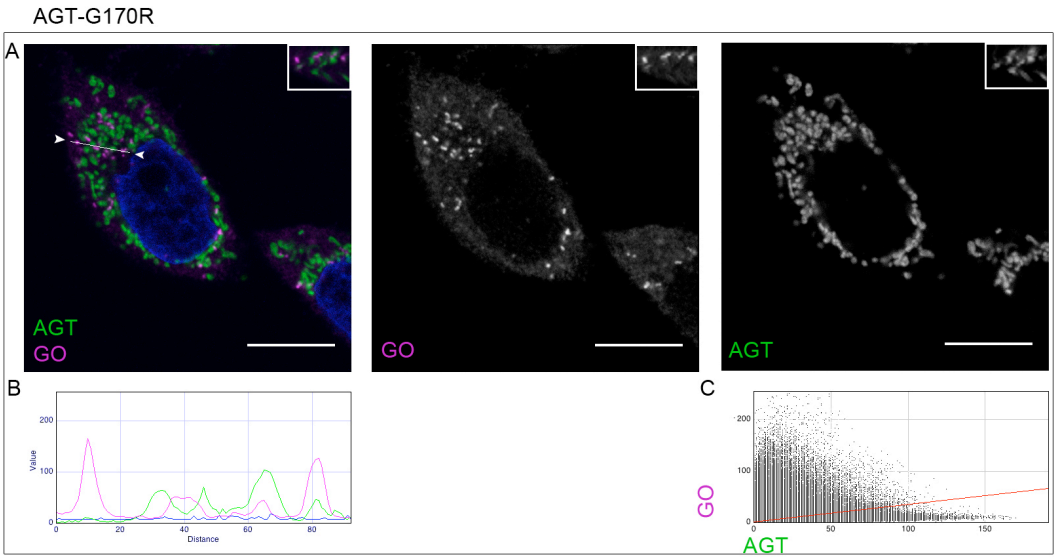

Figure IV-19. **Subcellular distribution of AGT-170 as shown by immunofluorescence microscopy - 1.** CHO GO AGT-170 cells were cultured in standard conditions (see Methods III.2), stained with anti AGT (green), anti GO (magenta), Hoechst (blue). Scale bar: 10 µm. Merged and single channel images from a single z-plane are shown in (A). Insert: reslice along the z-axis along the line drawn in the merged image (A). The RGB profile (B) is plotted along the line drawn in the merged image, the scatter plot (C)shows AGT (x-axis) and GO (y-axis). Pearson's coefficient 0.376, Manders' coefficient (thresholded): M1 (AGT): 0.081, M2 (GO): 0.291.

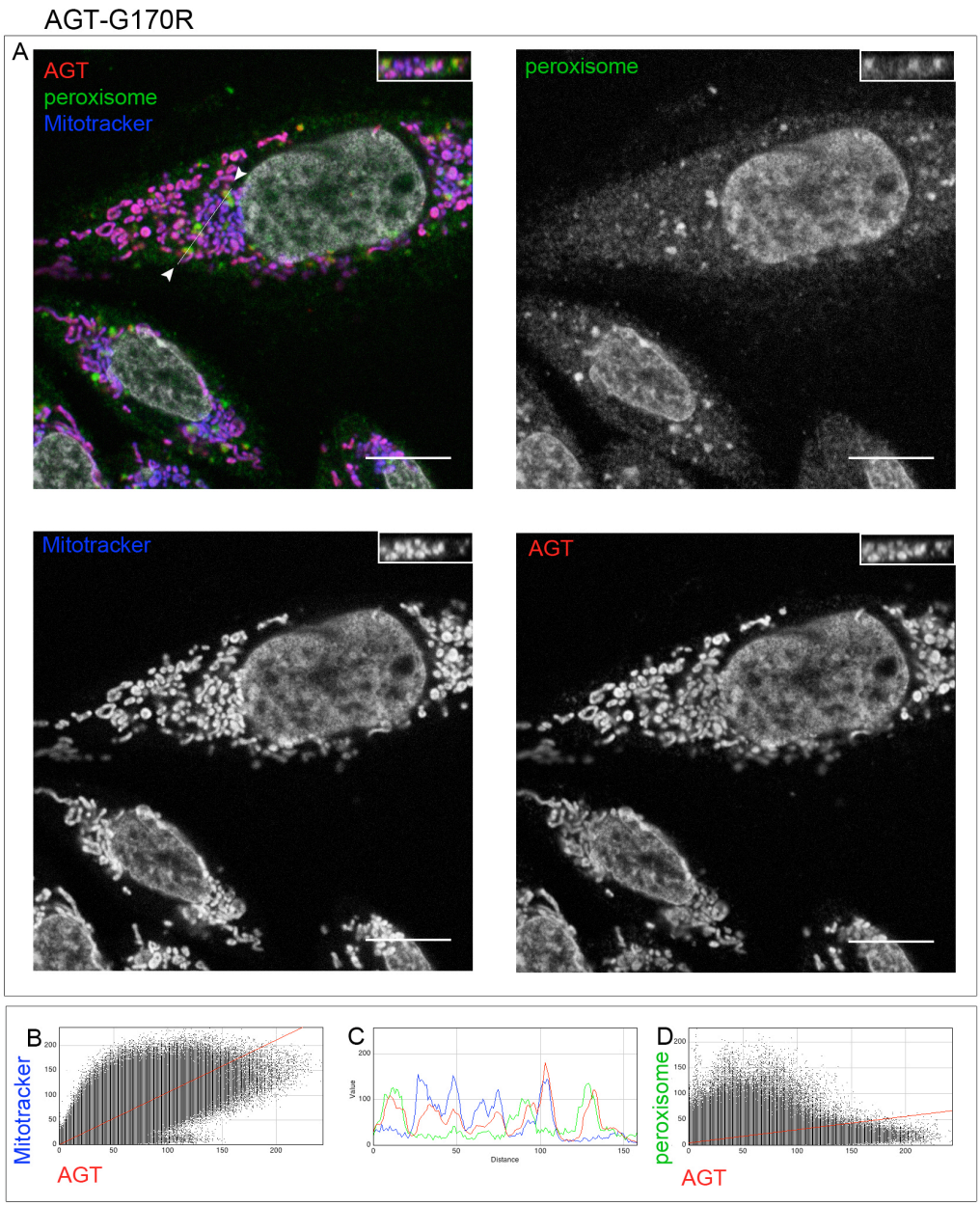

Figure IV-20. **Subcellular distribution of AGT-170 as shown by immunofluorescence microscopy - 2.** A: CHO GO AGT-170 cells were cultured in standard conditions (see Methods III.2), stained with anti AGT (red), anti peroxisomes (green), MitoTracker (blue). Nuclei stained with Hoechst (grey). Scale bar : 10 µm. Merged and single channel images from a single z-plane (A). Insert: reslice along the z-axis along the line drawn in the merged image in (A). B & D: scatter plots showing AGT (x-axis) and MitoTracker (y-axis) (B) and AGT (x-axis) and peroxisomes (y-axis) (D). C: RGB profile plotted along the line drawn in the merged image. Colocalization coefficients for the couples AGT / peroxisomes and AGT / mitochondria are as follows. For the couple AGT-170 / peroxisomes: Pearson's coefficient: 0.449, Manders' coefficient (thresholded): M1 (AGT): 0.054, M2 (peroxisomes): 0.383. For the couple AGT-170 / mitochondria: Pearson's coefficient: 0.897, Manders' coefficient (thresholded): M1 (AGT): 0.869, M2 (mitochondria): 0.728.

IV.2.1.7.2 EM of CHO GO AGT-170

The dual localization of AGT-170 was confirmed in IEM. The fraction of peroxisomal AGT was more easily seen than on IMF, due to the higher sensitivity of the IEM technique (Fig IV.21).

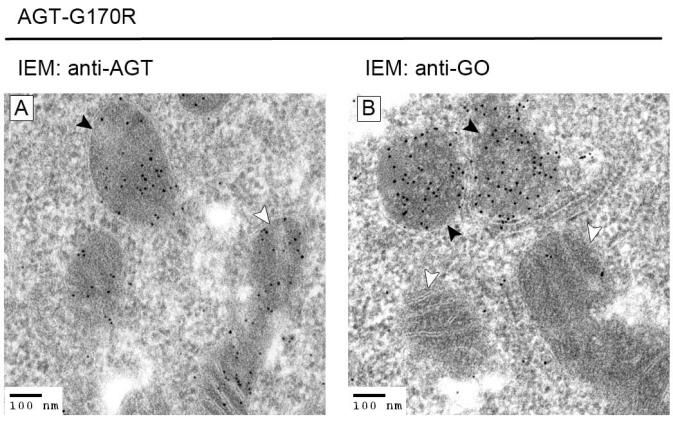

Figure IV-21. **Subcellular distribution of AGT-170 (A) and GO (B) in CHO GO AGT-170 cells as shown by immuno-electron microscopy**. A: immuno-electron microscopy, staining with anti-AGT (10 nm gold particles); B: immuno-electron microscopy, staining with anti-GO (10 nm gold particles). Black arrowheads: peroxisomes, white arrowheads: mitochondria (electron microscopy kindly carried out by J Lewin, see Methods III.7).

IV.2.1.8 AGT-F152I

IV.2.1.8.1 IMF of AGT GO AGT-152

Like AGT-170, the subcellular localization of AGT-152 was dual, mitochondrial and peroxisomal in stable (Fig IV.22 & IV.23) or transiently transfected cells (data not shown). The majority of AGT-152 was mitochondrial with Pearson's and Manders' coefficient >0.5 for mitochondria. As with the other dual-targeted AGT variants, the two populations of AGT could be distinguished on scatter plots (Fig IV.22 C, Fig IV.23 B&D).

There was no IEM study performed on AGT-152.

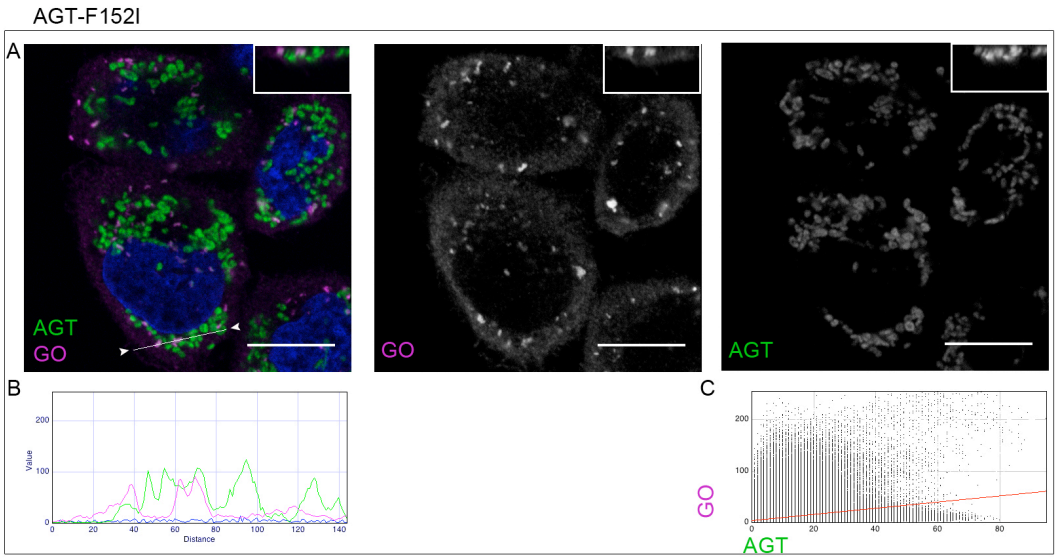

Figure IV-22. **Subcellular distribution of AGT-152 as shown by immunofluorescence microscopy - 1.** CHO GO AGT-152 cells were cultured in standard conditions (see Methods III.2), stained with anti AGT (green), anti GO (magenta), Hoechst (blue). Scale bar: 10 µm. Merged and single channel images from a single z-plane are shown in (A). Insert: reslice along the z-axis along the line drawn in the merged image (A). The RGB profile (B) is plotted along the line drawn in the merged image, the scatter plot (C)shows AGT (x-axis) and GO (y-axis). Pearson's coefficient 0.359, Manders' coefficient (thresholded): M1 (AGT): 0.052, M2 (GO): 0.307.

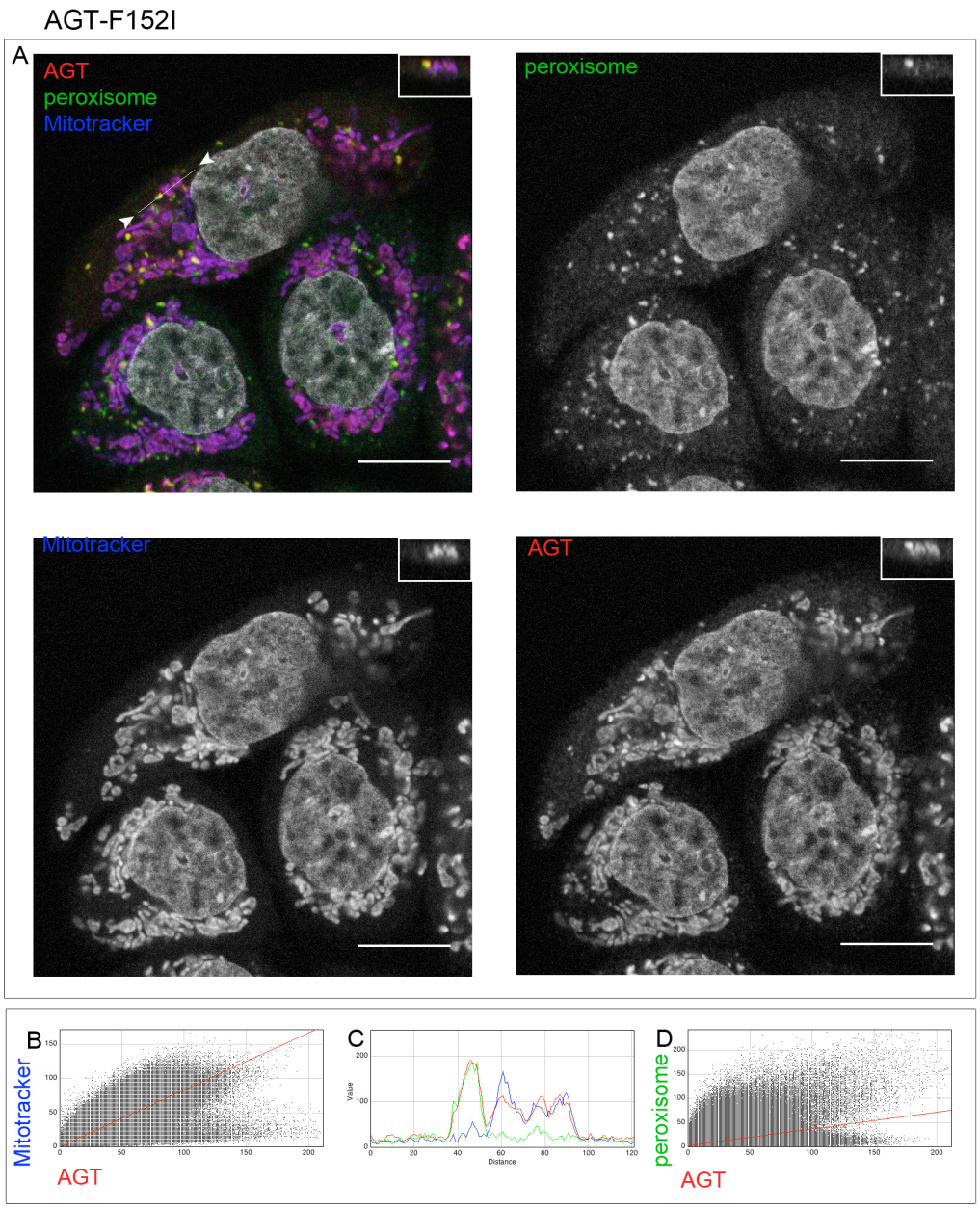

Figure IV-23. **Subcellular distribution of AGT-152 as shown by immunofluorescence microscopy - 2.** A: CHO GO AGT-152 cells were cultured in standard conditions (Methods III.2), stained with anti AGT (red), anti peroxisomes (green), MitoTracker (blue). Nuclei stained with Hoechst (grey). Scale bar : 10 µm. Merged and single channel images from a single z-plane (A). Insert: reslice along the z-axis along the line drawn in the merged image in (A). B & D: scatter plots showing AGT (x-axis) and MitoTracker (y-axis) (B) and AGT (x-axis) and peroxisomes (y-axis) (D). C: RGB profile plotted along the line drawn in the merged image. Colocalization coefficients for the couples AGT / peroxisomes and AGT / mitochondria are as follows. For the couple AGT-152 / peroxisomes: Pearson's coefficient: 0.517, Manders' coefficient (thresholded): M1 (AGT): 0.130, M2 (peroxisomes): 0.437. For the couple AGT-152 / mitochondria: Pearson's coefficient: 0.900, Manders' coefficient (thresholded): M1 (AGT): 0.675, M2 (mitochondria): 0.772.

IV.2.1.9 AGT-I244T

IV.2.1.9.1 IMF of AGT GO AGT-244

The localization of AGT-244 in stable CHO transformants was both mitochondrial and peroxisomal (Fig IV.24 & IV.25). The peroxisomal fraction of AGT was more marked than other dual-targeted AGT variants and Pearson's coefficient was >0.5 both for analysis with peroxisomes (0.675 – 0.624) and mitochondria (0.843). Although reciprocal Manders' coefficient for AGT/mitochondria were both high, only the M2 (peroxisomal) was >0.5 in the couple AGT/peroxisome.

However, in transient transfection in CHO cells, AGT-244 was predominantly peroxisomal, with a mitochondrial fraction that varied between low and undetectable on IMF (Fig IV.31). In transient transfection in COS cells, AGT-244 appeared to be purely peroxisomal (Fig IV.31).

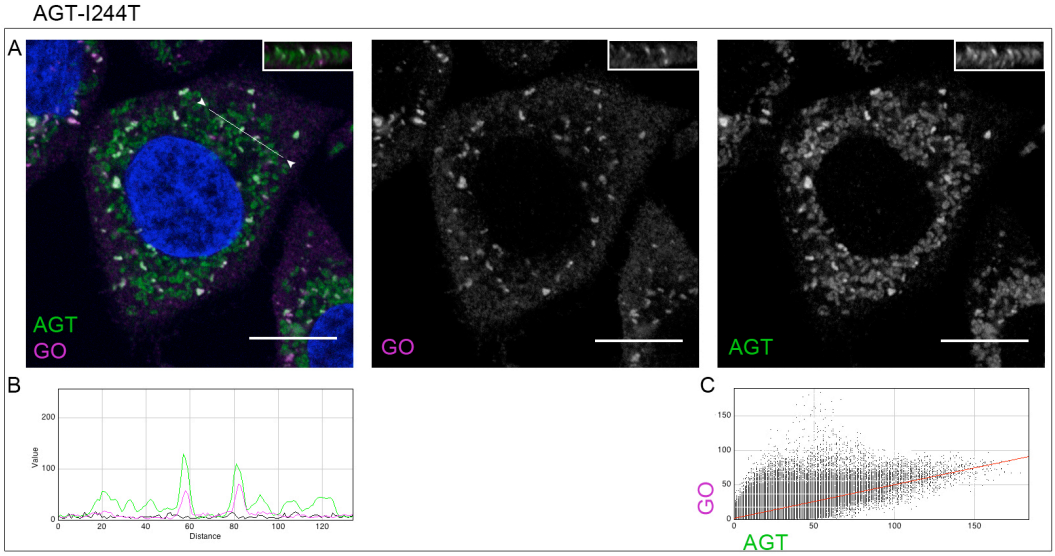

Figure IV-24. **Subcellular distribution of AGT-244 as shown by immunofluorescence microscopy - 1.** CHO GO AGT-244 cells were cultured in standard conditions (see Methods III.2), stained with anti AGT (green), anti GO (magenta), Hoechst (blue). Scale bar: 10 µm. Merged and single channel images from a single z-plane are shown in (A). Insert: reslice along the z-axis along the line drawn in the merged image (A). The RGB profile (B) is plotted along the line drawn, the scatter plot (C)shows AGT (x-axis) and GO (y-axis). Pearson's coefficient 0.675, Manders' coefficient (thresholded): M1 (AGT): 0.352, M2 (GO): 0.782.

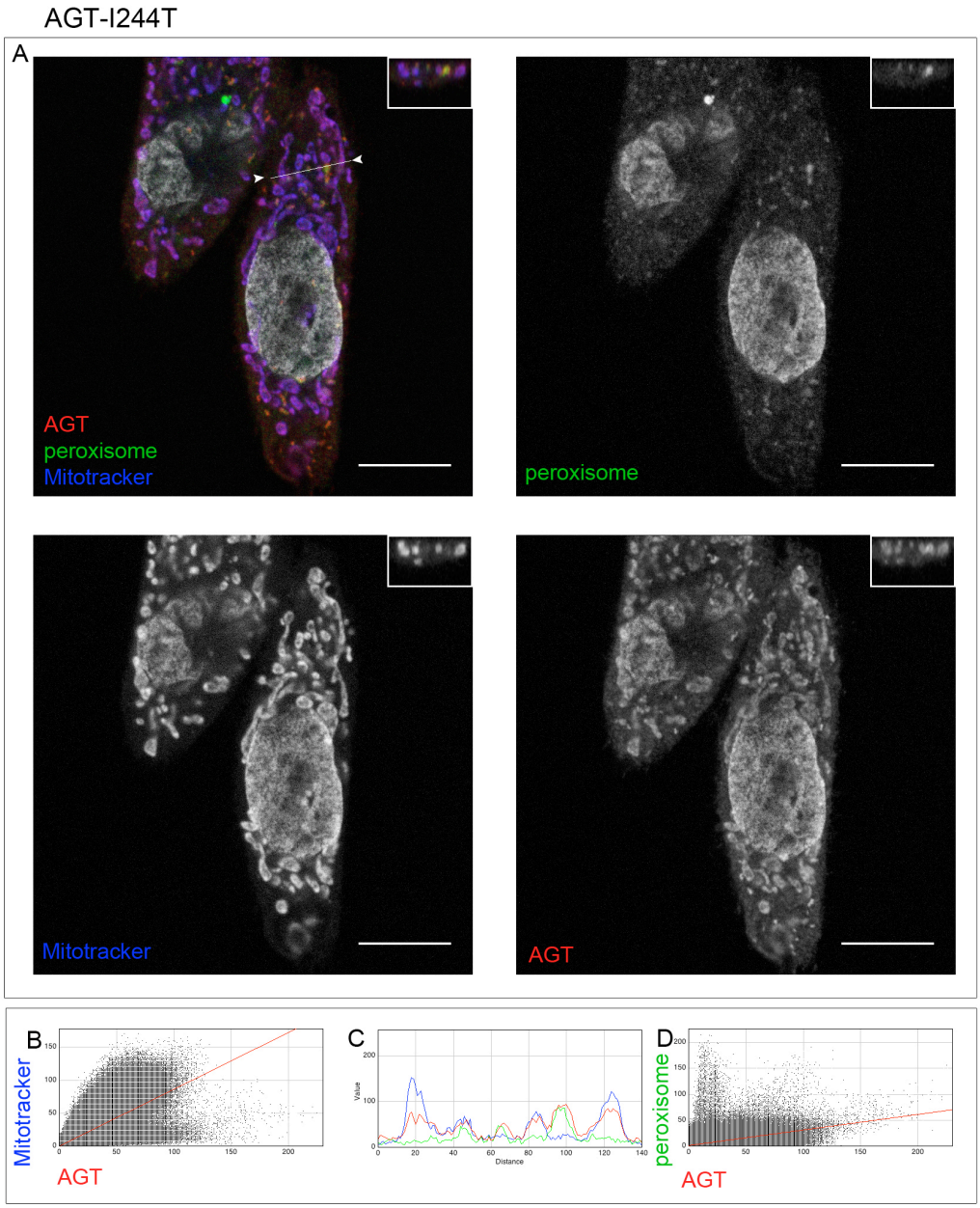

Figure IV-25. **Subcellular distribution of AGT-244 as shown by immunofluorescence microscopy - 2.** A: CHO GO AGT-244 cells were cultured in standard conditions (see Methods III.2) stained with anti AGT (red), anti peroxisomes (green), MitoTracker (blue). Nuclei stained with Hoechst (grey). Scale bar : 10 µm. Merged and single channel images from a single z-plane (A). Insert: reslice along the z-axis along the line drawn in the merged image in (A). B & D: scatter plots showing AGT (x-axis) and MitoTracker (y-axis) (B) and AGT (x-axis) and peroxisomes (y-axis) (D). C: RGB profile plotted along the line drawn. in the merged image Colocalization coefficients for the couples AGT / peroxisomes and AGT / mitochondria are as follows. For the couple AGT-244 / peroxisomes: Pearson's coefficient: 0.624, Manders' coefficient (thresholded): M1 (AGT): 0.060, M2 (peroxisomes): 0.521. For the couple AGT-244 / mitochondria: Pearson's coefficient 0.843, Manders' coefficient (thresholded): M1 (AGT): 0.724, M2 (mitochondria): 0.694.

IV.2.1.9.2 EM of AGT GO AGT-244

The presence of AGT-244 in both peroxisomes and mitochondria was confirmed in IEM in stable transformants. Both compartments showed significant staining (Fig IV.26). The structure of peroxisomes and mitochondria was similar to that of the cells expressing normal AGTs.

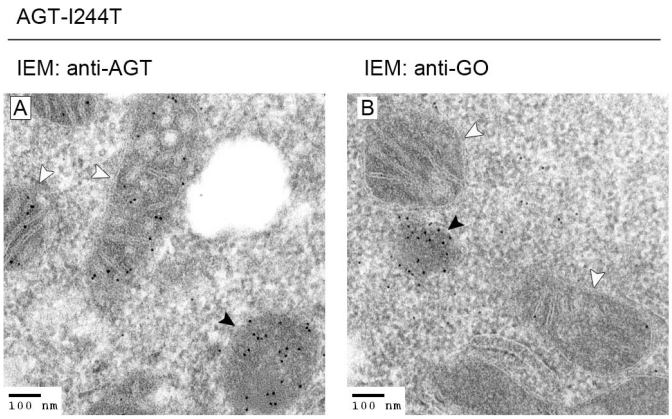

Figure IV-26. **Subcellular distribution of AGT-244 (A) and GO (B) in CHO GO AGT-244 cells as shown by immuno-electron microscopy**. A: immuno-electron microscopy, staining with anti-AGT (10 nm gold particles); B: immuno-electron microscopy, staining with anti-GO (10 nm gold particles). Black arrowheads: peroxisomes, white arrowheads: mitochondria (electron microscopy kindly carried out by J Lewin, see Methods III.7).

IV.2.1.10 AGT-G41R

IV.2.1.10.1 IMF of AGT GO AGT-41

The localization of AGT-41 was also both mitochondrial and peroxisomal (Fig IV.27 & IV.28) in stably transformed CHO cells. The mitochondrial localization appeared to be predominant (Pearson's coefficient 0.884 *vs*. 0.416 for AGT/mitochondria and AGT/peroxisomes respectively). There was variability in the proportions of peroxisomal and mitochondrial AGT between experiments and type of transfection (stable *vs*. transient) although both were detectable (Fig IV.27 & IV.28 & IV.31). In transiently transfected COS cells, AGT-41 appeared purely peroxisomal using IMF technique (Fig IV.31).

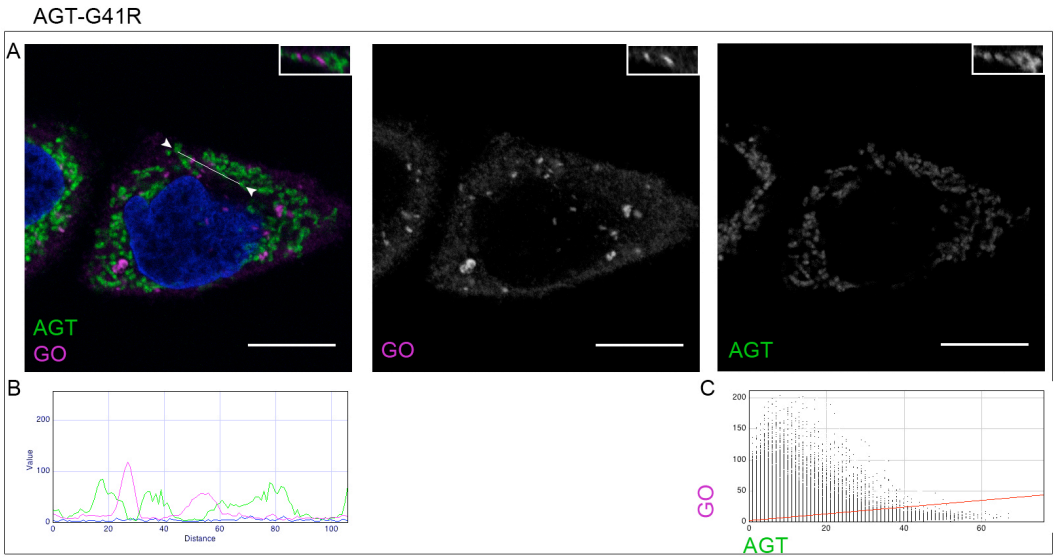

Figure IV-27. **Subcellular distribution of AGT-41 as shown by immunofluorescence microscopy - 1.** CHO GO AGT-41 cells were cultured in standard conditions (see Methods III.2), stained with anti AGT (green), anti GO (magenta), Hoechst (blue). Scale bar: 10 µm. Merged and single channel images from a single z-plane are shown in (A). Insert: reslice along the z-axis along the line drawn in the merged image (A). The RGB profile (B) is plotted along the line drawn, the scatter plot (C)shows AGT (x-axis) and GO (y-axis). Pearson's coefficient 0.360, Manders' coefficient (thresholded): M1 (AGT): 0.034, M2 (GO): 0.235.

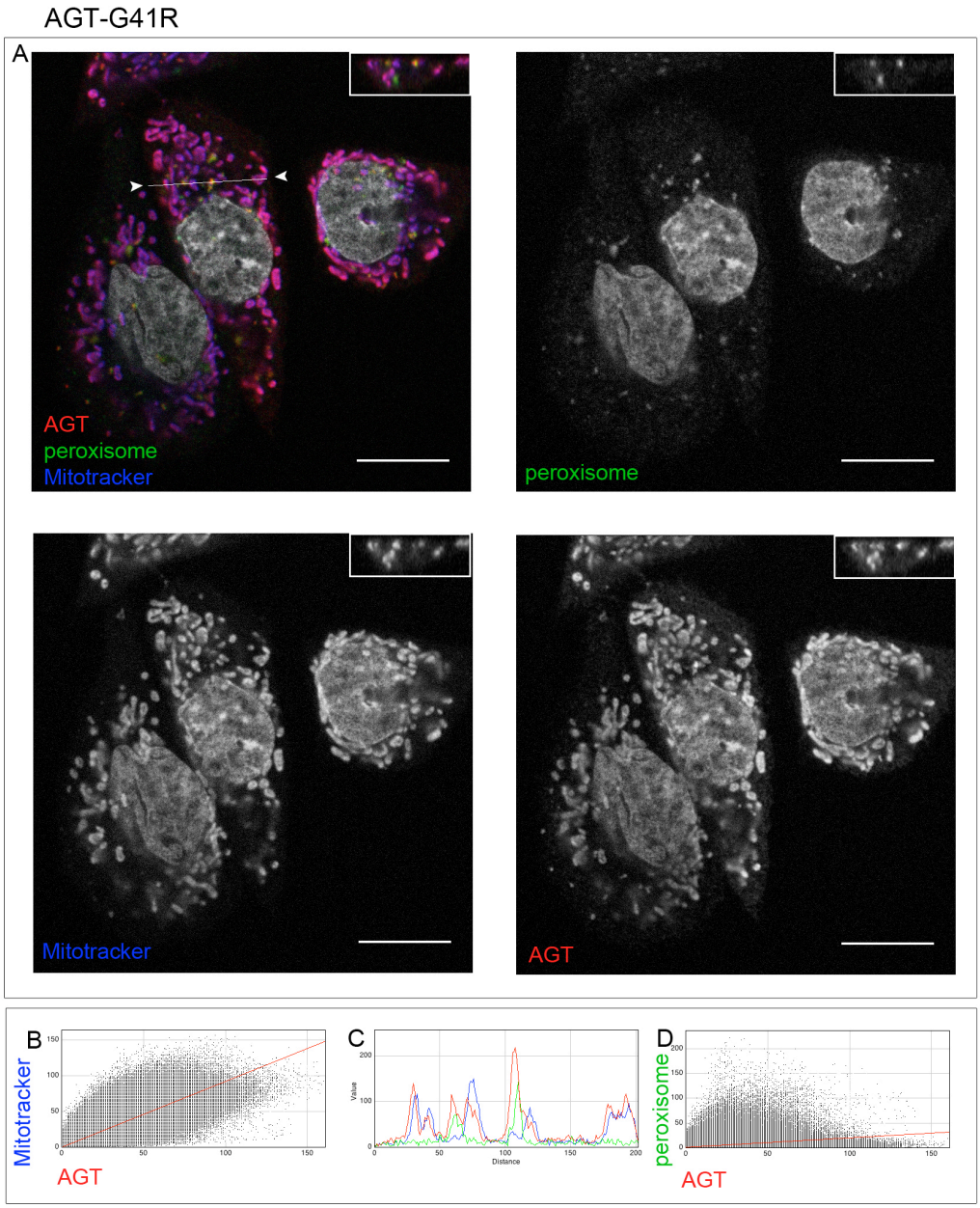

Figure IV-28. **Subcellular distribution of AGT-41 as shown by immunofluorescence microscopy - 2.** A: CHO GO AGT-41 cells were cultured in standard conditions (see Methods III.2), stained with anti AGT (red), anti peroxisomes (green), MitoTracker (blue). Nuclei stained with Hoechst (grey). Scale bar : 10 µm. Merged and single channel images from a single z-plane (A). Insert: reslice along the z-axis along the line drawn in the merged image in (A). B & D: scatter plots showing AGT (x-axis) and MitoTracker (y-axis) (B) and AGT (x-axis) and peroxisomes (y-axis) (D). C: RGB profile plotted along the line drawn in the merged image. Colocalization coefficients for the couples AGT / peroxisomes and AGT / mitochondria are as follows. For the couple AGT-41 / peroxisomes: Pearson's coefficient: 0.416, Manders' coefficient (thresholded): M1 (AGT): 0.037, M2 (peroxisomes): 0.450. For the couple AGT-41 / mitochondria: Pearson's coefficient: 0.884, Manders' coefficient (thresholded): M1 (AGT): 0.639, M2 (mitochondria): 0.744.

IV.2.1.10.2 EM of AGT GO AGT-41

In IEM, AGT-41 was found both in mitochondria and peroxisomes in stable CHO cells (Fig IV.29). In addition, to AGT staining in the peroxisomal matrix, there was a strong staining for large dense structures in the peroxisomes (Fig IV.29 A&C). These dense structures could occupy the totality of the peroxisomes and alter its form (Fig IV.29 C). Such structures also stained more weakly with GO (Fig IV.29 B) and could be detected on transmission EM (Fig IV.29 D). No such structures could be seen either in the cytosol or mitochondria.

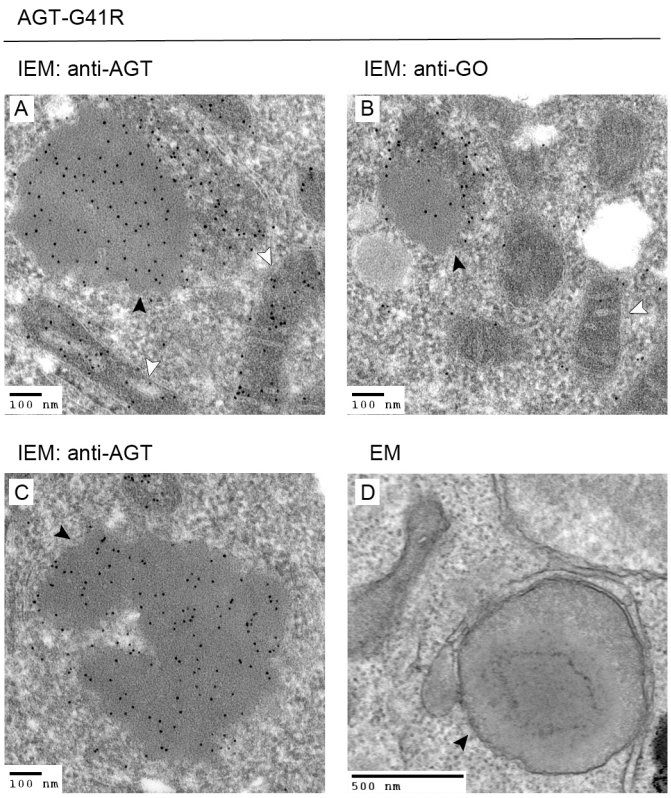

Figure IV-29. **Subcellular distribution of AGT-41 (A, B) and GO (C) in CHO GO AGT-41 cells as shown by electron microscopy**. A, C: immuno-electron microscopy, staining with anti-AGT (10 nm gold particles); B: immuno-electron microscopy, staining with anti-GO (10 nm gold particles); D: transmission electron microscopy. Black arrowheads: peroxisomes, white arrowheads: mitochondria (electron microscopy kindly carried out by J Lewin, see Methods III.7).

IV.2.1.11 Peroxisomal cores

All transformed cell lines showed rare intra-peroxisomal dense structures staining for GO in CHO GO cells or for AGT and GO in CHO GO AGT cells (Fig IV.30). The size of those structures usually did not exceed a quarter to a third of the peroxisomes they occupied. These structures could be detected on transmission EM, without accompanying change in outer morphology or shape of the peroxisome. Such amorphous structures were very different in size

and consequences on peroxisome outline from those observed in the CHO GO AGT-41 cell lines and to a lesser extent in the CHO GO AGT-Δ cell line. In contrast with CHO WT, all transformed CHO cells, including CHO GO and CHO GO AGT cells, showed in EM and IMF to be populated with a significant proportion of large peroxisomes, fewer in numbers than in CHO WT (data not shown). The effect was more marked in double transformants CHO GO AGT compared to CHO GO single transformants and was to some extent reversible in cells grown several days without antibiotic selection pressure, in which the intensity of staining for GO and AGT was decreased (data not shown). These modifications in regard to CHO WT cells did not affect the growth or multiplication of transformed CHO cells.

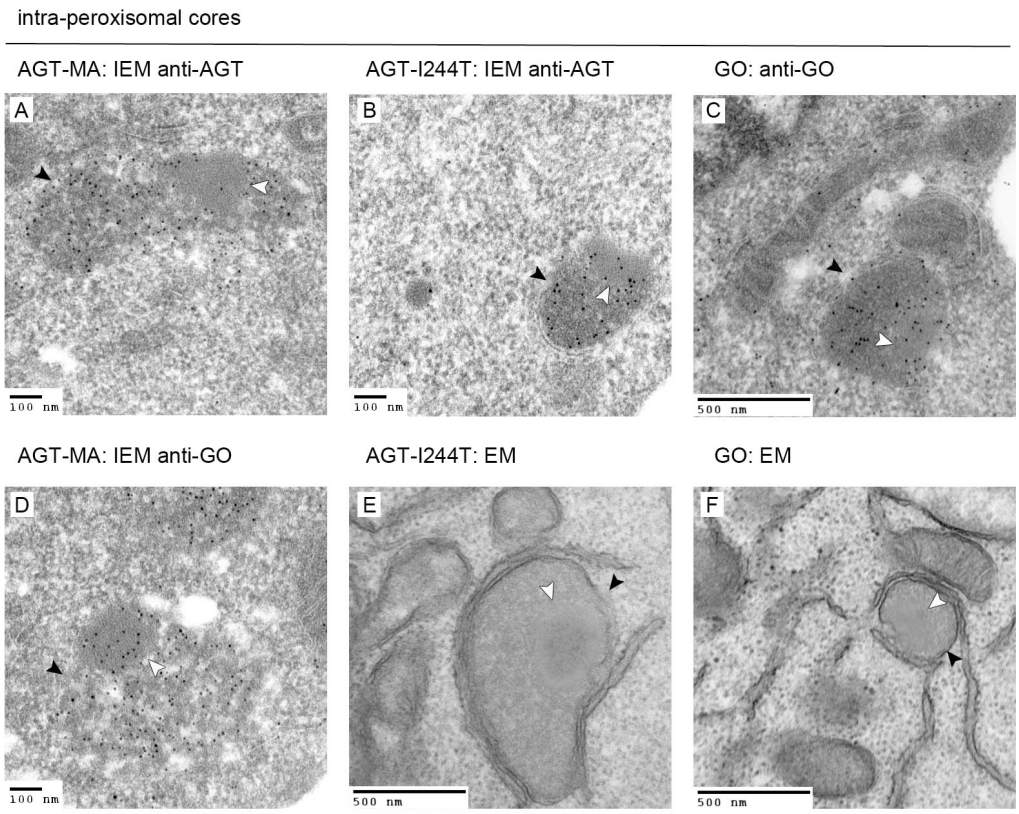

Figure IV-30. **Intra-peroxisomal cores in CHO GO AGT and CHO GO cells as shown by electron microscopy.** A, B: immuno-electron microscopy, staining with anti-AGT (10 nm gold particles); C, D: immuno-electron microscopy, staining with anti-GO (10 nm gold particles); E, F: transmission electron microscopy. AGT-MA: A, D, AGT-244: B, E, GO: C, F Black arrow heads: peroxisomes, white arrow heads: intra-peroxisomal cores (electron microscopy kindly carried out by J Lewin, see Methods III.7).

IV.2.2 Transient transfection in CHO and COS cells – Variability of targeting in transformed cells.

IV.2.2.1 Influence of cell and transfection type on targeting of AGT.

The subcellular targeting of some of the AGT constructs varied in different cell lines when transfection was stable or transient. The two AGT variants where this was clear were AGT-244 and AGT-41. The mitochondrial localization of all mutant constructs was stronger in stable transformants than in transiently transfected cells (Fig IV.31, Table IV.2). There was a difference between cell types also in transient transfection with a stronger mitochondrial localization in CHO compared to COS cells (Fig IV.31). Since both cell types are grown with different culture media (see Methods III.2), the targeting of AGT in CHO cells was studied in the medium used for DMEM, which has a higher vitamin B6 content (Fig IV.31). The mitochondrial targeting of AGT-244 and AGT-41 was stronger in CHO cells grown in their standard medium (Ham's F12) compared to the medium used for COS cells (DMEM). Overall a gradient of mitochondrial *vs*. peroxisomal targeting could be identified taking into account cell type, growth conditions and transfection type (Table IV.2).

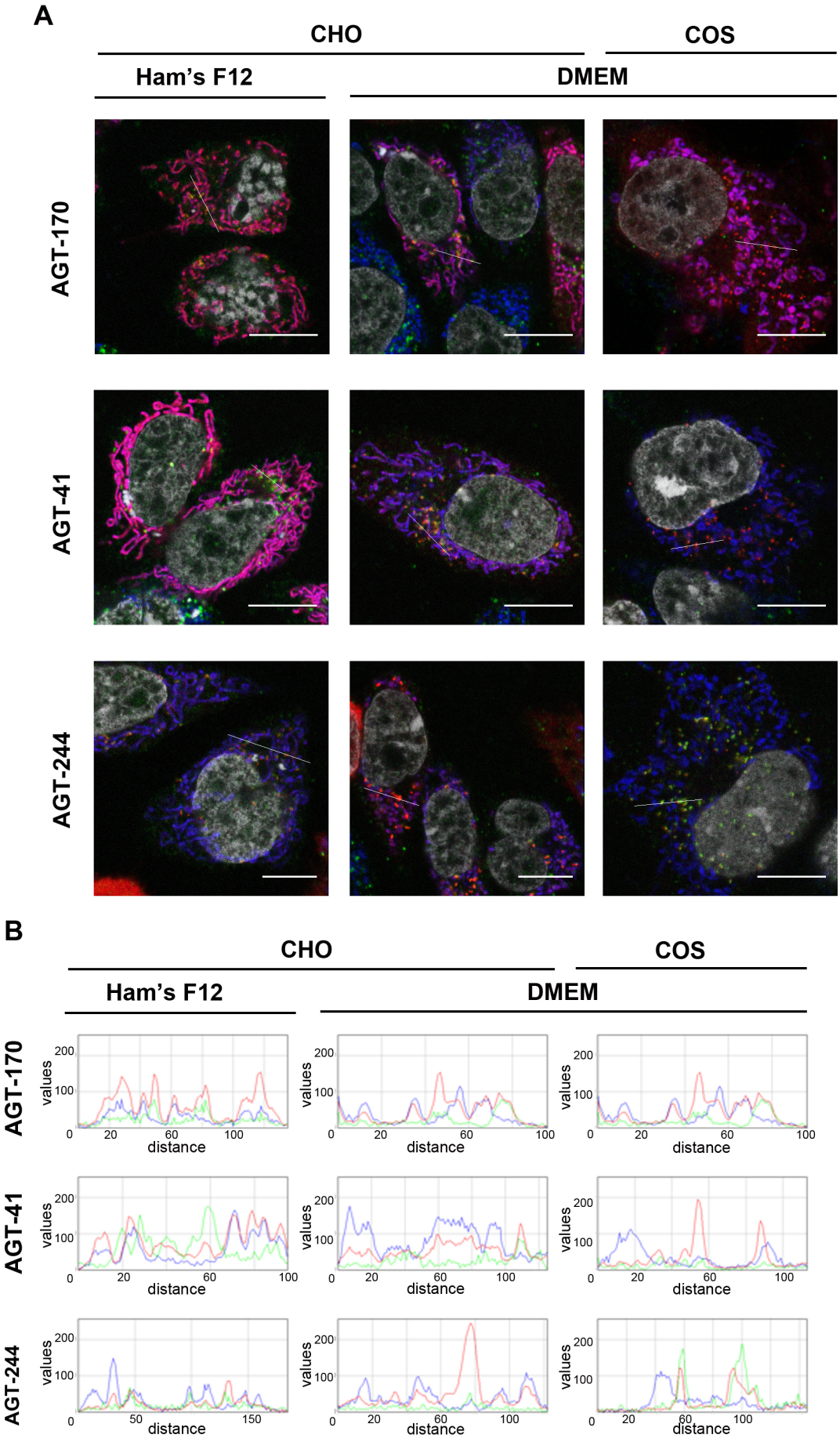

Fig IV.31. **Different subcellular targeting of AGT in transient transfection and in CHO *vs.* COS cells.**

Figure IV-31. **Different subcellular targeting of AGT in transient transfection and in CHO vs. COS cells**. CHO WT cells and COS cells were transiently transfected with AGT variants: AGT-170, AGT-41, AGT-244 and the cells were fixed and immunostained 24 h after transfection. For CHO cells, two different culture conditions were tested: in Ham's F12 (standard conditions for CHO cells) or in DMEM (standard conditions for COS cells). One z-plane only is shown, scale bar: 10 µm. (A): the merged image is shown with AGT in red, peroxisomes in green and mitochondria in blue. (B): RGB profile along the line drawn in the corresponding images in (A).

In the table below (Table IV.2), the behaviour of AGT variants in terms of subcellular targeting is summarized. Whereas agreement was good for normal AGTs, AGT-170 and AGT-152, the localization of AGT-244 and AGT-41 varied. Both appeared more peroxisomal in transient compared to stable transfection and in COS compared to CHO cells. The localization of AGT-244 and AGT-41 in COS cells transiently transfected appeared almost entirely peroxisomal in IMF(Fig IV.31).

Table IV-2. **Subcellular localization of the AGT variants in different mammalian cell systems.** M: mitochondrial localization, P: peroxisomal localization. For liver, the localization is the one found in the published literature in human liver based on electron microscopy. For localization in tissue culture cell lines, targeting was based on immunofluorescence experiments in the present study. Targeting in stable expression was only studied in stable CHO transformants. For expression in transient system, both CHO and COS were studied. The levels of pyridoxine are standard levels (see Methods III.2). For AGT-mi the (-/+) sign indicates that though none (-) was found by IMF, some localization (+) was found by immunelectron microscopy.

	AGT-MA		AGT-mi		AGT-anc		AGT-170		AGT-152		AGT-244		AGT-41	
	M	P	M	P	M	P	M	P	M	P	M	P	M	P
liver [a]	-	+++	+	+++	+++	+	++	+	[+	-] [d]	[+/-	-] [e]	[-	+] [f]
stable CHO [c]	-	+++	-/+	+++	+++	+	+++	+	+++	+	+++	++	+++	+
transient CHO [b]	-	+++	-	+++	+++	+	+++	+	+++	+	+/-	+++	+++	++
transient COS [b]	-	+++	-	+++	+++	+	+++	+	+++	+	-/+	+++	-/+	+++

a, as judged by IEM; b, as judged by IMF; c, as judged by IMF & IEM. For c, the IMF & IEM results were the same except for AGT-mi, which was [M-] by IMF and [M+] by IEM. d & f, extrapolation from compound heterozygotes and heterozygotes (Danpure, 1993); e, IEM on one patient (personal communication P Cochat, University of Lyon, France).

IV.2.2.2 Influence of temperature on subcellular targeting of AGT.

As an indication of the potential to increase the stability of AGT variants, it has been shown previously that lowering the temperature from 37 to 30 ºC caused a shift in the distribution of AGT-170 to a peroxisomal localization in transiently transfected COS cells (Lumb et al., 2003).

In order to see whether the same occurred in CHO cells expressing different AGT mutants, the effect of lowering the temperature (to 30 ºC) on the subcellular targeting of AGT variants was studied in CHO and COS cells transiently transfected under normal conditions (pyridoxine levels those of commercially available standard media, *i*.e. Ham's F12 and DMEM, respectively). The table below (Table IV.3) summarizes the results obtained. All the AGT variants which had a dual mitochondrial & peroxisomal targeting, showed an increase in the proportion of peroxisomal targeting. The effect was true for both cell types, CHO and COS. For identical temperature and transfection conditions, the targeting was more mitochondrial in CHO cells than in COS cells.

Table IV-3. **Effect of lowering temperature on the subcellular distribution of AGT variants**. CHO and COS cells were transiently transfected with AGT variants and placed either at 37 or 30ºC for 2 days before fixing and IMF analysis. The results are expressed qualitatively. Capital P or M: predominant targeting, small p or m: minor targeting, (±): sometimes associated with.

	CHO transient		**COS** transient	
	37°C	30°C	37°C	30°C
AGT-MA	P	P	P	P
AGT-mi	P	P	P	P
AGT-anc	M + p	M + p	M + p	M + p
AGT-G170R	M + p	P ± m	M + p	P
AGT-F152I	M + p	P	M + p	P
AGT-G41R	M + p	P ± m	P	P
AGT-I244T	P ± m	P	P	P

IV.2.3 Summary

AGT could be detected in all cell lines transformed with AGT variants.

The localization of AGT-MA was entirely peroxisomal. The localization of AGT-mi was peroxisomal with a very small fraction of mitochondrial localization only detectable on IEM. The localization of AGT-Δ was entirely peroxisomal. The localization of AGT-anc was both mitochondrial and peroxisomal. The localization of all the mutant AGTs was both peroxisomal and mitochondrial to varying extents. The most mitochondrial of AGT mutants was AGT-170, followed by AGT-152.

Both AGT-41 and AGT-Δ formed intra-peroxisomal cores, the largest seen with AGT-41.

There was a difference in subcellular distribution between transient and stable transformants and between cell lines (CHO, COS cells). The mitochondrial targeting of the AGT mutants was the strongest in stably transformed CHO cells, followed by transiently transformed CHO cells and by transiently transformed COS cells.

The stably transformed cell lines showed a smaller number of peroxisomes, which were also enlarged, compared with CHO WT cells. Small intra-peroxisomal cores staining non-specifically for AGT and GO were often found in transformed cells.

IV.3 Expression of AGT in the different cell lines

The expression of AGT was assessed by immunoblotting in stable CHO cell transformants.

IV.3.1 Expression of AGT in stably transformed CHO cells compared to HepG2 and mouse tissues

In contrast to liver and HepG2 cells (a human hepatic carcinoma derived cell line), CHO WT do not express AGT (Fig IV.32). On a denatured SDS gel, the AGT dimer is resolved as its monomeric sub-unit of approximately 43 kD and dimers between 80 and 110 kD. Non-specific bands are also revealed with the rabbit anti-human AGT, staining between the 52 and 76 kD marker. Compared to HepG2 cells, the level of expression of AGT is much higher in the transformed CHO cells.

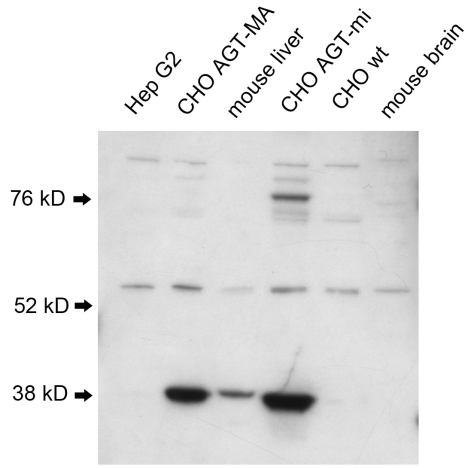

Figure IV-32. **Expression of AGT in different cells and mouse tissues as shown by immunoblotting.** Whole cell extracts from CHO WT, CHO GO AGT-MA and CHO GO AGT-mi cells were compared to HepG2 cells and mouse liver and brain tissue extracts. The same amount of total cell protein (5 μg) was loaded per lane and the membrane was incubated with rabbit anti human AGT. Arrows indicate protein size markers. The band corresponding to AGT is close to the 38 kD size marker, non-specific bands have different sizes.

Despite the high level of staining on the immunoblots (and in IMF and IEM), the transformed CHO cells do not show any modification of the total protein profile when a total protein stain is done on the whole cell lysate (Fig IV.33). No difference can be seen between CHO WT cells and CHO transformed with GO or GO + AGT. In (Fig IV.33), the size of the band expected for AGT is indicated by comparison with immunoprecipitated ^{35}S-labelled AGT (left lane, panel B) and the corresponding flow-through (right lane panel B). This shows that GO and AGT do not substantially interfere with the protein expression machinery as neither GO nor AGT could be detected on the whole protein stained gel.

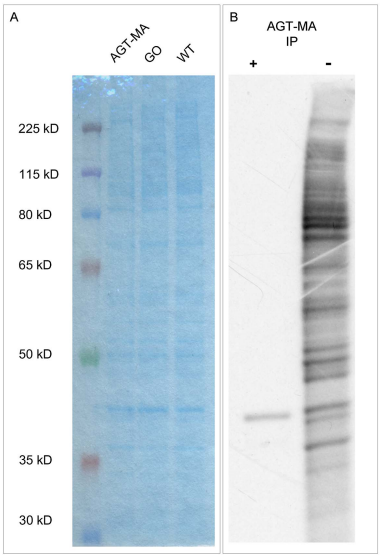

Figure IV-33. **Total protein expression in stably transformed CHO GO and CHO GO AGT-MA cells and non-transformed cells.** A: whole cell lysates from CHO WT cells, CHO GO or CHO GO AGT-MA cells have been fractionated on a SDS-PAGE gel followed by a protein stain (Bluestain). B: CHO GO AGT-MA cells have been labelled with ^{35}S-methionine, the cell lysate was immunoprecipitated and the eluate (+) and flow-through from immunoprecipitation (-) fractionated on a SDS-PAGE gel followed by transfer on a nitrocellulose membrane and exposed to a film. Protein size markers are indicated on the left.

IV.3.2 Level of expression of AGT in the different stably transformed CHO cell lines

A 43 kD band, corresponding to the monomer, could be detected in all types of stably transformed CHO cell lines, except for the AGT-Δ for which the monomer size was approximately 41 kD. The shorter size of AGT-Δ is expected, due to the absence of the N-terminal 21st amino-acids (Fig IV.34 & IV.35).

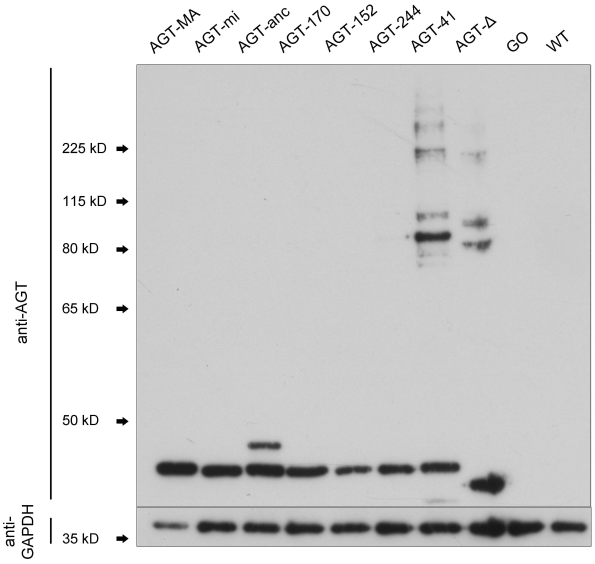

Figure IV-34. **Expression of the different AGT variants in stably transformed CHO cells shown by immunoblotting**. Whole cell lysates were obtained from culture in normal conditions and 2.5 μg of cell protein were loaded on each lane of the gel. The membrane was incubated with guinea-pig anti human-AGT and then with rabbit anti GAPDH as a loading control. Arrows indicate protein size markers

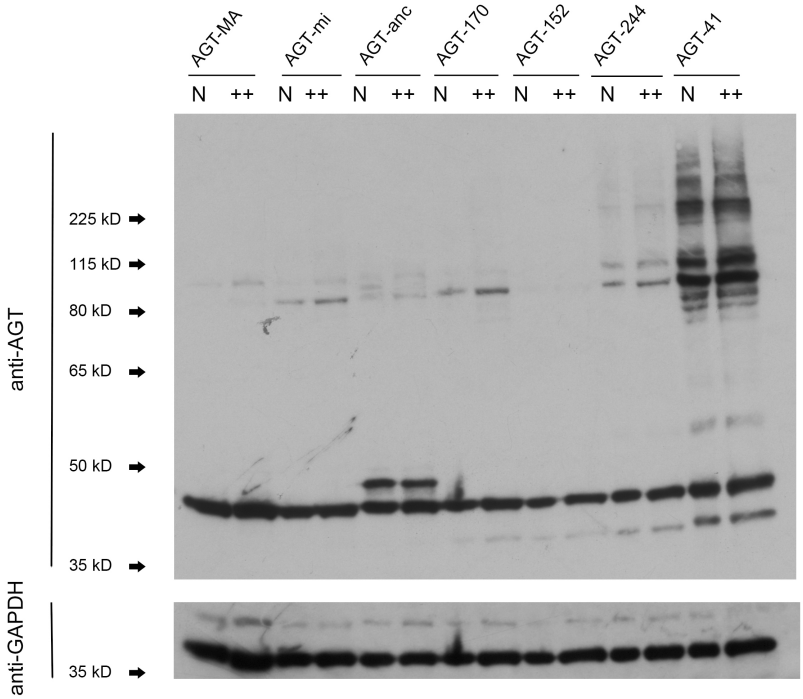

Figure IV-35. **Expression of AGT variants in stable transformants shown by immunoblotting.** Whole cell lysates were obtained from culture in standard culture conditions (N) or with pyridoxine supplementation (250 μM: ++) and 5 μg of cell protein were loaded on each lane of the gel. The membrane was incubated with guinea-pig anti human-AGT and then with rabbit anti GAPDH as a loading control. (see V Results part2). Arrows indicate protein size markers.

In addition to this band, AGT-anc was also present at a higher molecular weight (MW) of approximately 47 kD. This corresponds to the full-size AGT-anc, which has an added N-terminal MTS of 22 amino-acids before post-import intra-mitochondrial cleavage.

Some cell lines showed the presence of a shorter fragment of AGT, around 37 kD. This was the strongest in the AGT-41 cell line, but could also be detected in all the mutants: AGT-Δ (at a correspondingly smaller size), AGT-244, AGT-152 and AGT-170 (Fig IV.35). The shorter AGT fragment could even be detected in the AGT-mi, although at a much lower level and only detectable on gels loaded with more cell protein or overstained (data not shown). Both AGT-41 and AGT-Δ consistently displayed both the normal sized monomer (~ 43 and 41 kD, respectively), a shorter fragment of 37 kD for AGT-41 and less for AGT-Δ, and high MW bands starting at 90 kD/110 kD for AGT-41 (75/85 for AGT-Δ), followed by ~ 170 kD and > 220 kD.

Two specific AGT-staining bands were also detected in most cell-lines between 80 and 115 kD on more loaded or longer stained gels. The exception was AGT-152 for which this was not seen (Fig IV.35). Depending on the allele background (AGT-MA or AGT-mi), the shorter or longer of these two bands was the strongest in the cell lines. In the minor allele background the strongest of the two bands was consistently the lower. The intensity of these higher molecular weight bands was low compared with the ~ 43 kD band, except for AGT-41 and AGT-Δ, for which these high MW bands were as strong (or stronger) than the normal monomer (43 kD). On a couple of gels, bands smaller than the 90/110 kD pair were detected, which might correspond to twice the shorter AGT fragment of 37 kD occasions (Fig IV.35).

The overall level of AGT expression varied for different AGT constructs (Table IV.4). The cell line expressing the highest level of AGT (including all AGT bands) was AGT-41 followed by AGT-anc, AGT-MA, AGT-mi, AGT-170, AGT-244 and AGT-152. When only the full size-monomer was considered (43-47 kD), the cell expressing the highest level was AGT-anc, followed by AGT-MA, AGT-mi, AGT-170, AGT-41, AGT-244 and AGT-152.

Although the relative order of the level of expression of AGT in the cell lines stayed the same, the quantification of the expression of AGT by densitometry analysis showed a high inter-experimental variability.

Table IV-4. **Estimate of the relative expression of AGT in the different cell lines used as assessed by densitometry on immunoblots.** Whole cell lysates of cells grown in normal conditions were immunoblotted and incubated with anti-AGT antibodies. A densitometry analysis was performed on the resulting membrane either exposed to film or to a digital camera. Both monomer and dimer were measured. n: number of experiments. Results are given as mean and range of measures.

AGT		AGT-MA	AGT-mi	AGT-anc	AGT-170	AGT-152	AGT-244	AGT-41
		(n=8)	(n=6)	(n=5)	(n=7)	(n=5)	(n=5)	(n=5)
monomer	mean	99	79	115	65	33	44	63
	min	97	37	37	28	21	30	42
	max	100	116	153	124	49	64	79
total	mean	[100]	82	118	69	34	56	216
	min	100	41	43	34	23	30	70
	max	100	116	160	124	50	92	370

IV.3.3 Presence of very high molecular weight aggregates of AGT

In order to investigate the presence of high MW bands in some cell-lines, whole cell lysates from cells grown under standard conditions were obtained as usual, in a Triton-based lysis buffer, and pelleted at 600g for 10 minutes, to identify the presence of very large aggregates. Both pellets and supernatant were separated on a SDS-PAGE before blotting with anti-AGT. There was no detectable AGT in the pellet of almost all cell lines. The only cell line, which had a significant proportion of its AGT in the pellet fraction was the CHO GO AGT-41R cell line. The profile of the AGT bands was similar in the supernatant and the pellet with both a normal 43 kD monomer and high MW bands detected (Fig IV.36).

This supports the idea that AGT-41 forms large aggregates, which partly break down during the electrophoresis procedure. The same is also true for AGT-Δ.

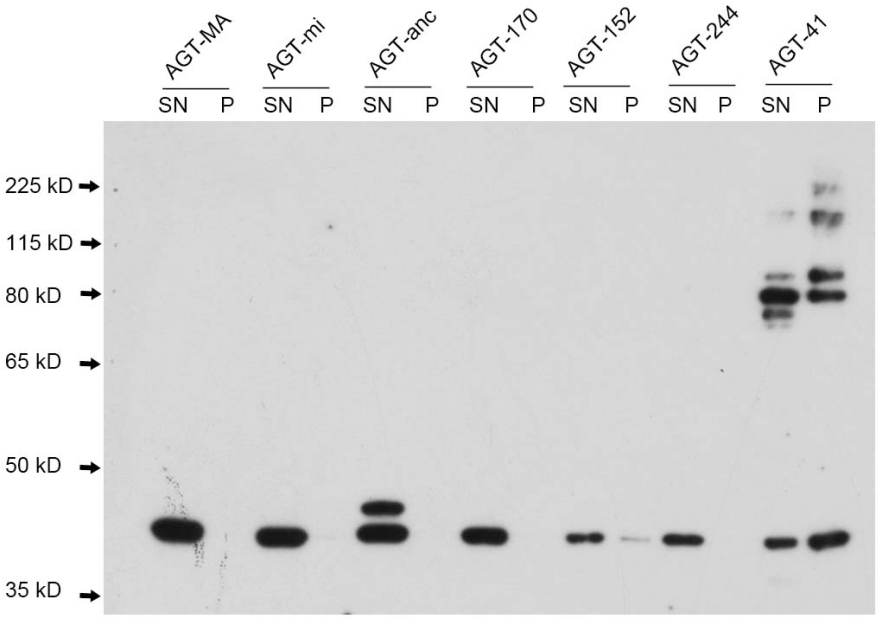

Figure IV-36 **Presence of aggregates of AGT in certain CHO cell lines stably expressing AGT variants.** Whole cell extracts of CHO cells stably expressing AGT variants grown in standard conditions were centrifuged at 600 * g for 10 min and the resulting supernatant (SN) and pellet (P) were immunoblotted against guinea-pig anti human AGT. Each lane was loaded with 5 µg of total cell protein. Arrows indicate protein size markers.

IV.3.4 Effect of cross-linking, urea and SDS on the AGT aggregates

The stability of the AGT aggregates in the CHO GO AGT-41 cell line was studied by adding a detergent (SDS 1%) to the lysis buffer and cross-linking the lysate with BS_3. Whereas AGT dimers of AGT-MA were separated by the addition of SDS, resulting in a greater proportion of monomer compared to dimer after cross-linking, only a small fraction of AGT-41 could be recovered from the aggregate and migrated as monomer or as dimer and intermediate high MW bands (Fig IV.37).

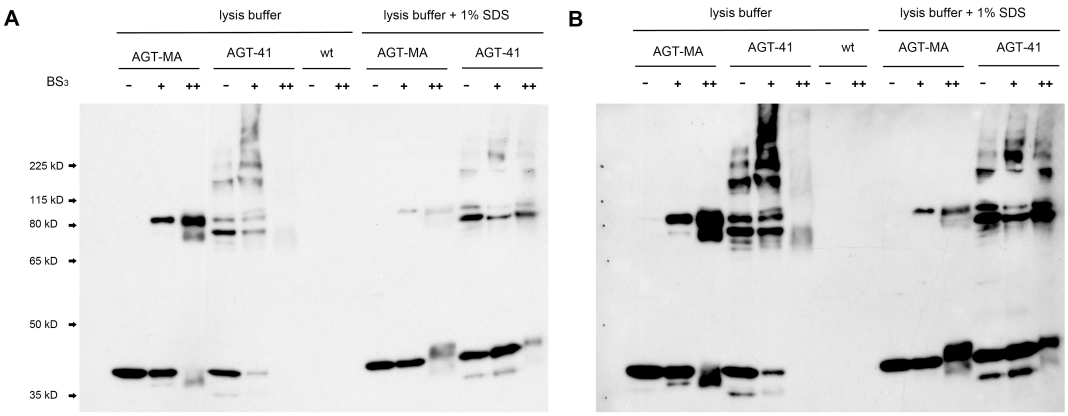

Figure IV-37 **Resistance of high molecular weight bands of AGT-41 to detergents.** Whole cell lysates from CHO GO AGT-MA, CHO GO AGT-41 or CHO WT cells were extracted in the presence or absence of SDS at 1% concentration and cross-linked with BS_3 before being separated by electrophoresis and immunoblotted with rabbit anti-human AGT. BS_3 concentrations: [-]: 0, [+]: 30 µM, [++]: 1250µM. Each lane was loaded with 2 µg of total cell protein. Arrows indicate protein size markers. A and B are short (A) and long (B) exposure of the same membrane. AGT monomers are between the 35 and 50 kD size markers, dimers between the 65 and 115 kD markers.

In addition, AGT-41 non cross-linked lower multimeric bands were of the same size as AGT-MA cross-linked bands (*i.e.* dimer). Higher multimeric bands of AGT-41 had a size compatible with multiples of monomer (43 kD). The AGT-41 aggregate was also resistant to unfolding in urea at 10 M concentration (Fig IV.38).

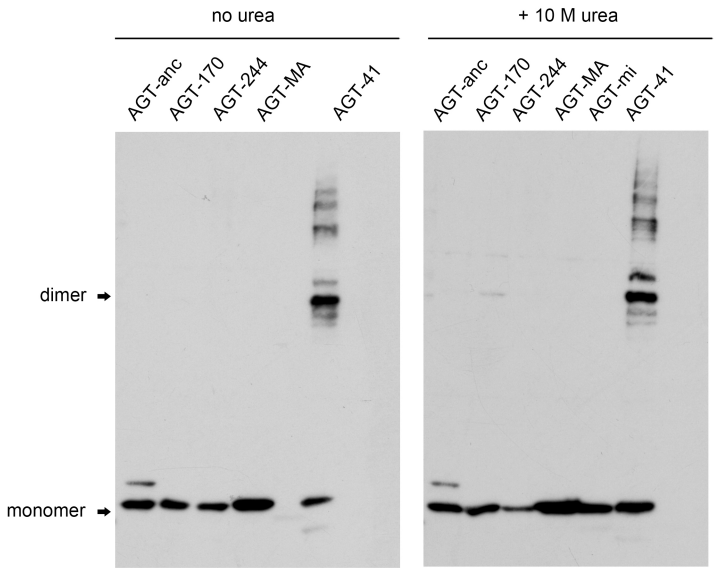

Figure IV-38. **Resistance of high molecular weight bands of AGT-41 to urea denaturation.** Whole cell lysates from CHO cells expressing AGT variants were incubated with 10 M urea at 37ºC for 1 hour. Samples with and without urea denaturation were fractionated on a 10% denaturing polyacrylamide gel in reducing conditions and immunoblotted against rabbit anti human AGT. Arrows indicate protein size markers.

IV.3.5 Summary

AGT was expressed in varying overall levels in all the double transformed CHO cells. A monomer of ~ 43 kD was found in all the AGT expressing cell lines except for AGT-Δ which was shorter and AGT-anc which in addition to the 43 kD monomer, had a larger monomer, ~ 47 kD. Some traces of dimer were detectable in most cell lines and a shorter fragment (< 41kD) in the mutant AGTs. AGT-41 formed very large aggregates.

IV.4 Effect of amino-acid changes on the dimerization of AGT

IV.4.1 Cross-linking of AGT-MA with different cross-linkers

IV.4.1.1 Cross linking AGT

In order to study the state of dimerization of AGT variants in the cells, whole cell lysates were freshly cross-linked after cell lysis and separated on SDS-PAGE before blotting against AGT (Fig IV.39). The efficiency and results of several cross-linkers were compared on AGT-MA. Both monomeric and dimeric forms could be identified. For the AGT dimer, two bands were identified at ~ 90 and 110 kD. These bands were also sometimes visible at low levels on the non-cross-linked AGT mutants (see fig IV.34 – IV.38), suggesting that these bands were small amounts of very stable dimer having escaped the denaturation and monomerization expected during the preparation for SDS-PAGE gel loading.

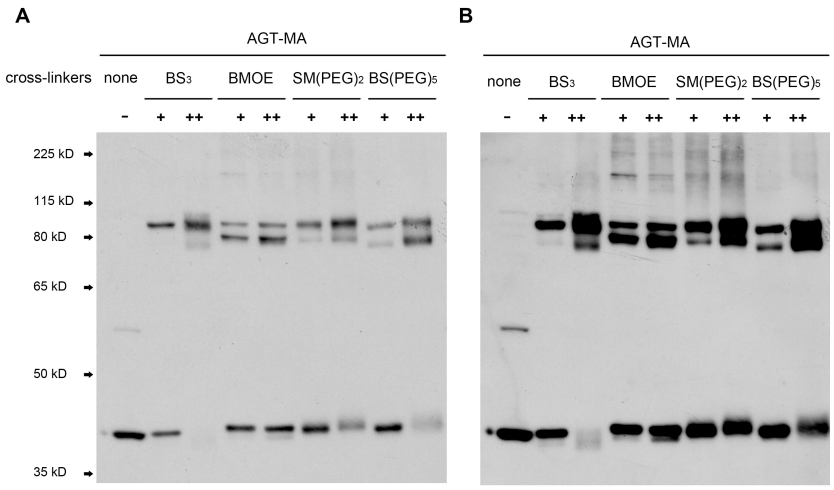

Figure IV-39 **Efficiency of cross-linkers on AGT in CHO GO AGT-MA cells.** Whole cell lysates at 0.25 mg/ml protein concentration were cross-linked with either BS_3 (+: 30 µM, ++: 1250 µM), BMOE (+: 30 µM, ++: 60 µM), $SM(PEG)_2$ (+: 30 µM, ++: 60 µM) or $BS(PEG)_5$ (+: 60 µM, ++: 1250 µM). AGT was visualized by incubation with rabbit anti human AGT. Each lane was loaded with 2 µg of total cell protein. A and B are short (A) and long (B) exposure of the same membrane. Arrows indicate protein size markers.

IV.4.1.2 Cross linking GO

The expression of GO in all transformed cell lines was similar and cross-linking with BS_3 produced bands corresponding both to the dimer and the tetramer (Fig IV.40).

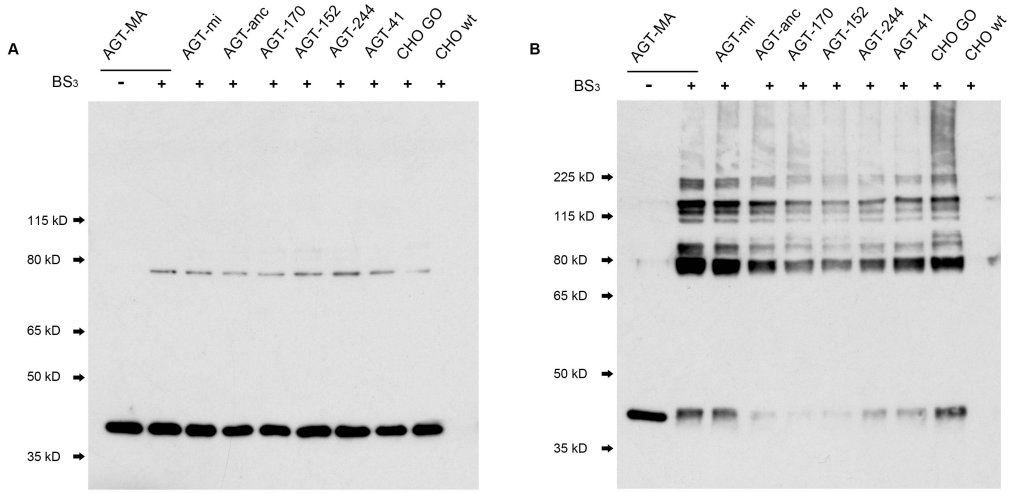

Figure IV-40 **Oligomerization status of GO in the stably transformed CHO cell lines** . Whole cell lysates at 0.25 mg/ml protein concentration were cross-linked (+) with either BS_3 at 30 μM, panel A, or at 1250 μM, panel B. No cross-linker (-). GO was visualized by incubation with rabbit anti human GO. Each lane was loaded with 2 μg of total cell protein. Arrows indicate protein size markers. GO monomers are visible between the 35 and 50 kD markers, dimers between the 65 and 80 kD markers and tetramers between the 80 and 225 kD markers.

IV.4.2 Dimerization status of AGT variants in BSPEG

All the AGT variants, except the AGT-41 produced bands at the expected size for the putative dimer after cross-linking with $BS(PEG)_5$ (Fig IV.41 A&B). As was seen at low levels, without cross-linking in the mutants and after cross-linking AGT-MA, the putative AGT dimer was seen as two distinct bands of ~ 90 and 110 kD. At high concentration of cross-linkers (Fig IV.41 B), higher MW weight bands were seen, which could correspond to cross-linking of forced interaction between AGT dimers with other AGT dimers or other proteins. Cross-linking with BS_3 showed similar results (data not shown).

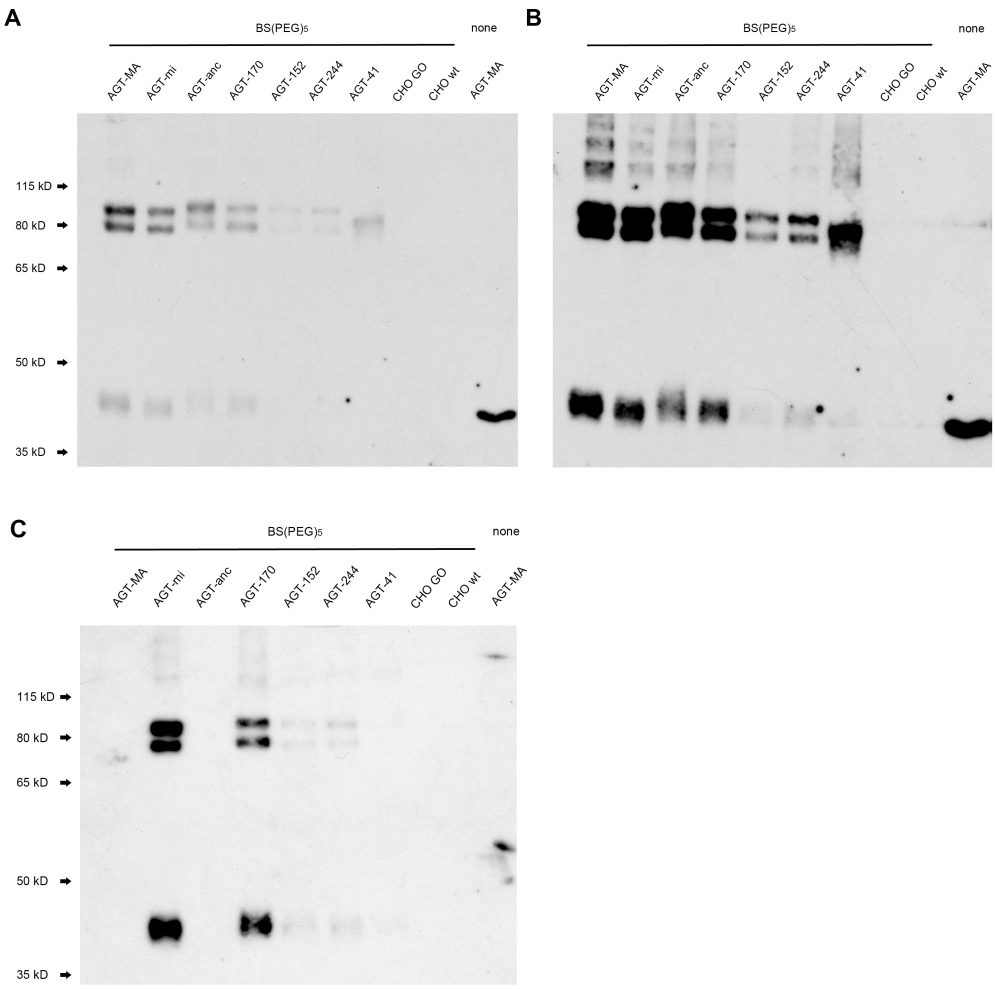

Figure IV-41 **Dimerization status of AGT variants in stably transformed CHO cells.** Whole cell lysates at 0.25 mg/ml protein concentration were cross-linked with $BS(PEG)_5$ at 30 μM and the western blot was incubated with guinea-pig anti human AGT (panel A and B, short and long exposure). Each lane was loaded with 2 μg of total cell protein. A and B are short (A) and long (B) exposure of the same membrane. The same membrane was stripped and re-blotted with a rabbit antibody targeted at the minor allele-specific N-terminus (polypeptide with Leu11) (panel C, bottom). In (C) the dimers for AGT-152 and AGT-244 are only faintly visible at this exposure. Arrows indicate protein size markers.

Using an antibody specific to the N-terminal arm carrying the P11L substitution, both monomer and dimers could be identified in variants on the minor allele, except for the AGT-41 dimer (for AGT-152 and AGT-244, the bands appear faintly in Fig IV.41). The size of the dimer expected to be recognized by the P11L antibody was the same as that of the normal dimer, this result could be explained by a different conformation of the N-terminal arm in a AGT-41 dimer, which would hide the epitope from the antibody. The smaller fragment of AGT usually detectable in AGT-41 was not recognized either by the N-terminal P11L anti-AGT in another experiment (data not shown).

IV.4.3 AGT expressed in cells *vs*. purified recombinant AGT

In order to test whether the two bands of the dimer and the higher MW bands were constituted purely of AGT or associated with other proteins, AGT expressed in cells was compared to purified recombinant AGT (kindly provided by Dr Cellini, Verona).

Both 90 and 110 kD forms of the dimer found in cells could be identified in pure protein after cross-linking (Fig IV.42). In addition, the same higher MW bands found in AGT-41 and AGT-Δ were also found with purified recombinant AGT, suggesting that the high MW bands are exclusively formed out of AGT. The only difference between AGT expressed in cells compared to recombinant AGT was its propensity to form high molecular weight multimers. For both AGT-41 and AGT-Δ, the pattern seen in non-cross-linked lysate from cells was more similar to cross-linked purified AGT. The apparent loss of monomer and dimer in cross-linked cell lysate is most probably due to the fact that AGT-41 and AGT-Δ are cross-linked as large aggregates unable to enter the SDS-PAGE-gel.

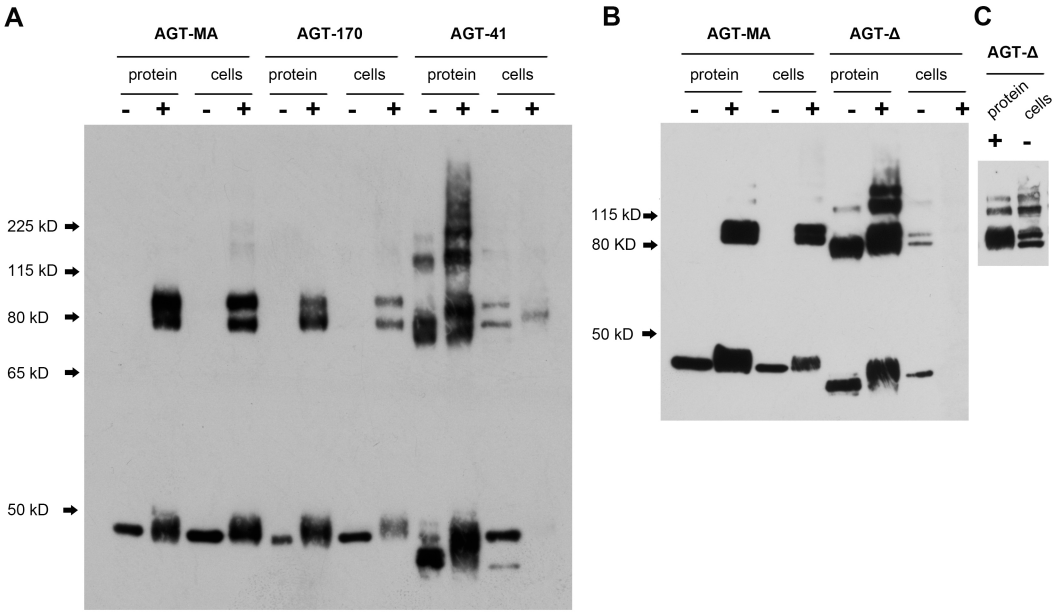

Figure IV-42 **Dimerization status of AGT expressed in CHO cells compared to purified recombinant AGT**. Whole cell lysates from CHO GO AGT-MA, CHO GO AGT-170, CHO GO AGT-41 and CHO GO AGT-Δ cells, at 0.25 mg/ml protein concentration, were cross-linked with $BS(PEG)_5$ at 1250 µM (+) or not (-). The purified recombinant AGT variants AGT-MA, AGT-170, AGT-41, AGT-Δ (kind gift from Dr Cellini, Verona) were cross-linked at 1250 µM. For cell samples 6 µg of protein were loaded per lane, for purified AGT 50 ng were loaded. AGT was visualized by incubation with guinea-pig anti-human AGT. Panel A: AGT-MA, AGT-170, AGT-41. Panel B AGT-MA and AGT-Δ. Due to different levels of AGT expression in cell lines, the inset in (C) shows the results of a repeated experiment from the experiment shown in (B) after adjusting for different level of protein expression. Arrows indicate protein size markers.

IV.4.4 Summary

Dimers of AGT were detected in all AGT expressing cell lines. Electrophoresis of purified recombinant AGT show that the AGT dimer appears to exist as two respective bands, possibly due to the existence of different conformers. Both AGT-41 and AGT-Δ form very large multimers of pure AGT. Those aggregates form more easily in the cell environment than in purified recombinant protein.

IV.5 Stability of AGT variants on pulse chase analysis

The turnover of the different AGT variants was studied by pulse-chase analysis. Transformed CHO cells were grown under standard conditions and labelled with ^{35}S-methionine. The cell lysates at different chase times were immuno-precipitated with rabbit anti-human AGT. The level of labelled AGT was quantified by autoradiography and densitometry. The half-life was calculated, based on the standard assumption that the level of decay of the radio-labelled protein over time follows a rate that is proportional to the removal rate (Methods III.13).

IV.5.1 Half-life of AGT variants

The turnover of AGT-MA was studied over time periods ranging between 1 h and 72 h. Since several cell divisions will have occurred by 72 h, the total amount of AGT present in the cell lysate increases. The radio-labelled AGT, however does not. There was only a small decrease in ^{35}S-AGT over the 72 h period, suggesting that the half-life of AGT-MA in CHO cells is longer than the length of time of the experiment (Fig IV.43, Fig IV.44).

Given such technical limits, no reliable half-life calculation can reasonably be determined for AGT-MA (Table IV.5), except to say that $t_{1/2}$ (AGT) > 72 h.

For AGT-mi and AGT-170, a degree of decay was observed over the 72 h, although the spread of data points makes the reliability of the half-life questionable. Therefore, the half-life of these variants was categorized as long (FigIV.43, Fig IV.44, Table IV.5).

No decrease could be reliably discovered for AGT-anc either over 24h studied for this variant.

Both AGT-152 and AGT-244 showed a marked decrease over the 24 h period studied with a shorter estimated half-life than AGT-MA.

By contrast, the decrease of AGT-41 occurred immediately and very rapidly, with an estimated half-life < 6 h (FigIV.43, Fig IV.44, Table IV.5).

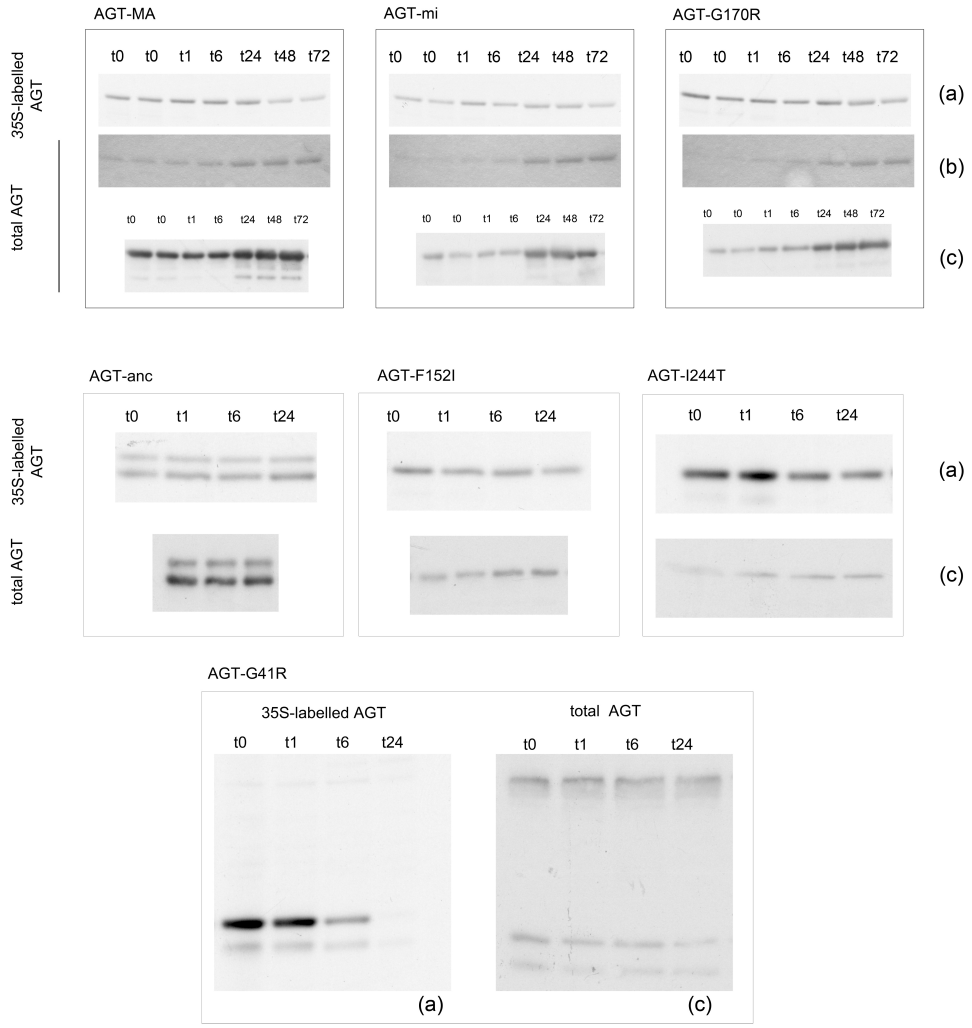

Figure IV-43 **Turnover of AGT variants in stably transformed CHO cells assessed by pulse-chase analysis over 72h.** CHO GO AGT-MA, CHO GO AGT-mi and CHO GO AGT-170 and CHO GO AGT-anc, CHO GO AGT-152, CHO GO AGT-244 cells were pulse-labelled with ^{35}S-methionine and harvested at different chase times. The cell lysate were immunoprecipitated with rabbit anti-human AGT before being separated on a SDS-PAGE gel. Immunoprecipitated samples were analysed by autoradiography (a) (after being stained for total (AGT) protein (b) and dried); other samples were run on SDS-PAGE and immunoblotted with guinea-pig anti AGT (c). The same volume was loaded in each lane of each gel: 10 µl for (a) and (b), 1 µl only for (c).

Table IV-5 **Calculated half-lives of AGT variants in stably transformed CHO cells**. The equation for the linear regression was extracted from pulse-chase experiments (Annexe IX.8) and used to calculate degradation rates and the half-lives ($t_{1/2}$). n: experiments included in the analysis.

		AGT-MA (n=5)	AGT-mi (n=2)	AGT-G170R (n=3)	AGT-anc (n=1)	AGT-F152I (n=2)	AGT-I244T (n=2)	AGT-G41R (n=2)
t 1/2	**calculated (h)**	1873.4	51.8	36.4	28.2	21.7	26.9	3.1
	category	long	long	long	long	intermediate	intermediate	short

Two groups of AGT variants could be identified. The first was a group of stable AGTs, including AGT-MA, AGT-mi and AGT-anc, with long half-lives. A second group of less stable AGT mutants was composed of AGT-170, AGT-152 and AGT-244 with long or intermediate half-lives, contrasting with a very unstable AGT mutant: AGT-41 with a very short half-life. It can be noted from the pulse-chase graph (Fig IV.44) that the decrease of AGT-41 appeared to follow two steps: a first decrease occurring during the first 12 h and a slower decrease over the remaining time. Since all of the mutants, including AGT-41, can be detected with other techniques in CHO cells, the remaining AGT may be more stable either by virtue of its conformation or its subcellular localization.

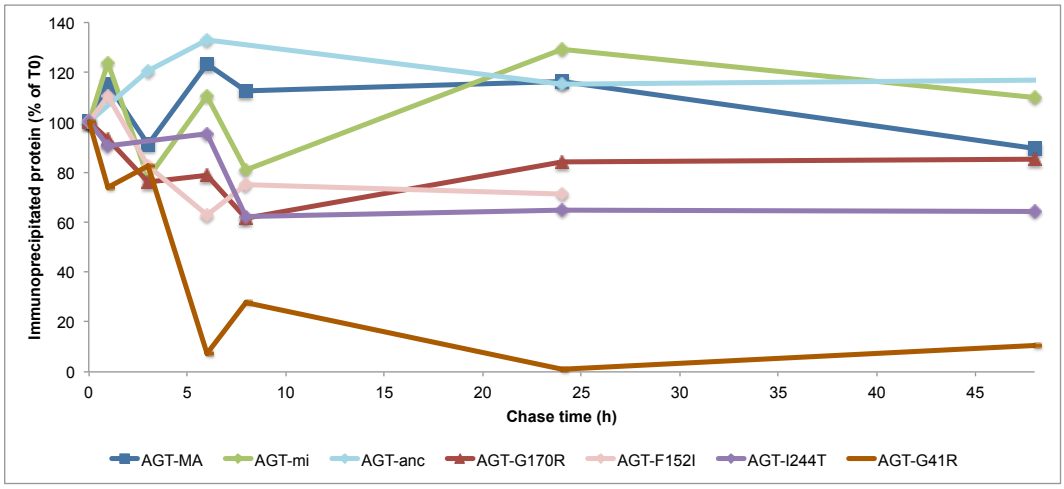

Figure IV-44. **Kinetics of degradation of AGT variants in stably transformed CHO GO AGT-MA, CHO GO AGT-mi, CHO GO AGT-anc, CHO GO AGT-170, CHO GO AGT-152, CHO GO AGT-244 and CHO GO AGT-41 cells.** The mean intensity of immunoprecipitated ^{35}S-labelled AGT at different chase time (Methods III.13) are plotted on the y axis (in % of intensity at t = 0h) for each chase time (x axis, h). The intensity was determined by densitometry analysis (Methods III.10).

IV.5.2 Summary

The half-life of AGT-MA, AGT-mi and AGT-anc was long and could not be precisely determined. The half-life of AGT-170, AGT-152 and AGT-244, though long was shorter than AGT-MA. The half-life of AGT-41 was very short.

IV.6 Catalytic activity of AGT variants in stably transformed CHO cells

IV.6.1 GO activity

All stably transformed CHO cell lines expressed similar amounts of GO and the activity of GO in cells was comparable, within a 64 to 107 % that of the CHO GO AGT-MA cell line (Fig IV.45, Table IV.6). The GO assay showed more variation than the AGT assay, even within a single cell line. This might be related to slight changes of GO expression at the different times of harvesting the cells or to a variability inherent to the technique of the assay itself (quality of the dialysis and removal of GO inhibitors in the cell lysate). The variability of GO expression between cell lines can be attributed to the effect of re-cloning the cell lines.

IV.6.2 AGT activity

IV.6.2.1 AGT activity in the presence of PLP in the assay

The intra-assay variability of the AGT assay was low but the variability between experiments was greater, although it stayed within a specific range characteristic for each construct (Fig IV.45, Table IV.6, Table IV.7, Annexe IX.9).

The activity of AGT was lower in CHO GO AGT-mi cells than it was in CHO GO AGT-MA cells (60%) but this does not take into account the different levels of AGT protein in the cell lines. The levels of AGT-mi expressed were lower than that of AGT-MA. An estimate of the specific catalytic activity of AGT variants (table IV.7) was carried out using the levels of expression determined by immunoblotting (see section IV.3). Different sets of experiments using different protocols were used for the determination of catalytic activites and levels of AGT expression. The corrected specific activity estimate for AGT-mi was similar to that of AGT-MA. The same was true for AGT-anc.

The uncorrected activity of AGT in CHO GO AGT-G170R cells was lower than in CHO cells expressing normal AGTs, but still significant. After correction, the estimated specific activity of AGT-170 remained lower than that of normal AGT but higher than the other mutant AGTs. The activity of AGT in CHO GO AGT-152 and CHO GO AGT-244 was low but still detectable and reached half that of AGT-MA in the estimated specific activity.

Even though AGT was expressed at levels comparable with CHO GO AGT-MA, the activity of AGT in CHO GO AGT-41 and CHO GO AGT-Δ was below detection level.

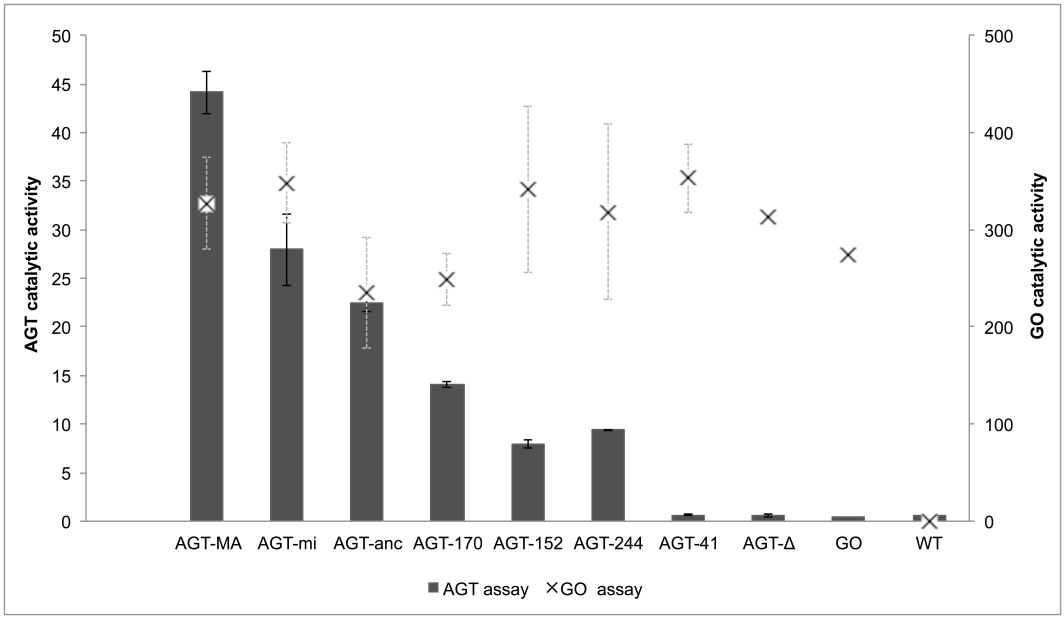

Figure IV-45 **AGT and GO catalytic activities in stably transformed CHO cell lines**. AGT activity in µmol pyruvate/h/mg of cell protein, GO in nmol/min/mg cell protein. The AGT assay was carried out in standard conditions (*i.e.* with added PLP at 150 µmol/l). The results are given as means ± ½ SD of several assays, n (number of experiments) between 3 and 9 for GO and AGT assays. Grey histograms: AGT activity; crosses: GO activity, vertical lines: ½ SD.

Table IV-6 **AGT and GO catalytic activities in stably transformed CHO cell lines**. AGT activity in µmol pyruvate/h/mg of cell protein, GO in nmol/min/mg cell protein. The AGT assay is carried out in standard conditions (*i.e.* with added PLP at 150 µmol/l). The results are given as means ± SD of several assays. References are activities in human liver (Rumsby et al., 1997). The limits of sensitivity of the AGT and GO assays are 3 and 4 respectively. The statistical significance of decreased activity of AGT variants compared to AGT-MA assessed by Student's test is marked with asterisks: (*) p< 0.05; (**) p< 0.01; (***) p< 0.001.

		CHO									
		AGT-MA (n=9)	**AGT-mi** (n=9)	**AGT-anc** (n=5)	**AGT-170** (n=7)	**AGT-152** (n=5)	**AGT-244** (n=5)	**AGT-41** (n=5)	**Δ1-21** (n=3)	**GO** (n=8)	**WT** (n=9)
AGT umol pyruvate/h/mg protein	mean	44.1	27.9	22.5	14.0	7.9	9.4	0.6	0.5	0.4	0.6
	SD	11.2	5.7	7.7	1.8	0.8	2.2	0.2	0.1	0.2	0.3
	% of AGT-MA cell line	[100]	63.3	50.9	31.8	17.9	21.2	1.3	1.1	0.9	1.3
ref range in human liver	19.1-47.9		**	**	***	***	***	***	***	***	***
GO nmol/min/mg protein	mean	327.0	348.2	235.5	249.1	340.9	318.2	313.7	299.0	274.6	0.1
	SD	75.1	112.1	95.9	153.1	54.2	170.9	182.8	42.0	119.4	0.4
	% of AGT-MA cell line	[100]	106.5	72.0	76.2	104.2	97.3	95.9	91.4	84.0	0.0
ref range in human liver	13.2-101.6										***

Table IV-7 **Estimated specific AGT activity in stably transformed CHO cells.** The level of expression of AGT in each cell line was estimated by densitometry analysis on immunoblotting with anti-AGT (mean and range normalized against AGT-MA expression) and the mean activity of AGT for each cell line was corrected by that factor. The statistical significance of decreased expression of AGT variants compared to AGT-MA assessed by Student's test is marked with asterisks: (*) p< 0.05; (**) p< 0.01; (***) p< 0.001.

		CHO						
with AGT		**AGT-MA** (n=5)	**AGT-mi** (n=5)	**AGT-anc** (n=3)	**AGT-170** (n=5)	**AGT-152** (n=3)	**AGT-244** (n=3)	**AGT-41** (n=3)
	AGT expression (mean)	1.00	0.82	1.18	0.69	0.34	0.56	2.16
	range	[1]	(0.41 - 1.16)	(0.43 - 1.60)	(0.34 - 1.24)	(0.23 - 0.50)	(0.30 - 0.92)	(0.70 - 3.70)
					*	***	*	
	estimated specific AGT	[100]	77.5	43.1	45.8	53.1	38.1	0.6

IV.6.2.2 AGT activity in the absence of PLP in the assay

In order to characterize the properties of AGT variants and the relative presence of apo- and holo-enzyme, the AGT assays were performed with and without added PLP in the assay (Fig IV.46). When the AGT assay is carried out with added PLP, the concentration of PLP in the sample is of a minimum of 150 µmol/l (150 µmol/l in addition to the PLP bound to AGT and present in the cell lysate). At this concentration, it has been shown that the activity of AGT is at its maximum (Wanders et al., 1990). Therefore what is assayed is the maximal activity of a given AGT variant.

There was no marked difference for all the active AGTs ([-PLP/+PLP] ratios from 0.7 to 1.1) apart from AGT-152, which lost all activity without addition of PLP ([-PLP/+PLP] ratio of 0.13), suggesting that all the AGT-152 is in apo-form in the cell lysate.

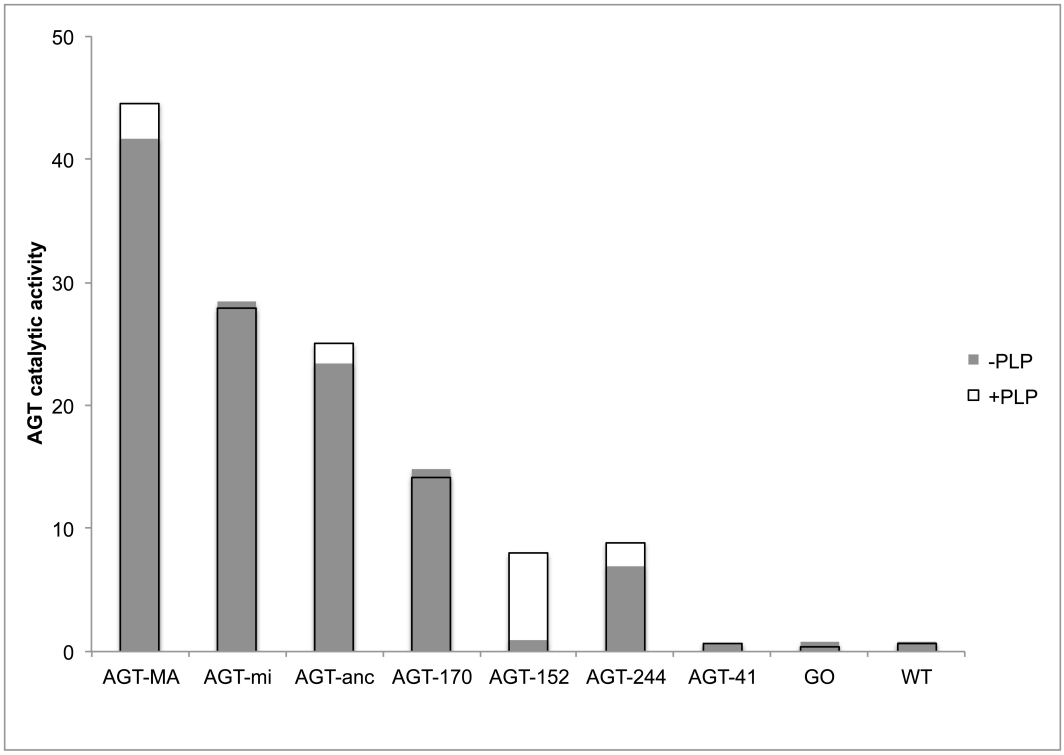

Figure IV-46 **Effect of presence or absence of PLP in the enzyme assay on the average catalytic activity of AGT in stably transformed CHO cell lines.** Empty histogram: activity in the presence of added PLP in the assay (150 μmol/l), shaded histogram: activity without added PLP in the assay. AGT activity in μmol pyruvate/h/mg of cell protein, The AGT activity in the presence of PLP is the same as in (Fig IV.45 & table IV.6). The results are given as means of several assays (4 to 8, see Annexe IX.10).

IV.6.3 Summary

All the CHO cells transformed with GO had GO catalytic activity in a comparable range.

The AGT activities in all the double transformants varied. After correction for the level of expression of AGT in the cell lines, a specific AGT catalytic activity was derived. The normal AGTs had similar activities, and AGT-mi had slightly higher specific activity than AGT-MA. There were three mutant AGTs with detectable activity: AGT-170, which had the highest AGT activity of all mutants, AGT-152 and AGT-244 with similar activities. Neither AGT-41 nor AGT-Δ had any AGT activity at all.

In the standard conditions of cell culture, there was no difference in the AGT activity whether the assay was done with added PLP or not, except for AGT-152 which lost all activity in the absence of added PLP in the assay.

IV.7 Discussion of Results Part 1

IV.7.1 AGT subcellular distribution

The subcellular localization of some AGT variants has been described in the literature in different settings. For AGT-MA, AGT-mi and AGT-170, the subcellular localization is known in human liver as well as in tissue culture cells transiently transfected (COS). The localization in the stably transformed CHO cells was similar to what was expected from the previous studies with a few minor exceptions. The localization of AGT-mi was known to be peroxisomal in cells and human liver with 5% localized to mitochondria in IEM studies of liver (Purdue et al., 1990). The results shown here agree with both since the IMF localization was apparently entirely peroxisomal but IEM study of the cells showed the presence of higher than background staining for AGT-mi in the mitochondria. This highlights the difference in sensitivity of the two techniques, IEM being more sensitive than IMF.

The targeting of AGT-anc was dual, both peroxisomal and mitochondrial, as was expected (Oatey et al., 1996). For AGT-170, the localization in CHO cells was mostly mitochondrial as expected from previous work (Purdue et al., 1990; Leiper et al., 1996). However, the respective amounts of mitochondrial and peroxisomal AGT-170 did vary to some extent between experiments over time, possibly partly due to changing experimental conditions discussed later (Results Part 2). The localization of the other mutants was not definitively known, however. The localization of AGT-152 was supposedly mitochondrial. This relied on the analysis of compound PH1 heterozygotes and healthy heterozygotes (Danpure et al., 1993). The targeting of AGT-152 in the transformed CHO cells confirmed this hypothesis and demonstrated that AGT-152 is mostly mitochondrial, although like AGT-170, a peroxisomal fraction is still seen as well. The current knowledge on AGT-41 and AGT-244 localization suggested that they would be peroxisomal. This relied on transient transfection in COS cells for AGT-244 as there is no published data on localization in liver. However, there might be some indication that in liver, where expression is more similar to stable transfection than transient expression, AGT-244 might be localized in peroxisomes (IEM in one liver of one PH1 patient homozygote for AGT-244, Cochat, personal communication). The dual localization of AGT-244 to peroxisomes and mitochondria in the stably transformed CHO cells, is surprising. But the localization of AGT-244 was also strongly, and sometimes mostly, peroxisomal as was seen in transient transfection experiments. The localization of AGT-41 to both peroxisomes and mitochondria was also very surprising as the localization inferred from PH1 compound heterozygotes and carrier heterozygotes suggested that it was peroxisomal and formed intra-peroxisomal cores (Danpure et al., 1993). The mitochondrial localization was stronger for AGT-41 than for AGT-244 and less than for AGT-170 and AGT-152.

Overall, some degree of mitochondrial localization was seen in all the stable CHO cells expressing the four mutant AGTs and even in AGT-mi as well as the AGT-anc which has a normal MTS. The mitochondrial localization of the mutants results from the presence of the P11L polymorphism, which creates a new MTS. The fact that AGT-mi on its own only directed a very small amount to mitochondria emphasizes the necessity of a synergy between the Leu11-MTS and an additional factor. This second factor, in this case the additional presence of a mutation on AGT, is needed to allow the mitochondrial targeting to take place in competition with the peroxisomal targeting mediated by the PTS1.

More factors seemed to be involved as well, since the mitochondrial targeting varied depending on whether the transfection was transient or stable in some of the CHO cell lines for some AGT variants (AGT-244 and AGT-41 to a lesser extent). Some difference was also found between cell type: CHO or COS in transient transfection experiments. CHO cells seemed to favour mitochondrial targeting compared to COS cells. It is difficult to compare the situation of COS or CHO cells with liver since the data on the localization of some of the mutants is not definitively known, but it would seem that the situation in liver may be closer to what is seen in COS cells, with less of mitochondrial targeting. The targeting in other cell lines has not been studied here but might prove useful. At least two factors could explain the difference of behaviour of cell lines. The first factor is the level of protein detected with the method used. As was seen for AGT-mi, IMF is less sensitive than IEM and the absence of detection of mitochondrial localization by IMF does not exclude the possibility of detection by IEM of lower levels of mitochondrial localization. This means that mutant AGTs expressed in COS cells may still have significant mitochondrial targeting but relatively less than in CHO cells. The second factor is the total level of protein detectable and available for staining. The immunoreactivity of most mutant AGTs in PH1 patients' livers is often much lower than normal AGT, consistent with an instability of mutant AGT leading to degradation (G Rumsby, London, personal communication) (Danpure, 1991; Danpure et al., 1994c). In contrast the immunoreactivity of mutant AGTs in both COS and CHO cells was similar to normal AGT although the number of copies of plasmids in the cells may vary between cell lines since they are episomal vectors. This could indicate that the degradation of mutant AGT occurs at a lower level in CHO and COS cells than in liver, allowing detection of otherwise low levels of degraded AGT (notably AGT targeted for mitochondria). A third explanation could be the level of vitamin B6 available in the cell if vitamin B6 could play a role in targeting and protein stabilisation as has been suggested. In fact liver cells have high levels of B6 vitamers (Coburn, 1990). The standard media used for cell culture vary widely in terms of vitamin B6 content. Whereas the medium used for CHO cells (*i.e.* Ham's F12) contains 0.3 μM pyridoxine hydrochloride, the medium used for COS cells (*i.e.* DMEM) contains approximately 20 μM, over 50 times more. Lastly, the organelle protein import kinetics and capacity, the organelle half-life and protein half-life may play a role in the final visualized localization of a given protein.

The factors involved in the targeting of proteins with more than a single subcellular localization are complex. In the case of AGT on the background of the minor allele, the protein has two competing targeting signals, a C-terminal PTS1 and a N-terminal Leu11-MTS. The potential of the Leu11-MTS to act as an MTS has been shown not only by the 5% of mitochondrial AGT-mi in human liver (Purdue et al., 1990) but also by the efficient mitochondrial targeting of Leu11-MTS-GFP constructs (Leiper et al., 1996; Lumb et al., 1999). Other authors have shown that the speed and stability of dimerization, a conformation incompatible with mitochondrial import, plays a crucial role in the mitochondrial targeting of proteins (other than AGT) that have dual targeting (mitochondrial + other) (Strobel et al., 2002). The hypothesis put forward by Lumb *et al.* was that with Leu11-MTS only, the kinetics of folding and/or dimerization of AGT are in favour of peroxisomal versus mitochondrial targeting (Lumb et al., 1999). When the G170R mutation is added to the Leu11-MTS, this balance is upset, *i.e.* folding and dimerization are slower, and the folding kinetics are in favour of mitochondrial targeting. Since some substitution mutations on proteins are expected to result in less stable proteins, which could lead to the same result as the G170R change on the AGT-mi background, it was therefore surprising that the mistargeting of mutant AGT on the minor allele background did not always result in mitochondrial targeting for all mutant constructs.

The results discussed here demonstrate that the potential of the P11L substitution in the N-terminus of AGT to act as a MTS is indeed general and that a slight perturbing of the folding/dimerization kinetics is indeed enough to send the protein to mitochondria. This may be more easily visualized in CHO cells than COS or liver cells because of a lesser AGT degradation.

Lowering the temperature has been used to stabilize proteins and was shown to retarget all AGT-170 in peroxisomes in transiently transfected COS cells (Lumb et al., 2003). In the present study, lowering the temperature increased the peroxisomal targeting of all four mistargeting mutants in transiently transfected CHO and COS cells and even completely normalized the targeting of all the AGT mutants in COS cells. This demonstrates that protein stabilization is an important factor in the final destination of AGT for all the mutants concerned, but the difference between CHO and COS reinforces the idea that other factors are still involved.

The stably transformed CHO cells showed signs of small peroxisomal morphological changes with a lesser number and larger size of peroxisomes compared to CHO WT. The peroxisomes in transformed cells often contained small intra-peroxisomal cores non-specifically staining with AGT and seeming to also react with GO, although possibly non-exclusively. This could be due to the overexpression of the two peroxisomal proteins in a compartment of limited size. The peroxisomal turnover might be slowed as some AGT constructs appeared to have half-lives longer than the peroxisomal half-life (1-3 days) determined in other systems (Poole et al., 1969). However the overall viability of cells was not impaired and peroxisomal targeting was

maintained and these changes probably have no significant impact on the conclusions drawn in the present study.

A different form of intra-peroxisomal cores was detected in two cell lines: CHO GO AGT-41 and CHO GO AGT-Δ. The presence of intra-peroxisomal cores has been described on IEM in the liver from patients with PH1 carrying at least one allele with the G41R mutation (Danpure et al., 1993). The formation of intra-peroxisomal cores was found in the CHO GO AGT-Δ cells as well. It has been shown on purified recombinant protein that AGT-41 is prone to aggregation and the very large intra-peroxisomal cores detected in CHO cells could be large aggregates of AGT-41 (Cellini et al., 2010b). The other AGT variants, which have been shown to be unstable, like AGT-41, is AGT-Δ (Montioli et al., 2012). The subcellular localization of AGT-Δ was peroxisomal, as expected from the presence of a PTS1 and absence of the first 21 amino acids of the N-terminus. In CHO GO AGT-Δ cells, intra-peroxisomal cores were detected, although their size was much smaller than those in CHO GO AGT-41 cells. There were no cytosolic or mitochondrial cores detected for any of the constructs, which could be either because the conditions for their formation are not met or because they are degraded.

The co-localization analysis in the cells relied on study of merged images and also on global statistics methods, with co-localization coefficients of Pearson and Manders. Manual thresholding was performed in order to selectively identify the structures of interest: peroxisomes and mitochondria. Automated methods of thresholding proved unable to deal with some of the intrinsic characteristics of the system: background staining probably due to some cytosolic staining (GO and anti-peroxisomal proteins antibodies mostly - some of which is catalase - possibly due to slow uptake kinetics) and the dual targeting of AGT with possible different intensities between compartments and cells. Object-based methods using the JACoP plugin of ImageJ (Bolte and Cordelières, 2006) were also performed and confirmed the conclusions drawn with other methods (data not shown).

The stable transformed cell system does not allow a direct study of folding, dimerization and organelle uptake kinetics but rather the long-term result of such. The suspected lesser capacity of protein degradation in CHO cells may, in fact, be useful here in that it allows us to detect the fate of some AGT variants, which would otherwise be of too low a level to be detectable. Such knowledge, however, may be of importance when trying to find pharmacological treatments for PH1.

IV.7.2 Expression and dimerization of AGT

The stably transformed CHO cells over-express AGT and GO. If the level of AGT or GO protein was excessively high, this could potentially interfere with the normal metabolism of the cells. However, neither AGT nor GO could be detected by a non-specific protein stain of a whole cell lysate, which indicates that levels of AGT or GO remain minimal compared to the other cell proteins.

All transformed cell lines expressed GO and all double transformants expressed AGT as well. The level of AGT varied between cell lines in a consistent manner for each cell line with CHO GO AGT-MA displaying the highest level of AGT. The expression of AGT in the CHO cells allowed detection of significant amounts of AGT mutants, which are usually only detectable at low levels in the livers of patients. The reason for that could be a lower efficiency of the degradation machinery in CHO cells compared to hepatocytes.

The AGT-anc presented as two different sized monomers on immunoblotting. The main form was a normal-sized monomer of ~ 43 kD compatible with cleavage of the N-terminal MTS, after mitochondrial import and the other, smaller fraction, was a larger monomer of ~ 47 kD. The intra-cellular localization of the 47 kD monomer could be the peroxisome which is not equipped with proteases cleaving the MTS.

The mutant AGTs on the minor background showed the presence in addition to full-size monomers of ~ 43 kD, a shorter fragment of AGT, ~ 37 kD (smaller for AGT-Δ). This shorter fragment was more obvious in the more unstable mutants (AGT-41, AGT-Δ). The short fragment of AGT did not stain with an antibody against the N-terminus of AGT suggesting that the shorter size resulted from either a removal of some of the N-terminal part of AGT or that the N-terminus was not accessible by being hidden in the folded shorter protein. A limited proteolysis of AGT has been shown to be possible on some AGT mutants, but not AGT-MA by different authors (Coulter-Mackie and Lian, 2006; Cellini et al., 2010b). Both authors have described the appearance of a fragment of ~ 40 kD after partial proteolysis of AGT-41 and Coulter-Mackie and Lian report that AGT-mi was also partially susceptible too, as well as other mutants. The size of the fragment here appears smaller, which may be due to an underestimation of the size. This does suggest that partial proteolysis may take place in the cell as a result of the instability of the mutant AGTs studied. MTS are usually cleaved after mitochondrial import and in mistargeted AGT mutants, the shorter fragment detected seemed to miss the N-terminus. It would be interesting to know where the suspected partial proteolysis of the mutant AGT N-terminus could take place, in the cytosol or in mitochondria.

In addition to the full-size monomer and a shorter fragment, AGT-41 appeared as strongly interacting high molecular weight bands, as did AGT-Δ. In both cell lines, these high molecular weight AGT species could be spun down at 600 g, whereas the only AGT detectable in the

pellets of other AGT variants was monomeric. This suggests that these immunoreactive bands had formed dimers, tetramers and even higher order multimers in the cell lysate. The nature of these aggregates will be discussed below (see section IV.7.3). These high molecular species were very stable as they could not be broken down by increasing the SDS concentration or denatured by 10 M urea. The presence of interacting subunits in denaturing gels and resistant to mild/strong denaturing agents has been reported but usually with membrane proteins, unlike AGT (Frischholz et al., 1998; Nouwen et al., 2000). It is possible that these high molecular weight species form part of a very large aggregate, like that seen in the peroxisomal cores, which would partially protect it, but allowing the release of some lower order species (monomers, dimers, tetramers) during the preparation of the samples for electrophoresis. In the absence of subcellular fractionation, the exact relationship between these high molecular species and the intra-peroxisomal cores remains a matter of speculation.

Although the high molecular species were specific to both AGT-41 and AGT-Δ, the other cell lines expressing AGT, except AGT-152, showed the presence of two AGT bands staining around 80/100 kD. They were present at very low levels in the cells since it could only be detected when large amounts of AGT were loaded or the immunostaining was revealed by long exposure. The presence of such species for AGT-MA was even lower than in the other cell lines. The size of these bands associated to the fact that they were absent in AGT-152, which has a tendency to monomerize in purified recombinant protein, suggests that these are dimers of AGT (Cellini et al., 2009). The presence of two bands staining for cross-linked normal AGT around 90 kD in human liver was reported by Leiper *et al.* (Leiper et al., 1996). The explanation for the presence of dimers on denaturing gels is puzzling and may results either from low denaturing conditions used or from a strong interaction between dimers of AGT. The fact that these dimers appear in two different sizes could result from the existence of two different conformers of AGT, more or less tightly linked and migrating at different speed. In support of that, it is to be noticed that of the two bands, the one migrating the slowest was always the most visible for AGT-MA whereas in AGT variants on the minor allele background it was the band migrating the fastest, which was the more visible, even after cross-linking.

Cross-linking in human liver extracts has shown the presence of dimeric AGT (Leiper et al., 1996). The cross-linking of AGT from transformed CHO cells showed that normal AGT formed dimers in the CHO cells as well and that all the mutant AGT could exist as dimers, even AGT-152. The presence of two bands staining for AGT around 80/100 kD in cross-linked AGT confirms that the two bands of the same sizes seen on non cross-linked gels were dimers and that the AGT dimer separates as two different species on a gel, possibly because of the existence of two conformers as discussed above. The possibility that the two bands could exist by the interaction of AGT or AGT dimer with another protein was excluded by comparison of cross-

linked AGTs from cell lysates and from purified recombinant AGTs which showed the bands to be identical in the two situations and therefore composed exclusively of AGT.

In non cross-linked immunoblots, AGT-41 and AGT-Δ were present as high molecular species. After cross-linking, most of the AGT-41 and AGT-Δ was not visible on gels suggesting that they still formed part of such a large order aggregate that it could not enter the gel. This is compatible with the propensity towards the formation of large aggregates found for AGT-41 and AGT-Δ in experiments on purified recombinant AGT protein (Cellini et al., 2010b; Montioli et al., 2012). The nature of the high molecular weight bands proved to be exclusively AGT when cell lysates were compared with purified recombinant AGT-41 and AGT-Δ. The comparison between the two also demonstrated that the AGT variants, which form aggregates do so to a much greater extent in the cell environment compared to purified recombinant AGT. This may be related to the fact that AGT-41 has been found to aggregate more easily in physiological conditions which was attributed to an electrostatically-driven process (Cellini et al., 2010b).

Previous studies had suggested that both AGT-244 and AGT-152 could aggregate (Santana et al., 2003; Cellini et al., 2009). For AGT-152, this had been shown in purified recombinant AGT, and is a monomer-driven process (Cellini et al., 2009). No aggregates of AGT-152 were detected in the present study and this may be due the different conditions in the cell environment. For AGT-244, indirect evidence for the presence of aggregates had been shown in transfected COS cells expressing AGT-244 (Santana et al., 2003). In the present study, no large aggregates could be detected for AGT-244, although faint dimers and very faint traces of higher order multimers could sometimes be detected on non cross-linked SDS-PAGE gels.

Whereas the final dimer state can be studied in transformed cells, the dimerization process itself cannot be studied in such a system. Transient transfection would not be appropriate either, since dimerization is a fast process and expression in transient transfection starts a few hours after transfection and is not synchronized between cells. Cell-free translation experiments coupled with cross-linking could offer insight into the dimerization process of the different variants. Molecular chaperones could be expected to play a role in the acquisition of the native conformation, at least for abnormal AGT. The recent work done by Albert *et al.* has shown the potential of a molecular chaperone (GroEL, though not a mammalian chaperone) to be involved in the folding of AGT-244 in *E. coli* (Albert et al., 2010).

IV.7.3 AGT stability

In the stably transformed CHO cells, the half-life of AGT was very long. The half-life of peroxisomes has been estimated to be between 1 and 3 days and the half-lives of normal AGTs in the present study were probably longer or at least equal to such an estimate (Poole et al., 1969). The normal AGTs, AGT-MA, AGT-mi and AGT-anc, were all stable over the time period studied and contrasted with AGT mutants, which were less stable. One mutant, AGT-41, was more unstable compared to the other mutants. The very short half-life seen for AGT-41 contrasted with the detection of AGT-41 by the other techniques (IMF, IEM and WB). This could be the result of the slow accumulation of non-degraded AGT-41 in the relatively protected environment of the peroxisome, maybe as aggregates, and mitochondria. The AGT-41 could be protected by incorporation in aggregates as in peroxisomes or as a lesser misfolded structure in the mitochondria.

The stability of AGT variants had previously only been studied on purified recombinant AGT. Hopper *et al.* have shown both in yeast (by a decrease in total protein expressed) and on purified protein (by a variety of techniques including DSF, SUPREX analysis and activity at lower temperature) that AGT mutants are less stable than AGT-MA (Hopper et al., 2008). The instability of the mutants studied here, as well as AGT-mi, was first suggested by Lumb and Danpure, in studies in *E. coli* (Lumb and Danpure, 2000). All the mutants on the minor background were found to form aggregates and even AGT-mi showed a tendency to aggregate and pellet down. Coulter-Mackie and Lian have shown that AGT mutants are more sensitive to trypsin degradation that normal AGT (AGT-MA and AGT-mi) (Coulter-Mackie and Lian, 2006, 2008). The stability of AGT-mi was found to be decreased compared with AGT-MA, by Hopper or by Cellini but not by Coulter-Mackie and Lian. However, these last authors only mention that the half-life is > 23 h, which does not exclude the possibility that it is still less than that of AGT-MA, as is suggested by Hopper and Cellini. The latter authors have shown by pulse-chase in cell-free translation that the half-life of AGT-170 is decreased compared to normal AGT with a half-life estimated at 21h, which is compatible with the estimate in the present study. For Cellini *et al.* the decrease in stability of AGT mutants (AGT-152, AGT-170) is a characteristic of the apo-form and not the holo-form (Cellini et al., 2009, 2010a).The high instability of AGT-41 has been found by both Coulter-Mackie and Lian and by Cellini *et al.* (Coulter-Mackie and Lian, 2006, 2008; Cellini et al., 2010b). Using pulse-chase in cell-free translation, the half-life of AGT-41 was very similar to that estimated in this work, with a $t_{1/2}$ of 3 h. For the AGT-244 variant, Santana et al have studied the stability of AGT-244 in cell free translation coupled with pulse-chase (Santana et al., 2003). No difference in turnover of AGT-244 could be shown compared to AGT-MA. However, the decreased stability indicated in the present study is not large and the limit of 48h study in Santana's work, may very well be within the variation of what the present study is suggesting (12-36h).

Techniques other than pulse-chase by ^{35}S-labelling would have to be used in order to determine a precise half-life for the more stable AGT variants.

IV.7.4 AGT and GO catalytic activities

Although the activity of AGT varied between cell lines, the activity of GO was comparable between the cell lines (70-100%). This was achieved by using a single CHO GO cell line, cloned to almost 100% of GO-expressing cells, as the background cell line into which AGT was transformed.

For the AGT activity, the activity in CHO GO AGT-MA was higher than that described in Behnam *et al.* (45.4 μmol/h/mg protein *vs*. 22.5) but still within the normal human range in human liver (19.1 – 47.9) with the same method (Rumsby et al., 1997; Behnam et al., 2006). The range of activity may reflect the variability of AGT expression in the cells over the period of the present study.

The published data on the activity of AGT-mi do not all agree and values vary between 45% and 100% of that of AGT-MA depending on the study (Lumb and Danpure, 2000; Coulter-Mackie et al., 2005; Coulter-Mackie and Lian, 2006; Williams and Rumsby, 2007; Coulter-Mackie and Lian, 2008; Hopper et al., 2008; Cellini et al., 2010a). The activity in human liver published described one patient homozygote for the minor allele was normal (92%) (Purdue et al., 1990). Both the raw and the estimated specific (corrected for overall level of AGT expression) activity found here fall in the range previously described for AGT-mi but the estimated specific activity is higher than described in purified recombinant AGT-mi. This may either reflect the variability of the methods used here or an intrinsic difference between AGT produced in *E. coli* compared to mammalian cells.

The estimated specific activity of AGT-anc was similar to that of AGT-MA and reflects both the activity of mitochondrial AGT-anc, with the MTS cleaved off, identical to AGT-MA, and the fraction (smaller) of peroxisomal AGT-anc, which still bears the MTS. Preliminary results on purified recombinant AGT-anc showed that the activity of full-length AGT-anc is similar to that of AGT-MA (data not shown, work kindly carried out by Dr Cellini, Verona). This would suggest that the presence of the additional ancestral MTS, although normally removed, does not prevent full-length AGT-anc from acquiring a conformation compatible with catalytic activity. However, the stability of such a variant may not be that of normal AGT and this may not be reflected in the CHO cells since they have proved to allow significant expression of otherwise unstable AGT variants.

The activities found for the active AGT mutants (AGT-170, AGT-152, AGT-244) were higher than the activities known in the livers of patients with the corresponding mutations (van Woerden et al., 2004; Monico et al., 2005b; a; Williams and Rumsby, 2007; Harambat et al.,

2010). One explanation for the difference may be that the net level of immunoreactive protein in the liver of patients bearing these mutations is very low whereas the net level of expression in the CHO cells is high. In stably transformed CHO cells, the activity of AGT-170 was higher than the activity of other AGT mutants, as is seen in the liver of PH1 patients homozygotes for AGT-170 compared with other mutations or heterozygotes for AGT-170.

The AGT-152 mutant was very sensitive to the presence of PLP and lost all activity in the absence of added PLP in the assay. This is compatible with the results of Cellini *et al.* on purified recombinant AGT-152, showing that this variant has a lower affinity for PMP and turns to the apo-form, which is more unstable than normal AGT and has a tendency to monomerize (Cellini et al., 2009).

In the culture conditions used, there was very little difference in the AGT activity assayed in the presence or absence of PLP which suggests that most of the AGT, which has folded in a catalytically-competent form, is a holo-enzyme, except for AGT-152.

IV.7.5 Conclusion

The results discussed above are based on the analysis of AGT synthesized in a mammalian cell environment. However, they address different aspects of the efficiency of a given AGT variant, oligomeric state, catalytic activity, subcellular targeting. The biological or metabolic efficiency of AGT is a result of the combination of these characteristics. The direct testing of the global efficiency of AGT variants would require a functional test, which will be discussed in chapter VI. Since some of the AGT variants had a dual, mitochondrial and peroxisomal, distribution, it would have been interesting to assess separately the characteristics of peroxisomal AGT and mitochondrial AGT. This would have required subcellular fractionation on the cell lysates, which was not done here. Nonetheless, the results presented in this chapter, can lead to certain conclusions and speculations on the AGT mutants studied and the role of the N-terminus and its polymorphism.

Three of the four mutants described here, AGT-170, AGT-152 and AGT-244, were shown to have significant activity, more than was expected from the data published in PH1 patients' liver.

The mitochondrial mistargeting was shown to be less mutation-specific than had been known before. The synergy between the P11L polymorphism and co-segregating mutations in leading to mitochondrial mistargeting shown previously only for AGT-170, was suggested here for all the other mutants studied. These results confirm the crucial role of the P11L polymorphism and its potential as an MTS. In order to be manifested, the MTS potential needs an additional modification on AGT. Such additional elements have been suggested to be a slowing down of folding and/or dimerization or the instability of the dimer.

The presence of an N-terminal extension, normal or otherwise, did not seem to be required for a dimerization of AGT, since AGT-Δ and the other AGT mutants did form dimers. One can

easily speculate that the N-terminal extension is important for the correct positioning of the monomeric subunits in the dimer.

Although the dimeric nature of the AGT-Δ did not seem to be modified, its propensity to aggregate and lack of activity may indicate that the N-terminal arm is involved in the process of folding. Work by Cellini has indicated that the region at the end of the N-terminal arm forms a hinge in connection with the catalytic site. The absence of the N-terminal arm and even its modification, as with the P11L polymorphism, could have as a consequence a modification of the active site, and decrease the catalytic activity.

So the presence of the P11L could have several effects in AGT mutants, decreasing further the activity in addition to mutation specific change in the AGT structure, affecting the kinetics of folding/dimerization and allowing the MTS formed to play its role. Lumb *et al.* showed that the stability of AGT mutation was greatly decreased by the additional presence of the P11L polymorphism (Lumb and Danpure, 2000).

This pathogenic role of the P11L polymorphism had been suggested before and the results shown here confirm this view. Indeed, all the techniques used here showed that the minor allele-encoded AGT (AGT-mi) behaved as an intermediate between AGT-MA and the AGT mutants.

V RESULTS part 2: Mechanisms of action of pyridoxine in PH1

V.1 Introduction

Vitamin B6 is the cofactor of more than a hundred enzymes in humans, which are involved in a variety of reactions including: synthesis and catabolism of neurotransmitters, transamination of amino acids, decarboxylation in phospholipid synthesis, reactions involving the side-chains of certain amino acids as well as acting as a phosphate buffer to glycogen phosphorylase, terminating the actions of steroid and other nuclear-acting hormones and a potential role as anti-oxidant {reviewed in (Bender, 1999)}.

Six different vitamin B6 vitamers are known: pyridoxal (PL), pyridoxine (PN), pyridoxamine (PM) and their 5'-phosphates (PLP, PNP, PMP respectively) (Fig V.1). The metabolism of vitamin B6 is well known but there are still some uncertainties as to the intracellular transport and levels of its vitamers at the subcellular level (Fig V.2).

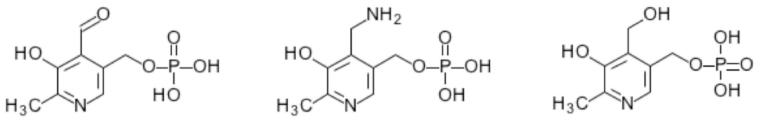

Figure V-1 **Phosphorylated B6 vitamers.** PLP: pyridoxal 5'-phosphate; PMP: pyridoxamine 5'-phosphate; PNP: pyridoxine phosphate

There are three key enzymes in the metabolism of vitamin B6, pyridoxal kinase (PDXK), pyridoxine 5'-phosphate oxidase (PNPO) and pyridoxal phosphatase (PDXP). These three enzymes, PDXP, PNPO, PDXP, are expressed ubiquitously but the level of transcription is regulated in a tissue-specific manner (Kang et al., 2004). The tissue with the highest expression of PNPO is the liver. The end product of PLP degradation is pyridoxic acid (PA) which is excreted in the urine, where it represents 90% of all forms of vitamin B6 metabolites.

PLP, which is the active form of vitamin B6, is formed in the liver and can be released in the blood, where it is the main circulating form of vitamin B6 followed by PN (Table V.1) (Lumeng et al., 1980). Normal plasma levels for PLP range between 12 and 75 nmol/l, but plasma levels found in normal human subjects as well as pyridoxine treated patients vary in the literature, as do the plasma levels of other B6 vitamers and PA (Table V.1) (Lumeng et al., 1980; Edwards et al., 1990a, b; Bor et al., 2003; Midttun et al., 2005; Footitt et al., 2011, 2012).

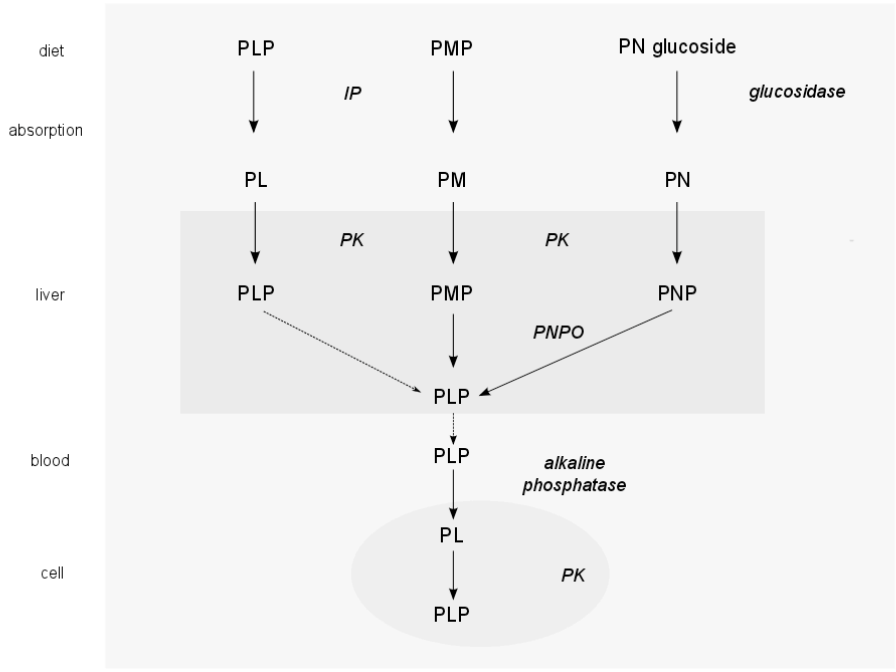

Figure V-2 **Metabolism of vitamin B6 in humans.** PL: pyridoxal; PLP: pyridoxal 5'-phosphate; PM: pyridoxamine; PMP: pyridoxamine 5'-phosphate; PN: pyridoxine; PNP: pyridoxine phosphate; PNPO: pyridoxamine 5'-phosphate oxidase; PK: pyridoxal kinase; IP: intestinal phosphatase. Enzymes are labelled in italics. After (Clayton, 2006).

Table V-1. **Variability of plasma levels of B6 vitamers without or with pyridoxine treatment in the literature**. PL: pyridoxal; PLP: pyridoxal 5'-phosphate; PM: pyridoxamine; PMP: pyridoxamine 5'-phosphate; PN: pyridoxine; PNP: pyridoxine phosphate; nd : not detectable. The range of plasma levels in the published literature is given in nmol/l. (Lumeng et al., 1980; Edwards et al., 1990a; b; Bor et al., 2003; Midttun et al., 2005; Footitt et al., 2011, 2012).

Pyridoxine treatment	[PLP], nM	[PL], nM	[PMP], nM	[PM], nM	[PNP], nM	[PN], nM	[4-PA], nM
untreated	12 - 102.3	nd - 28	nd - 3	nd - 6	nd - 4	nd - 31	11 - 88
treated 40 - 800 mg/day	234 - 826	144 - 11 100	nd - 3	0.1 - 6	nd - 410	nd - 4 666	167 - 8 613

The intracellular metabolism of vitamin B6 has also been studied in whole animal liver and isolated hepatocytes (Fig V.3). The transport of PL, PN and PM through the cell membranes seems to occur by passive or facilitated diffusion, driven by metabolic trapping of vitamin B6 in the cell once it is phosphorylated (Mehansho et al., 1980; Kozik and McCormick, 1984). A diffusion through the mitochondrial membrane driven by the binding of PLP and PMP to enzymes in the matrix has been shown (Lui et al., 1982). Studies using normal and labelled

pyridoxine in rat liver and rat hepatocytes have shown that the main forms of vitamin B6 in the cell are PLP and PMP (Fig V.3) (Bosron et al., 1978; Lumeng et al., 1980; Lui et al., 1981, 1982). Approximately 65% of the PLP is localized in the cytosol and 10 to 18% in the mitochondria. In the cytosol, 80% of the PLP is bound to proteins, a third of which are transaminases in liver (but glycogen phosphorylase for 90% in muscle). The bound PLP forms a slow turn-over pool compared to the 20% of free PLP which can diffuse to subcellular organelles like mitochondria (Fig V.3). Protein binding plays an important role in the distribution and elimination of vitamin B6.

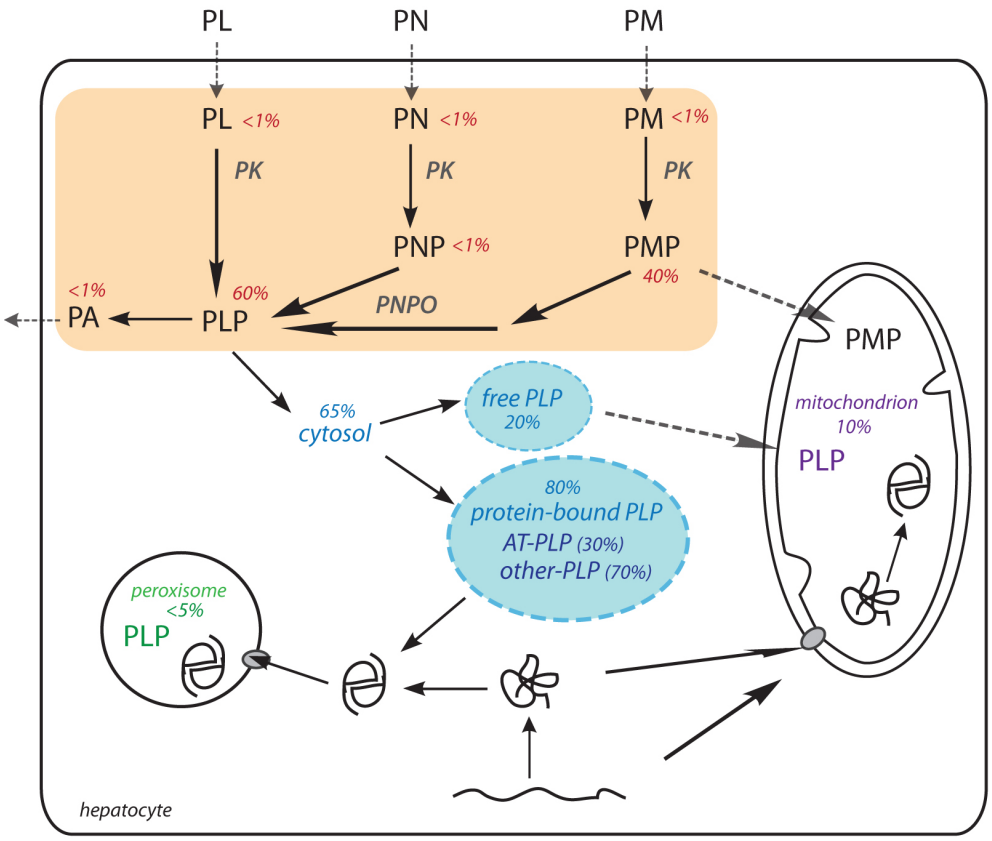

Figure V-3 **Metabolism of vitamin B6 in hepatocytes.** Diagram based on rat liver and rat hepatocytes studies (Bosron et al., 1978; Lumeng et al., 1980; Lui et al., 1981, 1982). PL: pyridoxal; PLP: pyridoxal 5'-phosphate; PM: pyridoxamine; PMP: pyridoxamine 5'-phosphate; PN: pyridoxine; PNP: pyridoxine phosphate; PA: pyridoxic acid; PNPO: pyridoxamine 5'-phosphate oxidase; PK: pyridoxal kinase.; AT: amino transferase. The relative proportion of B6 vitamers in hepatocytes are given in red (% of total intracellular vitamin B6). The distribution of PLP (% of total intracellular PLP) in the cell is given in blue (cytosolic PLP), green (peroxisomal and microsomal PLP), purple (mitochondrial PLP). Nuclear PLP is not represented (20% of intracellular PLP). Dashed arrows indicate transport by diffusion. The proportion in peroxisome (labelled < 5%) is understood as being included in the larger microsomal fraction which is given as < 5%.

The dietary sources of vitamin B6 are varied and overt vitamin B6 deficiency is rare, although marginal deficiency has been described in some groups of population (young children, pregnant women, elderly subjects) (Bender, 1999). The symptoms of vitamin B6 deficiency {reviewed in (Clayton, 2006)} are mainly neurological and psychological, but include among other signs an increased excretion of urinary oxalate, which has been described both in human patients and in rats (Gershoff et al., 1959; Takada and Noguchi, 1982).

Apart from dietary insufficiency in vitamin B6, an increased requirement for vitamin B6 can occur in different situations such as malabsorption of B6 vitamers, increased loss of vitamin B6, side-effects of drugs, inborn errors in the metabolism of vitamin B6 or metabolic diseases causing the production of small molecules interacting with B6 vitamers, and inborn errors of PLP-dependent enzymes (such as PH1). In the latter case the patients require a supplementation of pharmacological doses of vitamin B6 for their whole life {reviewed in (Bender, 1999; Clayton, 2006)}.

The B6-responsiveness of some patients with PH1 has been known for a long time (Gibbs and Watts, 1970; Watts et al., 1979; Kopp and Leumann, 1995, 1995; Hoppe and Langman, 2003). More recent work has shown that of the 30% of PH1 patients who are B6-responsive, two genotypes, at least, are associated with B6-responsiveness: the G170R and F152I mutations (van Woerden et al., 2004; Monico et al., 2005b; a). Although the response of other mutations to pyridoxine has not been excluded, the fact that B6-responsiveness does not occur in all patients is not in favour of a mechanism involving another enzyme than AGT.

In order to understand how pyridoxine could increase the effectiveness of AGT, thereby leading to the decrease in urinary oxalate observed in patients, we have tried to vary the intracellular concentrations of B6 vitamers, and studied the overall expression levels of AGT variants, the catalytic activity, apo- to holo-enzyme ratio and subcellular localization of AGT variants in stably transformed CHO cells

V.2 Increase of vitamin B6 in tissue culture cells

In order to study the mechanisms of action of pyridoxine on AGT, the different CHO cells studied in this project have been grown in different pyridoxine concentrations.

Five different concentrations of pyridoxine were chosen, some below and some above the expected plasma levels of PLP in untreated human patients (Table V.2 & V.1). The cell lines were grown at least 4 weeks in the different pyridoxine levels to allow for a wash-out period and the possible long half-life of peroxisomal AGT.

Table V-2. **Levels of pyridoxine in different culture conditions**. PN: pyridoxine, PN HCL: pyridoxine hydrochloride, PLP: pyridoxal-5'-phosphate, FBS: foetal bovine serum (Methods III.2).

culture conditions for B6	final [PN]	Medium used	[PN HCl] in medium	FBS used	[PLP] in FBS	PN HCl added (final)
No B6	≈ 0 µmol/l	B6-free Ham's F12	0	dialysed FBS	< 4 nmol/l	0
low B6	< 0.3 µmol/l	B6-free Ham's F12	0	normal FBS	< 4 nmol/l	0
standard B6	≈ 0.3 µmol/l	normal Ham's F12	292 nmol/l	normal FBS	< 4 nmol/l	0
high B6	≈ 50 µmol/l	normal Ham's F12	292 nmol/l	normal FBS	< 4 nmol/l	50 µmol/l
very high B6	≈ 250 µmol/l	normal Ham's F12	292 nmol/l	normal FBS	< 4 nmol/l	250 µmol/l

The intracellular content in B6 vitamers was measured in 3 cell lines: CHO GO, CHO GO AGT-MA, CHO GO AGT-170 (Fig V.4), after culture in different pyridoxine concentrations for at least 4 weeks.

The total content of vitamin B6 in the cells increased with increasing pyridoxine concentrations in culture (Fig V.4). The change in intracellular B6 levels did not change in proportion to the changes in concentration in the medium. Significant levels of B6 vitamers could still be detected in cells grown in medium nominally containing no B6. The total amount of B6 vitamers (mainly PLP) was higher in CHO GO AGT-MA and CHO GO AGT-170 cells than CHO GO cells at intermediate concentrations of pyridoxine (Annexe IX.11). No PA or PM could be measured in the cells, even at the highest levels. The main form of vitamin B6 in the cells was PLP.

At the two highest levels of added pyridoxine, an increasing amount of pyridoxine and pyridoxine-phosphate could be detected in all three cell lines, whereas it was undetectable at lower levels.

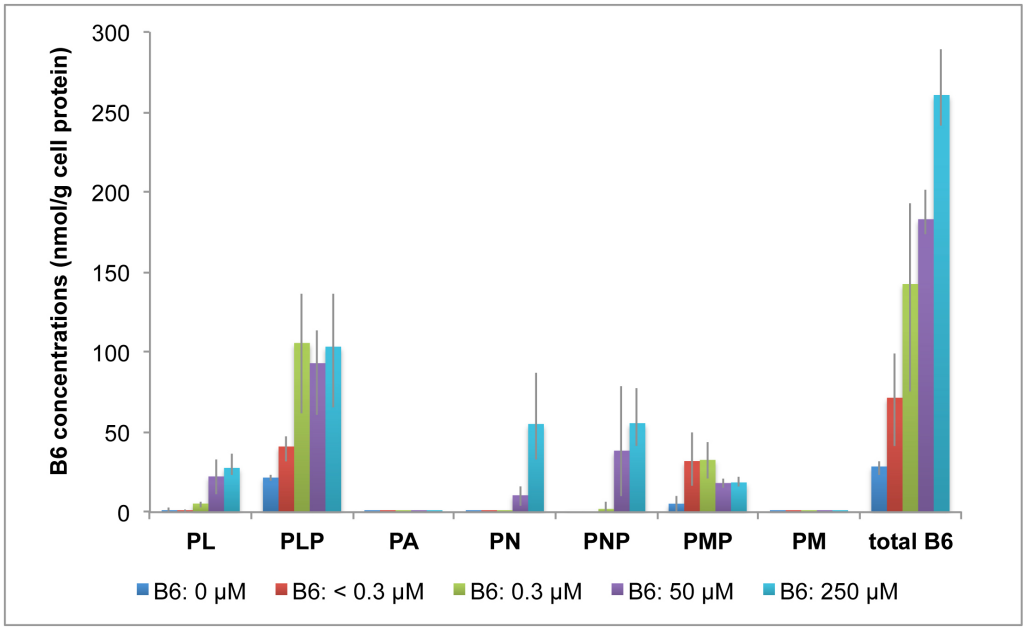

Figure V-4. **Increased levels of vitamin B6 vitamers in transformed CHO cells.** Cell lysates (n=3) were obtained from transformed CHO cells grown at least 4 weeks with different levels of pyridoxine (0, < 0.3 µM, 0.3 µM, 50 µM, 250 µM; see Methods III.2) and the B6 vitamers content was analysed by HPLC followed by tandem mass-spectrometry, the measurements were kindly carried out by E Footitt (see Methods III.3). The results are averaged from three different CHO cell lines: CHO GO, CHO GO AGT-MA, CHO GO AGT-170, and the range indicated by the vertical bars. PL: pyridoxal; PLP: pyridoxal 5'-phosphate; PA: pyridoxic acid; PN: pyridoxine; PNP: pyridoxine phosphate; PMP: pyridoxamine 5'-phosphate; PM: pyridoxamine.

V.3 Effect of pyridoxine on AGT expression

In order to test whether pyridoxine had an effect on the overall level of AGT expression in stably transformed CHO cells, the AGT expressed in the cell lines grown at least 4 weeks in various concentration of pyridoxine was studied by immunoblotting followed by a densitometry analysis (see Methods II.2 & III.10). The proportion of monomer to the total of (monomer and dimer) forms detected on non cross-linked immunoblots was determined (Fig V.5, V.6, V.7, Annexe IX.12).

Pyridoxine had a small effect on the level of AGT-MA, although the presence of dimer could only be detected at the lower concentrations of pyridoxine (0, < 0.3 µM). The total level of AGT-mi was not significantly influenced by pyridoxine concentration in the medium. However, the relative proportion of dimer to the total protein, was much greater at the lowest levels of pyridoxine than at the higher ones. The expression of AGT-170 increased as pyridoxine concentration in the medium increased up to twice its lowest level. Significant amounts of dimer were present at all pyridoxine concentrations. The presence of a short fragment of AGT (≈37 kD) was detectable only at low levels of pyridoxine for AGT-MA and AGT-170 (Fig V.6).

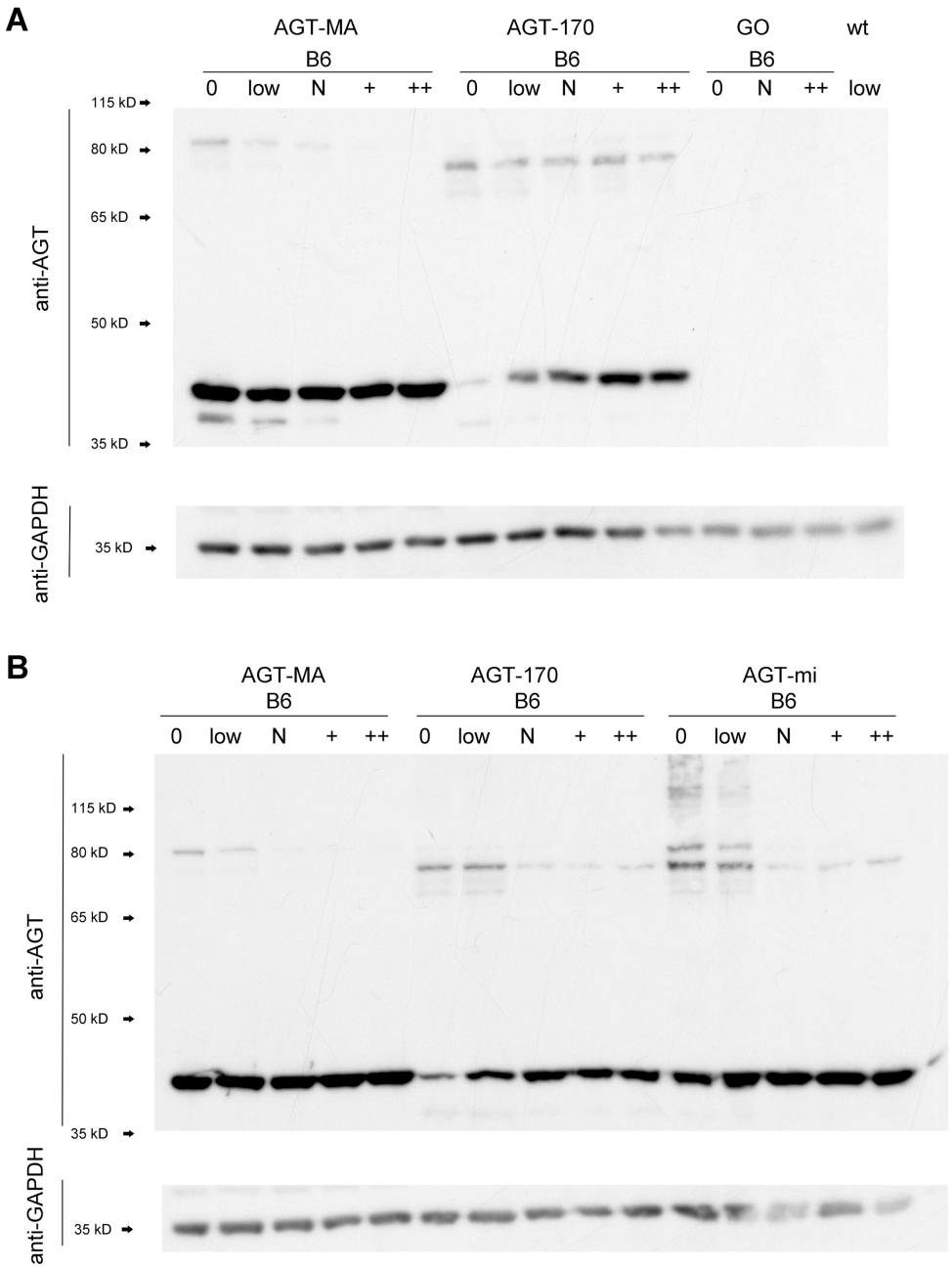

Figure V-5. **Effect of pyridoxine levels on the expression of AGT-MA, AGT-mi and AGT-170 in stably transformed CHO cells.** Whole cell lysates were obtained from culture of transformed CHO cells grown at least 4 weeks in various concentrations of pyridoxine (B6) (0: 0 μM, low: < 0.3 μM, N: 0.3 μM, +: 50 μM, ++: 250 μM, see Methods III.2). For the immunoblot, 5 μg of cell protein (non cross-linked) were loaded on each lane of a SDS-PAGE gel. The membrane was incubated with guinea-pig anti human-AGT and then with rabbit anti GAPDH as a loading control. A: CHO GO AGT-MA, CHO GO AGT-170, CHO GO, CHO WT cells; B: CHO GO AGT-MA, CHO GO AGT-170, CHO GO AGT-mi cells. A shorter fragment of AGT monomer (≈37 kD) is faintly visible for AGT-MA (A) and AGT-170 (A, B) at the lowest pyridoxine concentrations. Arrows indicate protein size markers.

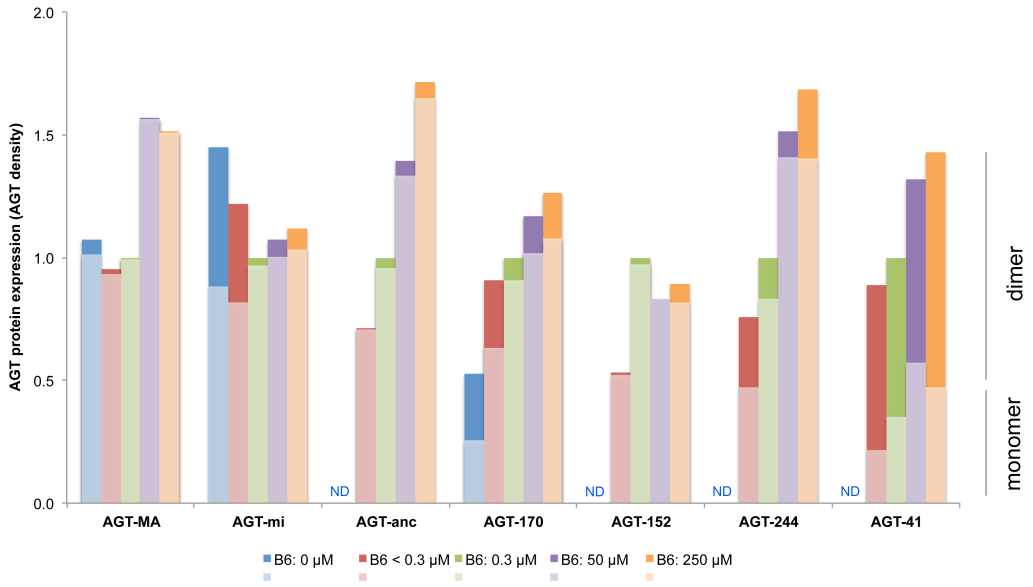

Figure V-6. **Estimation of the average effect of pyridoxine on the expression of AGT in CHO stable transformants as assessed by densitometry.** Whole cell lysates of cells were obtained from cells grown at least 4 weeks in various concentrations of pyridoxine (B6) (0, < 0.3 µM, 0.3 µM, 50 µM, 250 µM, see Methods III.2) and immunoblotted with anti-AGT antibodies A densitometry analysis was performed on the resulting membrane either exposed to film or to a digital camera. Both monomers (lightly coloured histograms) and dimers – or multimers in the case of AGT-41 - (brightly coloured histograms, tiered) were measured (n ≥ 2). The results are normalized to the total AGT in 0.3 µM pyridoxine concentration for each AGT variant and averaged. Only CHO GO AGT-MA, CHO GO AGT-mi, CHO GO AGT-170 were tested in the whole range of pyridoxine concentrations, CHO GO AGT-anc, CHO GO AGT-152, CHO GO AGT-244 and CHO GO AGT-41 were tested in 4 levels of pyridoxine only (< 0.3 µM, 0.3 µM, 50 µM, 250 µM). ND: not done.

The effect of pyridoxine on the expression of other variants of AGT was only studied at four pyridoxine concentrations (< 0.3 µM, 0.3 µM, 50 µM, 250 µM) (Fig V.6, V.7, Annexe IX.12)

There was a trend towards a higher overall expression of AGT with increasing pyridoxine concentrations in culture for AGT-anc, AGT-152, AGT-244 and AGT-41.

There was almost no detectable AGT-152 dimer, whatever the level of pyridoxine.

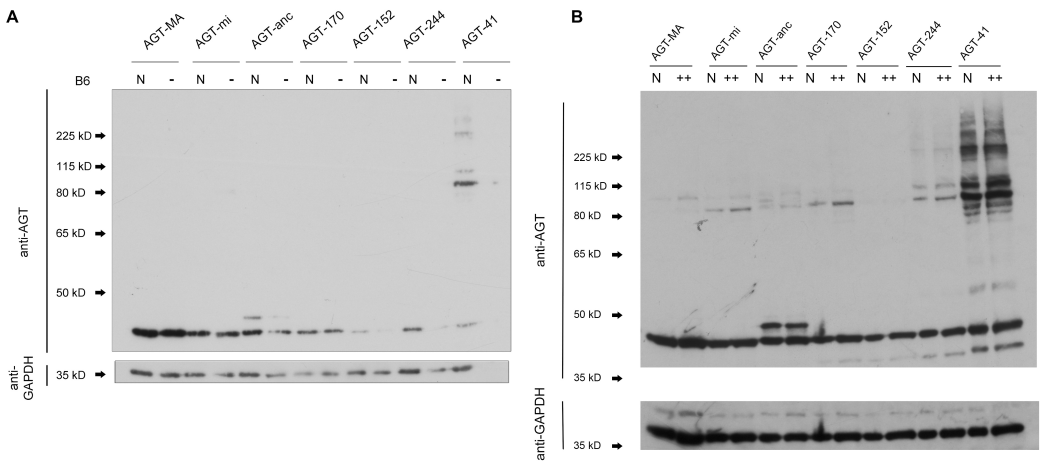

Figure V-7. **Effect of decreasing and increasing pyridoxine concentrations on AGT expression in stable transformants.** Whole cell lysates were obtained from transformed CHO cells grown at least 4 weeks in standard F12 culture conditions (0.3 μM pyridoxine (B6 N)), low levels of pyridoxine (< 0.3 μM, (B6 -)) (A) or with pyridoxine supplementation (250 μM, (B6 ++)) (B). For the immunoblots, 5 μg of cell protein (non cross-linked) were loaded on each lane of a SDS-PAGE gel. The membrane was incubated with guinea-pig anti human-AGT and then with rabbit anti GAPDH as a loading control. B: the same figure was shown in Results: part1 (Fig IV.35). Arrows indicate protein size markers.

V.4 Effect of pyridoxine on the catalytic activity of AGT

In order to test the effect of pyridoxine in culture on the intra-cellular levels of holo-and apo-AGT, stably transformed CHO cells were grown at least 4 weeks in various concentrations of pyridoxine (0, < 0.3 μM, 0.3 μM, 50 μM, 250 μM) and assayed in the presence (150 μM) or absence of PLP (Methods III.2 & III.8) (Fig V.8).

The normal assay, *i.e.* with added PLP (150 μM), indicates the maximal activity attainable at a particular level of immunoreactive AGT protein. The assay in the absence of PLP indicates the proportion of its existing in the holoform within the cells.

V.4.1 Effect of pyridoxine on maximum catalytic activity

The catalytic activity of AGT assayed with added PLP in the assay (150 μM) indicated the maximum recoverable activity of AGT variants (Fig V.8, Annexe IX.13).

Even in the absence of pyridoxine in the culture medium, the activity of AGT-MA was fully recoverable and was similar to that found in cells grown in pyridoxine concentrations ≤ 0.3 μM.

For AGT-mi, the activities at < 0.3 and = 0.3 μM were close to each other, but the activity in the absence of pyridoxine was severely decreased indicating a chaperone effect of vitamin B6

on AGT-mi, opposed to the absence of vitamin B6 requirement for the proper folding of AGT-MA.

In the absence of pyridoxine, there was no detectable activity for AGT-170, which showed an even greater requirement of vitamin B6 for the folding of AGT-170.

For mutants with residual activity (AGT-170, AGT-152, AGT-244), the activity in pyridoxine concentration < 0.3 μM was greatly decreased compared to 0.3 μM pyridoxine, below the detection level for AGT-152 and AGT-244. The main increase in activity was seen between < 0.3 μM and 0.3 μM pyridoxine, and plateaued at higher concentrations of pyridoxine.

The activity of AGT-41 was below or around the detection level of the assay whatever the concentration of pyridoxine, with a slight increase above detection level at pyridoxine >50 μM.

A decrease in the activity of the normal AGT variants, AGT-MA, AGT-mi, AGT-anc, was seen at the highest pyridoxine concentrations in culture (50 and 250 μM).

V.4.2 Effects of pyridoxine on AGT catalytic activity

The catalytic activity of AGT was also studied in the absence of added PLP in the assay (Fig V.8, Annexe IX.13).

In the absence of pyridoxine in culture, AGT-MA, which has the highest activity in standard conditions, had almost no activity. A small residual activity was measured in accordance with the small levels of PLP found in those cells (Chapter V.2). The other variants tested at this level of pyridoxine (AGT-mi, AGT-170) had no detectable activity.

In cell lines expressing AGT variants with detectable activity without added PLP in the assay (AGT-MA, AGT-mi, AGT-anc, AGT-170, AGT-244), AGT activity was decreased when pyridoxine was < 0.3 μM compared to 0.3 μM. For the two mutants AGT-170 and AGT-244, the activity increased with pyridoxine and plateaued above 0.3 μM pyridoxine. On the contrary, for the normal AGTs, AGT-MA, AGT-mi, AGT-anc, the changes in catalytic activity were biphasic. The activity increased and reached a maximum at 0.3 μM pyridoxine and then decreased at higher levels of pyridoxine (50 and 250 μM), without any difference between 50 and 250 μM pyridoxine. No activity was detected for AGT-41 whatever the level of pyridoxine and the activity of AGT-152 remained below detection level in the absence of added PLP.

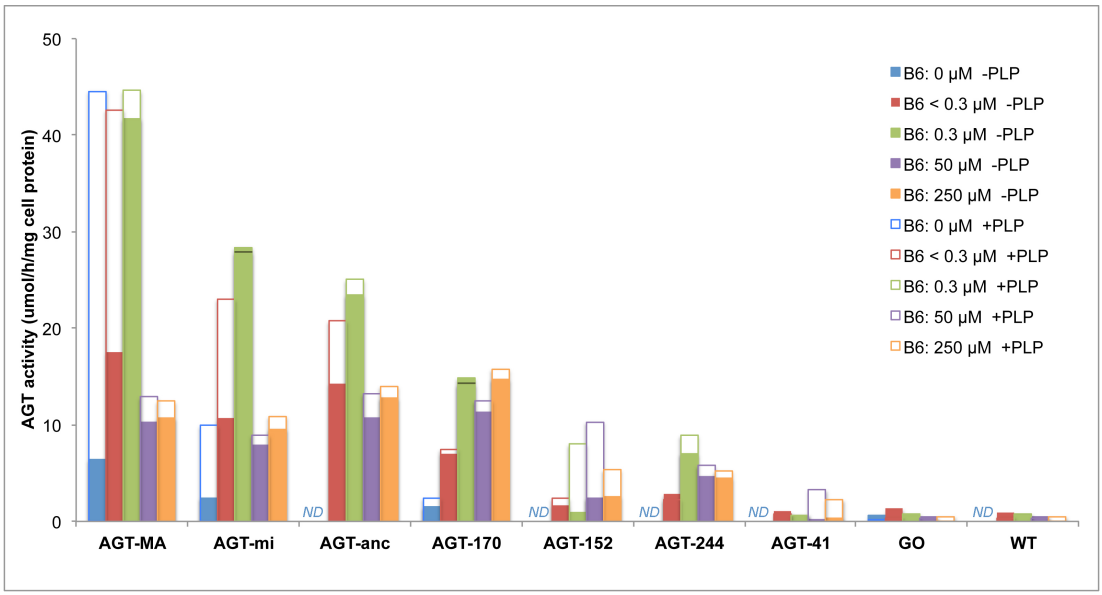

Figure V-8. **Effect of pyridoxine on the catalytic activity of AGT in transformed CHO cell lines.** Cell lysates were obtained from cells grown at least 4 weeks in the various pyridoxine (B6) concentrations (0, < 0.3 µM, 0.3 µM, 50 µM, 250 µM, see Methods). The standard pyridoxine concentration in Ham's F12 medium is 0.3 µM. Empty histogram (superimposed): activity in the presence of added PLP in the assay (150 µmol/l), full coloured histogram (superimposed): activity without added PLP. AGT activity in µmol pyruvate/h/mg of cell protein. ND: not done. The results are given as means of several assays (2 to 8, see Annexe IX.13). The limit of sensitivity of the AGT assay is 3 µmol pyruvate/h/mg of cell protein.

V.4.3 Summary

The catalytic activity of some of the mutant AGTs was increased by pyridoxine (AGT-170, AGT-152, AGT-244). Whereas in the absence of pyridoxine all the activity of AGT-MA was recovered by addition of PLP in the assay, the recoverable activity of AGT-mi and AGT-170 was not maximum. The activity of AGT-MA, AGT-mi and AGT-anc was decreased at pyridoxine concentrations > 0.3 µM.

V.5 Effect of pyridoxine on the subcellular localization of AGT

In order to assess whether the subcellular localization of AGT variants was modified by pyridoxine, stably transformed CHO cells expressing various AGT constructs were grown at least 4 weeks in different pyridoxine concentrations (see Methods III.2) and studied by immunofluorescence microscopy (Fig V.9 to V.21). An analysis of the subcellular localization was carried out by visual and analytical methods (Methods III.6) (Table V.3 to V.8, Fig V.22 & V.23).

V.5.1 Pyridoxine and the subcellular localization of AGT-MA

The intra-cellular localization of AGT-MA in CHO GO AGT-MA cells remained peroxisomal at all pyridoxine concentrations in culture (Fig V.9, V.10, Table V.3).

The colocalization coefficients calculated, both Pearson's and thresholded Manders', remained high and stable between GO and AGT at all pyridoxine levels (Fig V.19, V.20, see below).

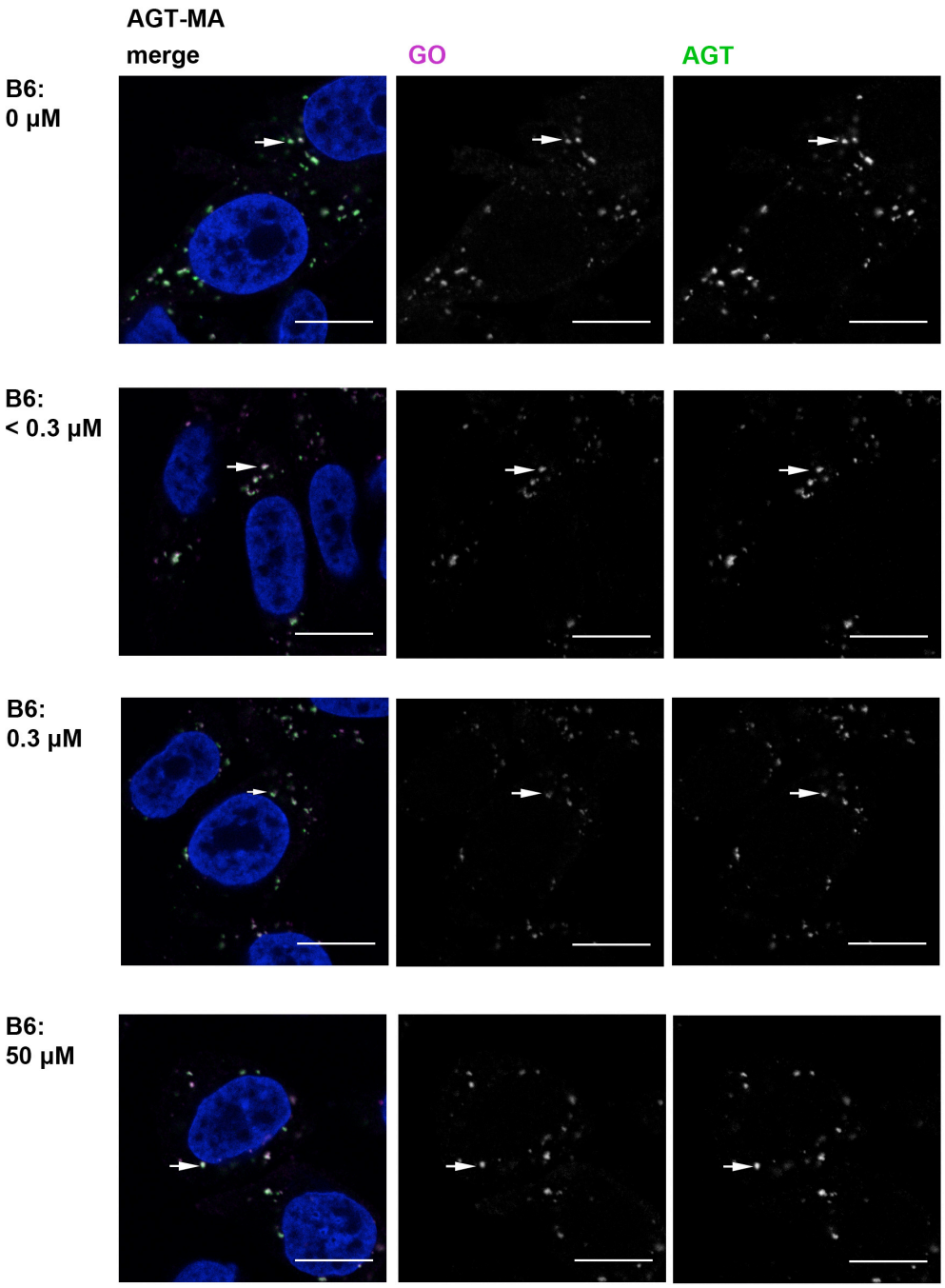

Figure V-9. **Effect of pyridoxine on the subcellular distribution of AGT-MA as shown by immunofluorescence microscopy - 1.** CHO GO AGT-MA cells were grown at least 4 weeks in the various concentrations of pyridoxine (B6) (0, < 0.3 µM, 0.3 µM, 50 µM) (see Methods III.2) and stained with anti AGT (green), anti GO (magenta), Hoechst (blue). Scale bar : 10 µm. Merged and single channel images from a single z-plane are shown for each pyridoxine level. White arrows point to a peroxisome.

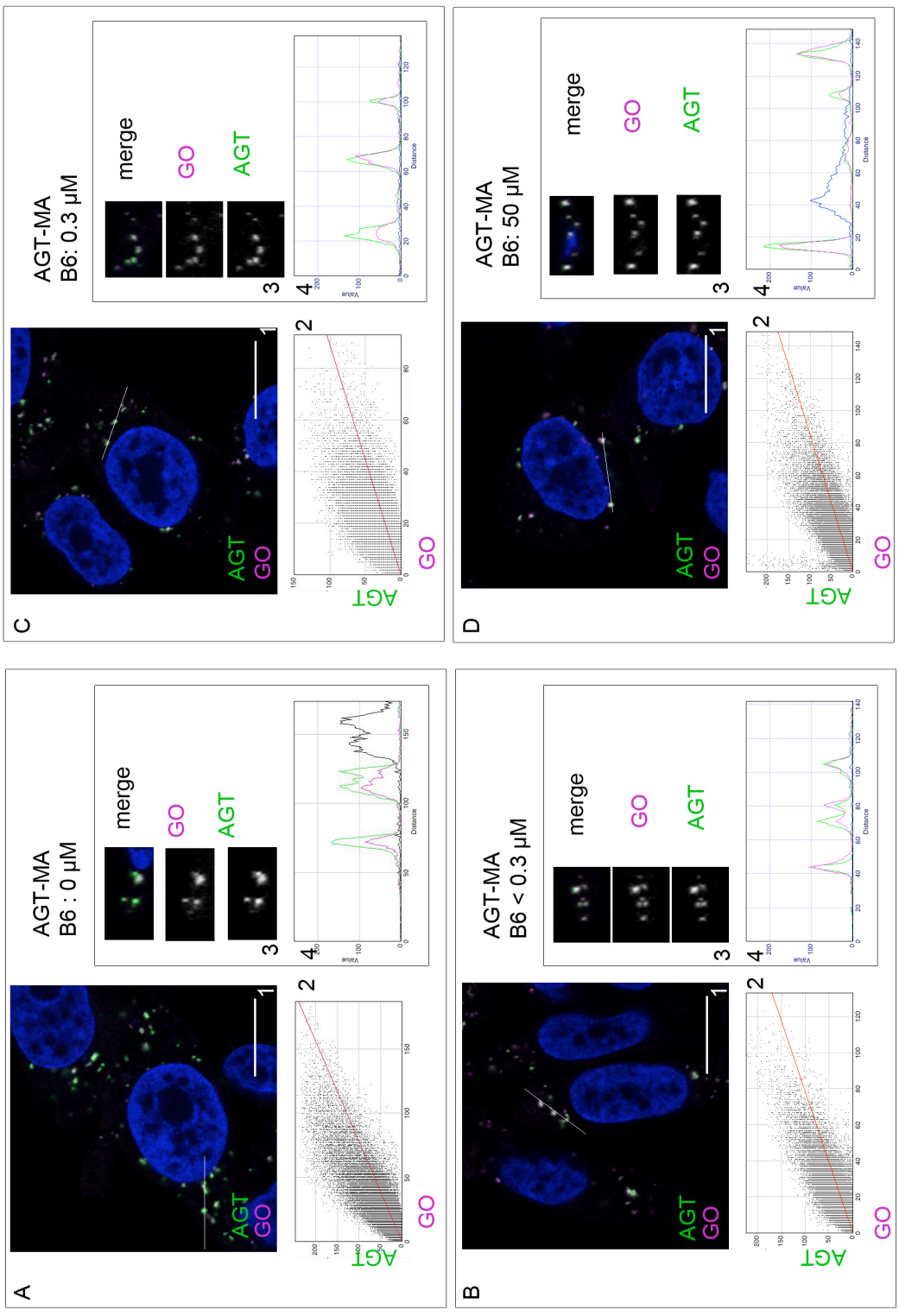

Figure V-10. Effect of pyridoxine on the subcellular distribution of AGT-MA as shown by IMF. CHO GO AGT-MA cells - 2in 0 µM (A); < 0.3 µM (B); 0.3 µM (C); 50 µM(D) pyridoxine (Methods III.2). AGT (green), GO (magenta), Hoechst (blue). (1): merged image from a single z-plane ; (2): cytofluorogram for the whole z-stack. Reslice along the z-axis (3) and RGB profile (4) plotted along the line drawn in (1). Scale bar : 10 µm. Colocalization coefficients in (TableV.3).

Figure V-10. **Effect of pyridoxine on the subcellular distribution of AGT-MA as shown by IMF- 2**.

GO/AGT	AGT-MA		
pyridoxine	*P*	*M1 (GO)*	*M2 (AGT)*
0 µM	0.810	0.836	0.839
< 0.3 µM	0.794	0.876	0.743
0.3 µM	0.731	0.666	0.643
50 µM	0.788	0.910	0.724

Table V-3. **Colocalization coefficients for Fig V.10.** Pearson's coefficient: P; Manders' M1 (GO) and M2 (AGT). Coefficients are manually thresholded.

V.5.2 Pyridoxine and the subcellular localization of mutant AGTs

V.5.2.1 Effect of pyridoxine on the peroxisomal localization of AGT-170

The subcellular localization of AGT-170 was studied by IMF at four levels of pyridoxine (0 µM; < 0.3 µM; 0.3 µM; 50 µM). Pyridoxine had a strong positive effect on peroxisomal localization of AGT-170, shown by all indicators used. In the absence of pyridoxine (0 µM) AGT-170 appeared completely mitochondrial (Fig V.11, Fig V.12 A1-4) with an exclusion pattern on the cytofluorogram (Fig V.12 A2). Both Pearson's and Manders' coefficients being unequivocal in favour of exclusion (Table V.4, Fig V.19 & V.20). The low scores of Pearson's and Manders' for peroxisomal localization of AGT (between AGT and GO markers) in the absence of pyridoxine was confirmed by several experiments in stable transformants (Fig V.19 & V.20).

With increasing pyridoxine, peroxisomal AGT-170 was increasingly detected. At low levels of pyridoxine, some peroxisomal AGT-170 could be detected, but of low intensity compared to the mitochondrial fraction (Fig V.12 B2). There was more variability of targeting at this level of pyridoxine as peroxisomal AGT-170 could be detected in some cells and not in some adjacent cells. Overall, however, the colocalization coefficients for AGT and GO at low pyridoxine concentrations were low (Fig V.19 & V.20). At both 0.3 µM and 50 µM pyridoxine, significant peroxisomal AGT-170 was detected alongside mitochondrial AGT-170, as was seen in Chapter IV.2. The difference between 0.3 µM and 50 µM pyridoxine mainly seemed to be a higher intensity of AGT signal at higher pyridoxine (Fig V.11 & V.12). The increase in Pearson's and Manders' colocalization coefficients between AGT-170 and GO alongside increased pyridoxine levels was obvious (Fig V.19 & V.20). Even at 50 µM pyridoxine, when the peroxisomal fraction of AGT-170 was the strongest, most of AGT-170 appeared to remain in the mitochondria.

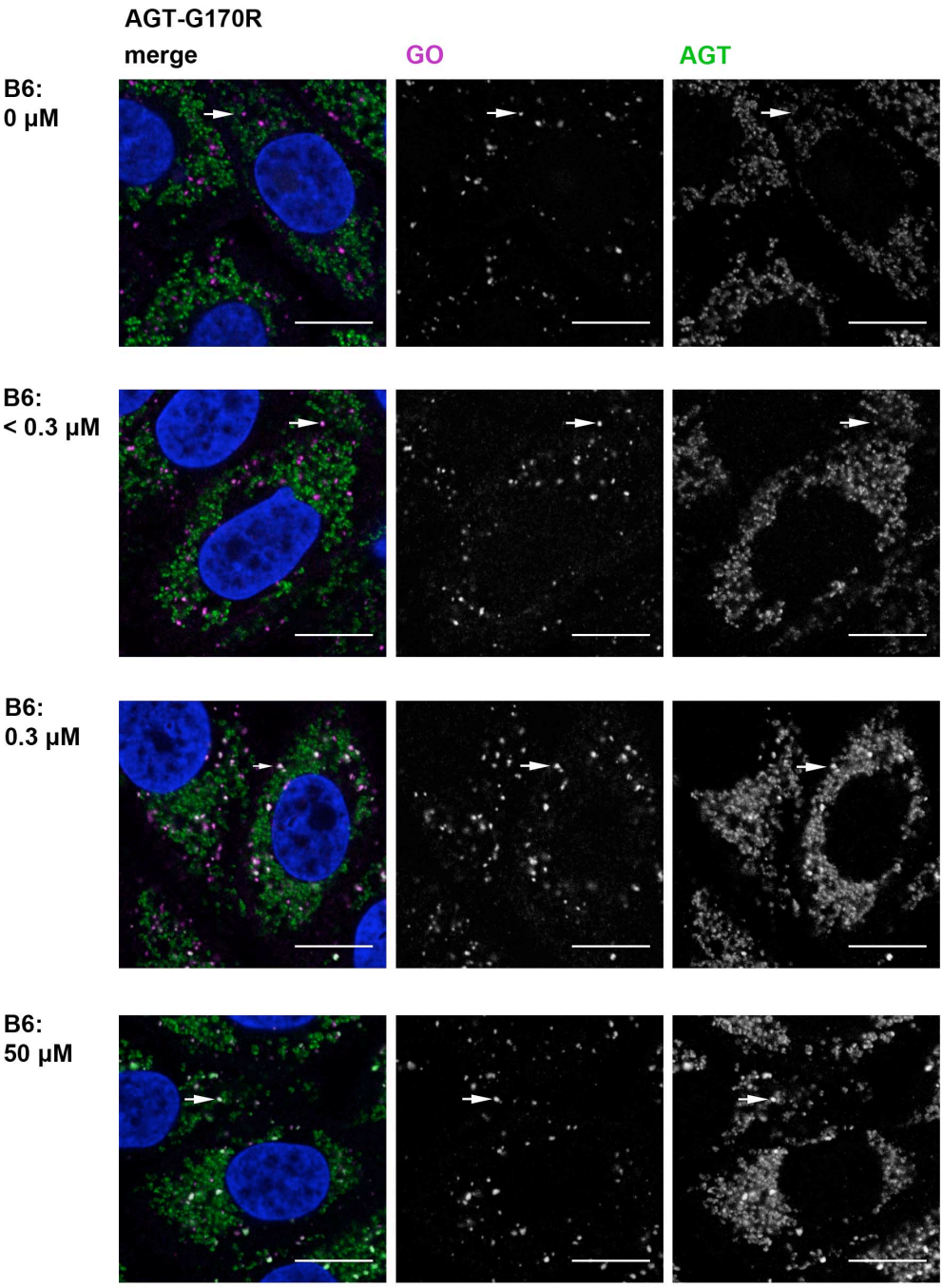

Figure V-11. **Effect of pyridoxine on the subcellular distribution of AGT-170 as shown by immunofluorescence microscopy - 1.** CHO GO AGT-170 cells were grown at least 4 weeks in the various concentrations of pyridoxine (B6) (0, < 0.3 µM, 0.3 µM, 50 µM, Methods III.2) and stained with anti AGT (green), anti GO (magenta), Hoechst (blue). Scale bar : 10 µm. Merged and single channel images from a single z-plane are shown for each pyridoxine level. White arrows point to a peroxisome.

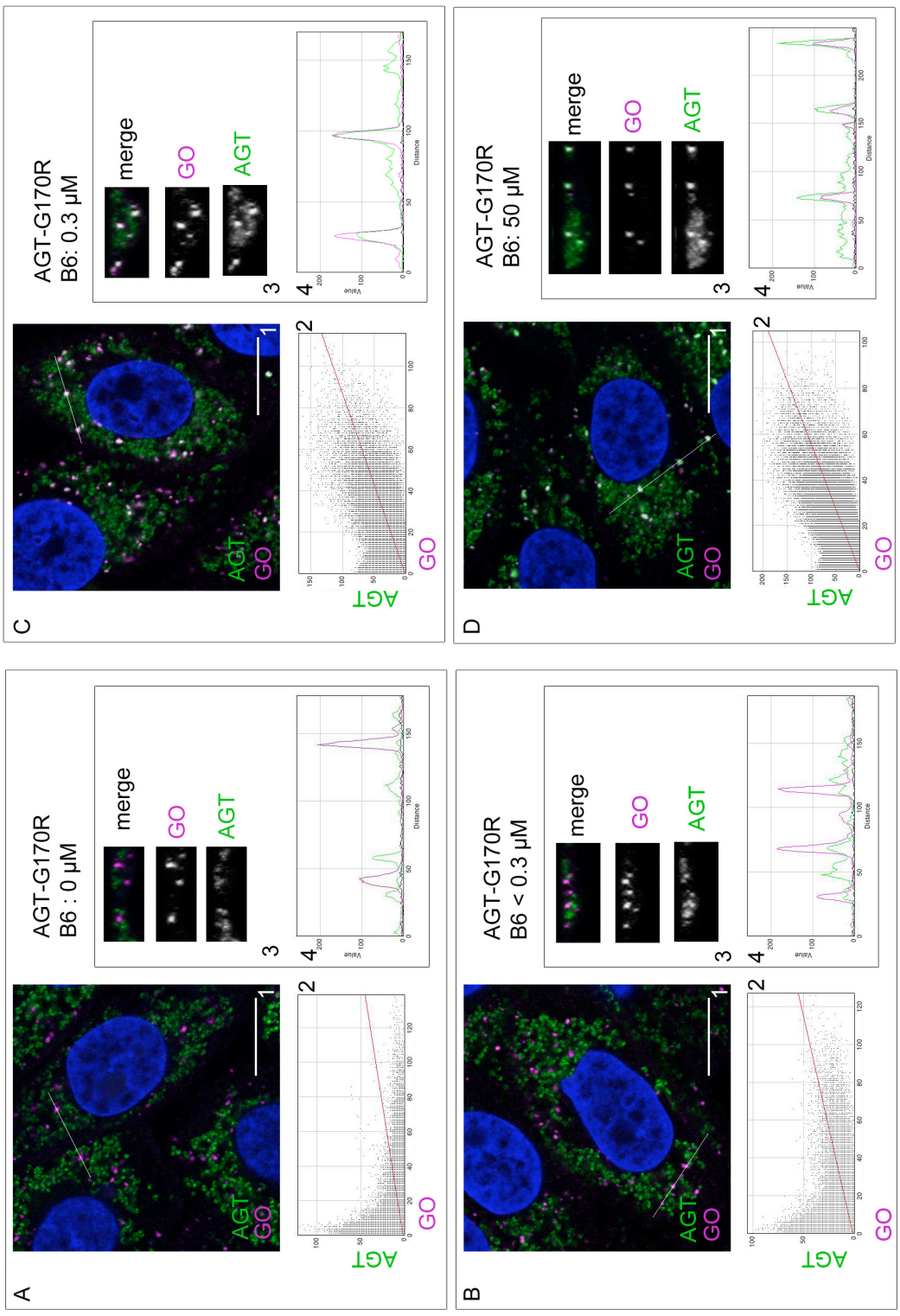

Figure V-12. **Effect of pyridoxine on the subcellular distribution of AGT-170 as shown by IMF - 2.** CHO GO AGT-170 cells in 0 µM (A); < 0.3 µM (B); 0.3 µM (C); 50 µM(D) pyridoxine (Methods III.2). AGT (green), GO (magenta), Hoechst (blue). (1): merged image from a single z-plane ; (2): cytofluorogram for the whole z-stack. Reslice along the z-axis (3) and RGB profile (4) plotted along the line drawn in (1). Scale bar : 10 µm. Colocalization coefficients in (Table V.4).

GO/AGT	AGT-170		
pyridoxine	*P*	*M1 (GO)*	*M2 (AGT)*
0 µM	0.196	0.003	0.002
< 0.3 µM	0.254	0.036	0.019
0.3 µM	0.534	0.620	0.323
50 µM	0.632	0.828	0.329

Table V-4. **Colocalization coefficients for Fig V.12.** Pearson's coefficient: P; Manders' M1 (GO) and M2 (AGT). Coefficients are manually thresholded.

V.5.2.2 Effect of pyridoxine on the peroxisomal localization of AGT-152

For AGT-152, three concentrations of pyridoxine were used, (< 0.3 µM, 0.3 µM, 50 µM) in stable transformants. The presence of peroxisomal AGT-152 in the complete absence of pyridoxine can therefore not be tested. At low levels of pyridoxine, most of the AGT-152 was detected in mitochondria, (Fig V.13, V.14, Table V.5) but some was also detectable in peroxisomes (Fig V.14 A2). With increasing pyridoxine, increasing levels of peroxisomal AGT-152 were detected, both by qualitative and quantitative methods (Fig V.13, V.14, Table V.5, Fig V.19, V.20). As was seen for AGT-170, the main difference of AGT-152 targeting was observed between < 0.3 µM and 0.3 µM pyridoxine, there was less difference between 0.3 and 50 µM pyridoxine.

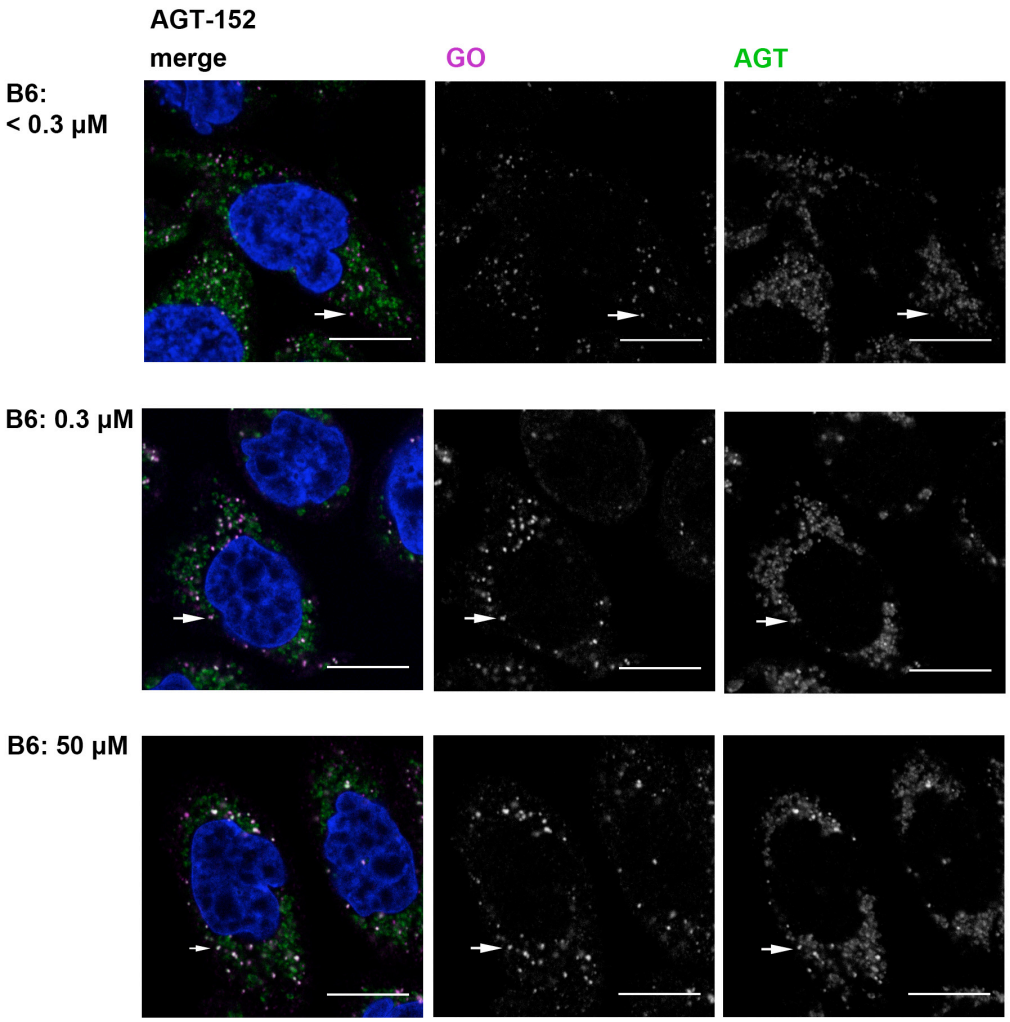

Figure V-13 **Effect of pyridoxine on the subcellular distribution of AGT-152 as shown by immunofluorescence microscopy - 1.** CHO GO AGT-152 cells were grown at least 4 weeks in the various concentrations of pyridoxine (B6) (< 0.3 µM, 0.3 µM, 50 µM) (Methods III.2) and stained with anti AGT (green), anti GO (magenta), Hoechst (blue). Scale bar : 10 µm. Merged and single channel images from a single z-plane are shown for each pyridoxine level. White arrows point to a peroxisome.

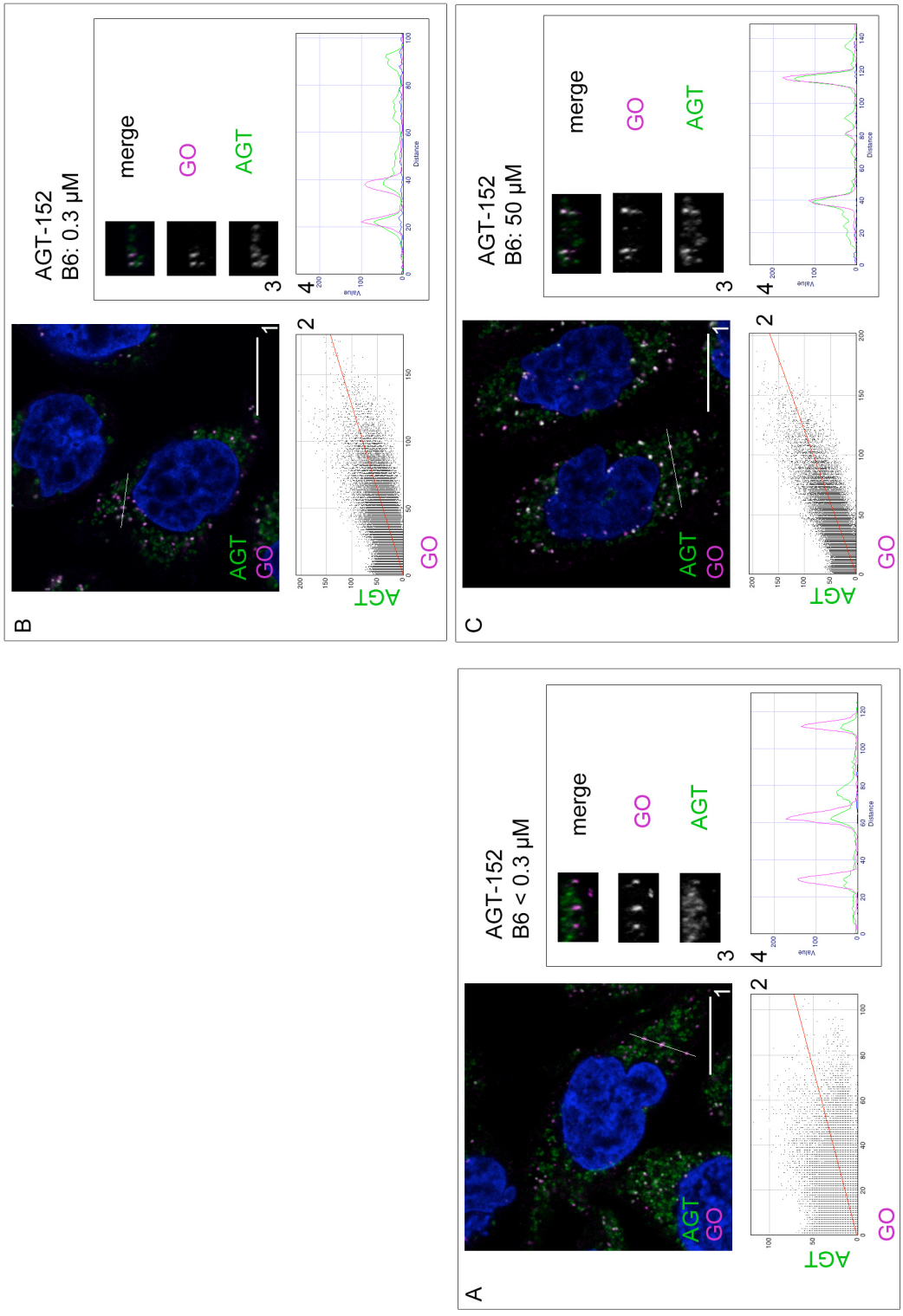

Figure V-14. **Effect of pyridoxine on the subcellular distribution of AGT-152 as shown by IMF - 2.** CHO GO AGT-152 cells in < 0.3 µM (A); 0.3 µM (B); 50 µM(C) pyridoxine (Methods III.2). AGT (green), GO (magenta), Hoechst (blue). (1): merged image from a single z-plane ; (2): cytofluorogramfor the whole z-stack. Reslice along the z-axis (3) and RGB profile (4) plotted along the line drawn in (1). Scale bar : 10 µm. Colocalization coefficients in (Table V.5).

Figure V-14 **Effect of pyridoxine on the subcellular distribution of AGT-152 as shown by IMF – 2.**

GO/AGT	AGT-152		
pyridoxine	*P*	*M1 (GO)*	*M2 (AGT)*
< 0.3 µM	0.438	0.591	0.149
0.3 µM	0.653	0.863	0.259
50 µM	0.745	0.899	0.411

Table V-5. **Colocalization coefficients for Fig V.14.** Pearson's coefficient: P; Manders' M1 (GO) and M2 (AGT). Coefficients are manually thresholded.

V.5.2.3 Effect of pyridoxine on the subcellular localization of AGT-244

The subcellular localization of AGT-244 was studied at three concentrations of pyridoxine (< 0.3 µM, 0.3 µM, 50 µM) in stable transformants (Fig V.15, V.16, Table V.6). In all levels studied, the peroxisomal fraction of AGT-244 was predominant, even more so than had been shown in earlier experiments (Chapter IV.2). The mitochondrial fraction of AGT-244 could still be detected at and below 0.3 µM pyridoxine (Fig V.15, Fig V.16 A4 & B4) and is also indicated by the lower M1 (GO in AGT) Manders' coefficient compared to the M2 (AGT in GO). At higher pyridoxine concentrations (50 µM), however, there was almost no detectable mitochondrial AGT-244 (Fig V.15, Fig V.16, Table V.6, Fig V.19, V.20) with correspondingly high M1 and M2 Manders' coefficients.

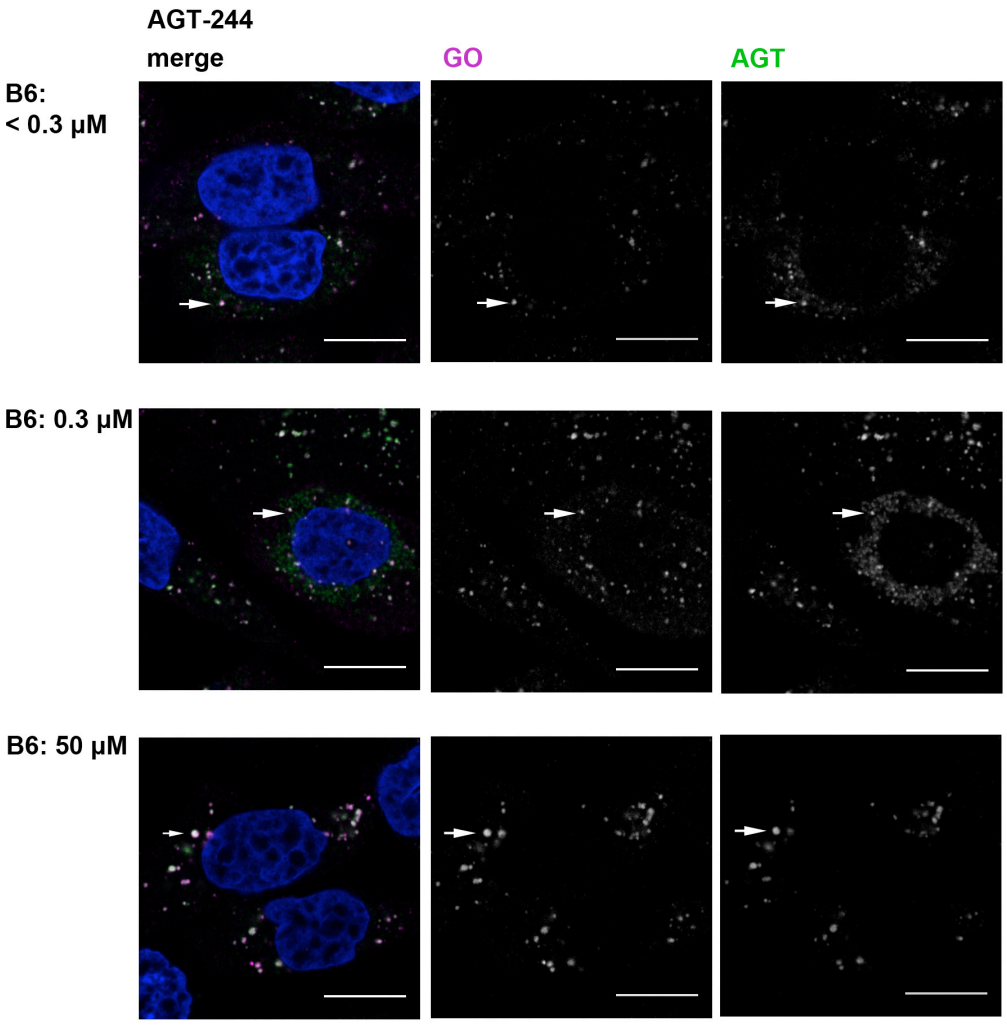

Figure V-15 **Effect of pyridoxine on the subcellular distribution of AGT-244 as shown by immunofluorescence microscopy - 1.** CHO GO AGT-244 cells were grown at least 4 weeks in the various concentrations of pyridoxine (B6) (< 0.3 µM, 0.3 µM, 50 µM) (Methods III.2) and stained with anti AGT (green), anti GO (magenta), Hoechst (blue). Scale bar : 10 µm. Merged and single channel images from a single z-plane are shown for each pyridoxine level. White arrows point to a peroxisome.

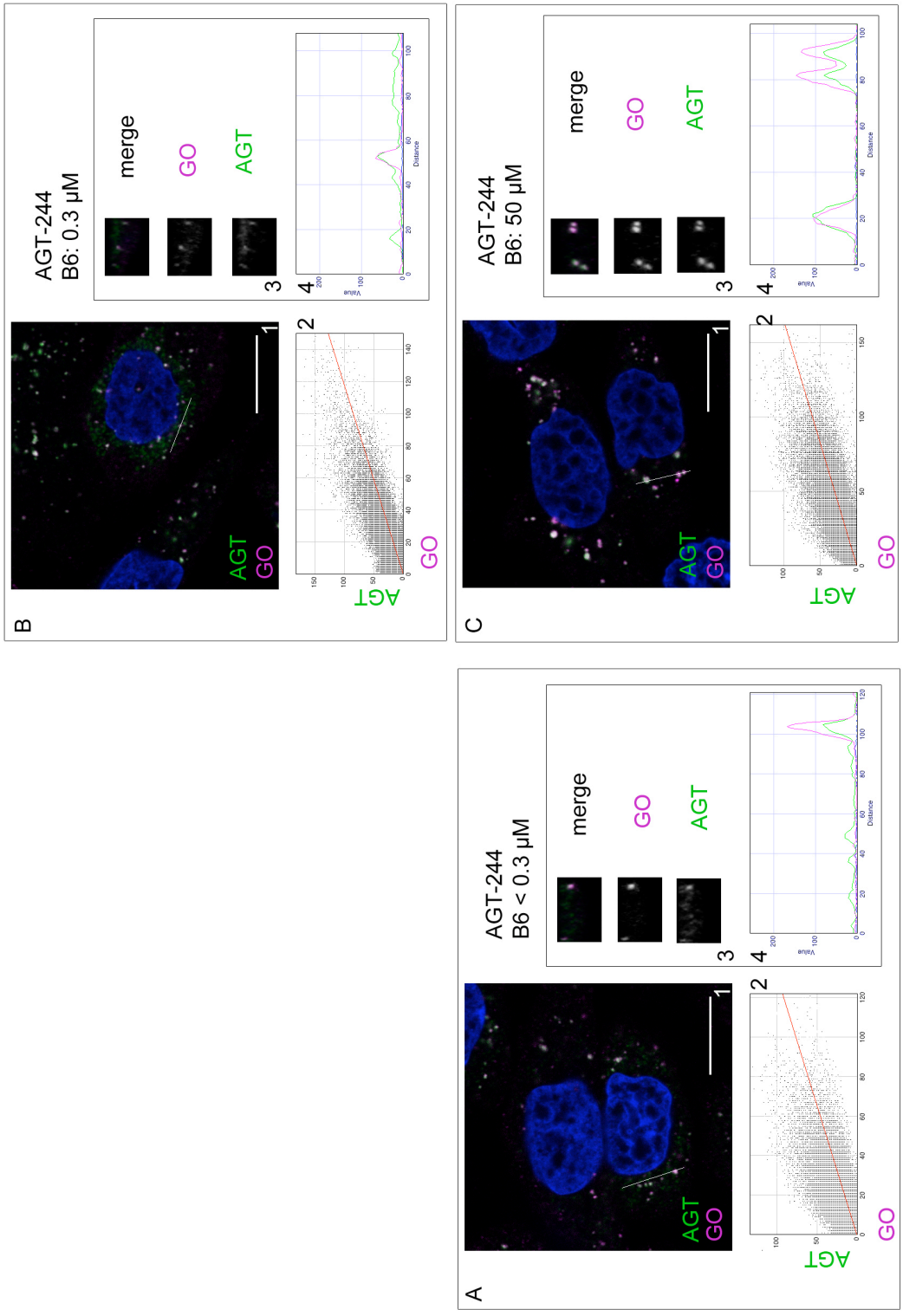

Figure V-16. . **Effect of pyridoxine on the subcellular distribution of AGT-244 as shown by IMF - 2.** CHO GO AGT-244 cells in < 0.3 µM (A); 0.3 µM (B); 50 µM(C) pyridoxine (Methods III.2). AGT (green), GO (magenta), Hoechst (blue). (1): merged image from a single z-plane ; (2): cytofluorogram for the whole z-stack. Reslice along the z-axis (3) and RGB profile (4) plotted along the line drawn in (1). Scale bar : 10 µm. Colocalization coefficients in (Table V.6).

GO/AGT	AGT-244		
pyridoxine	*P*	*M1 (GO)*	*M2 (AGT)*
< 0.3 µM	0.631	0.769	0.574
0.3 µM	0.734	0.965	0.325
50 µM	0.822	0.987	0.965

Table V-6. **Colocalization coefficients for Fig V.16.** Pearson's coefficient: P; Manders' M1 (GO) and M2 (AGT). Coefficients are manually thresholded.

V.5.2.4 Effect of pyridoxine on the subcellular localization of AGT-41

The subcellular localization of AGT-41 was studied at three levels of pyridoxine (<0.3 µM, 0.3 µM, and 50 µM) in stable transformants (Fig V.17, V.18, Table V.7). Although AGT-41 was dually targeted to mitochondria and peroxisomes below and at 0.3 µM pyridoxine concentrations, the majority of AGT-41 appeared peroxisomal in this experiment. At high pyridoxine level, most but not all of the AGT-41 was peroxisomal. (Table V.7, Fig V.19, V.20). Although the mitochondrial fraction seemed fainter at 50 µM pyridoxine, there was no obvious change in the colocalization coefficients, contrasting with results shown earlier (Chapter IV.2).

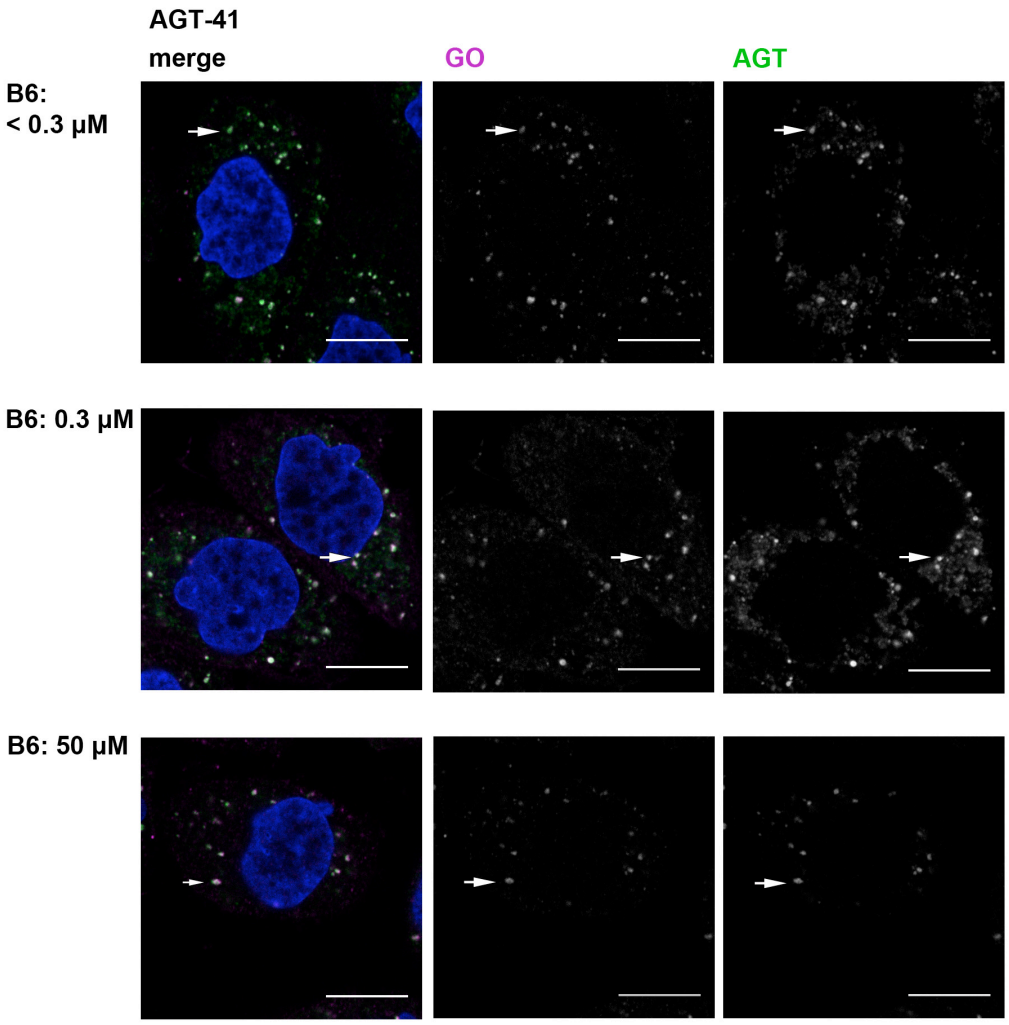

Figure V-17 **Effect of pyridoxine on the subcellular distribution of AGT-41 as shown by immunofluorescence microscopy - 1.** CHO GO AGT-41 cells were grown at least 4 weeks in the various concentrations of pyridoxine (B6) (< 0.3 µM, 0.3 µM, 50 µM) (Methods III.2) and stained with anti AGT (green), anti GO (magenta), Hoechst (blue). Scale bar : 10 µm. Merged and single channel images from a single z-plane are shown for each pyridoxine level. White arrows point to a peroxisome.

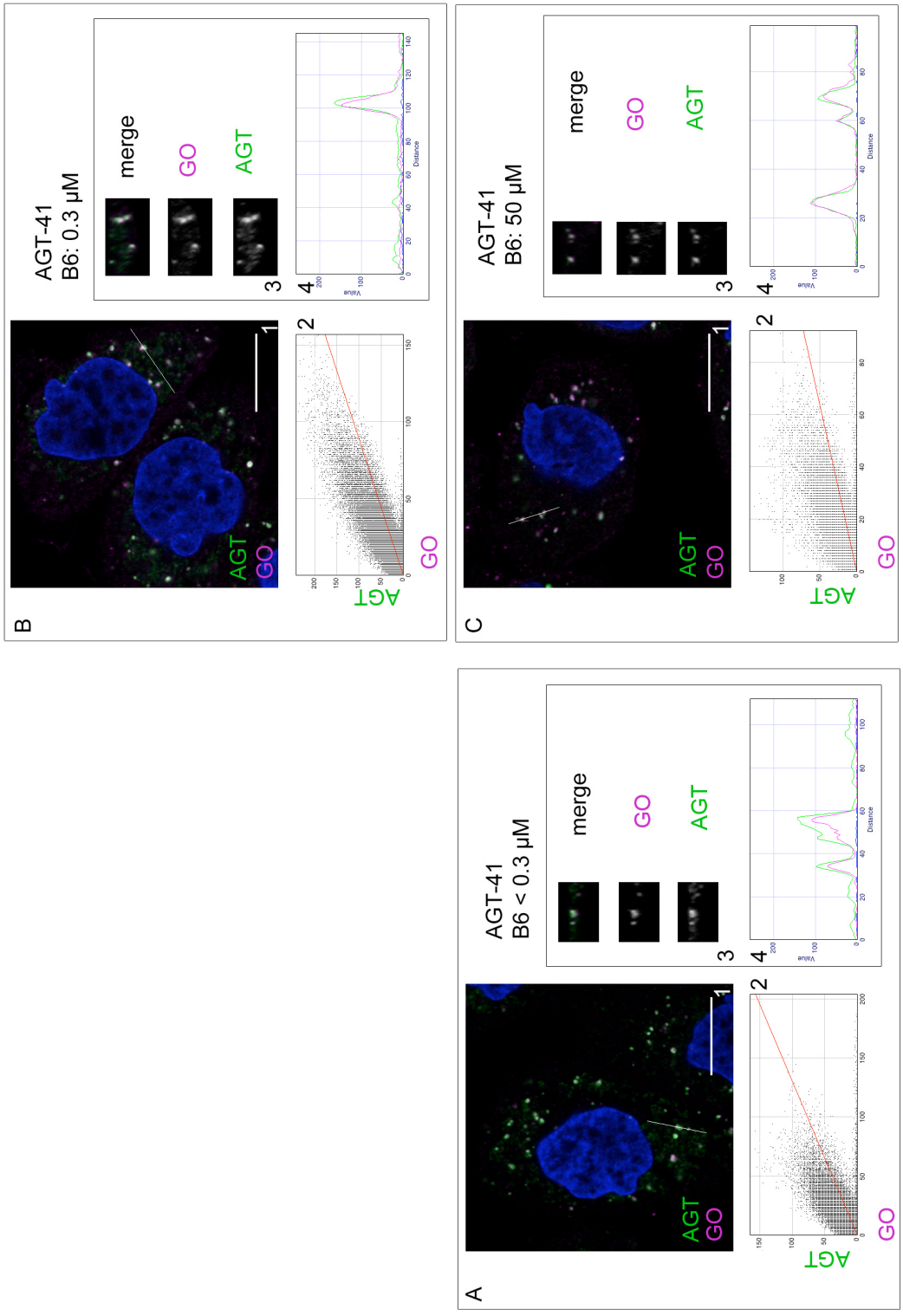

Figure V-18. **Effect of pyridoxine on the subcellular distribution of AGT-41 as shown by IMF - 2.** CHO GO AGT-42 cells in < 0.3 µM (A); 0.3 µM (B); 50 µM(C) pyri-doxine (Methods III.2). AGT (green), GO (magenta), Hoechst (blue). (1): merged image from a single z-plane ; (2): cyto-fluorogram the whole z-stack. Reslice along the z-axis (3) and RGB profile (4) plotted along the line drawn in (1). Scale bar : 10 µm. Colocalization coefficients in (Table V.7).

Figure V-18. **Effect of pyridoxine on the subcellular distribution of AGT-41 as shown by IMF - 2.**

GO/AGT	AGT-41		
pyridoxine	*P*	*M1 (GO)*	*M2 (AGT)*
< 0.3 µM	0.654	0.822	0.559
0.3 µM	0.732	0.903	0.535
50 µM	0.687	0.856	0.558

Table V-7. **Colocalization coefficients for Fig V.18.** Pearson's coefficient: P; Manders' M1 (GO) and M2 (AGT). Coefficients are manually thresholded.

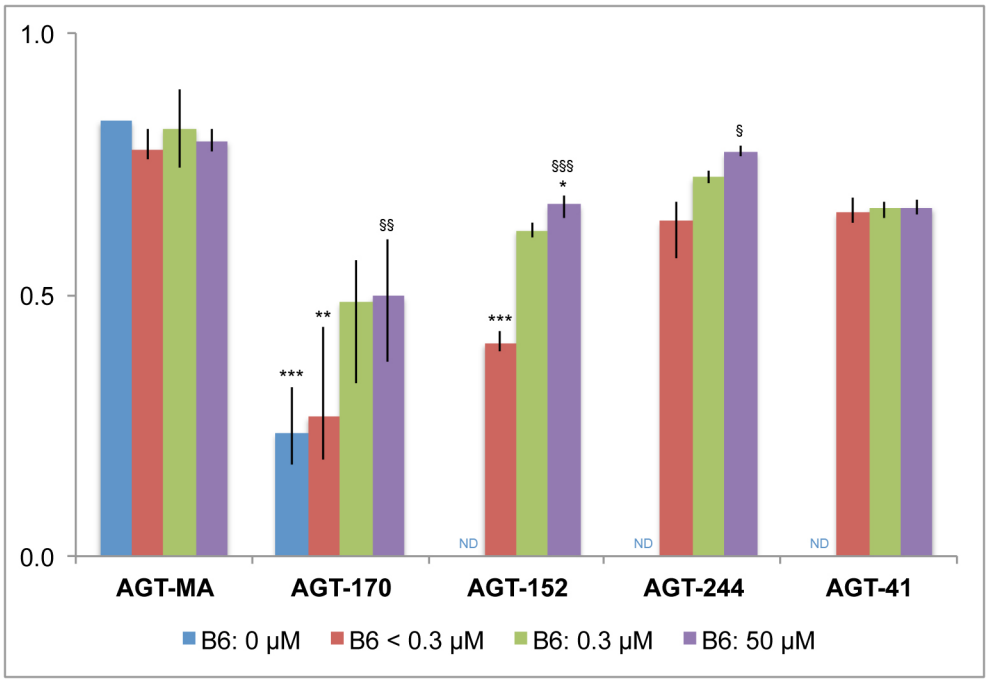

Figure V-19 **Analysis of the effect of pyridoxine on the subcellular distribution of AGT variants based on immunofluorescence microscopy - Pearson's colocalization coefficients.** CHO GO AGT cells were grown at least 4 weeks in various concentrations of pyridoxine (B6) (0; < 0.3 µM; 0.3 µM; 50 µM) (Methods III.2) and stained with anti AGT and anti GO. Pearson's coefficients were calculated on manually thresholded images for each pyridoxine level and each construct. The results are given as means of several images (n images ≥ 3, n cells ≥ 10). The range is displayed by the vertical bars. The statistical signifance is marked with (*) if compared to pyrtidoxine=0.3 µM or (§) if compared to pyridoxine < 0.3 µM. p< 0.05 (*/§), p< 0.01 (**/§§), p< 0.001 (***/§§§).

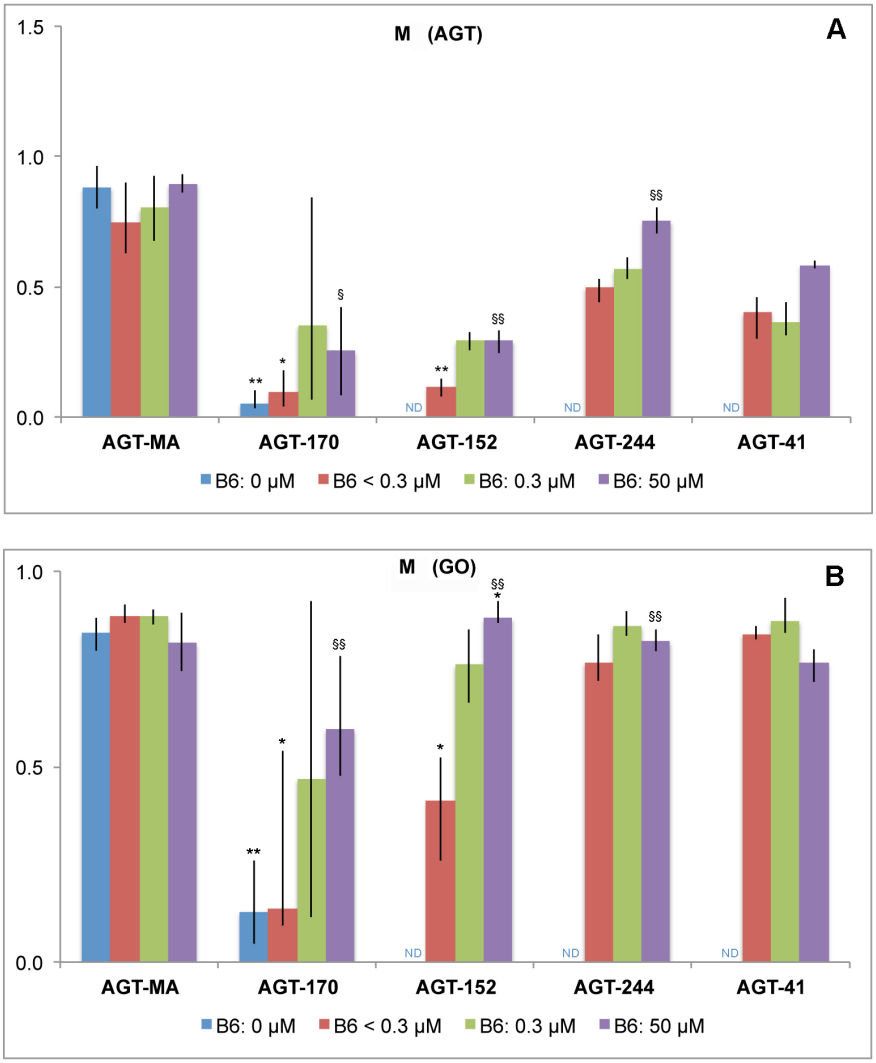

Figure V-20 **Analysis of the effect of pyridoxine on the subcellular distribution of AGT variants based on immunofluorescence microscopy – Manders' colocalization coefficients.** CHO GO AGT cells were grown at least 4 weeks in various concentrations of pyridoxine (B6) (0; < 0.3 µM; 0.3 µM; 50 µM) (Methods III.2) and stained with anti AGT and anti GO. Manders' coefficients were calculated on manually thresholded images for each pyridoxine level and each construct. (A): Manders' M(AGT) coefficient for AGT; (B): Manders' M(GO) coefficient for GO. The results are given as means of several images (n images ≥ 3, n cells ≥ 10), the range is displayed by the vertical bars. The statistical signifance is marked with (*) if compared to pyrtidoxine=0.3 µM or (§) if compared to pyridoxine < 0.3 µM. p< 0.05 (*/§), p< 0.01 (**/§§), p< 0.001 (***/§§§).

V.5.3 Summary

The peroxisomal localization of AGT-170, AGT-152 and AGT-244 increased with increasing pyridoxine concentrations. The effect of pyridoxine was greater when comparing low levels of pyridoxine (0, < 0.3 µM) to higher concentrations. Both AGT-244 and AGT-41 were more peroxisomal than previously shown (Chapter IV.2).

V.6 Discussion on the mechanisms of action of pyridoxine on AGT

V.6.1 Levels of B6 vitamers in transformed CHO cells

In order to study the effect of pyridoxine on AGT it was essential to be able to vary the concentration of vitamin B6 in the cells. The measurement of B6 vitamers in transformed CHO cells was carried out after at least 4 weeks of culture at the chosen pyridoxine concentration. Four weeks was chosen to allow a full turn-over of AGT so that all the AGT would have been synthesized, folded and targeted in the presence of the required pyridoxine concentration.

The measurement of B6 vitamers in the CHO cells demonstrated that B6 vitamers, especially PLP, could be increased by culture with excess pyridoxine. The increase in vitamin B6 in the cells, however, did not parallel that of extra-cellular pyridoxine since the latter varied between near zero and 250 μM, whereas the intra-cellular B6 content varied ten-fold (the PLP varied between 23 -31 nmol/g cell protein to 241 -289 nmol/g cell protein). This is not unexpected as intra-cellular levels of vitamin B6 have been described as regulated. A complete depletion of intra-cellular PLP could not be obtained, and residual levels of PLP (22 nmol/g cell protein) were seen even in the absence of pyridoxine added to the culture. Later experiments have shown that such low levels were sufficient to deprive some AGTs of their activity and can represent therefore a "no B6" control. The reason for the persistence of PLP could be the presence of trace vitamin B6 in the dialysed serum used for culture, recycling or slow turn-over of PLP bound to long-life proteins in the cells.

Intra-cellular levels of PLP have been determined in rat liver and rat hepatocytes and levels range between 35 and 49 nmol/g wet weight (Bosron et al., 1978; Lumeng et al., 1980). Assuming that the protein content of such cells would be 18% (Alberts B, Johnson A, Lewis J, et al., 2002), the intra-cellular PLP content in such studies would range between 195 and 272 nmol/g cell protein. The intra-cellular PLP levels found in the present work are lower (between 32 and 136 nmol/g cell protein for extra-cellular pyridoxine between <0.3 – 250 μM) but rely on different techniques of measurements. However they remain comparable and physiologically relevant for the purpose of this study.

The main B6 vitamer detected was PLP, followed by PMP in concentrations of extra-cellular pyridoxine up to 0.3 μM as is seen in hepatocytes (Lumeng et al., 1980). The intra-cellular PLP levels reached a maximum at 0.3 μM pyridoxine in culture, the standard pyridoxine level in Ham's F12 medium. All three cell lines tested displayed increased PL concentrations, as has been found both in hepatocytes exposed to increased pyridoxine and in patients treated with pyridoxine (Table V.1) (Lumeng et al., 1980; Edwards et al., 1990a, b; Bor et al., 2003; Midttun et al., 2005). No increased PA could be detected in the CHO cells at high pyridoxine levels in contrast to what is seen in patients and rat hepatocytes, which indicates that the CHO cells,

though equipped with PNPO and PDXK as seen from the presence of all B6 vitamers, have low capacity for the degradation of vitamin B6 compared to other cell lines or release all PA in the medium (Fig V.2, V.3).

Intra-cellular PN and PNP were only detectable at the highest extra-cellular pyridoxine concentrations (50 & 250 μM). Levels of PN and PNP are very low or non-detectable in the absence of vitamin B6 treatment, both in patients and hepatocyte studies (Lumeng et al., 1980; Edwards et al., 1990a, b; Bor et al., 2003; Midttun et al., 2005). However, several authors have reported detectable (Midttun et al., 2005; Footitt et al., 2012) to very high (Edwards et al., 1990a; Bor et al., 2003) levels of PN and PNP in humans treated with pyridoxine, the more so with very high doses of pyridoxine (up to 7 times greater than the level of PLP for doses of 800 mg/day for (Edwards et al., 1990a)). In CHO GO AGT cells, PN and PNP accounted for more than PLP and PMP at the two highest levels of pyridoxine (50 & 250 μM). The biological significance in the CHO system of such levels of PN and PNP will be discussed later and may have some clinical relevance in treated patients.

V.6.2 Effect of pyridoxine on the overall expression of AGT

These results show that the overall level of expression of some of the AGT variants was modified by the concentration of pyridoxine in culture. Increasing extra-cellular pyridoxine concentrations increased the expression of the AGT mutants with a varying intensity.

The greatest effect of pyridoxine was seen on AGT-170 and AGT-244 especially between the two lowest levels of pyridoxine (0 and < 0.3 μM) compared to higher concentrations. In no instance did the increase in AGT expression exceed three-fold between the lowest and highest levels. There was no major effect on AGT-mi and a slight effect on AGT-MA at very high levels of pyridoxine.

The second effect of pyridoxine on AGT expression was the relative presence of monomer and dimer or higher order multimers detectable on non-cross-linked immunoblots. At standard levels of pyridoxine (0.3 μM) only mutant AGT-170, AGT-244 and AGT-41 showed presence of a non cross-linked dimer, and only traces for AGT-mi.

Non-cross-linked dimers comprised a much greater proportion of the total immunoreactive AGT at low pyridoxine concentrations. At lower levels of pyridoxine, there was much more detectable AGT dimers for the AGT mutants (except AGT-152 which has a tendency to monomerize) and also for AGT-mi. Some dimeric species could even be detected for AGT-MA in the absence of pyridoxine, although at very low levels. The presence of the dimer and multimers (for AGT-41) on non cross-linked immunoblots, is presumably related to the formation of highly stable misfolded aggregated AGT protein. It is possible that the increase of

detectable dimer on immunoblots is linked with the presence of more unstable conformers of AGT in the absence of pyridoxine.

A stabilizing effect of pyridoxine has been shown both for AGT and for other PLP-dependent enzymes as well (like TAT (Gross-Mesilaty et al., 1997)). Hopper *et al.* have shown that the stability of both purified recombinant AGT-MA and AGT-mi was increased by increasing pyridoxine in studies using different methods (thermal inactivation, SUPREX analysis of stability and differential scanning fluorimetry) (Hopper et al., 2008). Santana et al showed that the solubility of AGT-244 was increased in transfected COS cells by increasing the PLP concentration in the medium (Santana et al., 2003). Coulter-Mackie and Lian also showed a stabilizing effect of pyridoxine on purified recombinant AGT after partial trypsin digestion and an increased half-life for AGT-41 in proteasomal degradation experiments (Coulter-Mackie and Lian, 2006, 2008).

The overall level of AGT expressed results from the balance between the rate of synthesis and rate of degradation. In order to assess if pyridoxine decreased the degradation rate of mutant AGTs in CHO cells, the half-life of a mutant AGT like AGT-41, with a very short half-life, could be studied in varying pyridoxine concentrations.

V.6.3 Effect of pyridoxine on the catalytic activity of AGT

Increased activity of PLP-dependent enzymes in response to increased pyridoxine concentrations has been shown for different enzymes (tyrosine transaminase, ornithine ketoacid transaminase (OKT)) by several groups (Greengard and Gordon, 1963; Weleber et al., 1978; Kennaway et al., 1980; Ramesh et al., 1988; Shih et al., 1988; Gross-Mesilaty et al., 1997). The results showed that this is also true for AGT.

The presence of B6 vitamers (PLP 21.58 nmol/mg cell protein) in CHO cells cultured over four weeks in B6-free medium and dialysed FBS shows the near impossibility of removing B6 entirely from the cells. It is, therefore, not surprising that a residual AGT activity was detected in AGT-MA even under these culture conditions (6.39 μmol pyruvate/h/mg protein).

The pyridoxine concentration in culture had an effect on the activity of AGT variants that was quantitatively and qualitatively different between the variants.

In the absence of pyridoxine in culture and PLP in the assay, the activity of AGT-MA was decreased seven-fold but all the activity, *i.e.* the maximum activity assayed for AGT-MA in pyridoxine ≤ 0.3 μM, was recovered after addition of PLP in the assay. For some mutants, like AGT-170, the maximum activity increased with increasing pyridoxine. These two types of response to vitamin B6 can be interpreted as corresponding to two types of effect of vitamin B6. The first is a chaperone effect, the second is a prosthetic group effect.

The chaperone effect of PLP is one that takes place during the folding of the protein (affecting the overall expression, dimerization and targeting of AGT), whereas the prosthetic group effect takes place after the folding and targeting of AGT, in a mature dimer form and affects the catalytic activity of AGT. Both mechanisms were involved in different relative importance depending on the AGT variant.

The full recovery of activity of AGT-MA in the assay with PLP even without pyridoxine in culture, suggests that AGT-MA is able to fold and dimerize into its normal conformation even in the absence of its cofactor. This contrasts with the conclusion drawn by Hopper *et al.* who found that PLP stabilized purified recombinant AGT-MA (Hopper et al., 2008).

A prosthetic group effect was seen for AGT-mi, but a chaperone role was also shown as in the absence of pyridoxine in culture, the recovered activity was not maximum (35% of the maximum). This indicates that the presence of PLP is required for the correct acquisition of a fully functional dimer of AGT-mi. Other authors have shown that the stability of AGT-mi is decreased compared to AGT-MA, and it may be that the stabilizing effect of PLP found by Hopper *et al.*is also true in the cell (Hopper et al., 2008; Lumb and Danpure, 2000; Cellini et al., 2010a).

The AGT-anc variant was not assessed in the absence of pyridoxine in culture, but showed simply a prosthetic group effect, like AGT-MA.

The effect of pyridoxine on AGT-170 was both that of chaperone and prosthetic group. In the absence of pyridoxine in culture, AGT-170 had almost no activity (15% of its maximum activity at 250 μM pyridoxine). The increase of activity with increased pyridoxine in culture is the result of both prosthetic group and chaperone effect and cannot be attributed entirely to the increased overall expression level (also a chaperone effect) as this did not exceed a two-fold increase whereas the increase in activity was over six-fold. The chaperone effect of PLP on AGT could result in more stable protein and increased total levels but also in more correct folding and active protein.

Both AGT-152 and AGT-244 showed an increased activity with increasing pyridoxine in culture, but to a lesser extent than AGT-170, and participated of both mechanisms. The main effect on AGT-152 was a prosthetic group effect with loss of activity in the absence of PLP in the assay, but some chaperone effect was also present. For AGT-41, the activities remained below the detection level of the assay, whatever the pyridoxine concentration in culture.

The reason for the paradoxical decrease in activity seen at the highest levels of pyridoxine in culture for the three normal AGT variants (AGT-MA, AGT-mi, AGT-anc) is possibly related to the presence of high levels of intra-cellular PN and PNP at these concentrations of extra-cellular pyridoxine in the culture medium. It is possible that PN or PNP may bind to AGT and act as inhibitors to decrease the activity. In order to investigate this, it would be interesting to study

the affinities of the respective B6 vitamers on AGT variants, which could be done on purified recombinant AGT. It should be noted that while there was a decrease in activity in high pyridoxine only for AGT-MA, AGT-mi and AGT-anc, the activity of the mutants plateaued at these levels. Such a paradoxical effect on a PLP-dependent enzyme is not widely known. In one study, a decrease in the activity of a normal variant of a PLP-dependent enzyme, ornithine ketoacid transaminase (OKT), was found in the presence of very high PLP concentrations in the assay (> 0.5 mM), whereas the mutant OKT showed an increased activity at these same levels (Kennaway et al., 1980). The decrease in normal OKT activity was moderate (20 to 25%) and no explanation was suggested by the authors.

V.6.4 Effect of pyridoxine on the intra-cellular targeting of AGT

These results show that pyridoxine has an effect on the targeting of mutant AGT in the cells. More precisely, pyridoxine increased the peroxisomal targeting of three out of four mutant AGTs.

The greatest shift in targeting was seen when comparing the lowest pyridoxine concentrations (0 and < 0.3 μM) and higher concentrations. This may be extrapolated to the situation in untreated versus B6-treated patients.

The subcellular localization of AGT was assessed qualitatively, by study of merged images, and quantitatively by colocalization coefficient analysis. An object-based approach was carried out (data not shown) as well as global statistic methods (JACoP) (see Methods III.6) (Bolte and Cordelières, 2006). Since the subcellular localization of most of the AGT mutants is dual (peroxisomal and mitochondrial) and no complete retargeting was obtained, two methods were finally chosen: Pearson's and Manders' coefficients. Thresholding was done manually because of the background cytosolic staining, added to the fact that GO and AGT staining, though localized in the same physical space, do not necessarily covary in intensity and that the intensity of AGT staining in peroxisome and mitochondria was not equal. However criteria for the setting of the threshold were consistent in analyses (identification of all structures marked with GO or AGT while retaining minimal cytosolic marking). The discrepancy between a lower Mander's M1 (AGT in GO) compared to the M2 (GO in AGT) in the dually targeted AGT variants reflects the fraction of non-peroxisomal AGT but the presence of some AGT in most peroxisomes.

The peroxisomal targeting of AGT-MA or AGT-anc (data not shown) was not affected by pyridoxine. This shows that the increased peroxisomal targeting did not result from an inhibition of the mitochondrial import machinery. Since, unlike peroxisomal proteins, mitochondrial protein have to be unfolded or loosely folded in order to be imported into mitochondria, the shift in distribution from mitochondria to peroxisomes is more likely to result

from an increase in the rapidly folded and cofactor bound AGT due to increased pyridoxine. Although increased pyridoxine concentrations led to a significant increase in the proportion of AGT-170 and AGT-152 targeted to peroxisomes, most still remained mitochondrial and complete peroxisomal retargeting of AGT was not achieved. It is possible that even in the absence of pyridoxine some AGT-170 was still targeted to peroxisomes but was below the level of detection of the method used in these experiments (IMF being less sensitive than IEM). It is interesting to note that, whereas the localization of AGT-170 in the absence of pyridoxine was clearly mitochondrial and the peroxisomal localization of AGT-170 was strong at high pyridoxine concentrations, there was inter-cellular heterogeneity in the intra-cellular distribution of AGT-170 at intermediate concentrations of pyridoxine.

The total staining intensity of AGT mutants at low levels of pyridoxine, and even more so in the absence of pyridoxine, was lower than the total staining intensity at high pyridoxine. This is consistent with the data discussed earlier (Chapter II.2), which showed that AGT expression is low in the absence or low levels of pyridoxine. Alternatively this could result from the presence of misfolded AGT and hidden epitopes undetectable by the anti-AGT antibodies used at low pyridoxine concentrations in culture.

There was a difference in the subcellular localization seen for AGT-244 and AGT-41 in pyridoxine concentration of 0.3 μM (standard F12 medium concentrations) between these and previous experiments (Chapter IV.2). In both Chapters IV.2 and V.5 a dual localization of the mutants was shown. However, the relative proportions of mitochondrial versus peroxisomal AGT mutants were different (the AGT was less mitochondrial). Although no formal proof can be obtained, it is possible that this difference is a result of different concentrations of pyridoxine and B6 vitamers in the FBS used (which had changed over the length of time devoted to this project and is not guaranteed by the manufacturer). The same trend in a higher peroxisomal localization was also detected in the other dual targeted AGT variants, although since their distribution is more heavily mitochondrial, a shift in localization does not result in a qualitative change in distribution of AGT, unlike AGT-244 and AGT-41. The greater peroxisomal localization of AGT-244, and AGT-41, can be discussed in view of the little that is known in human liver. For both, there is evidence of peroxisomal localization, although the additional presence of mitochondrial AGT cannot be excluded. Despite these differences, the combined data from Chapter IV and V indicate that the potential of pyridoxine to redirect the targeting of AGT variants destined for mitochondria to the peroxisomes instead is not restricted to AGT-170 and AGT-152 but applies also to AGT-244 and probably to AGT-41. The potential of pyridoxine to affect the targeting of AGT-41 was suggested in transient transfection experiments in COS and CHO cells where there was a distinct effect of medium added to the effect of cell type and type of transfection (Chapter IV.2.2).

The mechanism by which this preferential localization occurs has not been investigated in the present study and is only a matter of conjecture for AGT, although some data exists for other proteins. The increased peroxisomal targeting of AGT-170 and AGT-152, in addition to the main mitochondrial targeting, as well as the increased catalytic activity, may contribute to the pyridoxine responsiveness of patients bearing these mutations.

If glyoxylate detoxification has to occur in the same physical location as its production, *i.*e. in the peroxisome, then it is the peroxisomal activity of AGT, not the mitochondrial, which is biologically relevant in terms of metabolic efficiency. A doubling of the peroxisomal AGT could be significant in terms of the detoxification capabilities of mutant AGT and lead to a significant decrease in urinary oxalate (defined as a minimum 30% decrease), even though the total amount of mitochondrial AGT would hardly change. Whether the retargeting of AGT leads to an increased metabolic efficiency of mutant AGT or not will be discussed more fully in Part III of the Results (Chapter VI).

The kinetics of folding versus the kinetics of protein targeting is likely to play a crucial role in the final localization of AGT in the cell. Since mitochondrial import requires a non-folded or loosely folded conformation, a shift towards a faster and more stable folded conformation would result in a relative decrease of mitochondrial localization and relative increase in peroxisomal localization of AGT. The results shown here support this hypothesis. Compared to human liver, where immunoreactivity is low for many of the mutant AGTs, the transformed CHO cells have high overall levels of mutant AGT, which is mainly or partly targeted to mitochondria. Some effect of pyridoxine, with varying intensity depending on the mutation, on targeting can be detected for the AGT mutants. A non-mutation-specific effect such as stabilization of folded mutant AGT (chaperone effect), would allow faster dimer formation, making the MTS formed by the N-terminus less accessible to the mitochondrial import machinery or making the unfolding of AGT less easy and so allowing greater peroxisomal targeting of AGT instead of mitochondrial targeting (Leiper et al., 1996; Zhang et al., 2003).

A dual localization of proteins is known for a number of proteins, sometimes both peroxisomal and mitochondrial (Elgersma et al., 1995; Lee et al., 2000; Petrova et al., 2004). Different mechanisms governing this distribution have been described {reviewed in (Danpure, 1995; Karniely and Pines, 2005; Wolf et al., 2010)}. For AGT-anc, the dual targeting may result from the competition between two different targeting signals, similar to the other mutants (on the minor allele background). The AGT mutants studied here, have only one transcript and all possess the MTS created by the P11L change in the N-terminus. For them, the mechanism of dual targeting is likely to be a balance between the kinetics of folding and the kinetics of mitochondrial import. The role of protein folding in the targeting of a partly mitochondrial protein has been shown for other enzymes and supports the hypothesis that this mechanism controls AGT targeting. For fumarase, the presence of folded cytosolic protein can either result

from initial folding in the cytosol or import to mitochondria followed by export of folded enzyme (Stein et al., 1994; Knox et al., 1998; Sass et al., 2003). The speed of folding has been shown to have an impact on the final distribution of fumarase. Strobel *et al.* have shown that adenylate kinase has a weak N-terminal MTS (not cleaved after import) and that the enzyme folds rapidly in the cytosol without molecular chaperones (Strobel et al., 2002). In addition to cytosolic localization, adenylate kinase is targeted to the mitochondria and this targeting is decreased when folding is fast.

The mechanistic and kinetics of targeting and the role of PLP were not directly studied in the present work. Rather, it is the resulting, final, targeting which is observed. However, the stabilizing effect of PLP on AGT shown and the absence of evidence for some of the mechanisms described above, make the hypothesis of a change in the balance between the kinetics of folding and the kinetics of mitochondrial import the most probable (Hopper et al., 2008; Cellini et al., 2009, 2010a).

V.6.5 Conclusion

The results presented here have shown that a positive effect of pyridoxine on the effectiveness of some AGT mutants can be demonstrated *in vitro*, in transformed CHO cells. Several mechanisms have been observed: an increased expression of AGT, an increased catalytic activity due to both prosthetic group effect and chaperone effect and an increased peroxisomal targeting of AGT.

The relative importance of the different mechanisms involved depends on the mutation present on AGT and the strength of the effect of pyridoxine also depends on the mutation. The effect of pyridoxine can be understood as either a chaperone effect, promoting protein folding, reducing the presence of misfolded protein, all of which could increase the expression and activity of the mutant proteins. Or the role of PLP could be that of a prosthetic group effect, the cofactor of the enzyme, pyridoxine could increase the holo- to apo-enzyme ratio, thereby increasing the enzyme activity. In the case of PH1, an alternative could be to increase the activity of PLP-dependent enzymes other than AGT, such as GGT, which would rescue the phenotype. There is little evidence for that in the published data in patients, as the pyridoxine response is not generalized to all PH1 patients.

The mutation that showed the best response to pyridoxine in the present work was AGT-170, on which a strong chaperone role was shown, leading to increased overall expression, or decreased degradation, activity and peroxisomal targeting. In contrast, the main mechanism for AGT-152 seemed to be that of a prosthetic group effect, which had been predicted by the work on recombinant AGT-152 by Cellini *et al.* (Cellini et al., 2009). Surprisingly AGT-244 also

displayed evidence of B6-responsiveness in vitro, whereas B6-response (or absence of response) is not documented in patients with this mutation. It is known however that the immunoreactivity of AGT-244 in liver from patients is low, so that the full benefit of pyridoxine therapy perhaps requires a sufficient level of protein stabilization and overall expression level in the cell. Conversely, a vitamin B6 response has been shown in vitro for TAT deficiency without response in patients with TAT deficiency (Greengard and Gordon, 1963; Gross-Mesilaty et al., 1997). So pyridoxine responsiveness may or may not be present in PH1 patients carrying the I244T mutation.

This implies that the mechanisms of action of pyridoxine suggested in this study are non-mutation-specific even if the final, global, response varies between mutants and the effect of vitamin B6 are achieved by different mechanisms in different mutants. Therefore it could be that many more AGT mutants with missense mutations could benefit from pyridoxine therapy in varying degrees, ranging from the well-described sensitivity of AGT-170 to lesser responses.

The use of a mammalian cell system to study the effect of pyridoxine relies on a certain number of assumptions. One of these is that the conditions observed in patients can be reproduced in the simplified system, notably where levels of pyridoxine are concerned. As was mentioned before, even though normal levels of B6 vitamers are known in normal subject, and pyridoxine is used for treatment in a variety of situations, the plasma levels to aim for in patients treated are not defined. The plasma levels reported in the literature vary (Table V.1), but show that in general, the levels of PLP are increased by a factor of 10 or more (Lumeng et al., 1980; Edwards et al., 1990a; b; Bor et al., 2003; Midttun et al., 2005; Footitt et al., 2011, 2012). It appears, in the present study, that PLP concentrations are more regulated than concentrations of the other B6 vitamers. In the published literature, levels of PLP have been reported to remain increased by 10 times at increasingly high doses of pyridoxine, whereas PA and PL kept increasing to 400 – 900 times the basal levels. At high doses of pyridoxine (> 100 mg/day) some authors mention that B6 vitamers like PN and PNP, which are very low or undetectable in the absence of vitamin B6 treatment, can become detectable and even be greater than the level of PLP (Edwards et al., 1990a; Bor et al., 2003; Midttun et al., 2005).

In addition intracellular levels of vitamin B6 in the liver are not known in human, nor in tissue culture cell lines, like CHO cells. Most tissue culture cell growth conditions have been optimized over the years without regard for physiological significance. This is true also for pyridoxine levels. The levels of vitamin B6 supplementation in tissue culture media may vary by more than a factor of 50 depending on the medium used (0.3 μM for CHO cell medium Ham's F12 and 20 μM for COS cells medium DMEM). So that standard levels of pyridoxine in cell culture medium may be greater than the equivalent circulating levels of vitamin B6 in

human blood (normal plasma PLP range is 15 to 75 nM and represent a little over half the total vitamin B6).

A retrospective analysis of the results discussed above indicate that the pyridoxine level in culture most relevant to an untreated human patient is probably the "low" level of pyridoxine (< 0.3 μM). This conclusion was based on the targeting of the AGT mutants as well as the expression and catalytic activity of AGT mutants and normal AGT (which is not maximal without PLP in the assay in human liver {G Rumsby, London, personal communication}. Therefore the "standard" conditions (0.3 μM pyridoxine, Ham's F12 medium) may already mimic what happens in some treated patients and levels as high as 50 and 250 μM pyridoxine probably do not occur in patients, or rarely, though level between 0.3 and 50 μM may. No extra positive effect was shown at 250 μM compared to 50 μM pyridoxine and little between 0.3 and 50 μM, except for the inhibition of normal AGTs. Furthermore, very high levels of pyridoxine may lead to undesirable effects such as the decrease in AGT activity seen in normal AGTs for pyridoxine levels of 50 -250 μM, though mutant AGTs did not display a decrease in activity at these concentrations. This may be related to the fact that most B6-responsive PH1 patients who do so respond at low doses (5 to 10 mg/kg) and very few patients require higher doses to respond (Monico et al., 2005b).

The effects of pyridoxine discussed here have been shown on cell lysates or IMF. The translation into an increased metabolic efficiency of AGT mutants would require a test bringing together all the mechanisms described here in live cells. Such a test will be described in the following section of the present study (Chapter VI).

VI RESULTS part 3: Cell-based metabolic assay of AGT

The characterization of the various forms of AGT has been done in a wide variety of different systems. Several groups have published work based on purified recombinant AGT protein (Lumb and Danpure, 2000; Zhang et al., 2003; Coulter-Mackie and Lian, 2006; Cellini et al., 2007; Williams and Rumsby, 2007; Coulter-Mackie and Lian, 2008; Cellini et al., 2009, 2010a, b), in transiently transfected mammalian cells (see Chapters IV & V) (Leiper et al., 1996; Knott et al., 2000; Lumb et al., 2003; Huber et al., 2005), liver tissue (Noguchi and Takada, 1979) and yeast (Hopper et al., 2008).

Each type of approach has been used to address different aspects of AGT function. Studies on pure protein can give information on the stability, structure and catalytic properties of AGT variants in a controlled environment. Studies in cells can be used to yield more restricted information in a more complex environment, closer to the physiological one (human hepatocytes), mammalian cells being theoretically closer to human hepatocytes than yeast, while retaining a simplicity and flexibility absent in even more complex models such as mouse model.

The results described earlier in the present work (Chapter IV & V) come under this second, cellular, approach. However, the metabolic efficiency of AGT results from a combination of overall expression, catalytic activity and correct subcellular targeting, all addressed separately in the previous sections of the present study.

The stably transformed CHO cells system described by Behnam opened up the possibility of creating a metabolic assay of the functional efficiency of AGT (Behnam et al., 2006). The development of a system expressing both GO and AGT (and/or GR) was shown to recapitulate sequential steps of the metabolism of glyoxylate in which AGT plays a crucial role (Fig VI.1).

The expression of GO by the cells allows glycolate added to the culture medium to be converted to glyoxylate (see Introduction, Chapter II). Whereas glycolate is harmless for cells, glyoxylate is toxic. The co-expression of functional AGT and GO allowed the glyoxylate formed to be converted to harmless glycine. This was demonstrated by Behnam *et al.* (Behnam et al., 2006).

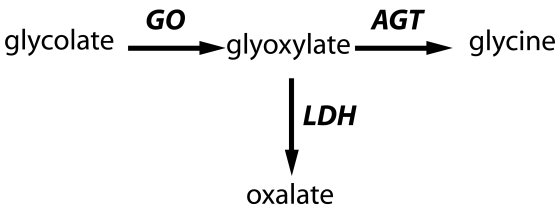

Figure VI-1. **Basis for the indirect glycolate toxicity in transformed CHO cells**. CHO cells expressing GO can catalyse the conversion of glycolate into glyoxylate, which is cytotoxic for cells. CHO cells expressing functional AGT as well as GO, can detoxify glyoxylate by converting it to glycine, which is harmless.

Following the same principle, any change in the efficiency of AGT, or GO, by the addition of pharmaceutical agents or chemical chaperones, could also be reflected in the response of transformed cells to the indirect toxicity induced by glycolate, and so, form a metabolic assay of the functional efficiency of AGT. These two points, *i.e.* the difference in response of AGT variants to the metabolic assay of indirect glycolate toxicity and the possibility to detect induced changes in the (biological) function of AGT variants following the addition of pyridoxine to the cell culture, are developed in this section.

In order to address them, the toxicity of different metabolites of glyoxylate was studied in the double transformed CHO cells. The ability of the different AGT variants to protect CHO cells from the indirect toxicity of glycolate, compared to normal AGT, was then studied. Finally, the effect of modifying the pyridoxine content of cells in culture on the response of transformed CHO cell lines to the indirect glycolate toxicity was studied.

VI.1 Cell-based metabolic assay

VI.1.1 Metabolic pathway of glycolate to glyoxylate conversion in transformed cells – Principle of the cell-based metabolic assay

The cell-based model of CHO cells expressing GO and AGT is based on the fact that it mimics a simplified hepatic metabolic pathway of glyoxylate metabolism. As is the case for hepatocytes, glycolate can be converted to glyoxylate, catalysed by GO. If AGT is present and functional, glyoxylate can be further converted to glycine (Fig IV.1 & IV.2). Glyoxylate could also be converted to oxalate catalysed by cytosolic LDH. Both glyoxylate and oxalate are thought to be cytotoxic whereas glycolate and glycine are harmless. In this way, exposing cells to glycolate in the culture medium (relying on expression of GO) or exposing cells directly to glyoxylate is sufficient to reveal the absence or the activity of AGT.

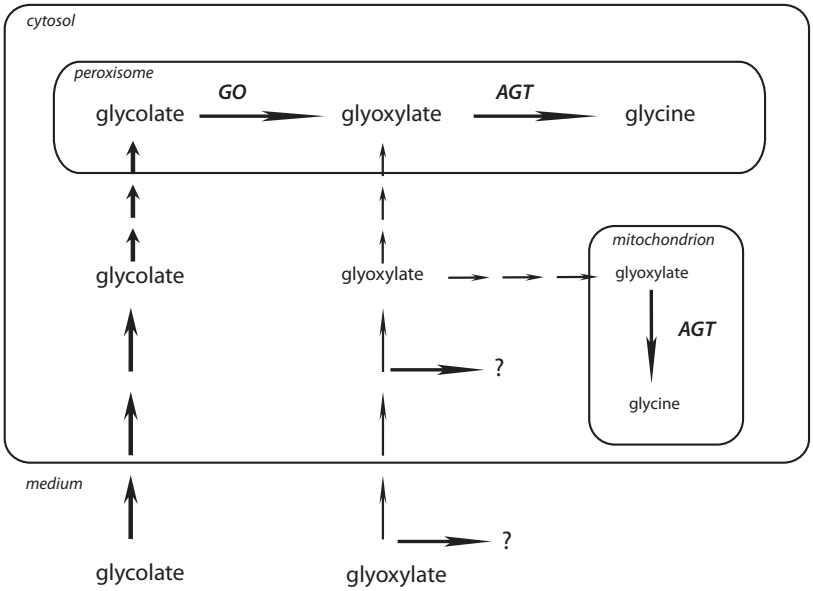

Figure VI-2. **Direct glyoxylate toxicity versus indirect glycolate toxicity in transformed CHO cells.** In indirect toxicity, glycolate is fed to the cells in the culture medium and can be catalysed to glyoxylate by GO in the peroxisomes, where it can be transformed into glycine catalysed by AGT. In the direct toxicity, glyoxylate added to the culture medium has to be taken up by the cell and then penetrate the peroxisome or the mitochondria in order to be transformed into the harmless glycine.

VI.1.2 Glyoxylate is toxic to CHO cells

Before the CHO transformants were metabolically assayed, the baseline sensitivity of CHO WT to the metabolites involved (glycine, glyoxylate, glycine, glycolate, oxalate) was tested. Whereas glycine and glycolate were harmless to CHO WT cells, even at high concentration, both glyoxylate and oxalate were toxic and resulted in decreased cell number in cultures exposed to concentrations in the millimolar range (Fig VI.3). Only 25% of the CHO WT cells exposed for 2 days to glyoxylate at 1 mM survived and almost all cells were killed (<1% survival) at 10 mM of glyoxylate.

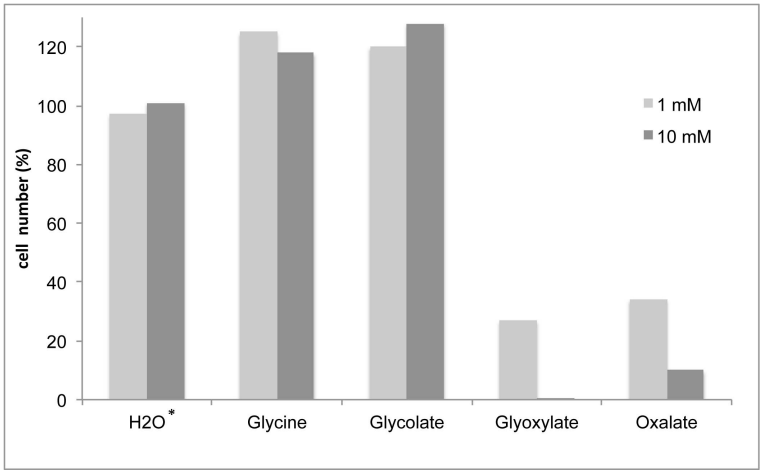

Figure VI-3. **Sensitivity of CHO WT to glyoxylate and its metabolites.** CHO WT cells were exposed for 2 days to two concentrations (1 and 10 mM) of glycine, glycolate, glyoxylate, oxalate or water (*: used as dilution control). The number of surviving cells was normalized against a control grown in normal medium.

VI.1.3 Functional AGT protects from glyoxylate toxicity

The toxicity of glyoxylate, as assessed by the survival of cells grown with different concentrations of glyoxylate, was tested on different CHO cell lines (Fig VI.4). Both CHO WT and CHO GO showed a sensitivity to glyoxylate exposure. Only 10 to 20% of the cells survived in concentrations at or above 800 μM and 60% do at 400 μM. In contrast, CHO GO AGT-MA and CHO GO AGT-mi were resistant to glyoxylate in the range of concentrations tested, with ~ 85% surviving at 1200 μM. The response of CHO GO AGT-170 fell between the two cases. While initially not sensitive to glyoxylate, the CHO GO AGT-170 cell line displayed a sensitivity for the higher glyoxylate concentrations with only 25% surviving at 1200 μM.

These results show that normal AGT, such as AGT-MA and AGT-mi, can protect the cells from glyoxylate poisoning, presumably by converting it to glycine. The presence of a mutant AGT, less functional, such as AGT-170, does not protect the cells as well as normal AGT, but in line with some residual catalytic activity of AGT (peroxisomal or not), the toxicity appears to be less than it is for cells without any AGT, such as CHO WT or CHO GO.

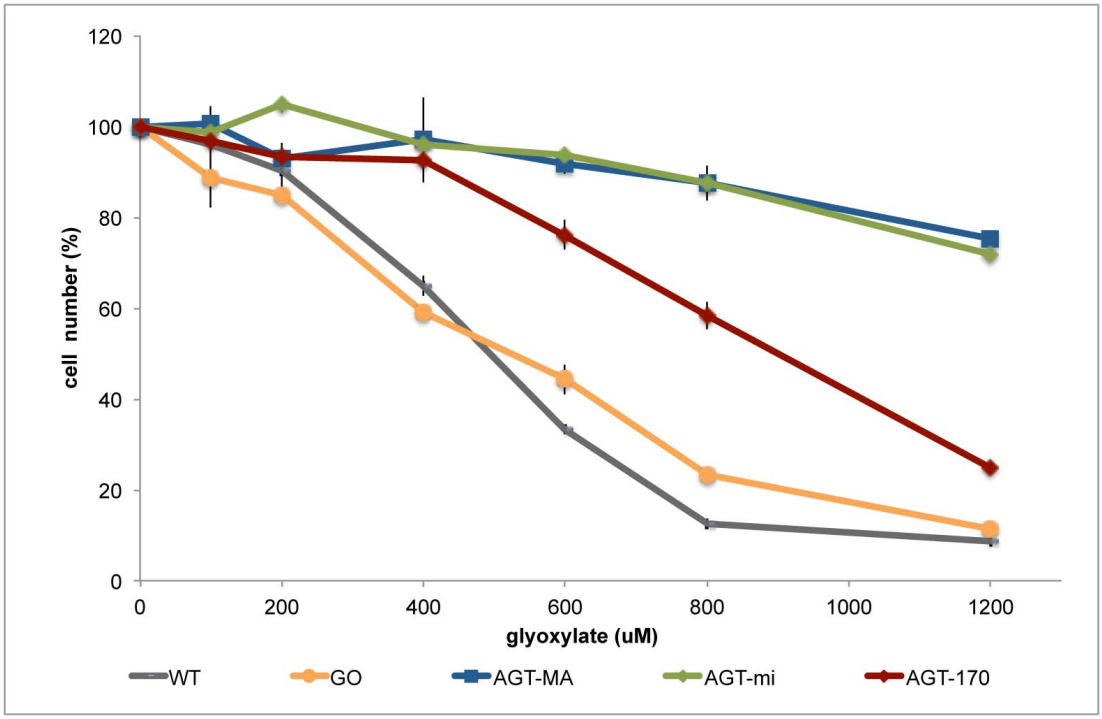

Figure VI-4. **Effect of AGT on the sensitivity of CHO cells to glyoxylate.** Different CHO cell lines (CHO, CHO WT GO, CHO GO AGT-MA, CHO GO AGT-mi, CHO GO AGT-170) grown under standard conditions (see Methods III.2), were exposed for 2 days to different concentrations of glyoxylate (0 to 1200 μM) The toxicity of glyoxylate was assessed by the decrease in surviving cells after 2 days of exposure. The results (n=2) are expressed as mean % of the control without glyoxylate for each cell line, vertical bars: range.

VI.2 Indirect toxicity of glycolate in the cell-based metabolic assay

VI.2.1 . Glycolate is indirectly toxic in CHO cells expressing GO but not AGT

As it had been shown by Behnam *et al.*, the presence of GO in CHO cells makes glycolate toxic due to its conversion to glyoxylate (Fig VI.5) (Behnam et al., 2006). Different CHO cell lines (CHO WT, CHO GO, CHO GO AGT-MA) were exposed to 2 days of either glycine, glycolate, glyoxylate or oxalate. As was shown earlier, CHO WT cells were not affected by high concentrations of glycolate, and CHO GO AGT-MA cells were only moderately affected. However the survival of CHO GO cells was close to that of CHO GO cells exposed to glyoxylate, confirming the role of GO in the generation of glyoxylate in the cells exposed to glycolate. At the high concentrations chosen, CHO GO AGT-MA did not protect entirely from glycolate and not at all from glyoxylate, showing that the relative levels of GO and AGT in the cells are relevant to the final degree of protection. This also confirms that glyoxylate, and possibly oxalate, are responsible for the cell toxicity observed.

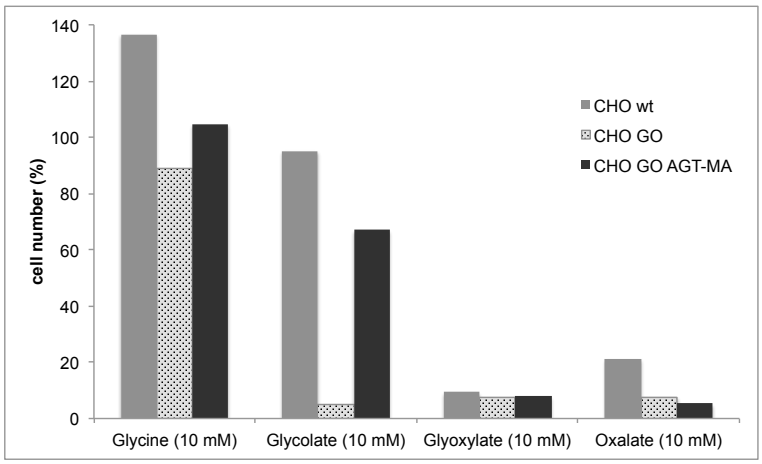

Figure VI-5. **Influence of GO and AGT on the sensitivity of CHO cells to glyoxylate metabolites.** CHO WT, CHO GO and CHO GO AGT-MA were exposed to 10 mM concentration of either glycine, glycolate, glyoxylate or oxalate for 2 days. The number of surviving cells was normalized against a control grown in standard medium and expressed as % of the control.

VI.2.2 Effect of AGT variants on the indirect toxicity of glycolate

VI.2.2.1.1 AGT mutants offer less protection against glycolate indirect toxicity than normal AGT

In order to characterize further the activity of AGT variants and to test the metabolic effectiveness of AGT variants, the indirect toxicity of glycolate was tested on all the different AGT variants described in this project. The CHO cell lines (CHO WT, CHO GO, CHO GO AGT-MA, CHO GO AGT-mi, CHO GO AGT-anc, CHO GO AGT-170, CHO GO AGT-152, CHO GO AGT-244, CHO GO AGT-41) were exposed to different concentrations of glycolate for 2 days, in standard conditions of pyridoxine concentrations (Fig VI.6, Annexe IX.14). As had been shown before, CHO WT were not affected by glycolate. CHO GO were very sensitive, with only 20% surviving at 250 µM and less than 10% at higher concentrations. All CHO GO AGT cell lines showed a sensitivity to the indirect toxic effects of glycolate but to different degrees. Less than 10% cells of all CHO AGT cell lines survived at 1500 µM glycolate and less than 25% at 1000 µM glycolate. For concentrations between 250 and 750 µM the response was different for the AGT variants. The best protection against glycolate indirect toxicity with ~ 80 % cells surviving at 500 µM was AGT-MA. Second came AGT-mi, AGT-anc and AGT-244 with similar survival, ~ 60 % for glycolate concentrations of 500 µM. AGT-170 and AGT-152 showed less than 50% survival at 500 µM, with AGT-170 being more resistant (40 % survival) than AGT-152 (~ 20 % survival). Lastly, CHO GO AGT-41 showed the same sensitivity as

CHO GO to glycolate. After two days of exposure to glycolate, the lowest survival rate was between 2 and 10 %. The time needed to kill all the cells at high concentrations of glycolate, as well as glyoxylate, was longer than 2 days (data not shown).

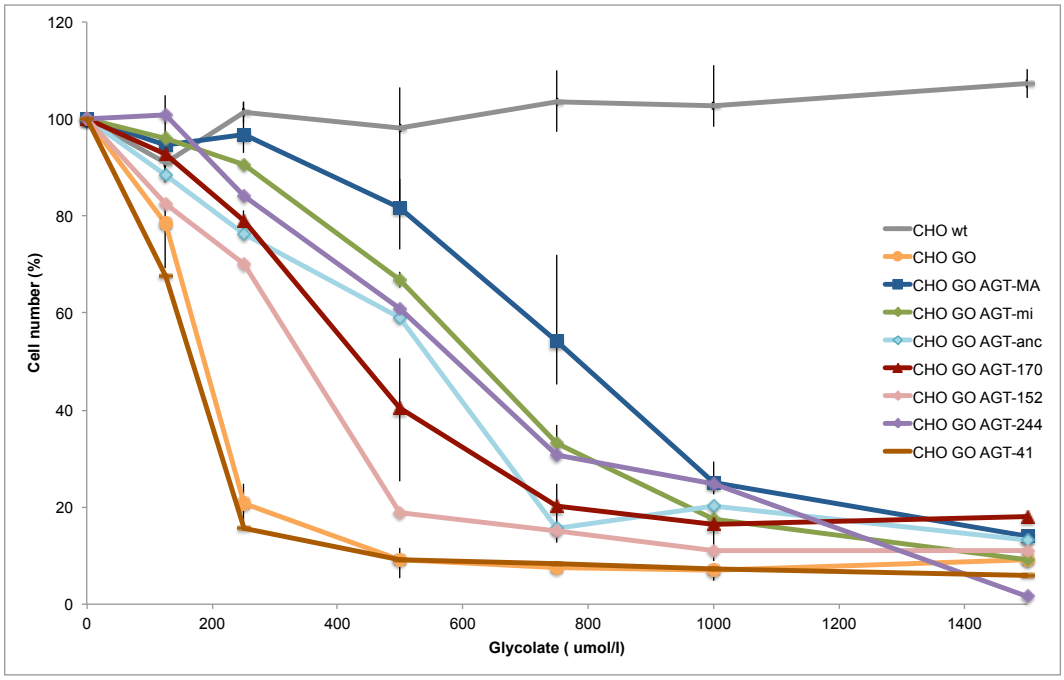

Figure VI-6. **Effect of AGT variants on the sensitivity of CHO cells to indirect glycolate toxicity.** Different CHO cell lines (CHO WT, CHO GO, CHO GO AGT-MA, CHO GO AGT-mi, CHO GO AGT-anc, CHO GO AGT-170, CHO GO AGT-152, CHO GO AGT-244, CHO GO AGT-41) grown under standard conditions (see Methods III.2), were exposed for 2 days to different concentrations of glycolate (0 to 1500 µM). The indirect toxicity of glycolate was assessed by the decrease in surviving cells after 2 days of exposure. The results (n=1 – 3) are expressed as mean % of the control without glycolate for each cell line, vertical bars: range (see Annexe IX.14).

VI.2.2.2 The survival of cells to the indirect toxicity of glycolate is due to the presence of AGT and not loss of GO

In order to confirm that the survival of cells to the indirect glycolate toxicity was due to the presence of AGT, the cells surviving the metabolic assay were stained for GO and AGT and studied by IMF (FigVI.7).

The cells surviving at high concentrations of glycolate, at which the presence of AGT and GO was assessed, showed a decreased growth rate. In order to stain these cells for IMF, it was necessary to wait a further 3 days before fixing. In order to maximize the cell recovery, no antibiotic selection was applied during these additional 3 days, so that the total number of days without antibiotic selection for GO and AGT was 5 days. It had been shown before (data not shown) that transformed CHO still express GO and AGT after a week in the absence of

antibiotic selection, but at significantly lower levels. As was therefore expected, the levels of AGT and GO staining (Fig VI.7) were lower than in standard conditions (see section IV.2) both after exposure to glycolate and in the controls.

All the cell lines expressed GO, showing that survival was not due to loss of GO and therefore absence of production of glyoxylate. All CHO GO AGT cells also expressed AGT, confirming the role of AGT in the protection afforded to the surviving cells. The subcellular localization of AGT was not radically modified by the addition of glycolate and remained dually localized for all mutants and AGT-anc and peroxisomal for AGT-MA and AGT-mi. Since the level of AGT staining was low, the mitochondrial fraction of AGT in mutants required image adjustments to be clearly visible in IMF (Fig VI.7, boxed squares: increased brightness).

In some transformed cells lines with mutant AGTs, the average level of AGT staining appeared greater in the cells surviving high concentrations of gycolate than controls (CHO GO AGT-152, CHO GO AGT-41) (Fig VI.7).

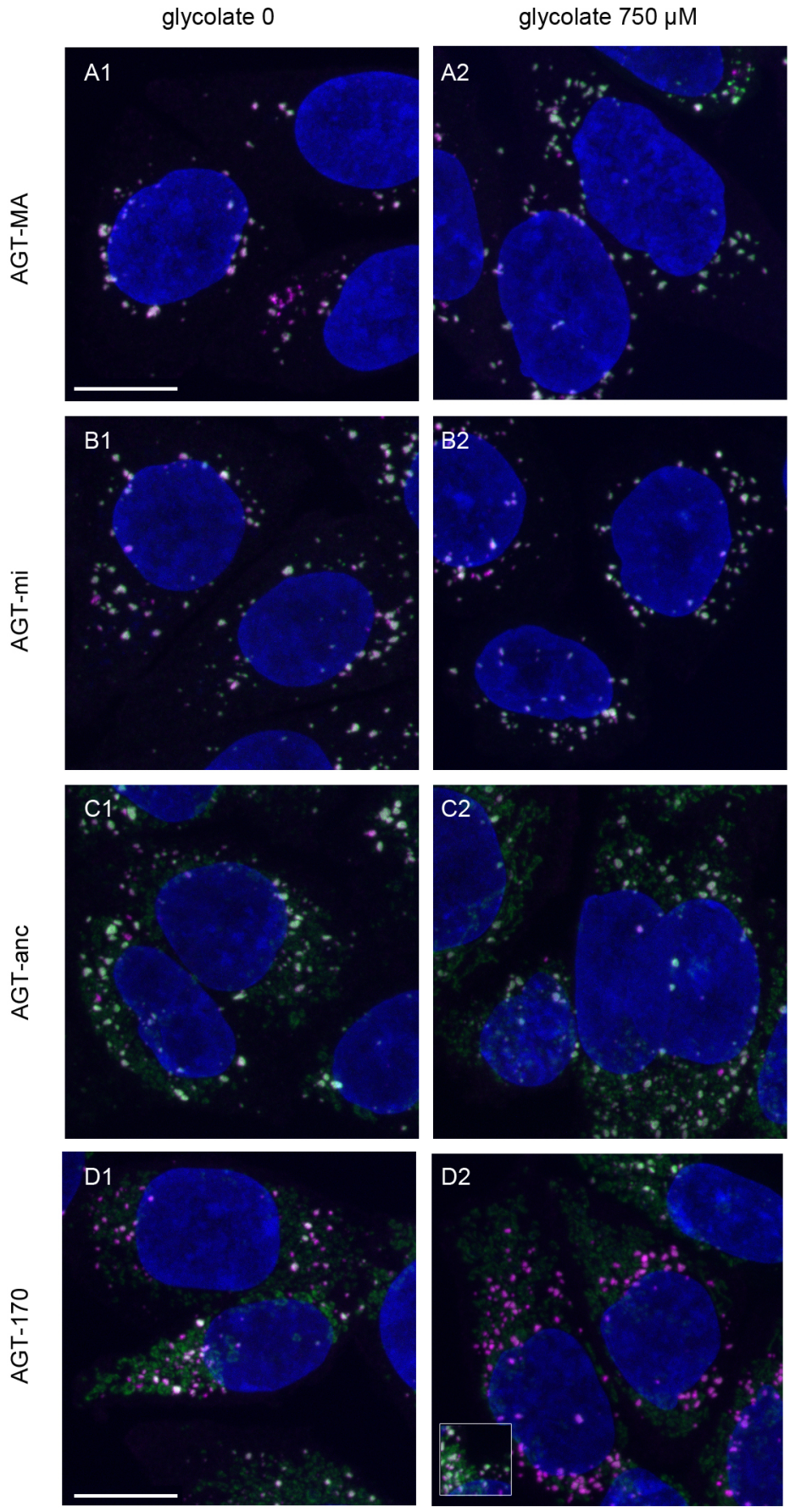

Fig VI.7. **Expression of GO and AGT in CHO GO AGT cell lines after exposure to glycolate**

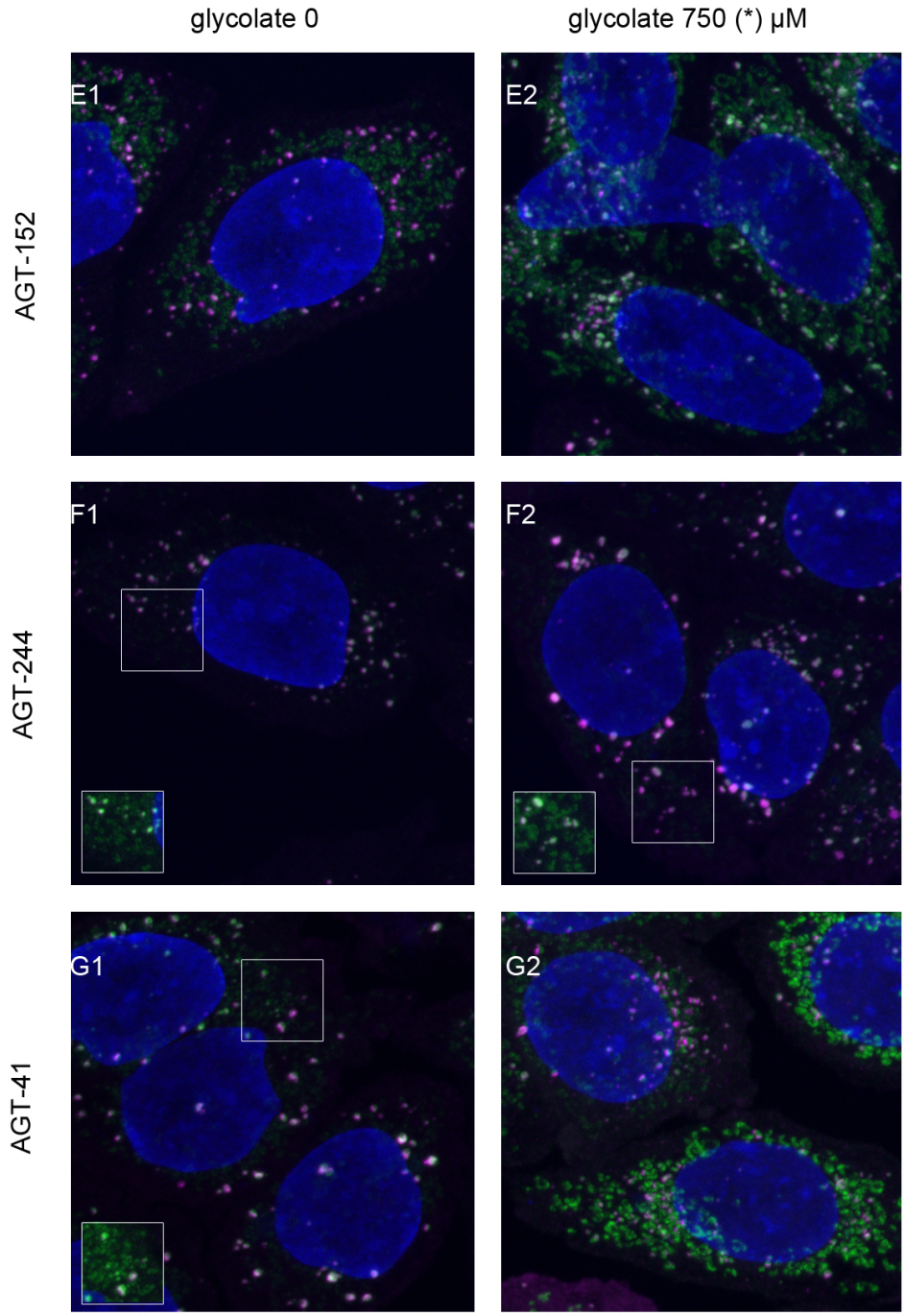

Figure VI-7. **Expression of GO and AGT in CHO GO AGT cell lines after exposure to glycolate**. The cells from the different CHO GO AGTs surviving the indirect glycolate toxicity assay were seeded on cover-slips and grown for a further 3 days without antibiotic selection. After a total of 5 days without antibiotic selection pressure (including 2 days for the metabolic assay), the cells were fixed and stained against GO (magenta) and AGT (green). Areas in the white boxes have been displayed with an increased brightness in the square box on the bottom left. Scale bar 10 µm. *: for CHO GO AGT-41 the glycolate concentration was 250 µM (no cell were surviving at 750 µM).

VI.3 Effect of pyridoxine on the indirect toxicity of glycolate in the cell-based metabolic assay

VI.3.1 Pyridoxine does not affect WT or GO expressing cells

Before studying the effect of pyridoxine on AGT variants by the cell-based metabolic assay described above, the robustness of the metabolic assay in different pyridoxine concentrations was tested. The level of pyridoxine had no impact on the survival of either CHO WT or CHO GO after exposure to glycolate (Table VI.1). CHO WT were not sensitive to glycolate and CHO GO showed less than 10% surviving at 500 and 750 µM whatever the pyridoxine level.

	Glycolate	Pyridoxine				
		0 µM	< 0.3 µM	0.3 µM	50 µM	250 µM
CHO wt	0 µM	100	100	100	100	100
	500 µM	97	89	101	93	100
	750 µM	92	82	106	89	104
CHO GO	0 µM	100	100	100	100	100
	500 µM	9	8	9	8	7
	750 µM	7	6	6	6	4

Table VI-1**. Effect of pyridoxine on the sensitivity of CHO cells to indirect glycolate toxicity.** CHO WT and CHO GO cells grown for > 1 month in different concentrations of pyridoxine (0, low = < 0.3, 0.3, 50, 250 µM, see Methods III.2) were exposed to glycolate at 500 and 750 µM in the different pyridoxine levels. The indirect toxicity of glycolate was assessed by the decrease in surviving cells after 2 days of exposure. The results (n=2) are expressed as mean % of the control for each cell line.

VI.3.2 Effect of pyridoxine on AGT variants

The different CHO GO AGT cell lines studied in this project were grown for more than a month in different pyridoxine levels (see Methods III.2). Briefly, cells were grown in five different conditions: absence of pyridoxine ("B6: 0 µM"), low levels of pyridoxine (no pyridoxine in the medium, but some in the FBS, "B6: < 0.3 µM"), standard levels of pyridoxine (Ham's F12 medium at 0.3 µM pyridoxine in addition to the FBS, "B6: 0.3 µM"), increased pyridoxine: medium at 0.3 µM pyridoxine, normal FBS and supplementation in pyridoxine at 50 µM ("B6: 50 µM") or 250 µM (B6: 250 µM"). All five concentrations were tested for CHO WT, CHO GO, CHO GO AGT-MA, CHO GO AGT-mi and CHO GO AGT-170. For the other mutant cell lines, CHO GO AGT-152/244/41, only three levels of pyridoxine were tested: < 0.3 µM, 0.3 µM and 50 µM. The different concentrations of pyridoxine were maintained during a metabolic assay of indirect glycolate toxicity (Fig VI.8, Annexe IX.15). Two concentrations of

glycolate only were used for this assay, 500 and 750 μM, at which there was the greatest difference in survival between the cell lines (section VI.2.2.1).

At the lowest level pyridoxine (~ 0 μM) only CHO WT and CHO GO AGT-MA survived, though the latter showed a strongly decreased survival, at 30 % for 500 μM glycolate. The survival of the cells increased with increased pyridoxine with a maximum at 0.3μM of pyridoxine (Ham's F12 medium) for cells expressing AGT-MA, AGT-mi and AGT-anc. For pyridoxine concentrations higher than 0.3 μM, the survival decreased or stayed stable (Fig VI.8). The highest survival occurred in cells with AGT-MA, followed by cells with AGT-mi and then AGT-anc.

In CHO cells expressing mutant AGTs, the cell line showing the best survival was CHO GO AGT-170, followed by cells expressing AGT-244. The survival of cells expressing AGT-170 was increased with increased pyridoxine. As was seen for AGT-MA, AGT-mi and AGT-anc expressing cells, the highest survival was seen at 0.3 μM pyridoxine with a slight decrease at higher concentrations. Although only three concentrations of pyridoxine were tested for CHO GO AGT-244, increasing pyridoxine was associated with a better survival, which plateaued at levels higher than 0.3 μM pyridoxine. CHO GO AGT-152 showed a poor survival no matter what the level of pyridoxine at the concentrations of glycolate tested. CHO GO AGT-41 showed the same survival as CHO GO whatever the concentration of pyridoxine, *i.e.* no protection at all.

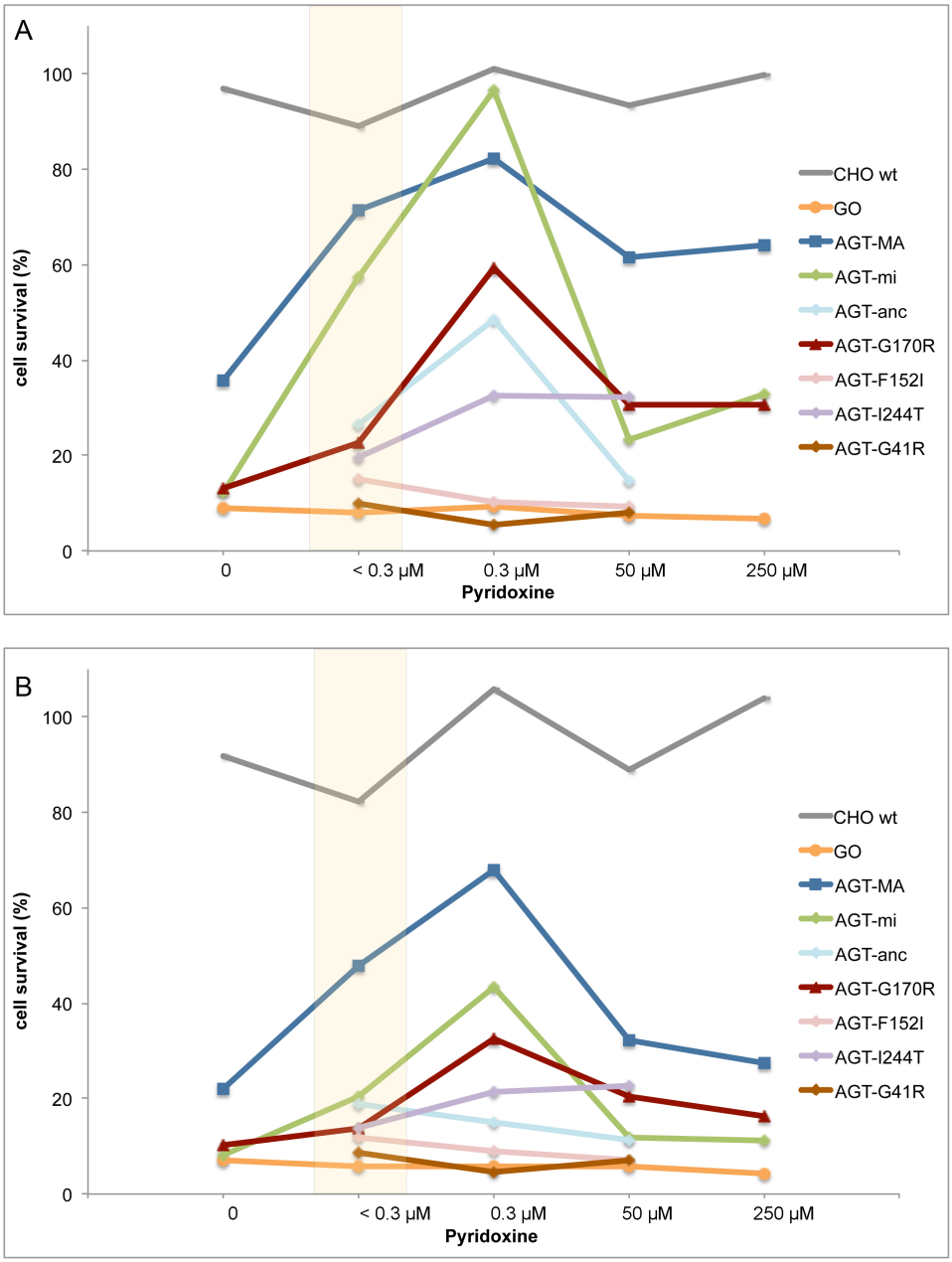

Figure VI-8. **Effect of pyridoxine on the sensitivity of CHO GO AGT cells to indirect glycolate toxicity.** Different CHO cell lines (CHO WT, CHO GO, CHO GO AGT-MA, CHO GO AGT-mi, CHO GO AGT-anc, CHO GO AGT-170, CHO GO AGT-152, CHO GO AGT-244, CHO GO AGT-41) grown at least 4 weeks in different concentrations of pyridoxine (0, < 0.3, 0.3, 50, 250 µM, see Methods III.2), were exposed to glycolate at 500 and 750 µM. The indirect toxicity of glycolate was assessed by the decrease in surviving cells after 2 days of exposure to glycolate. The results (n=2) are expressed as mean % of the control for each cell line. For AGT-anc, AGT-152, AGT-244 and AGT-41, only 3 levels of pyridoxine were studied: <0.3, 0.3, 50 µM. A: survival at 500 µM glycolate, B: survival at 750 µM glycolate. Normal plasma levels of pyridoxine are expected to fall between the < 0.3 µM and 0.3 µM categories (yellow area).

Table .VI-2 **Summary of the effect of pyridoxine on the metabolic efficiency of AGT variants**. Arrows indicate the trend of the changes in metabolic efficiency of AGT, (=) indicates that no change was detectable.

Changes in pyridoxine concentrations	AGT-MA	AGT-mi	AGT-anc	AGT-G170R	AGT-F152I	AGT-I244T	AGT-G41R	GO	CHO wt
0 ➔ <0.3 µM ➔ 0.3 µM	↑	↑	↑	↑	=	↑	=	=	=
0.3 µM ➔ 50 µM ➔ 250 µM	↓	↓	↓	↓	=	=	=	=	=

VI.3.3 Summary

The cell survival after exposure to glycolate was influenced by the pyridoxine concentration in culture. There was an improved survival in cells expressing AGT-MA, AGT-mi, AGT-anc, AGT-170 and AGT-244, ranging from 1.7 to 8-fold, with increasing pyridoxine concentrations in culture up to 0.3 µM. A decrease, or plateau, in survival was seen at higher pyridoxine concentration.

VI.4 Discussion

VI.4.1 Direct and indirect cell-based toxicity assay

As Behnam *et al.* have shown, the presence of glycolate added to GO expressing cells results in cell toxicity, manifested by a decreased cell survival in the metabolic assay (Behnam et al., 2006). The toxicity is the result of the production of glyoxylate. This was confirmed here indirectly and not by a direct measurement of glyoxylate in the cells, glyoxylate being a reactive metabolite and difficult to measure in biological samples.

The addition of glyoxylate proved to be toxic for both CHO GO and CHO WT cells, but not, or less so, for cells expressing functional AGT. AGT variants with lower activity, like AGT-170, could only partially protect the cells from glyoxylate, either from a direct addition of glyoxylate on the cells or indirectly by addition of glycolate in GO expressing cells. However, in the direct glyoxylate toxicity assay, the glyoxylate added has to be taken up by cells and then by peroxisomes or mitochondria. During this process the glyoxylate added may be diverted to other reactions in the cells, decreasing its efficiency and the mitochondrial glyoxylate can be also catalysed by the mitochondrial mistargeted AGT.

The indirect glycolate toxicity assay takes advantage of the intra-peroxisomal localization of GO and AGT. Glycolate can be taken up by cells, as was shown by its effect in some cell lines. However, the conversion of glycolate to glyoxylate, the substrate of AGT only takes place where GO is expressed, which is almost exclusively the peroxisomes. This recapitulates more closely the physiological reaction in hepatocytes where glyoxylate is produced in the same organelle as normal, peroxisomal, AGT, or in a different organelle for mistargeted mutant AGT.

In addition to being a better metabolic assay of AGT, the indirect glycolate toxicity method theoretically offers the opportunity to test for inhibitors of GO.

Despite not having selected for GO and AGT expression by antibiotic during the metabolic assay, all cell lines still expressed GO and AGT at the end of the assay, if at a lower level than before. The situation described by Behnam *et al.* of loss of GO at the end of the assay is different to the situation here (Behnam et al., 2006). That difference could result from a non-homogenous expression of GO in the CHO GO cell lines used by Behnam whereas the cell lines used here have more than 90% cells expressing GO with comparable levels on IMF. The selection of low GO expressing cells may, therefore, not have had time to occur during the 5 days of the experiment.

The AGT variants with the best survival was AGT-MA, which is consistent with all previous results. Even CHO GO AGT-MA cells show a decrease of cell survival at the higher glycolate concentrations, as had also been found by Behnam *et al.* The reason for this could be that at higher glycolate concentrations the enzymatic capacity of AGT-MA to convert glyoxylate to glycine is less than the capacity of GO to produce glyoxylate. As stated before, comparison between cell lines is difficult because of the different AGT expression levels in the cell lines.

At standard pyridoxine concentrations, both AGT-anc and AGT-mi's response to glycolate were towards a higher toxicity than CHO GO AGT-MA. Both cell lines have similar GO expression levels and activity but lower expression levels than AGT-MA. In addition, AGT-anc is dually located to peroxisomes and mitochondria. Although the estimated specific catalytic activity of AGT-anc is close to that of AGT-MA, it is possible that mitochondrial AGT-anc would be less able than AGT-MA or AGT-mi to protect from peroxisomal glyoxylate, as has been suggested for AGT-170.

In accordance with the lower catalytic activity of AGT-170 and its mitochondrial localization, CHO GO AGT-170 cells were more sensitive to glycolate than the normal cell lines (AGT-MA, AGT-mi, AGT-anc).

CHO GO AGT-41 cells, as was expected from their lack of catalytic activity in the AGT assay but presence of GO, had no better survival than CHO GO cells. As for AGT-41, CHO GO AGT-Δ cells, which have no AGT catalytic activity in the AGT assay, showed no survival after glycolate exposure (data not shown).

Although both CHO GO AGT-152 and AGT-244 cell lines showed more sensitivity to glycolate than normal AGTs, as expected from their lower AGT catalytic activities and partial mitochondrial localization, their respective response was somewhat surprising. CHO GO AGT-152 cells were the most sensitive of the cell lines expressing functional mutant AGT. Although their GO expression levels are similar to the other cell lines, their AGT expression levels are

lower. In addition the mitochondrial localization is very high, close to that of AGT-170, where AGT could be expected to be less efficient in glyoxylate detoxification.

In contrast, CHO GO AGT-244 behaved more like CHO GO AGT-anc and AGT-mi cells. Immunoblotting analyses showed that CHO GO AGT-244 expressed AGT and GO in similar levels to that of CHO GO AGT-mi but have an estimated specific catalytic activity of AGT lower than AGT-mi. It is possible that the cells used for the metabolic assay expressed lower GO levels than previously shown (section IV & V), although this was not apparent in the IMF analysis of these cells. A decreased permeabilisation to glycolate in the specific CHO GO AGT-244 is unlikely as none of these other cell lines ever showed evidence of such a mechanism. The quality of the glycolate cannot be the cause either, as the experiments were done in parallel with the same solutions and media. Another possibility would be that there was enough functional AGT-244 in the peroxisomes (peroxisomal localization of AGT-244 was strong in these experiments) and enough pyridoxine (0.3 μM) in the medium to rescue AGT-244 and protect CHO GO AGT-244 cells from the indirect glycolate toxicity. Conversely, it is possible that levels of GO in the other cell lines were higher during the experiment whereas the specific catalytic activity of AGT was not affected at the levels of B6 used (already at maximum activity).

The results of the indirect glycolate toxicity assay were expressed here by the survival of cells compared to each control cell line. The survival was not corrected for the levels of GO or AGT expressed in the cells although the survival results from the balance between these two enzymes. For a comparison between different transformed cell lines expressing AGT variants, the levels of GO expression should be taken into account. The results shown in Chapter IV demonstrated that although all transformed CHO cells lines had comparable GO expression, the catalytic activity of GO in the assay varied by less than a third (235 to 348 nmol/min/mg cell protein, 70 to 100%) between cell lines. The GO protein expression judged by immunoblotting showed very similar levels also. This was achieved by transforming the same CHO GO cell lines with the different AGT variants. The overall level of expression of AGT in the cells, however, varied more: between a third to twice that of AGT-MA. Some of this variation can be attributed to episomal plasmid copies and transcription in the cells but also to the stability or degradation of the AGT variant, a true characteristic of a given AGT variant. Although conclusions based on the comparison between the survival of cell lines must take into account the different levels of expression of AGT in the cell lines, this would not be necessary when comparing each cell line to itself.

VI.4.2 Effect of pyridoxine in the indirect glycolate toxicity assay

The effect of pyridoxine on AGT shown in the previous chapter (Chapter V) were recapitulated using the indirect glycolate toxicity assay.

In the absence of pyridoxine in culture, only CHO GO AGT-MA retained a measure of cell survival after glycolate exposure (36%). As was shown by the catalytic activity of AGT in the same conditions, both CHO GO AGT-mi and AGT-170 showed an absence of better cell survival compared to CHO GO in the absence of pyridoxine. All cell lines expressing functional AGT, except AGT-152, showed an improved cell survival at increased pyridoxine levels in culture up to 0.3 μM pyridoxine concentration. The effect was more pronounced at 500 μM glycolate but was also noticeable at 750 μM glycolate.

Although CHO GO AGT-mi showed a higher sensitivity to B6-depletion than CHO GO AGT-MA, the cell survival at low (<0.3 μM) pyridoxine or standard (0.3 μM) pyridoxine concentration was very similar to that of AGT-MA, compatible with the results from the AGT assay (see section V.4). As had been found for higher levels of pyridoxine (50 & 250 μM) on the AGT assay, the survival of CHO GO AGT-MA, AGT-mi, AGT-anc, and even AGT-170, cells decreased compared to the survival at 0.3 μM pyridoxine. So the paradoxical effect of pyridoxine in culture on AGT activities was reproduced in the indirect glycolate metabolic assay.

The effect of increasing pyridoxine in culture on AGT mutants was to increase the cell survival as well. The mutant whose response was the greatest was AGT-170. Contrary to the results of the AGT assay, the cell survival of CHO GO AGT-170 at the highest pyridoxine levels (50 & 250 μM) was less than at 0.3 μM, following the same trend as normal AGTs. For these cell lines (CHO GO AGT-MA, AGT-mi. AGT-170), which showed a paradoxical negative effect of pyridoxine on cell survival, the survival at 500 μM glycolate still remained greater than in the absence of pyridoxine, closer to the response obtained at low levels of pyridoxine (<0.3 μM).

Whereas the moderate positive effect of pyridoxine in culture on CHO GO AGT-244 cells was reproduced in the metabolic assay, no effect at all could be detected for CHO GO AGT-152 cells despite the positive effect seen on AGT activity and targeting.

Since CHO GO AGT-152 had shown to be more sensitive to glycolate concentrations than the other cell lines in the standard levels of pyridoxine, this absence of effect of B6 could be explained by using glycolate concentrations that were too high for this assay. It is possible, but has not been proven, that the survival of CHO GO AGT-152 at lower concentrations of glycolate (more sensitive conditions) would be improved by increasing pyridoxine in culture.

In support of this, the results of low glycolate exposure (250 μM) on CHO GO AGT-41 at higher pyridoxine levels showed a better survival than expected for standard B6 levels (data not shown). This would suggest that for mutant AGTs with low activities, the effect of B6 on the indirect glycolate toxicity assay should be studied at lower glycolate concentrations in order to improve the sensitivity of the assay. Alternatively, using a wider range and more numerous glycolate concentrations could prove to be more sensitive to changes in the efficiency of AGT.

VI.4.3 Conclusion

The indirect glycolate toxicity assay proved to reflect the functional efficiency of the different AGT variants.

The potential of the metabolic assay to act as a screening assay for active molecules on AGT was confirmed. The changes in catalytic activity shown in Chapter V, both increase and decrease seen with changes in pyridoxine levels for AGT-MA and AGT-mi, were reflected with the metabolic assay. Changes in the activity of AGT-170, AGT-244 and AGT-anc were also detectable in the metabolic assay. Changes in the survival of different CHO GO AGT cell lines were detectable at both the concentrations of glycolate chosen (500 and 750 μM).

The criteria chosen to express the toxicity of glycolate on transformed CHO cells, was the final cell number at the endpoint (2 days of exposure to glycolate), which represents a surrogate marker for AGT functional efficiency. Since the number of cells at the endpoint was less than the number of cells seeded, the effect of glyoxylate had to include cell death. The mechanism of the toxicity induced by glyoxylate in the cells was not investigated and a more detailed study could have included cell viability assays using tetrazolium dye assays, which reflect the metabolic activity of cells (like MTT or XTT assays).

The response of the cell survival to the addition of glycolate to the culture medium described a rough sigmoid curve. With a greater number of experiments per cell line and glycolate concentration points, it should be possible to characterize each cell line's response to glycolate in the same manner as for pharmacological assays and derive a half lethal concentration (LD50) of glycolate, which would be characteristic of each cell line and culture condition. This would allow easier comparison of the effect of drugs on each AGT variant. A decrease in LD50 would characterize a drug decreasing the efficiency of AGT whereas an increase of LD50 would be characteristic of a drug increasing the metabolic efficiency of AGT. The effect of pyridoxine on the metabolic assay was only studied here with 3 glycolate concentrations (0, 500, 750), which were chosen for their relevance to the majority of cell lines (greater difference between AGT-MA and AGT-170). The proof of the effect of pyridoxine, *i.e.* the potential of the indirect glycolate toxicity assay to detect a change in the efficiency of AGT in a cell line in which an effect of pyridoxine had been demonstrated before by alternative methods (see Chapter V), was

shown by the change in the cell line's survival at the different pyridoxine levels in cell culture. For a more precise characterization and a more sensitive detection of the effect of pharmacological chaperones of AGT, or GO inhibitors for example, it would be useful to carry out the metabolic assay with more glycolate concentrations points and derive LD50s, which would be a quantitative measure of the effect of the drug tested. This assay could also potentially be of use for higher throughput screening procedures provided the system could be scaled up and automatized.

In conclusion, the indirect toxicity assay has proven to be a valid system in which to test the metabolic efficiency of AGT variants. The surrogate marker chosen for AGT activity being cell survival after exposure of cells to glycolate.

In addition, such a metabolic assay could be used to detect and possibly measure, the effect of drugs on the rescue of mutant dysfunctional AGTs or even on the capacity of drugs to inhibit GO.

VII GENERAL DISCUSSION

The present work has led to several important discoveries:

1 - Several AGT mutants on the background of the minor allele can be mistargeted to mitochondria in addition to the one AGT mutant known to do so (AGT-170).

2 - The AGT-41 mutant forms peroxisomal aggregates in the cells and is less stable than other AGT variants.

3- Vitamin B6 increases the overall level of expression of AGT; increases the catalytic activity of AGT; increases the peroxisomal localization of dually, peroxisomal and mitochondrial, mistargeting AGT.

4 - Vitamin B6 has both a prosthetic group and chaperone effect on AGT and vitamin B6 has a non-mutation specific effect on AGT variants, although the degree of response is mutation-specific.

5 - Abnormal levels of some vitamin B6 vitamers (pyridoxine and pyridoxine 5‘-phosphate) can be detected in the cells at very high concentrations of pyridoxine in culture.

6 - The activity of normal AGT is decreased at very high concentrations of pyridoxine in culture.

7 - The glycolate indirect toxicity assay reflects the metabolic effectiveness of AGT variants and can detect changes in the metabolic effectiveness of a given AGT variant.

In conclusion, the present work has shown that the mitochondrial mistargeting of AGT is not specific to one mutation, but may be common to many mutations on the background on the minor allele of AGT. The mitochondrial mistargeting is the result of a shift in the balance between the kinetics of folding and the kinetics of subcellular targeting of an AGT variant carrying the P11L polymorphic MTS. The change in the kinetics of folding is caused by an additional mutation in AGT.

The synergy between the P11L polymorphism and a mutation on AGT was shown to extend even in the cell environment. Moreover, the P11L polymorphism was shown to represent an intermediate step between completely normal AGT (AGT-MA) and a full-blown mutation. This leads one to question if there could not be symptoms in P11L homozygotes in particular situations, like vitamin B6 deficiency or insufficiency. Such patients could be found among a kidney stone-forming population.

The results found here emphasize the role of the system used in the study of AGT and a confirmation of those results in human patients would be useful. The mistargeting of some mutants could be confirmed by IEM in PH1 patients’ liver, the effect of pyridoxine on targeting could also be studied if documentation could be obtained in the liver before and after treatment. It would be unethical to perform serial liver biopsies in a patient, but since liver transplantation

is currently the only curative approach and requires removal of the original liver, it should be possible to document post-treatment situation, and possibly a pre-treatment in a diagnostic biopsy, provided patients' samples were secured in a bank and approval obtained.

Vitamin B6 was found to have both a chaperone effect (affect folding, dimerization and targeting) and a prosthetic group effect on AGT (affect catalytic activity). Some measure of response to pyridoxine, was found for three out of four of the AGT mutants (AGT-170, AGT-152, AGT-244), but with varying degrees and with different involvement of the two types of mechanisms. Although the mutation with the most important clinical response to pyridoxine was also the most responsive in the CHO cells (AGT-170), the response of two other mutants (AGT-152 and AGT-244), one unknown to be responsive (AGT-244), suggest that patients carrying these mutations, and maybe others as well, could be clinically responsive to pyridoxine. Even if all mutations do not respond equally to pyridoxine, it is possible that pyridoxine might increase the effectiveness of other pharmacological treatments of PH1 and rescue AGT.

The bi-phasic response of AGT to pyridoxine, in terms of activity and metabolic efficiency, suggests that there is an optimal concentration of pyridoxine as far as AGT efficiency is concerned. The abnormal levels of some B6 vitamers (PN, PNP) at high concentrations of pyridoxine, raise the question of whether they interfere in the function of PLP-dependent enzymes or not.

Even though pyridoxine is used as a treatment for several diseases, pyridoxine-toxicity is rarely seen in treated patients. However, target plasma levels of B6 vitamers have not been established and the therapeutic window is defined on clinical symptoms. The negative effect on the efficiency of AGT, and the potential different effects of some of the B6 vitamers, both suggest that a better knowledge of pyridoxine as treatment is required in general.

A better knowledge is especially required in PH1 patients. The response to pyridoxine is defined as a 30% decrease of urinary oxalate, as urinary oxalate can vary by 25%. However, a true lower B6 response might still be useful in patients, especially in addition to other treatment. A formal testing of pyridoxine is not generally done but should be performed for all AGT missense mutations and the degree of response should be noted as well as the dose of pyridoxine at which it is obtained. Additionally, the plasma levels of B6 vitamers should be monitored and analysed in correlation with biochemical and clinical markers of PH1. Whether higher pyridoxine levels than those leading to the defined response, are harmless or lead to a decrease in the efficiency of AGT should be investigated.

Finally, the functional test for AGT first published by Behnam *et al.* proved to be able to distinguish functional AGT from non-functional mutants and to be able to detect changes in the metabolic efficiency of AGT following the addition of pharmacological agent (Behnam et al., 2006). Such a system could be used in the future to screen for drugs affecting AGT (or GO).

VIII REFERENCES

Abe, Y., T. Shodai, T. Muto, K. Mihara, H. Torii, S. Nishikawa, T. Endo, and D. Kohda. 2000. Structural basis of presequence recognition by the mitochondrial protein import receptor Tom20. *Cell*. 100:551–560.

Albert, A., C. Yunta, R. Arranz, A. Pena, E. Salido, J. Valpuesta, and J. Martin-Benito. 2010. Structure of GroEL in Complex with an Early Folding Intermediate of Alanine Glyoxylate Aminotransferase. *JOURNAL OF BIOLOGICAL CHEMISTRY*. 285:6371–6376.

Alberts B, Johnson A, Lewis J, et al. 2002. Molecular biology of the Cell. 4th ed. Garland Science, New York.

Allsop, J., P.R. Jennings, and C.J. Danpure. 1987. A new micro-assay for human liver alanine: glyoxylate aminotransferase. *Clin. Chim. Acta*. 170:187–193.

Behnam, J.T., E.L. Williams, S. Brink, G. Rumsby, and C.J. Danpure. 2006. Reconstruction of human hepatocyte glyoxylate metabolic pathways in stably transformed Chinese-hamster ovary cells. *Biochem. J*. 394:409–416.

Belostotsky, R., E. Seboun, G.H. Idelson, D.S. Milliner, R. Becker-Cohen, C. Rinat, C.G. Monico, S. Feinstein, E. Ben-Shalom, D. Magen, I. Weissman, C. Charon, and Y. Frishberg. 2010. Mutations in DHDPSL are responsible for primary hyperoxaluria type III. *Am. J. Hum. Genet*. 87:392–399.

Bender, D.A. 1999. Non-nutritional uses of vitamin B6. *Br. J. Nutr.* 81:7–20.

Bergstralh, E.J., C.G. Monico, J.C. Lieske, R.M. Herges, C.B. Langman, B. Hoppe, and D.S. Milliner. 2010. Transplantation outcomes in primary hyperoxaluria. *Am. J. Transplant.* 10:2493–2501.

Birdsey, G.M., J. Lewin, A.A. Cunningham, M.W. Bruford, and C.J. Danpure. 2004. Differential enzyme targeting as an evolutionary adaptation to herbivory in carnivora. *Mol. Biol. Evol.* 21:632–646.

Birdsey, G.M., J. Lewin, J.D. Holbrook, V.R. Simpson, A.A. Cunningham, and C.J. Danpure. 2005. A comparative analysis of the evolutionary relationship between diet and enzyme targeting in bats, marsupials and other mammals. *Proc. Biol. Sci.* 272:833–840.

Bolte, S., and F.P. Cordelières. 2006. A guided tour into subcellular colocalization analysis in light microscopy. *J Microsc*. 224:213–232.

Bor, M.V., H. Refsum, M.R. Bisp, Ø. Bleie, J. Schneede, J.E. Nordrehaug, P.M. Ueland, O.K. Nygard, and E. Nexø. 2003. Plasma vitamin B6 vitamers before and after oral vitamin B6 treatment: a randomized placebo-controlled study. *Clin. Chem*. 49:155–161.

Bosron, W.F., R.L. Veitch, L. Lumeng, and T.K. Li. 1978. Subcellular localization and identification of pyridoxal 5'-phosphate-binding proteins in rat liver. *J. Biol. Chem.* 253:1488–1492.

Broyer, M., F.P. Brunner, H. Brynger, S.R. Dykes, J.H. Ehrich, W. Fassbinder, W. Geerlings, G. Rizzoni, N.H. Selwood, and G. Tufveson. 1990. Kidney transplantation in primary oxalosis: data from the EDTA Registry. *Nephrol. Dial. Transplant*. 5:332–336.

Broyer, M., P. Jouvet, P. Niaudet, M. Daudon, and Y. Revillon. 1996. Management of oxalosis. *Kidney Int. Suppl*. 53:S93–98.

Casas-Melley, A.T., P.G. Thomas, L.J. Krueger, K.P. Falkenstein, L.M. Flynn, S.B. Conley, and S.P. Dunn. 2002. Domino as a bridge to definitive liver transplantation in a neonate. *Pediatr Transplant*. 6:249–254.

Cellini, B., M. Bertoldi, R. Montioli, A. Paiardini, and C. Borri Voltattorni. 2007. Human wild-type alanine:glyoxylate aminotransferase and its naturally occurring G82E variant: functional properties and physiological implications. *Biochem J*. 408:39–50.

Cellini, B., A. Lorenzetto, R. Montioli, E. Oppici, and C.B. Voltattorni. 2010a. Human liver peroxisomal alanine:glyoxylate aminotransferase: Different stability under chemical stress of the major allele, the minor allele, and its pathogenic G170R variant. *Biochimie*. 92:1801–1811.

Cellini, B., R. Montioli, A. Paiardini, A. Lorenzetto, F. Maset, T. Bellini, E. Oppici, and C.B. Voltattorni. 2010b. Molecular defects of the glycine 41 variants of alanine glyoxylate aminotransferase associated with primary hyperoxaluria type I. *Proc. Natl. Acad. Sci. U.S.A.* 107:2896–2901.

Cellini, B., R. Montioli, A. Paiardini, A. Lorenzetto, and C.B. Voltattorni. 2009. Molecular Insight into the Synergism between the Minor Allele of Human Liver Peroxisomal Alanine:Glyoxylate Aminotransferase and the F152I Mutation. *J. Biol. Chem*. 284:8349–8358.

Cellini, B., R. Montioli, and C.B. Voltattorni. 2011. Human liver peroxisomal alanine:glyoxylate aminotransferase: characterization of the two allelic forms and their pathogenic variants. *Biochim. Biophys. Acta*. 1814:1577–1584.

Chetyrkin, S.V., D. Kim, J.M. Belmont, J.I. Scheinman, B.G. Hudson, and P.A. Voziyan. 2005. Pyridoxamine lowers kidney crystals in experimental hyperoxaluria: a potential therapy for primary hyperoxaluria. *Kidney Int*. 67:53–60.

Cibrik, D.M., B. Kaplan, J.A. Arndorfer, and H.-U. Meier-Kriesche. 2002. Renal allograft survival in patients with oxalosis. *Transplantation*. 74:707–710.

Clayton, P.T. 2006. B6-responsive disorders: a model of vitamin dependency. *J. Inherit. Metab. Dis.* 29:317–326.

Coburn, S.P. 1990. Location and turnover of vitamin B6 pools and vitamin B6 requirements of humans. *Ann. N. Y. Acad. Sci*. 585:76–85.

Cochat, P., A. Deloraine, M. Rotily, F. Olive, I. Liponski, and N. Deries. 1995. Epidemiology of primary hyperoxaluria type 1. Société de Néphrologie and the Société de Néphrologie Pédiatrique. *Nephrol. Dial. Transplant*. 10 Suppl 8:3–7.

Cochat, P., S. Fargue, and J. Harambat. 2010. Primary hyperoxaluria type 1: strategy for organ transplantation. *Curr Opin Organ Transplant*. 15:590–593.

Cochat, P., A. Liutkus, S. Fargue, O. Basmaison, B. Ranchin, and M.-O. Rolland. 2006. Primary hyperoxaluria type 1: still challenging! *Pediatr. Nephrol*. 21:1075–1081.

Cochat, P., and A. Mahmoud. 1995. Transplantation in primary hyperoxaluria type 1. *Nephrol Dial Transplant*. 10:1293–6.

Cooper, P.J., C.J. Danpure, P.J. Wise, and K.M. Guttridge. 1988. Immunocytochemical localization of human hepatic alanine: glyoxylate aminotransferase in control subjects and patients with primary hyperoxaluria type 1. *J. Histochem. Cytochem*. 36:1285–1294.

Coulter-Mackie, M.B., and Q. Lian. 2006. Consequences of missense mutations for dimerization and turnover of alanine:glyoxylate aminotransferase: study of a spectrum of mutations. *Mol. Genet. Metab*. 89:349–359.

Coulter-Mackie, M.B., and Q. Lian. 2008. Partial trypsin digestion as an indicator of mis-folding of mutant alanine:glyoxylate aminotransferase and chaperone effects of specific ligands. Study of a spectrum of missense mutants. *Mol. Genet. Metab*. 94:368–374.

Coulter-Mackie, M.B., Q. Lian, D.A. Applegarth, J. Toone, P.J. Waters, and H. Vallance. 2008. Mutation-based diagnostic testing for primary hyperoxaluria type 1: survey of results. *Clin. Biochem*. 41:598–602.

Coulter-Mackie, M.B., Q. Lian, and S.G. Wong. 2005. Overexpression of human alanine:glyoxylate aminotransferase in Escherichia coli: renaturation from guanidine-HCl and affinity for pyridoxal phosphate co-factor. *Protein Expr. Purif*. 41:18–26.

Coulter-Mackie, M.B., A. Tung, H.E. Henderson, J.R. Toone, and D.A. Applegarth. 2003. The AGT gene in Africa: a distinctive minor allele haplotype, a polymorphism (V326I), and a novel PH1 mutation (A112D) in Black Africans. *Mol. Genet. Metab*. 78:44–50.

Cramer, S.D., P.M. Ferree, K. Lin, D.S. Milliner, and R.P. Holmes. 1999. The gene encoding hydroxypyruvate reductase (GRHPR) is mutated in patients with primary hyperoxaluria type II. *Hum Mol Genet*. 8:2063–9.

Crawhall, J.C., E.F. Scowen, and R.W. Watts. 1959. Conversion of glycine to oxalate in primary hyperoxaluria. *Lancet*. 2:806–9.

Cregeen, D.P., E.L. Williams, S. Hulton, and G. Rumsby. 2003. Molecular analysis of the glyoxylate reductase (GRHPR) gene and description of mutations underlying primary hyperoxaluria type 2. *Hum. Mutat*. 22:497.

Danpure, C.J. 1991. Molecular and clinical heterogeneity in primary hyperoxaluria type 1. *Am J Kidney Dis*. 17:366–9.

Danpure, C.J. 1993. Primary hyperoxaluria type 1 and peroxisome-to-mitochondrion mistargeting of alanine:glyoxylate aminotransferase. *Biochimie*. 75:309–315.

Danpure, C.J. 1995. How can the products of a single gene be localized to more than one intracellular compartment? *Trends Cell Biol.* 5:230–238.

Danpure, C.J. 2001. Primary Hyperoxaluria. *In* The Metabolic and Molecular Bases of Inherited Disease. B.A. Scriver CR, editor. McGraw-Hill, New-York. 3323–3367.

Danpure, C.J. 2004. Molecular aetiology of primary hyperoxaluria type 1. *Nephron Exp. Nephrol.* 98:e39–44.

Danpure, C.J., G.M. Birdsey, G. Rumsby, M.J. Lumb, P.E. Purdue, and J. Allsop. 1994a. Molecular characterization and clinical use of a polymorphic tandem repeat in an intron of the human alanine:glyoxylate aminotransferase gene. *Hum. Genet.* 94:55–64.

Danpure, C.J., P.J. Cooper, P.J. Wise, and P.R. Jennings. 1989. An enzyme trafficking defect in two patients with primary hyperoxaluria type 1: peroxisomal alanine/glyoxylate aminotransferase rerouted to mitochondria. *J Cell Biol*. 108:1345–52.

Danpure, C.J., P. Fryer, P.R. Jennings, J. Allsop, S. Griffiths, and A. Cunningham. 1994b. Evolution of alanine:glyoxylate aminotransferase 1 peroxisomal and mitochondrial targeting. A survey of its subcellular distribution in the livers of various representatives of the classes Mammalia, Aves and Amphibia. *Eur. J. Cell Biol.* 64:295–313.

Danpure, C.J., K.M. Guttridge, P. Fryer, P.R. Jennings, J. Allsop, and P.E. Purdue. 1990. Subcellular distribution of hepatic alanine:glyoxylate aminotransferase in various mammalian species. *J. Cell. Sci.* 97 (Pt 4):669–678.

Danpure, C.J., and P.R. Jennings. 1986a. Peroxisomal alanine:glyoxylate aminotransferase deficiency in primary hyperoxaluria type I. *FEBS Lett*. 201:20–4.

Danpure, C.J., and P.R. Jennings. 1986b. Peroxisomal alanine:glyoxylate aminotransferase deficiency in primary hyperoxaluria type I. *FEBS Lett.* 201:20–24.

Danpure, C.J., and P.R. Jennings. 1988. Further studies on the activity and subcellular distribution of alanine:glyoxylate aminotransferase in the livers of patients with primary hyperoxaluria type 1. *Clin Sci (Lond)*. 75:315–22.

Danpure, C.J., P.R. Jennings, P. Fryer, P.E. Purdue, and J. Allsop. 1994c. Primary hyperoxaluria type 1: genotypic and phenotypic heterogeneity. *J. Inherit. Metab. Dis.* 17:487–499.

Danpure, C.J., P.E. Purdue, P. Fryer, S. Griffiths, J. Allsop, M.J. Lumb, K.M. Guttridge, P.R. Jennings, J.I. Scheinman, and S.M. Mauer. 1993. Enzymological and mutational analysis of a complex primary hyperoxaluria type 1 phenotype involving alanine:glyoxylate aminotransferase peroxisome-to-mitochondrion mistargeting and intraperoxisomal aggregation. *Am. J. Hum. Genet.* 53:417–432.

Danpure, C.J. 1991. Scientific rationale for hepatorenal transplanttaion in primary hyperoxlauria type 1. *In* Tranplanttaion and Clinical Immunology. Excerpta Medica, Amsterdam. 91–98.

Detry, O., P. Honoré, A. DeRoover, M. Trimeche, J.-C. Demoulin, M. Beaujean, M. Moonen, J.-P. Godon, J. Boniver, N. Jacquet, and M. Meurisse. 2002. Reversal of oxalosis cardiomyopathy after combined liver and kidney transplantation. *Transpl. Int*. 15:50–52.

Djordjevic, S., X. Zhang, M. Bartlam, S. Ye, Z. Rao, and C.J. Danpure. 2010. Structural implications of a G170R mutation of alanine:glyoxylate aminotransferase that is associated with peroxisome-to-mitochondrion mistargeting. *Acta Crystallogr. Sect. F Struct. Biol. Cryst. Commun.* 66:233–236.

Donckier, V., I. El Nakadi, J. Closset, B. Ickx, H. Louis, O. Le Moine, N. Bourgeois, M. Adler, and M. Gelin. 2001. Domino hepatic transplantation using the liver from a patient with primary hyperoxaluria. *Transplantation*. 71:1346–1348.

Edwards, P., P.K. Liu, and G.A. Rose. 1990a. Liquid chromatographic studies of vitamin B6 metabolism in man. *Clin. Chim. Acta*. 190:67–80.

Edwards, P., S. Nemat, and G.A. Rose. 1990b. Effects of oral pyridoxine upon plasma and 24-hour urinary oxalate levels in normal subjects and stone formers with idiopathic hypercalciuria. *Urol Res*. 18:393–6.

Elgersma, Y., C.W. van Roermund, R.J. Wanders, and H.F. Tabak. 1995. Peroxisomal and mitochondrial carnitine acetyltransferases of Saccharomyces cerevisiae are encoded by a single gene. *EMBO J*. 14:3472–9.

Farese, S., N. Trost, D. Candinas, and U. Huynh-Do. 2005. Early renal failure after domino hepatic transplantation using the liver from a compound heterozygous patient with primary hyperoxaluria. *Nephrol. Dial. Transplant*. 20:2557–2560.

Fiji Is Just ImageJ.

Fodor, K., J. Wolf, R. Erdmann, W. Schliebs, and M. Wilmanns. 2012. Molecular Requirements for Peroxisomal Targeting of Alanine-Glyoxylate Aminotransferase as an Essential Determinant in Primary Hyperoxaluria Type 1. *PLoS Biol*. 10.

Footitt, E.J., P.T. Clayton, K. Mills, S.J. Heales, V. Neergheen, M. Oppenheim, and P.B. Mills. 2012. Measurement of plasma B(6) vitamer profiles in children with inborn errors of vitamin B(6) metabolism using an LC-MS/MS method. *Journal of inherited metabolic disease*.

Footitt, E.J., S.J. Heales, P.B. Mills, G.F.G. Allen, M. Oppenheim, and P.T. Clayton. 2011. Pyridoxal 5'-phosphate in cerebrospinal fluid; factors affecting concentration. *J. Inherit. Metab. Dis.* 34:529–538.

Franchello, A., G. Paraluppi, R. Romagnoli, M. Petrarulo, C. Vitale, A. Pacitti, A. Amoroso, M. Marangella, and M. Salizzoni. 2005. Severe course of primary hyperoxaluria and renal failure after domino hepatic transplantation. *Am. J. Transplant*. 5:2324–2327.

Frischholz, S., F. Beier, I. Girkontaite, K. Wagner, E. Pöschl, J. Turnay, U. Mayer, and K. von der Mark. 1998. Characterization of human type X procollagen and its NC-1 domain expressed as recombinant proteins in HEK293 cells. *J. Biol. Chem.* 273:4547–4555.

Fry, D.W., and K.E. Richardson. 1979. Isolation and characterization of glycolic acid oxidase from human liver. *Biochim. Biophys. Acta*. 568:135–144.

GERSHOFF, S.N., A.L. MAYER, and L.L. KULCZYCKI. 1959. Effect of pyridoxine administration on the urinary excretion of oxalic acid, pyridoxine, and related compounds in mongoloids and nonmongoloids. *Am. J. Clin. Nutr*. 7:76–79.

Giafi, C.F., and G. Rumsby. 1998. Primary hyperoxaluria type 2: enzymology. *J. Nephrol*. 11 Suppl 1:29–31.

Gibbs, D.A., S. Hauschildt, and R.W. Watts. 1977. Glyoxylate oxidation in rat liver and kidney. *J Biochem*. 82:221–30.

Gibbs, D.A., and R.W. Watts. 1970. The action of pyridoxine in primary hyperoxaluria. *Clin Sci*. 38:277–286.

Gould, S.J., G.A. Keller, N. Hosken, J. Wilkinson, and S. Subramani. 1989. A conserved tripeptide sorts proteins to peroxisomes. *J. Cell Biol.* 108:1657–1664.

GREENGARD, O., and M. GORDON. 1963. THE COFACTOR-MEDIATED REGULATION OF APOENZYME LEVELS IN ANIMAL TISSUES. I. THE PYRIDOXINE-INDUCED RISE OF RAT LIVER TYROSINE TRANSAMINASE LEVEL IN VIVO. *J. Biol. Chem.* 238:3708–3710.

Gross-Mesilaty, S., J.L. Hargrove, and A. Ciechanover. 1997. Degradation of tyrosine aminotransferase (TAT) via the ubiquitin-proteasome pathway. *FEBS Lett.* 405:175–180.

Guo, C., T.A. Cenac, Y. Li, and K.E. McMartin. 2007. Calcium oxalate, and not other metabolites, is responsible for the renal toxicity of ethylene glycol. *Toxicol Lett*. 173:8–16.

Harambat, J., S. Fargue, C. Acquaviva, M.-F. Gagnadoux, F. Janssen, A. Liutkus, C. Mourani, M.-A. Macher, D. Abramowicz, C. Legendre, A. Durrbach, M. Tsimaratos, H. Nivet, E. Girardin, A.-M. Schott, M.-O. Rolland, and P. Cochat. 2010. Genotype-phenotype correlation in primary hyperoxaluria type 1: the p.Gly170Arg AGXT mutation is associated with a better outcome. *Kidney Int.* 77:443–449.

Harambat, J., K.J. van Stralen, L. Espinosa, J.W. Groothoff, S.-A. Hulton, R. Cerkauskiene, F. Schaefer, E. Verrina, K.J. Jager, and P. Cochat. 2012. Characteristics and Outcomes of Children with Primary Oxalosis Requiring Renal Replacement Therapy. *Clinical Journal of the American Society of Nephrology: CJASN*.

Hatch, M., and R.W. Freel. 2003. Renal and intestinal handling of oxalate following oxalate loading in rats. *Am. J. Nephrol*. 23:18–26.

Hatch, M., R.W. Freel, and N.D. Vaziri. 1999. Regulatory aspects of oxalate secretion in enteric oxalate elimination. *J. Am. Soc. Nephrol.* 10 Suppl 14:S324–328.

Holbrook, J.D., G.M. Birdsey, Z. Yang, M.W. Bruford, and C.J. Danpure. 2000. Molecular adaptation of alanine:glyoxylate aminotransferase targeting in primates. *Mol. Biol. Evol.* 17:387–400.

Holmes, R.P., and D.G. Assimos. 1998. Glyoxylate synthesis, and its modulation and influence on oxalate synthesis. *J. Urol*. 160:1617–1624.

Hoppe, B., B.B. Beck, and D.S. Milliner. 2009. The primary hyperoxalurias. *Kidney Int.* 75:1264–1271.

Hoppe, B., C.J. Danpure, G. Rumsby, P. Fryer, P.R. Jennings, N. Blau, G. Schubiger, T. Neuhaus, and E. Leumann. 1997. A vertical (pseudodominant) pattern of inheritance in the autosomal recessive disease primary hyperoxaluria type 1: lack of relationship between genotype, enzymic phenotype, and disease severity. *Am. J. Kidney Dis*. 29:36–44.

Hoppe, B., D. Graf, G. Offner, K. Latta, D.J. Byrd, D. Michalk, and J. Brodehl. 1996. Oxalate elimination via hemodialysis or peritoneal dialysis in children with chronic renal failure. *Pediatr. Nephrol*. 10:488–492.

Hoppe, B., M.J. Kemper, A. Bökenkamp, A.A. Portale, R.A. Cohn, and C.B. Langman. 1999. Plasma calcium oxalate supersaturation in children with primary hyperoxaluria and end-stage renal failure. *Kidney Int*. 56:268–274.

Hoppe, B., and C.B. Langman. 2003. A United States survey on diagnosis, treatment, and outcome of primary hyperoxaluria. *Pediatr. Nephrol*. 18:986–991.

Hoppe, B., K. Latta, C. von Schnakenburg, and M.J. Kemper. 2005. Primary hyperoxaluria--the German experience. *Am J Nephrol*. 25:276–81.

Hopper, E.D., A.M.C. Pittman, M.C. Fitzgerald, and C.L. Tucker. 2008. In vivo and in vitro examination of stability of primary hyperoxaluria-associated human alanine:glyoxylate aminotransferase. *J. Biol. Chem*. 283:30493–30502.

Huber, P.A.J., G.M. Birdsey, M.J. Lumb, D.T.R. Prowse, T.J. Perkins, D.R. Knight, and C.J. Danpure. 2005. Peroxisomal import of human alanine:glyoxylate aminotransferase requires ancillary targeting information remote from its C terminus. *J. Biol. Chem.* 280:27111–27120.

ImageJ.

Inoue, Y., H. Masuyama, H. Ikawa, H. Mitsubuchi, and T. Kuhara. 2003. Monitoring method for pre- and post-liver transplantation in patients with primary hyperoxaluria type I. *J. Chromatogr. B Analyt. Technol. Biomed. Life Sci*. 792:89–97.

Jamieson, N.V. 2005. A 20-year experience of combined liver/kidney transplantation for primary hyperoxaluria (PH1): the European PH1 transplant registry experience 1984-2004. *Am. J. Nephrol*. 25:282–289.

Jones, J.M., J.C. Morrell, and S.J. Gould. 2000. Identification and characterization of HAOX1, HAOX2, and HAOX3, three human peroxisomal 2-hydroxy acid oxidases. *J. Biol. Chem*. 275:12590–12597.

Kamoda, N., Y. Minatogawa, M. Nakamura, J. Nakanishi, E. Okuno, and R. Kido. 1980. The organ distribution of human alanine-2-oxoglutarate aminotransferase and alanine-glyoxylate aminotransferase. *Biochem Med*. 23:25–34.

Kang, J.H., M.-L. Hong, D.W. Kim, J. Park, T.-C. Kang, M.H. Won, N.-I. Baek, B.J. Moon, S.Y. Choi, and O.-S. Kwon. 2004. Genomic organization, tissue distribution and deletion mutation of human pyridoxine 5'-phosphate oxidase. *Eur. J. Biochem*. 271:2452–2461.

Karniely, S., and O. Pines. 2005. Single translation[mdash]dual destination: mechanisms of dual protein targeting in eukaryotes. *EMBO Rep*. 6:420–425.

Kennaway, N.G., R.G. Weleber, and N.R. Buist. 1980. Gyrate atrophy of the choroid and retina with hyperornithinemia: biochemical and histologic studies and response to vitamin B6. *Am. J. Hum. Genet.* 32:529–541.

Knight, J., and R.P. Holmes. 2005. Mitochondrial hydroxyproline metabolism: implications for primary hyperoxaluria. *Am. J. Nephrol*. 25:171–175.

Knott, T.G., G.M. Birdsey, K.E. Sinclair, I.M. Gallagher, P.E. Purdue, and C.J. Danpure. 2000. The peroxisomal targeting sequence type 1 receptor, Pex5p, and the peroxisomal import efficiency of alanine:glyoxylate aminotransferase. *Biochem J*. 352 Pt 2:409–18.

Knox, C., E. Sass, W. Neupert, and O. Pines. 1998. Import into mitochondria, folding and retrograde movement of fumarase in yeast. *J. Biol. Chem*. 273:25587–25593.

Kopp, N., and E. Leumann. 1995. Changing pattern of primary hyperoxaluria in Switzerland. *Nephrol. Dial. Transplant*. 10:2224–2227.

Kozik, A., and D.B. McCormick. 1984. Mechanism of pyridoxine uptake by isolated rat liver cells. *Archives of Biochemistry and Biophysics*. 229:187–193.

Lee, I.S., Y. Muragaki, T. Ideguchi, T. Hase, M. Tsuji, A. Ooshima, E. Okuno, and R. Kido. 1995. Molecular cloning and sequencing of a cDNA encoding alanine-glyoxylate aminotransferase 2 from rat kidney. *J. Biochem.* 117:856–862.

Lee, J.G., S.P. Cho, H.S. Lee, C.H. Lee, K.S. Bae, and P.J. Maeng. 2000. Identification of a cryptic N-terminal signal in Saccharomyces cerevisiae peroxisomal citrate synthase that functions in both peroxisomal and mitochondrial targeting. *J. Biochem*. 128:1059–1072.

Leiper, J.M., P.B. Oatey, and C.J. Danpure. 1996. Inhibition of alanine:glyoxylate aminotransferase 1 dimerization is a prerequisite for its peroxisome-to-mitochondrion mistargeting in primary hyperoxaluria type 1. *J Cell Biol*. 135:939–51.

Leumann, E., and B. Hoppe. 2001. The primary hyperoxalurias. *J. Am. Soc. Nephrol*. 12:1986–1993.

Leumann, E., B. Hoppe, and T. Neuhaus. 1993. Management of primary hyperoxaluria: efficacy of oral citrate administration. *Pediatr. Nephrol*. 7:207–211.

Lieske, J.C., C.G. Monico, W.S. Holmes, E.J. Bergstralh, J.M. Slezak, A.L. Rohlinger, J.B. Olson, and D.S. Milliner. 2005. International registry for primary hyperoxaluria. *Am. J. Nephrol*. 25:290–296.

Liu, Y., H. Xu, X. Yuan, S.J. Rossiter, and S. Zhang. 2012. Multiple adaptive losses of alanine-glyoxylate aminotransferase mitochondrial targeting in fruit eating bats. *Molecular Biology and Evolution*.

Lui, A., L. Lumeng, and T.K. Li. 1981. Metabolism of vitamin B6 in rat liver mitochondria. *J Biol Chem*. 256:6041–6.

Lui, A., L. Lumeng, and T.K. Li. 1982. Transport of pyridoxine and pyridoxal 5'-phosphate in isolated rat liver mitochondria. *J. Biol. Chem.* 257:14903–14906.

Lumb, M.J., G.M. Birdsey, and C.J. Danpure. 2003. Correction of an enzyme trafficking defect in hereditary kidney stone disease in vitro. *Biochem. J*. 374:79–87.

Lumb, M.J., and C.J. Danpure. 2000. Functional synergism between the most common polymorphism in human alanine:glyoxylate aminotransferase and four of the most common disease-causing mutations. *J. Biol. Chem*. 275:36415–36422.

Lumb, M.J., A.F. Drake, and C.J. Danpure. 1999. Effect of N-terminal alpha-helix formation on the dimerization and intracellular targeting of alanine:glyoxylate aminotransferase. *J. Biol. Chem*. 274:20587–20596.

Lumeng, L., A. Lui, and T.K. Li. 1980. Plasma content of B6 vitamers and its relationship to hepatic vitamin B6 metabolism. *J. Clin. Invest.* 66:688–695.

Ma, C., G. Agrawal, and S. Subramani. 2011. Peroxisome assembly: matrix and membrane protein biogenesis. *J. Cell Biol.* 193:7–16.

Manders, E.M., J. Stap, G.J. Brakenhoff, R. van Driel, and J.A. Aten. 1992. Dynamics of three-dimensional replication patterns during the S-phase, analysed by double labelling of DNA and confocal microscopy. *J. Cell. Sci.* 103 (Pt 3):857–862.

Marangella, M., D. Cosseddu, M. Petrarulo, C. Vitale, and F. Linari. 1993. Thresholds of serum calcium oxalate supersaturation in relation to renal function in patients with or without primary hyperoxaluria. *Nephrol. Dial. Transplant*. 8:1333–1337.

Marangella, M., M. Petrarulo, D. Cosseddu, C. Vitale, and F. Linari. 1992. Oxalate balance studies in patients on hemodialysis for type I primary hyperoxaluria. *Am. J. Kidney Dis*. 19:546–553.

Marangella, M., C. Vitale, M. Petrarulo, A. Tricerri, E. Cerelli, A. Cadario, M.P. Barbos, and F. Linari. 1995. Bony content of oxalate in patients with primary hyperoxaluria or oxalosis-unrelated renal failure. *Kidney Int*. 48:182–187.

Mdluli, K., M.P.S. Booth, R.L. Brady, and G. Rumsby. 2005. A preliminary account of the properties of recombinant human Glyoxylate reductase (GRHPR), LDHA and LDHB with glyoxylate, and their potential roles in its metabolism. *Biochim. Biophys. Acta*. 1753:209–216.

Mehansho, H., D.D. Buss, M.W. Hamm, and L.M. Henderson. 1980. Transport and metabolism of pyridoxine in rat liver. *Biochim. Biophys. Acta*. 631:112–123.

Midttun, O., S. Hustad, E. Solheim, J. Schneede, and P.M. Ueland. 2005. Multianalyte quantification of vitamin B6 and B2 species in the nanomolar range in human plasma by liquid chromatography-tandem mass spectrometry. *Clin. Chem.* 51:1206–1216.

Milliner, D.S., J.T. Eickholt, E.J. Bergstralh, D.M. Wilson, and L.H. Smith. 1994. Results of long-term treatment with orthophosphate and pyridoxine in patients with primary hyperoxaluria. *N. Engl. J. Med*. 331:1553–1558.

Mistry J, D.C. 1988. Hepatic D-glycerate dehydrogenase and glyoxylate reductase deficiency in primary hyperoxaluria type 2; *Biochemical Society Transactions*. 16:626.

Monico, C.G., J.B. Olson, and D.S. Milliner. 2005a. Implications of genotype and enzyme phenotype in pyridoxine response of patients with type I primary hyperoxaluria. *Am J Nephrol*. 25:183–8.

Monico, C.G., S. Rossetti, J.B. Olson, and D.S. Milliner. 2005b. Pyridoxine effect in type I primary hyperoxaluria is associated with the most common mutant allele. *Kidney Int*. 67:1704–9.

Montioli, R., S. Fargue, J. Lewin, C. Zamparelli, C.J. Danpure, C. Borri Voltattorni, and B. Cellini. 2012. The N-terminal extension is essential for the formation of the active dimeric structure of liver peroxisomal alanine:glyoxylate aminotransferase. *The International Journal of Biochemistry & Cell Biology*.

Morgan, S.H., P. Purkiss, R.W. Watts, and M.A. Mansell. 1987. Oxalate dynamics in chronic renal failure. Comparison with normal subjects and patients with primary hyperoxaluria. *Nephron*. 46:253–257.

Motley, A., M.J. Lumb, P.B. Oatey, P.R. Jennings, P.A. De Zoysa, R.J. Wanders, H.F. Tabak, and C.J. Danpure. 1995. Mammalian alanine/glyoxylate aminotransferase 1 is imported into peroxisomes via the PTS1 translocation pathway. Increased degeneracy and context specificity of the mammalian PTS1 motif and implications for the peroxisome-to-mitochondrion mistargeting of AGT in primary hyperoxaluria type 1. *J. Cell Biol*. 131:95–109.

Neupert, W., and J.M. Herrmann. 2007. Translocation of proteins into mitochondria. *Annu. Rev. Biochem*. 76:723–749.

Nishiyama, K., T. Funai, R. Katafuchi, F. Hattori, K. Onoyama, and A. Ichiyama. 1991. Primary hyperoxaluria type I due to a point mutation of T to C in the coding region of the serine:pyruvate aminotransferase gene. *Biochem. Biophys. Res. Commun*. 176:1093–1099.

Noguchi, T., and Y. Takada. 1979. Peroxisomal localization of alanine: glyoxylate aminotransferase in human liver. *Arch. Biochem. Biophys.* 196:645–647.

Nouwen, N., H. Stahlberg, A.P. Pugsley, and A. Engel. 2000. Domain structure of secretin PulD revealed by limited proteolysis and electron microscopy. *EMBO J.* 19:2229–2236.

Oatey, P.B., M.J. Lumb, and C.J. Danpure. 1996. Molecular basis of the variable mitochondrial and peroxisomal localisation of alanine-glyoxylate aminotransferase. *Eur. J. Biochem*. 241:374–385.

Obita, T., T. Muto, T. Endo, and D. Kohda. 2003. Peptide library approach with a disulfide tether to refine the Tom20 recognition motif in mitochondrial presequences. *J. Mol. Biol.* 328:495–504.

Oppici, E., R. Montioli, A. Lorenzetto, S. Bianconi, C. Borri Voltattorni, and B. Cellini. 2012. Biochemical analyses are instrumental in identifying the impact of mutations on holo and/or apo-forms and on the region(s) of alanine:glyoxylate aminotransferase variants associated with primary hyperoxaluria type I. *Mol. Genet. Metab.* 105:132–140.

de Pauw, L., M. Gelin, C.J. Danpure, P. Vereerstraeten, M. Adler, D. Abramowicz, and C. Toussaint. 1990. Combined liver-kidney transplantation in primary hyperoxaluria type 1. *Transplantation*. 50:886–887.

Petrova, V.Y., D. Drescher, A.V. Kujumdzieva, and M.J. Schmitt. 2004. Dual targeting of yeast catalase A to peroxisomes and mitochondria. *Biochem. J*. 380:393–400.

Poldelski, V., A. Johnson, S. Wright, V.D. Rosa, and R.A. Zager. 2001. Ethylene glycol-mediated tubular injury: identification of critical metabolites and injury pathways. *Am J Kidney Dis*. 38:339–48.

Poole, B., F. Leighton, and C. De Duve. 1969. The synthesis and turnover of rat liver peroxisomes. II. Turnover of peroxisome proteins. *J. Cell Biol.* 41:536–546.

Poore, R.E., C.H. Hurst, D.G. Assimos, and R.P. Holmes. 1997. Pathways of hepatic oxalate synthesis and their regulation. *Am. J. Physiol.* 272:C289–294.

Purdue, P.E., J. Allsop, G. Isaya, L.E. Rosenberg, and C.J. Danpure. 1991a. Mistargeting of peroxisomal L-alanine:glyoxylate aminotransferase to mitochondria in primary hyperoxaluria patients depends upon activation of a cryptic mitochondrial targeting sequence by a point mutation. *Proc. Natl. Acad. Sci. U.S.A*. 88:10900–10904.

Purdue, P.E., M.J. Lumb, J. Allsop, and C.J. Danpure. 1991b. An intronic duplication in the alanine: glyoxylate aminotransferase gene facilitates identification of mutations in compound heterozygote patients with primary hyperoxaluria type 1. *Hum. Genet*. 87:394–396.

Purdue, P.E., M.J. Lumb, J. Allsop, Y. Minatogawa, and C.J. Danpure. 1992. A glycine-to-glutamate substitution abolishes alanine:glyoxylate aminotransferase catalytic activity in a subset of patients with primary hyperoxaluria type 1. *Genomics*. 13:215–218.

Purdue, P.E., M.J. Lumb, M. Fox, G. Griffo, C. Hamon-Benais, S. Povey, and C.J. Danpure. 1991c. Characterization and chromosomal mapping of a genomic clone encoding human alanine:glyoxylate aminotransferase. *Genomics*. 10:34–42.

Purdue, P.E., Y. Takada, and C.J. Danpure. 1990. Identification of mutations associated with peroxisome-to-mitochondrion mistargeting of alanine/glyoxylate aminotransferase in primary hyperoxaluria type 1. *J. Cell Biol*. 111:2341–2351.

Ramesh, V., A.I. McClatchey, N. Ramesh, L.A. Benoit, E.L. Berson, V.E. Shih, and J.F. Gusella. 1988. Molecular basis of ornithine aminotransferase deficiency in B-6-responsive and -nonresponsive forms of gyrate atrophy. *Proc. Natl. Acad. Sci. U.S.A.* 85:3777–3780.

Rodionov, R.N., D.J. Murry, S.F. Vaulman, J.W. Stevens, and S.R. Lentz. 2010. Human alanine-glyoxylate aminotransferase 2 lowers asymmetric dimethylarginine and protects from inhibition of nitric oxide production. *J. Biol. Chem.* 285:5385–5391.

Rucktäschel, R., W. Girzalsky, and R. Erdmann. 2011. Protein import machineries of peroxisomes. *Biochim. Biophys. Acta*. 1808:892–900.

Rumsby, G., and D.P. Cregeen. 1999. Identification and expression of a cDNA for human hydroxypyruvate/glyoxylate reductase. *Biochim. Biophys. Acta*. 1446:383–388.

Rumsby, G., T. Weir, and C.T. Samuell. 1997. A semiautomated alanine:glyoxylate aminotransferase assay for the tissue diagnosis of primary hyperoxaluria type 1. *Ann. Clin. Biochem*. 34 (Pt 4):400–404.

Salido, E.C., X.M. Li, Y. Lu, X. Wang, A. Santana, N. Roy-Chowdhury, A. Torres, L.J. Shapiro, and J. Roy-Chowdhury. 2006. Alanine-glyoxylate aminotransferase-deficient mice, a model for primary hyperoxaluria that responds to adenoviral gene transfer. *Proc. Natl. Acad. Sci. U.S.A*. 103:18249–18254.

Saner, F.H., J. Treckmann, J. Pratschke, H. Arbogast, A. Rahmel, U. Vester, and A. Paul. 2010. Early renal failure after domino liver transplantation using organs from donors with primary hyperoxaluria type 1. *Transplantation*. 90:782–785.

Santana, A., E. Salido, A. Torres, and L.J. Shapiro. 2003. Primary hyperoxaluria type 1 in the Canary Islands: a conformational disease due to I244T mutation in the P11L-containing alanine:glyoxylate aminotransferase. *Proc. Natl. Acad. Sci. U.S.A*. 100:7277–7282.

Sass, E., S. Karniely, and O. Pines. 2003. Folding of fumarase during mitochondrial import determines its dual targeting in yeast. *J. Biol. Chem.* 278:45109–45116.

Schmidt, O., N. Pfanner, and C. Meisinger. 2010. Mitochondrial protein import: from proteomics to functional mechanisms. *Nat. Rev. Mol. Cell Biol.* 11:655–667.

von Schnakenburg, C., and G. Rumsby. 1997. Primary hyperoxaluria type 1: a cluster of new mutations in exon 7 of the AGXT gene. *J. Med. Genet*. 34:489–492.

Sharma, V., and P.O. Schwille. 1997. Clofibrate feeding to Sprague-Dawley rats increases endogenous biosynthesis of oxalate and causes hyperoxaluria. *Metab. Clin. Exp.* 46:135–139.

Shih, V.E., R. Mandell, and E.L. Berson. 1988. Pyridoxine effects on ornithine ketoacid transaminase activity in fibroblasts from carriers of two forms of gyrate atrophy of the choroid and retina. *Am. J. Hum. Genet.* 43:929–933.

Stein, I., Y. Peleg, S. Even-Ram, and O. Pines. 1994. The single translation product of the FUM1 gene (fumarase) is processed in mitochondria before being distributed between the cytosol and mitochondria in Saccharomyces cerevisiae. *Mol. Cell. Biol.* 14:4770–4778.

Strobel, G., A. Zollner, M. Angermayr, and W. Bandlow. 2002. Competition of Spontaneous Protein Folding and Mitochondrial Import Causes Dual Subcellular Location of Major Adenylate Kinase. *Mol. Biol. Cell*. 13:1439–1448.

Swinkels, B.W., S.J. Gould, A.G. Bodnar, R.A. Rachubinski, and S. Subramani. 1991. A novel, cleavable peroxisomal targeting signal at the amino-terminus of the rat 3-ketoacyl-CoA thiolase. *EMBO J.* 10:3255–3262.

Swinkels, B.W., S.J. Gould, and S. Subramani. 1992. Targeting efficiencies of various permutations of the consensus C-terminal tripeptide peroxisomal targeting signal. *FEBS Lett*. 305:133–6.

Takada, Y., N. Kaneko, H. Esumi, P.E. Purdue, and C.J. Danpure. 1990. Human peroxisomal L-alanine: glyoxylate aminotransferase. Evolutionary loss of a mitochondrial targeting signal by point mutation of the initiation codon. *Biochem. J*. 268:517–520.

Takada, Y., T. Mori, and T. Noguchi. 1984. The effect of vitamin B6 deficiency on alanine: glyoxylate aminotransferase isoenzymes in rat liver. *Arch. Biochem. Biophys*. 229:1–6.

Takada, Y., and T. Noguchi. 1982. Subcellular distribution, and physical and immunological properties of hepatic alanine: glyoxylate aminotransferase isoenzymes in different mammalian species. *Comp. Biochem. Physiol., B*. 72:597–604.

Thompson, J.S., and K.E. Richardson. 1967. Isolation and characterization of an L-alanine: glyoxylate aminotransferase from human liver. *J. Biol. Chem.* 242:3614–3619.

Thompson, J.S., and K.E. Richardson. 1968. Determination of pyruvate in enzyme-catalyzed reactions in the presence of glyoxylate. *Anal. Biochem.* 24:197–201.

Toussaint, C., L. De Pauw, A. Vienne, P.A. Gevenois, J. Quintin, M. Gelin, and J.L. Pasteels. 1993. Radiological and histological improvement of oxalate osteopathy after combined liver-kidney transplantation in primary hyperoxaluria type 1. *Am. J. Kidney Dis.* 21:54–63.

Wanders, R.J., J. Ruiter, C.W. van Roermund, R.B. Schutgens, R. Ofman, S. Jurriaans, and J.M. Tager. 1990. Human liver L-alanine-glyoxylate aminotransferase: characteristics and activity in controls and hyperoxaluria type I patients using a simple spectrophotometric method. *Clin. Chim. Acta*. 189:139–144.

Watts, R.W., R.Y. Calne, K. Rolles, C.J. Danpure, S.H. Morgan, M.A. Mansell, R. Williams, and P. Purkiss. 1987. Successful treatment of primary hyperoxaluria type I by combined hepatic and renal transplantation. *Lancet*. 2:474–475.

Watts, R.W., R.Y. Calne, R. Williams, M.A. Mansell, N. Veall, P. Purkiss, and K. Rolles. 1985a. Primary hyperoxaluria (type I): attempted treatment by combined hepatic and renal transplantation. *Q. J. Med*. 57:697–703.

Watts, R.W., R.A. Chalmers, D.A. Gibbs, A.M. Lawson, P. Purkiss, and E. Spellacy. 1979. Studies on some possible biochemical treatments of primary hyperoxaluria. *Q. J. Med*. 48:259–272.

Watts, R.W., N. Veall, and P. Purkiss. 1983. Sequential studies of oxalate dynamics in primary hyperoxaluria. *Clin. Sci*. 65:627–633.

Watts, R.W., N. Veall, and P. Purkiss. 1984. Oxalate dynamics and removal rates during haemodialysis and peritoneal dialysis in patients with primary hyperoxaluria and severe renal failure. *Clin. Sci*. 66:591–597.

Watts, R.W., N. Veall, P. Purkiss, M.A. Mansell, and E.F. Haywood. 1985b. The effect of pyridoxine on oxalate dynamics in three cases of primary hyperoxaluria (with glycollic aciduria). *Clin. Sci*. 69:87–90.

Weleber, R.G., N.G. Kennaway, and N.R. Buist. 1978. Vitamin B6 in management of gyrate atrophy of choroid and retina. *Lancet*. 2:1213.

Williams, E., D. Cregeen, and G. Rumsby. 2000. Identification and expression of a cDNA for human glycolate oxidase. *Biochim Biophys Acta*. 1493:246–8.

Williams, E., and G. Rumsby. 2007. Selected exonic sequencing of the AGXT gene provides a genetic diagnosis in 50% of patients with primary hyperoxaluria type 1. *Clin. Chem*. 53:1216–1221.

Williams, E.L., C. Acquaviva, A. Amoroso, F. Chevalier, M. Coulter-Mackie, C.G. Monico, D. Giachino, T. Owen, A. Robbiano, E. Salido, H. Waterham, and G. Rumsby. 2009. Primary hyperoxaluria type 1: update and additional mutation analysis of the AGXT gene. *Hum Mutat*. 30:910–7.

Williams, H.E., and L.H. Smith. 1968. L-glyceric aciduria. A new genetic variant of primary hyperoxaluria. *N. Engl. J. Med*. 278:233–238.

Williams, E. L. 2003. Human liver glycolate oxidase. Gene identification and protein studies. (PhD Thesis).

van Woerden, C.S., J.W. Groothoff, F.A. Wijburg, C. Annink, R.J.A. Wanders, and H.R. Waterham. 2004. Clinical implications of mutation analysis in primary hyperoxaluria type 1. *Kidney Int*. 66:746–752.

Wolf, J., W. Schliebs, and R. Erdmann. 2010. Peroxisomes as dynamic organelles: peroxisomal matrix protein import. *FEBS J.* 277:3268–3278.

Zhang, X., S.M. Roe, Y. Hou, M. Bartlam, Z. Rao, L.H. Pearl, and C.J. Danpure. 2003. Crystal structure of alanine:glyoxylate aminotransferase and the relationship between genotype and enzymatic phenotype in primary hyperoxaluria type 1. *J. Mol. Biol*. 331:643–652.

IX ANNEXES

Annexe IX-1 **Standard mutagenesis primers used for the AGT-I244T construct.**

name	sequence	strand
AGXT-T852C F	5'-CCCTTCTCCTTCTACCTGGACACCAAGTGGCT-3'	(+)
AGXT-T852C R	5'-AGCCACTTGGTGTCCAGGTAGAAGGAGAAGGG-3'	(-)

Annexe IX-2. **Primers used for sequencing.**

name	sequence	strand	Tm
T7F	5'- TAATACGACTCACTATAGGG -3'	(+)	53º
Mit1	5'- CACCAATCCTCACCTCTCAC -3'	(+)	58º
TAK1040	5'- GGACCTTGCAGGGTCTGTTT -3'	(-)	61º
AGTXT-e2	5'- GAGATCAAGGAAGGCATCCA -3'	(+)	57º
AGXT-e4	5'- TCCACCTCCTGCAGTGTGTA -3'	(-)	59º
AGXT-e6	5'- AAAAAGAAGATGTACTCCCGC -3'	(+)	56º
GO-e5	5'- TCATGGGGCTCGACAACT -3'	(+)	57º
GO-e3	5'- GCTTCTTGGTGACTTCTCGGT -3'	(-)	60º

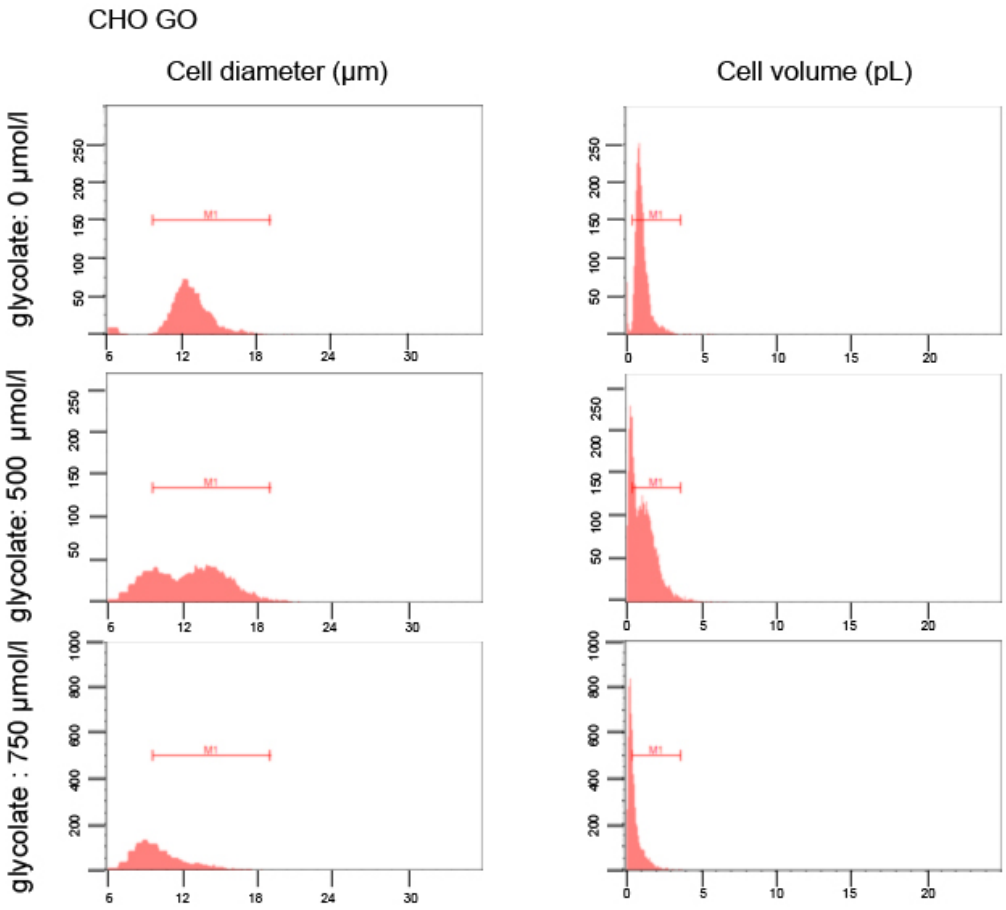

Annexe IX-3. **CHO cell size under different growth conditions**. The volume and diameter of CHO GO cells in a glycolate toxicity assay was determined with the Millipore Scepter. The majority of normal cells are distributed between 10 and 20 µm, as can be seen in the absence of glycolate. Under conditions of toxicity, as with added glycolate on CHO GO cells, a second population of smaller cells (diameter < 10 µm) can be seen.

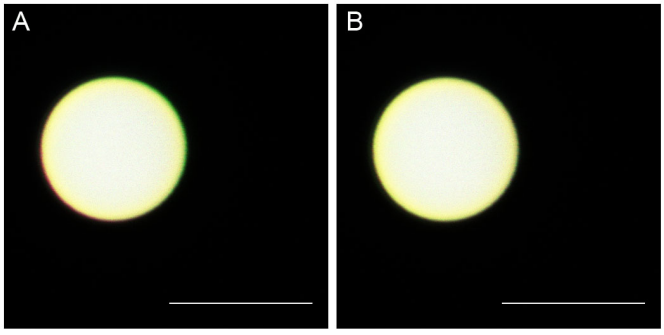

Annexe IX-4. **Registration correction on confocal acquired images**, red and green channels. Single z image of a coloured 10 micron bead, labelled in red, green and acquired with a 63x objective on the Leica TCS SPE used for experiments. Scale bar: 10 µm. Red channel displayed in red, green channel in green. A: no registration correction. B: after registration correction with the ImageJ TransformJ/Translate plugin.

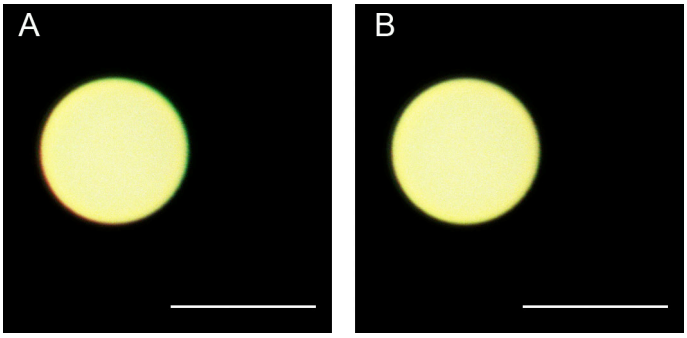

Annexe IX-5. **Registration correction on confocal acquired images,** red, green and far-red channels. Single z image of a coloured 10 micron bead, labelled in red, green, far-red and acquired with a 63x objective on the Leica TCS SPE used for experiments. Scale bar: 10 µm. Red channel displayed in red, green channel in green, far-red channel in blue. A: no registration correction. B: after registration correction with the ImageJ TransformJ/Translate plugin.

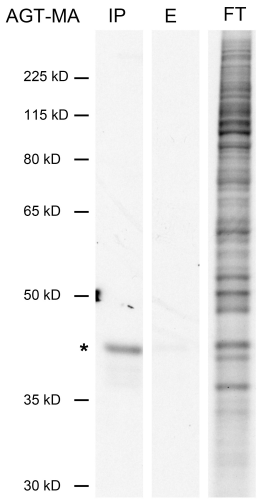

Annexe IX-6. **Immunoprecipitation of AGT-MA**. Cells lysates were obtained from CHO GO AGT-MA and immunoprecipitated on columns prepared with rabbit anti-human AGT. The immunoprecipitated fraction (IP) was collected, as well as the eluate post immunoprecipitation (E) and the flow-through (FT). All fraction were separated on a SDS-PAGE gel and the same volume was either immunoblotted with guinea-pig anti-human AGT and revealed by ECL, or if ^{35}S-Met had been used in the culture, as in pulse-chase experiments, the dried membrane was directly exposed to a film for autoradiography (shown on the figure). The (*) indicates the AGT monomer, seen on the IP fraction but absent from E or FT. Two bands of a size close to AGT are seen on the FT.

Annexe IX-7. **Colocalization coefficients determined on IMF in CHO cell lines**. CHO cells grown in standard conditions were stained either with anti AGT and anti GO or anti AGT, anti peroxisomes and MitoTracker. For CHO GO, anti AGT and anti GO or anti peroxisome and anti GO. Pearson's and Manders' coefficients were determined using the JACoP plugin of Image J on IMF of CHO cells (see methods III.6). P: Pearson's coefficient, M1: Manders' M1 (AGT, for CHO GO M1 is peroxisome), M2: Manders' M2 (either GO or mitochondria, for CHO GO M2 is GO).

construct	AGT-MA			AGT-mi			AGT-anc			AGT-D						WT		
	P	*M1*	*M2*	*P*	*M1*	*M2*	*P*	*M1*	*M2*	*P*	*M1*	*M2*				*P*	*M1*	*M2*
AGT/GO	0.853	0.773	0.712	0.849	0.794	0.815	0.473	0.081	0.291	0.642	0.634	0.584						
AGT / peroxisome	0.675	0.280	0.904	0.809	0.753	0.822	0.382	0.035	0.376	0.711	0.702	0.639			M/P	0.488	0.037	0.270
AGT / mitochondria	0.383	0.063	0.079	0.529	0.107	0.050	0.852	0.561	0.526	0.267	0.109	0.010						

construct	AGT-170			AGT-170			AGT-152			AGT-244			AGT-41			GO		
	P	*M1*	*M2*	*P*	*M1*	*M2*	*P*	*M1*	*M2*	*P*	*M1*	*M2*	*P*	*M1*	*M2*	*P*	*M1*	*M2*
AGT/GO	0.376	0.081	0.291				0.359	0.052	0.307	0.675	0.352	0.782	0.360	0.034	0.235	0.057	0.243	0.001
AGT / peroxisome	0.389	0.019	0.190	0.449	0.054	0.383	0.517	0.130	0.437	0.624	0.060	0.521	0.416	0.037	0.450			
AGT / mitochondria	0.940	0.781	0.906	0.897	0.869	0.728	0.900	0.675	0.772	0.843	0.724	0.694	0.884	0.639	0.744			

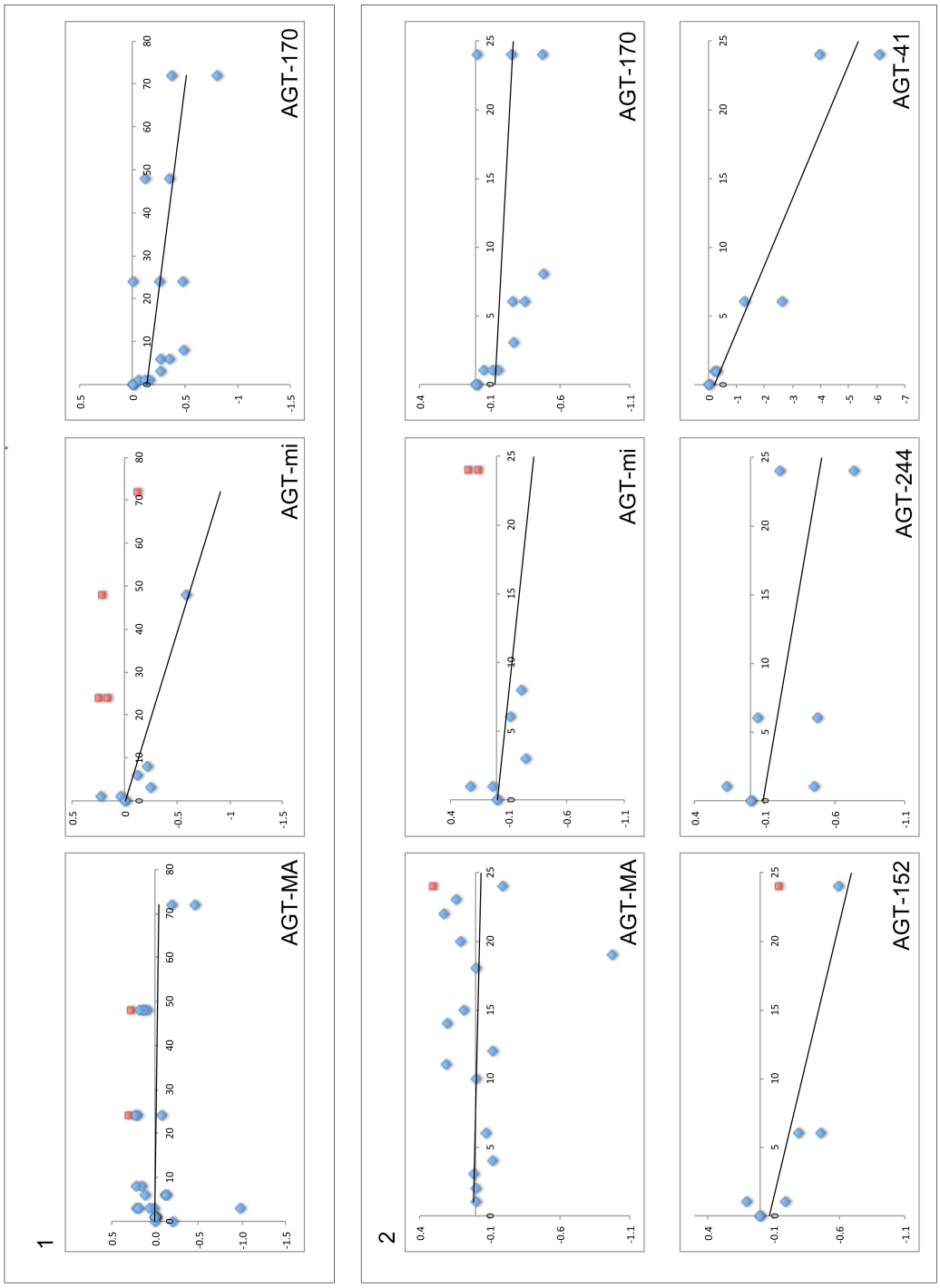

Annexe IX-8. . **Individual kinetics of degradation of AGT variants in CHO cells.** The intensity of immunoprecipitated AGT at different chase time is plotted on a log scale (y axis), chase time (x axis). Data (points) from all the experiments included in the calculation of half-life are shown in blue, data points not included for calculation are in red. The linear regression (full line) used for the calculation of the half-life is shown (full line). (1): chase time form 0 to 72 h; (2): chase time from 0 to 24 h.

Annexe IX-8. **Individual kinetics of degradation of AGT variants in CHO cells**

Annexe IX-9 **AGT and GO catalytic activities in stably transformed CHO cell lines.** AGT activity in µmol pyruvate/h/mg of cell protein, GO in nmol/min/mg cell protein. The AGT assay is carried out with added PLP (150 µmol/l). All results shown are those included for analysis in the present study. References are activities in human liver (Rumsby 1997). The limits of sensitivity of the AGT and GO are 3 µmol pyruvate/h/mg of cell protein and 4 nmol/min/mg cell protein. respectively.

	CHO GO AGT-MA	CHO GO AGT-mi	CHO GO AGT-anc	CHO GO AGT-170	CHO GO AGT-152	CHO GO AGT-244	CHO GO AGT-41	AGT-Δ	GO	WT
AGT										
	34.0	24.8	26.0	12.2	7.0	5.7	0.9	*	0.3	0.3
µmol pyruvate/h/mg protein	42.3	34.9	*	13.2	*	*	*	*	0.6	0.7
	34.3	19.2	*	13.8	*	*	*	*	0.1	0.7
	31.0	30.2	27.9	17.2	7.9	9.2	0.5	*	0.4	0.3
	54.9	32.2	29.7	15.7	7.8	10.0	0.6	*	0.4	0.5
	52.5	28.9	16.5	12.9	9.2	10.6	0.7	*	0.5	0.3
	34.2	19.2	12.2	13.3	7.7	11.3	0.5	0.5	0.3	0.4
	60.0	30.0	*	*	*	*	*	0.6	0.6	1.0
	54.0	32.0	*	*	*	*	*	0.6	*	1.0
mean	**44.1**	**27.9**	**22.5**	**14.0**	**7.9**	**9.4**	**0.6**	**0.6**	**0.4**	**0.6**
sd	**11.2**	**5.7**	**7.7**	**1.8**	**0.8**	**2.2**	**0.2**	**0.1**	**0.2**	**0.3**
% of CHO GOAGT-MA	**100.0**	**63.3**	**50.9**	**31.8**	**17.9**	**21.2**	**1.5**	**1.3**	**0.9**	**1.3**
GO										
	271	269	322	131	353	318	412	*	304	0
nmol/min/mg protein	392	542	*	513	*	*	*	*	510	0
	241	326	*	204	*	*	*	*	307	0
	215	266	168	112	301	200	185	*	127	0
	298	183	147	137	277	102	137	*	149	0
	374	486	355	243	416	494	551	*	322	1
	356	377	185	403	357	477	480	299	247	0
	354	310	*	*	*	*	*	361	231	0
	442	375	*	*	*	*	*	281	*	*
mean	**327**	**348**	**235**	**249**	**341**	**318**	**353**	**314**	**275**	**0.1**
sd	**75**	**112**	**96**	**153**	**54**	**171**	**183**	**42**	**119**	**0**
% of CHO GOAGT-MA	**100**	**106**	**72**	**76**	**104**	**97**	**108**	**96**	**84**	**0.0**

Annexe IX-10 **Effect of PLP on the catalytic activity of AGT in stably transformed CHO cell lines.** The ratio of activity with to without added PLP in the assay (PLP 150 µmol/l) in the assay is shown for each experiment included for analysis. Each ratio is calculated on the paired results with and without PLP. For the student t-test, the parameters have been set to one tail and paired data.

[0.3 µM B6]	ratio activity (-/+ PLP)	mean ratio	t-test (p)		ratio activity (-/+ PLP)	mean ratio	t-test (p)		ratio activity (-/+ PLP)	mean ratio	t-test (p)
AGT-MA	1.22	0.96	0.1670	**AGT-170**	0.85	1.06	0.3626	**GO**	1.00	1.78	0.0515
	0.81				0.85				1.00		
	1.00				0.97				3.00		
	0.87				1.00				2.23		
	1.26				1.69				0.86		
	0.77				0.99				2.58		
	0.92										
	0.88										
AGT-mi	0.84	1.05	0.4147	**AGT-152**	0.00	0.10	0.0003	**wt**	1.00	2.11	0.4572
	0.83				0.03				0.80		
	1.12				0.37				8.00		
	1.21				0.00				0.40		
	1.71								0.00		
	0.76								2.47		
	1.00										
	0.90										
AGT-anc	0.93	0.96	0.1764	**AGT-244**	0.60	0.80	0.0714				
	0.86				0.65						
	1.16				0.95						
	0.89				1.00						
				AGT-41	0.60	0.89	0.3426				
					0.67						
					1.43						
					0.88						

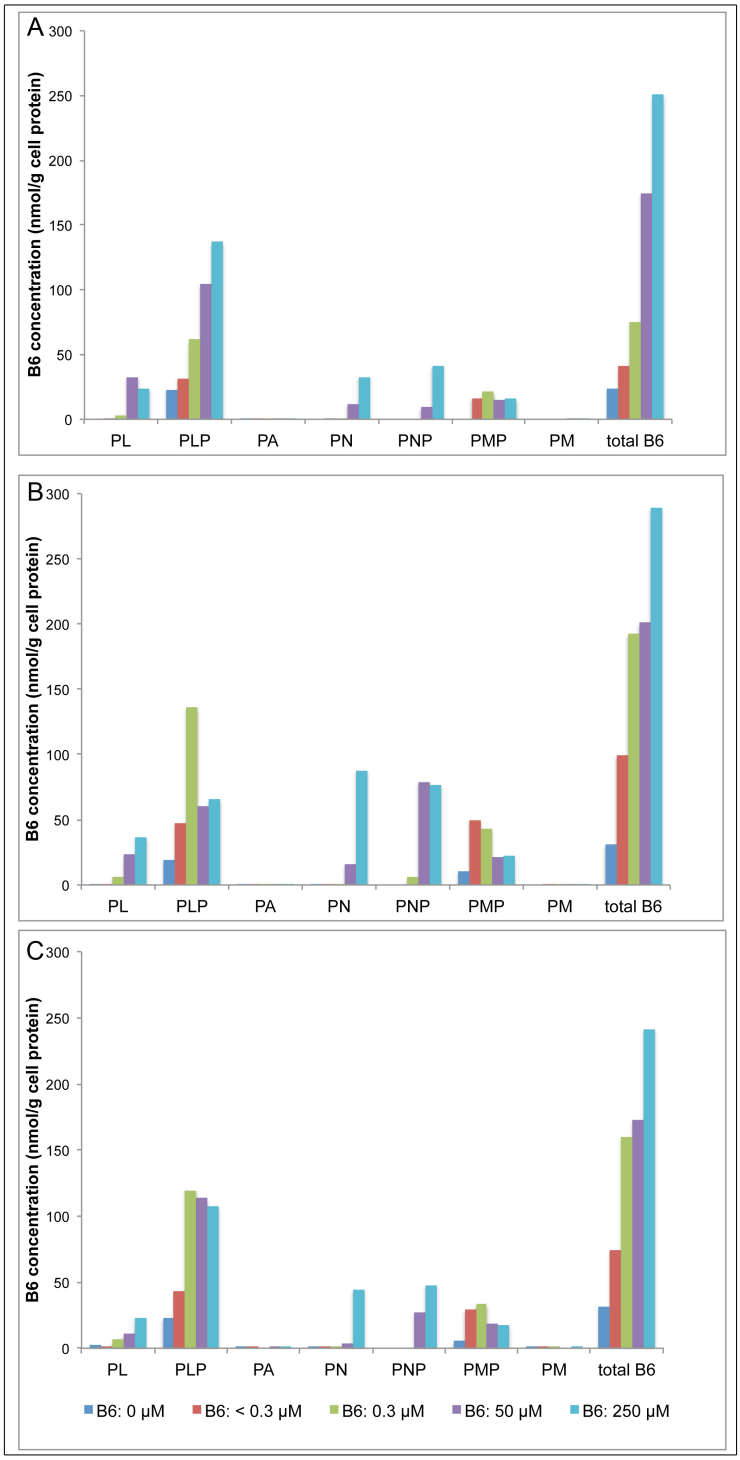

Annexe IX-11. **Increased levels of vitamin B6 vitamers in the transformed CHO cells tested**. Cell lysates (n=1) were obtained from three different CHO cell lines: CHO GO (A), CHO GO AGT-MA (B), CHO GO AGT-170 (C), grown at least 4 weeks with different levels of pyridoxine (0, < 0.3 µM, 0.3 µM, 50 µM, 250 µM, see methods III.2). PL: pyridoxal; PLP: pyridoxal 5'-phosphate; PA: pyridoxic acid; PN: pyridoxine; PNP: pyridoxine phosphate; PMP: pyridoxamine 5'-phosphate; PM: pyridoxamine. The B6 vitamers content was analysed by HPLC followed by tandem mass-spectrometry and expressed as nmol/g of cell protein (measurements kindly carried out by E Footitt, see Methods III.3).

Annexe IX-12. **Effect of pyridoxine on the AGT expression in stable transformants.**

Whole cell lysates were obtained from transformed CHO cells grown at least 4 weeks with different levels of pyridoxine (0, < 0.3 µM, 0.3 µM, 50 µM, 250 µM, see methods III.2). For the immunoblot, 5 µg of cell protein were loaded on each lane of the gel The membrane was incubated with guinea-pig anti human-AGT. A densitometry analysis was performed on the resulting membrane either exposed to film or to a digital camera. Both monomers and dimers were measured (n ≥ 2). The ratio between monomer to the total AGT detected on the immunoblots and the maximum increase of total AGT seen over the pyridoxine concentration range is given in the lower table.

		AGT-MA					AGT-mi				
AGT	**B6**	**0 µM**	**< 0.3 µM**	**0.3 µM**	**50 µM**	**250 µM**	**0 µM**	**< 0.3 µM**	**0.3 µM**	**50 µM**	**250 µM**
monomer	mean	1.01	0.94	0.99	1.56	1.51	0.88	0.82	0.97	1.00	1.03
	min	0.87	0.47	0.97	0.98	0.73	0.73	0.78	0.90	0.89	0.80
	max	1.23	1.41	1.00	2.56	3.07	1.04	0.85	1.00	1.20	1.51
total	mean	1.07	0.95	1.00	1.57	1.52	1.45	1.22	1.00	1.07	1.12
	min	0.87	0.47	1.00	0.98	0.73	1.04	0.94	1.00	0.99	0.88
	max	1.31	1.41	1.00	2.57	3.07	1.86	1.51	1.00	1.20	1.51

		AGT-anc				
AGT	**B6**	**0 µM**	**< 0.3 µM**	**0.3 µM**	**50 µM**	**250 µM**
monomer	mean	*	0.71	0.96	1.33	1.65
	min	*	0.61	0.86	1.09	1.15
	max	*	0.80	1.00	1.58	2.16
			0.82	1.00	1.58	2.16
total	mean	*	0.71	1.00	1.39	1.71
	min	*	0.61	1.00	1.21	1.27
	max	*				

		AGT-170					AGT-152				
AGT	**B6**	**0 µM**	**< 0.3 µM**	**0.3 µM**	**50 µM**	**250 µM**	**0 µM**	**< 0.3 µM**	**0.3 µM**	**50 µM**	**250 µM**
monomer	mean	0.26	0.63	0.91	1.02	1.08	*	0.52	0.97	0.83	0.82
	min	0.11	0.39	0.69	0.77	0.81	*	0.43	0.90	0.81	0.61
	max	0.37	0.82	1.00	1.35	1.58	*	0.61	1.00	0.86	1.03
total	mean	0.53	0.91	1.00	1.17	1.26	*	0.53	1.00	0.83	0.89
	min	0.28	0.69	1.00	0.83	0.96	*	0.46	1.00	0.81	0.61
	max	0.76	1.12	1.00	1.45	1.62	*	0.61	1.00	0.85	1.17

		AGT-244					AGT-41				
AGT	**B6**	**0 µM**	**< 0.3 µM**	**0.3 µM**	**50 µM**	**250 µM**	**0 µM**	**< 0.3 µM**	**0.3 µM**	**50 µM**	**250 µM**
monomer	mean	*	0.47	0.84	1.41	1.40	*	0.22	0.35	0.57	0.47
	min	*	0.43	0.69	1.25	1.24	*	0.21	0.21	0.45	0.35
	max	*	0.51	1.00	1.56	1.56	*	0.89	1.00	1.24	1.08
total	mean	*	0.76	1.00	1.51	1.68	*	0.89	1.00	1.32	1.43
	min	*	0.69	1.00	1.25	1.25	*	0.22	0.59	0.70	0.60
	max	*	0.83	1.00	1.77	2.12	*	0.89	1.00	1.40	1.78

	AGT-MA	AGT-mi	AGT-anc	AGT-170	AGT-152	AGT-244	AGT-41
(monomer / total AGT)							
B6: 0 µM	0.94	0.61	*	0.48	*	*	*
B6 < 0.3 µM	0.98	0.67	0.99	0.70	0.98	0.62	0.24
B6: 0.3 µM	0.99	0.97	0.96	0.91	0.97	0.84	0.35
B6: 50 µM	1.00	0.94	0.96	0.87	1.00	0.93	0.43
B6: 250 µM	0.99	0.92	0.96	0.85	0.92	0.83	0.33
maximum increase of total AGT	1.65	1.45	2.40	2.40	1.88	2.22	1.61

Annexe IX-13. **Effect of pyridoxine on the catalytic activity of AGT in transformed CHO cell lines.** Cell lysates were obtained from cells grown at least 4 weeks in various pyridoxine concentrations (0, < 0.3 µM, 0.3 µM, 50 µM, 250 µM, see Methods III.2). The AGT catalytic assay was carried out in the presence of PLP (150 µmol/l) or in its absence. The AGT activity is in µmol pyruvate/h/mg of cell protein. The limit of sensitivity of the AGT assay is 3. µmol pyruvate/h/mg protein.

mean activity [+PLP]	B6: 0 µM		B6: < 0.3 µM						B6: 0.3 µM				B6: 50 µM			B6: 250 µM		
AGT-MA	30.7	58.4	47.4	48	36.1	42.3	39.50	31.0	54.9	52.5	52.2	34.3	60	38	34.01	10.9	13.9	13.8	11.9	12.9	12.5
AGT-mi	8.07	11.8	19.2	46.8	13.2	16.8	19.12	30.2	32.2	28.9	34.9	19.2	30	22.6	24.83	7.5	9.2	10.1	9.69	14.3	8.7
AGT-anc	*	*	22.6	*	*	*	18.92	27.9	29.7	16.5	*	*	*	*	25.99	*	14.2	12.2	*	12.4	15.6
AGT-170	2.25	2.57	4.8	*	*	8.29	9.29	17.2	15.7	12.9	13.2	13.8	*	*	12.19	8.66	11.4	17.4	14.6	15.9	16.9
AGT-152	*	*	1.5	*	*	*	3.24	7.9	7.8	9.2	*	*	*	*	6.99	*	5.2	15.4	*	5.4	5.3
AGT-244	*	*	1.6	*	*	*	2.84	9.2	10	10.6	*	*	*	*	5.71	*	4.2	7.3	*	5.4	5.1
AGT-41	*	*	0.3	*	*	*	1.28	0.5	0.6	0.7	*	*	*	*	0.93	*	5.8	0.7	*	2	2.5
GO	0.3	0	0.5	*	*	*	0.29	0.3	0.4	0.5	0.56	0.35	0.6	0.3	0.32	0.33	0.3	0.2	0.54	*	*
WT	*	*	0	1	0.3	*	0.30	0.4	0.5	0.3	*	*	1.1	1.5	0.34	*	0.4	0.4	*	*	0.5

mean activity [-PLP]	B6: 0 µM		B6: < 0.3 µM						B6: 0.3 µM				B6: 50 µM			B6: 250 µM		
AGT-MA	6	6.78	21	15	15.3	16.2	19.94	37.8	44.5	52.3	45.1	43.1	46	35	29.77	10.5	9.6	10.7	11.8	10.7	9.5
AGT-mi	1.7	3.1	14	8.9	8.5	10.4	11.65	25.4	26.8	32.3	42.2	32.8	22.8	22.7	22.34	7.89	7.6	8.1	10.2	12.5	6.0
AGT-anc	*	*	16.3	*	*	*	12.28	25.9	25.5	19.1	*	*	*	*	23.11	*	11.4	10.1	*	12.3	13.2
AGT-170	0.7	2.2	5.1	*	*	7.35	8.69	14.7	13.3	12.5	13.2	23.3	*	*	12.05	9.73	9.4	14.8	15.5	14.5	14.1
AGT-152	*	*	1.4	*	*	*	2.05	0.0	0.2	3.4	*	*	*	*	0.00	*	2.1	2.6	*	2.4	2.7
AGT-244	*	*	2.3	*	*	*	3.36	5.5	6.5	10.1	*	*	*	*	5.72	*	3.3	6.1	*	4.7	4.2
AGT-41	*	*	1.3	*	*	*	0.76	0.3	0.4	1	*	*	*	*	0.82	*	0.0	0.2	*	0.3	0.3
GO	0	1.36	1.5	*	*	*	1.18	0.3	0.4	1.5	1.25	0.3	*	*	0.82	*	0.3	0.6	*	*	*
WT	*	*	1.2	0.4	1	*	0.86	0.4	0.4	2.4	*	*	0.44	0	0.83	*	0.4	0.5	*	*	0

Annexe IX-13 **Effect of pyridoxine on the catalytic activity of AGT in transformed CHO cell lines.**

Annexe IX-14. **Effect of AGT variants on the sensitivity of CHO cells to indirect glycolate toxicity.** Different CHO cell lines (CHO WT, CHO GO, CHO GO AGT-MA, CHO GO AGT-mi, CHO GO AGT-anc, CHO GO AGT-170, CHO GO AGT-152, CHO GO AGT-244, CHO GO AGT-41) grown under standard levels of pyridoxine (Ham's F12, 0.3 µM pyridoxine), were exposed for 2 days to different concentrations of glycolate (0 to 1500 µM) The indirect toxicity of glycolate was assessed by the decrease in surviving cells after 2 days of exposure. The results (n=1 - 3) are expressed as mean % (range) of the control for each cell line.

Pyridoxine : 0.3 µM	CHO wt (n=3)	CHO GO (n=3)	CHO GO AGT-MA (n=3)	CHO GO AGT-mi (n=2)	CHO GO AGT-anc (n=1)	CHO GO AGT-170 (n=3)	CHO GO AGT-152 (n=1)	CHO GO AGT-244 (n=1)	CHO GO AGT-41 (n=1)
Glycolate (0 µM)	[100]	[100]	[100]	[100]	[100]	[100]	[100]	[100]	[100]
Glycolate (125 µM)	91 (88-94)	79 (69-83)	95 (90-97)	96 (87-105)	89	93 (88-95)	82	101	68
Glycolate (250 µM)	101 (99-104)	21 (16-25)	97 (93-104)	91 (90-91)	76	79 (76-81)	70	84	16
Glycolate (500 µM)	98 (82-197)	9 (5-12)	82 (73-88)	67 (65-69)	59	40 (25-51)	19	61	9
Glycolate (750 µM)	104 (97-110)	7 (7-8)	54 (45-72)	33 (30-37)	16	20 (13-25)	15	31	8
Glycolate (1000 µM)	103 (98-111)	7 (5-8)	25 (23-29)	17 (17-18)	20	16 (9-21)	11	25	7
Glycolate (1500 µM)	107 (104-110)	9 (8-10)	14 (13-14)	9 (8-11)	13	18 (18-19)	11	2	6

Annexe IX-15**. Effect of pyridoxine on the sensitivity of CHO GO AGT cells to indirect glycolate toxicity.** Different CHO cell lines (CHO WT, CHO GO, CHO GO AGT-MA, CHO GO AGT-mi, CHO GO AGT-anc, CHO GO AGT-170, CHO GO AGT-152, CHO GO AGT-244, CHO GO AGT-41) were grown at least 1 month in different concentrations of pyridoxine (0, < 0.3, 0.3, 50, 250 µM), and exposed for 2 days to glycolate (500 or 750 µM). The indirect toxicity of glycolate was assessed by the decrease in surviving cells after 2 days of exposure to glycolate. The results (n=2) are expressed as mean % (range) of the control for each cell line. For AGT-anc, AGT-152, AGT-244 and AGT-41, only 3 levels of pyridoxine were studied: <0.3, 0.3, 50 µM.

Pyridoxine concentration		CHO wt (n=2)	CHO GO (n=2)	CHO GO AGT-MA (n=2)	CHO GO AGT-mi (n=2)	CHO GO AGT-anc (n=2)	CHO GO AGT-170 (n=2)	CHO GO AGT-152 (n=2)	CHO GO AGT-244 (n=2)	CHO GO AGT-41 (n=2)
B6: 0 µM	**0 µM**	[100]	[100]	[100]	[100]	*	[100]	*	*	*
	500 µM	97	9	36	12		13			
	750 µM	92	7	22	8		10			
B6: < 0.3 µM	**0 µM**	[100]	[100]	[100]	[100]	[100]	[100]	[100]	[100]	[100]
	500 µM	89	8	72	57	27	23	15	20	10
	750 µM	82	6	48	21	19	14	12	14	9
B6: 0.3 µM	**0 µM**	[100]	[100]	[100]	[100]	[100]	[100]	[100]	[100]	[100]
	500 µM	101	9	82	97	48	59	10	33	5
	750 µM	106	6	68	43	15	33	9	21	5
B6: 50 µM	**0 µM**	[100]	[100]	[100]	[100]	[100]	[100]	[100]	[100]	[100]
	500 µM	93	8	62	23	15	31	9	32	8
	750 µM	89	6	32	12	11	20	7	23	7
B6: 250 µM	**0 µM**	[100]	[100]	[100]	[100]	*	[100]	*	*	*
	500 µM	100	7	64	33		31			
	750 µM	104	4	28	11		16			